BIORESPONSE TO POLYMERIC SUBSTRATES: EFFECT OF SURFACE ENERGY, MODULUS, TOPOGRAPHY, AND SURFACE GRAFT COPOLYMERS

By

LESLIE HOIPKEMEIER WILSON

A DISSERTATION PRESENTED TO THE GRADUATE SCHOOL
OF THE UNIVERSITY OF FLORIDA IN PARTIAL FULFILLMENT
OF THE REQUIREMENTS FOR THE DEGREE OF
DOCTOR OF PHILOSOPHY

UNIVERSITY OF FLORIDA

2005

This document is dedicated to Cliff Wilson, my wonderful and supportive husband.

ACKNOWLEDGMENTS

I wish to express sincere gratitude for my advisor, Dr. Anthony Brennan, for his motivation and guidance in this endeavor. I would also like to thank my committee members Dr. Christopher Batich, Dr. Ronald Baney, Dr. Kenneth Wagener, and Dr. John Mecholsky Jr. I would also like to thank Dr. Elliot Douglas for agreeing to attend on my defense.

I could not have completed this task without the assistance of my colleagues, both past and present, who gave me all the necessary collaboration and support: Clay Bohn, Michelle Carmen, Thomas Estes, Adam Feinberg, Amy Gibson, Brian Hatcher, Kiran Karve, Nikhil Kothurkar, Jeanne MacDonald, Dr. Rodrigo Orifice, Jim Schumacher, Wade Wilkerson, Margaret Kayo and all the other students, faculty, and staff that made my experience at the University of Florida memorable. I would also like to thank the undergraduates who helped me on this project: Jennifer Brandt, Angela Dixon, and Cristina Fernandez.

I would like to thank those at the University of Florida that have assisted with instrumentation training and experimentation including Eric Lambers at the Major Analytical Instrumentation Center (MAIC), Dr Jim Rocca at the Brain Institute, and Gary Scheifelle at the Particle Engineering Research Center (PERC).

This work would not have been possible without the collaboration and financial support from the Office of Naval Research. I would specifically like to

thank Steve McElvaney and Dr. Irwin Singer. I gratefully acknowledge the assistance of my collaborators who performed the bioassays: Dr. Maureen Callow, Dr. James Callow, Dr. John Finlay, and Ruth Perry at the University of Birmingham.

I would like to thank my parents, my sister, and my extended family for supporting my continued education. Last, but not least, I would like to thank my husband, Cliff, for his love and support through the years of my education.

TABLE OF CONTENTS

LIST OF TABLES

LIST OF FIGURES

Abstract of Dissertation Presented to the Graduate School
of the University of Florida in Partial Fulfillment of the
Requirements for the Degree of Doctor of Philosophy

BIORESPONSE TO POLYMERIC SUBSTRATES: EFFECT OF SURFACE ENERGY, MODULUS, TOPOGRAPHY, AND SURFACE GRAFT COPOLYMERS

By

Leslie Hoipkemeier Wilson

August 2005

Chair: Anthony B. Brennan
Major Department: Materials Science and Engineering

Biofouling is the accumulation of biological matter on a substrate. It is essential to elucidate and model the major factors that affect both biological settlement and adhesion to substrates in order to develop coatings that minimize initial fouling or ease the removal of this fouling. To date, models that have estimated adhesion strength to coatings primarily included bulk elastic modulus and surface energy. Topography, however, has been found to dominate both these terms in the reduction of settlement and has been found to affect the adhesion strength as well.

Silicone foul release coatings have demonstrated moderate success in the prevention of marine biofouling because of their low modulus and low surface energy. Problems exist with durability and eventual fouling of the coating due to the overgrowth of foulants that prefer hydrophobic substrates. This research details the characterization and the surface and bulk modification of a

commercially available silicone elastomer. The modifications include bulk additives, surface topography, and surface graft copolymers. The effect of these modifications on biological response was then assayed using the alga *Ulva* as a model for marine biofouling.

The unmodified silicone elastomer has a bulk modulus of approximately 1MPa. The addition of vinyl functional polydimethylsiloxane oils allowed for a greater than 200% increase or a 90% decrease in the bulk modulus of the material. The addition of non-reactive polydimethylsiloxane oils allowed for a change in the surface lubricity of the elastomer without a significant change in the mechanical properties.

Topographical modifications of the surface show a profound effect on the bioresponse. Appropriately scaled engineered microtopographies replicated in the silicone elastomer can produce a 250% increase in algal zoospore fouling or an 85% reduction in settlement relative to a smooth silicone elastomer.

Finally, the modification of the surface energy of this material was achieved by acid catalyzed surface hydrolysis and subsequent grafting of poly(ethylene glycol), polysulfone, or perfluoropolyether. The water contact angle could be increased by16% or decreased by 60% relative to the silicone elastomer control. These surfaces were characterized by various contact angle techniques, ATR-FTIR, and XPS. These surface grafts were also combined with the topographical modifications to evaluate the relative significance of these two factors on bioresponse.

CHAPTER 1
BIOFOULING

Introduction

The purpose of the present research is the chemical manipulation of a polydimethylsiloxane elastomer in order to evaluate the factors that affect biological adhesion to polymers. The three main factors that will be modulated are surface chemistry, bulk modulus, and surface topography. The silicone elastomer can be modified with respect to each of these factors individually or in combination to ascertain their relative importance on bioadhesion, specifically the problem of biofouling.

Biofouling is the accumulation of biological matter on a surface. Any substrate in regular contact with water is likely to become fouled; and, as yet, no surface has been found that is completely resistant to fouling [1-3]. The presence of biofouling on ship hulls is a particularly vexing problem facing the US Navy. Biofouling is problematic for maritime vessels in view of the resulting increased roughness of the hull of a ship, which leads directly to increased drag and decreased fuel efficiency.

The composition of marine fouling can be divided into microfoulers and macrofoulers. Biofilms are classically defined as the layer composed of microfoulers such as bacteria, diatoms, and microalgae. Macrofoulers include macroalgae and large organisms such as oysters, mussels, tubeworms, and barnacles [4]. The formation of biofouling is a complex hierarchical process. The

establishment of a biofilm is essential for the attraction and adhesion of most macrofoulers.

A number of studies indicate that a correlation exists between the effectiveness of the antifouling and foul release coatings and the physico-chemical surface properties [5-13]. The key parameters influencing fouling of substrates include: surface/bulk chemistry, surface free energy, modulus, and surface topography/structure.

Biology/Surface Chemistry/Conditioning Layers

Within seconds of immersion in an aqueous system, all substrates will begin to acquire a conditioning film composed of salts, macromolecules, and proteins that become physadsorbed. In most natural systems, foulants will contact this previously absorbed biofilm rather than the native substrate, given that these conditioning films are present within hours of exposure to seawater on all substrates. Due to the extremely short-range nature of adhesion, it would be expected that all substrates would become virtually identical, indicating that initial substratum properties should have no influence on macroscopic fouling. However, initial substratum properties do influence the macroscopic fouling. Thus, substrate surface chemistry must directly or indirectly influence early surface colonization of the conditioning biofilms. Conditioning films are spatially heterogeneous and vary in terms of composition of absorbed biomolecules.

Protein adsorption is known to vary largely as a function of water chemistry and substrate surface chemistry. Additionally temperature and concentration are important factors. All of these factors will affect which biomolecules are laid

down as well as their surface concentration, conformation, and morphology. For instance, some proteins will denature upon adherence to a substrate.

In a study by Taylor, the surface free energy of an adsorbed monolayer of the same protein was 30 mN/m on a relatively hydrophobic substrate ($\gamma_{substrate}$=49 mN/m) and 43 mN/m on a more hydrophilic substrate ($\gamma_{substrate}$=54 mN/m) [14]. This shows that the surface properties of the conditioning film are controlled by the substrate properties. Subsequent bacterial attachment in this study was shown to vary significantly with the properties of this adsorbed conditioning layer.

Studies have shown that the presence of specific strains in bacterial biofilms may either enhance or inhibit settlement and adhesion of algae, such as *Ulva* [15, 16]. Similar studies show both inhibitory and advantageous effects for different bacterial strains on settlement of hard foulants such as barnacle larvae [17-19]. Naturally occurring biofilms are assemblages of a wide variety of bacterial strains; such assemblages encourage settlement. A study by Joint et al. [16] indicates that bacterial biofilm assemblages strongly and linearly increase settlement and attachment of *Ulva* whereas bacterial-free conditioning films behave similarly to pristine substrates with respect to *Ulva.* This result shows that the presence of “attractive” bacterial biofilm is especially problematic in terms of the biofouling cascade.

The biofouling cascade starts with the initial conditioning film, which allows for the attachment of bacterial assemblages and microfouling slimes. These biofilms are thus attractive to macrofouling. The depiction of the biofouling cascade shows the substrate, which is then covered with the biofilm assemblage,

composed of the conditioning film, slime, microfouling alga, and marine bacteria. The third layer depicts the macrofouling alga *Ulva*. This is depicted as a separate layer because this fouler bridges the gap between the microfoulers and macrofoulers. *Ulva* settles and adheres to a substrate as a micron sized zoospore, which then differentiates and grows into a macroalgal plant (Figure 1-1). The final stage is the adherence, differentiation, and growth of the calcareous organisms such as tubeworms and barnacles.

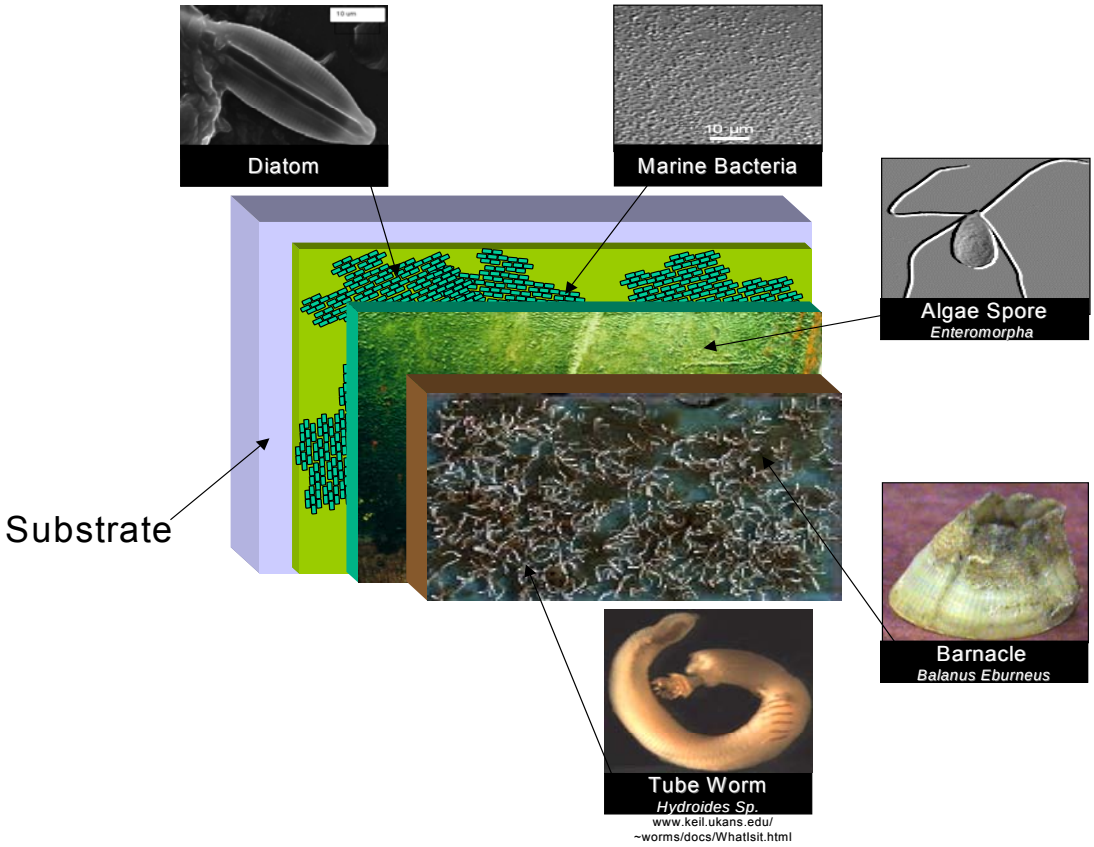

Figure 1-1: Schematic of hierarchical organization of the temporal evolution of biofouling formation [20]

Economic and Environmental Impact of Marine Biofouling

It is widely accepted that the most effective coatings devised for fouling minimization on ship and boat hulls are self-polishing antifouling paints incorporating tributyltin (TBT), as such, more than 70% of the world's fleet use

organotin coatings [21-24]. Due to environmental regulations, which aim to phase out and eliminate their use by 2008, new coatings must be developed which will be as effective.

According to a review of organotin regulatory strategies in 1985, the US Navy calculated that the cost savings of using TBT based antifouling paints versus no preventative measures would exceed $130 million annually. This figure considered fuel savings alone and was calculated with the assumption of fuel costs of $18/barrel and 600 ships [23]; today fuel cost is approximately $55/barrel and 300 ships in fleet [25, 26]. If we consider other commercial ships, fishing vessels, and private boats, this fuel savings could include another $300-$400 million annually for the US alone [23].

These figures also ignore the additional costs of necessary periodic underwater cleaning and dry-docking for the purposes of cleaning and repainting. Annually, the US Navy spends 6$22-44M on in-service underwater hull coating and dive cleaning operations [27]. When a ship hull becomes exceedingly fouled, the ship must be dry-docked, stripped, and recoated. According to the Commander of Atlantic Naval Surface Forces, in Norfolk, the average cost per ship is $500K for the docking/undocking total evolution, independent of any other repair work [28]. However, for larger ships, such as an aircraft carrier, the cost could exceed $1mil, according to a former aircraft carrier captain [29]. Estimations that are more recent place the cost of dry-docking per day at $350K [27].

The monetary cost of increased fuel consumption is not the only concern, as the byproducts of burning fossil fuels include carbon dioxide and sulfur dioxide, which are main contributing factors to air pollution. It is estimated that the decreased fuel consumption attributed to TBT coatings correlates to 22 million tons less carbon dioxide and 0.6 million tons less sulfur dioxide emitted to the environment annually [23, 24, 30].

Anti-Fouling/Foul-Release Coatings

Tributyltin Coatings

Self-polishing antifouling paints incorporating tributyltin (TBT) have been very successful antifouling coatings, but the environmental impact has been vast. Many reviews of the environmental, economical, and military impacts of the use and ban of TBT coatings are available in the literature [21-24, 30-38]. Organotin compounds were first developed in the 1920s to combat moths. Subsequent uses included fungicides and bactericides [36]. Organotin based paints were first used for marine paints in the early 1970s [23].

The TBT based paints are “self-polishing” in that the biocide is incorporated into the polymeric backbone, i.e. through an organotin-ester bond in a methacrylate based copolymer resin. The mechanism of biocide release is the systematic hydration, swelling, and degradation of the film allowing for release of biocide and exposure of a fresh paint surface. The polymer-COO-TBT surface is attacked by seawater (Na^+ and Cl^- ions). This causes hydrolysis of the organotin-ester linkage at the surface. The toxic organotin-chlorine salt species is released into the seawater. The partially reacted outer layer of the film, acidic Polymer-COO^- Na^+, is water-soluble and easily eroded exposing a fresh layer of

the organotin polymer [39]. This process is repetitive, leading to both the long lifetime and relatively constant biocide release rate of this coating type.

As early as 1974, oyster growers noticed abnormalities in *Crassostrea gigas*, the pacific oyster along the east coast of England. Imposex was observed in dogwelks, a marine mollusk; this condition leads to females developing male characteristics and a subsequent decline in population. The connection between these abnormalities and organotin paints was not realized until the mid 1980s, when researchers in France and the United Kingdom began to suggest that the antifoulant was adversely affecting non-target species. Since 1980, environmental studies have been showing the detrimental repercussions of the tributyltin.

Regulations and research were spearheaded by the European nations. France implemented a ban in 1982 [31, 37], and the United Kingdom in 1985. Shipyard workers in the coastal United States who dealt with application of tributyltin paints and cleaning of paint ship hulls began reporting a variety of health problems in 1986 [23]. By mid-1987, most of the coastal states had begun implementing restrictions on the use of organotins. Virginia, home to the largest naval port in the world, led the US in the implementation of TBT regulatory strategies. The subsequent federal regulations were based on Virginia's model to reduce environmental and public health risks [23]. The International Maritime Organization agreed upon the total ban on TBT paints in 1999.

Copper-Based Paints and Booster Biocides

Due to the restrictions against TBT paints, copper compounds such as cuprous oxide (Cu_2O), copper thyocyanate (CuSCN) and even metallic copper

are now employed as the principal biocide. Copper oxides were first successfully used as an antifoulant in paint in 1863 [35]. Copper exhibits broad-spectrum antifouling activity against many macrofoulants; however, several algal species including *Ulva* are highly tolerant of copper [8, 38]. The use of booster biocides is required to combat the copper-resistant organisms. Many booster biocides have been used in conjunction with copper to control copper-resistant fouling organisms. In fact, tributyltin was first introduced as a booster for copper resistant slimes and algae. Copper is used as the broad-spectrum biocide in many of the self-polishing copolymer paint formulations [39]. There are many additional booster biocides currently registered as active ingredients in antifouling products on the market: chlorothalonil, dichlofluanid, diuron, Irgarol 1051, sea-nine, zinc pyrithione, zineb, Kathon 5287, TCMTB, and TCMS pyridine [33, 34, 38].

The level of soluble copper and these alternative booster biocides are presently increasing in prevalence in waterways [38, 40, 41]. Many authors have predicted regulations against these compounds in the coming years [24]. As such, a completely novel system must be developed that has no leachable biocidal agents, but also acts across a wide range of species.

Foul Release Coatings

The basic premise of foul release (FR) coatings is that low surface free energy/low modulus coatings may become fouled but can be easily cleaned, ideally under the shear forces experienced during normal operations. Foul release coatings have gained favor in the private sector in recent years, because

the ban on TBT paints has been in effect for small private boats under 25 meters in length since 1988.

Polydimethylsiloxane elastomers (PDMSe) are useful FR coatings due to the combination of this materials inherent low modulus and low surface energy. The first reported use of PDMSe coatings for marine foul release was in 1970 by Dow Corning's Silastic®. The first patent for siloxane-based FR coatings was issued in 1972 to the Battelle Institute [42]. From that time, many patents have been rewarded to companies such as International Paint, Nippon Paint, General Electric, and many others [42-44].

Release coating formulations have incorporated hydrosilylation and condensation type elastomers, as well as copolymeric formulations including polyethylene glycol and polymethyl methacrylate. Siloxane oligomers have also been included to increase surface lubricity. Several problems exist with the siloxane based release coating:

- Coatings are not durable enough to withstand required abrasions and abuse associated with the operations of the ship and cleaning processes,
- Expensive application costs,
- Protein layers rapidly cover the siloxane coating, as proteins are attracted to hydrophobic substrates, leading to fouling of the coating occurs within a few years, well short of the Naval goal of 12 years.

Adhesion Models and Theory

In order to develop a coating that will minimize biofouling it is necessary to analyze the factors that control biological adhesion (Figure 1-2). The mechanical, surface, and biological aspects of adhesion will briefly be reviewed. This image depicts an *Ulva* zoospore probing a surface. The variables affecting its response to the surface include surface chemistry/energy, topography, and bulk modulus. The present research entails the modification of these three variables using a commercially available silicone elastomer.

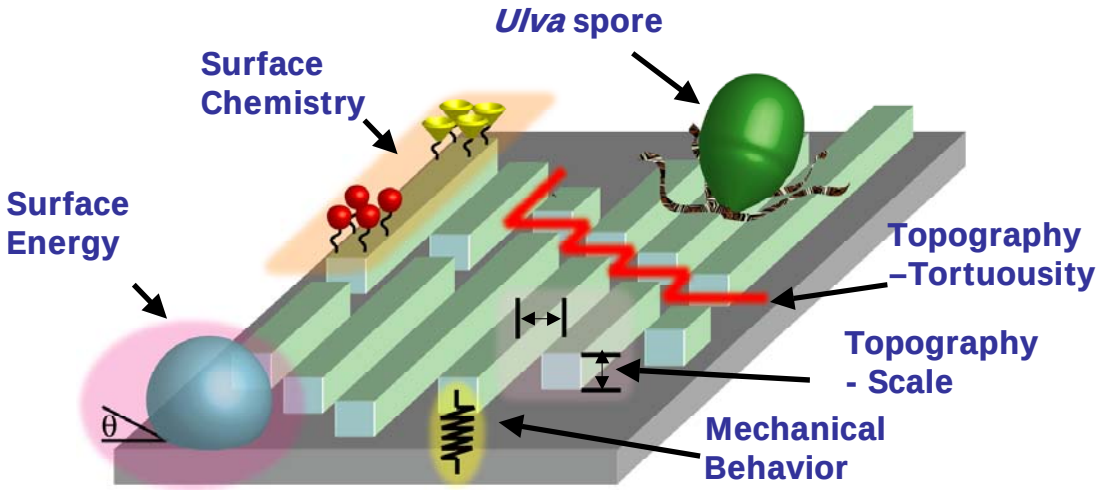

Figure 1-2: Schematic of various physico-chemical factors affecting marine biofouling [45]

Mechanical Aspects

The fracture strength of a solid material is related to the cohesive forces between atoms and the existence of flaws within the bulk and surface of that material [3, 46-48]. As derived by Griffith, the critical stress, σ_c, (Figure 1-3 A) required for crack propagation in a brittle material is described by

$$\sigma_c = ((2E\gamma_s)/(\pi a))^{1/2} \quad [1]$$

where σ_c is the critical stress for crack propagation, E is the modulus of the material, γ_s is surface energy, and 'a' is the radius of the flaw.

The most prominent theory regarding biological adhesion to substrates is the Johnson-Kendall-Roberts (JKR) theory, which equates work of adhesion to the area of contact, surface energy, bulk modulus, etc (Figure 1-3B). This theory is directly analogous to and derived from Griffith's brittle fracture theory. For polymeric substrates, one must also consider Poisson's ratio in these calculations. Therefore, the equation describing crack propagation in a solid polymeric material with a flaw of radius 'a' becomes:

$$\sigma_c = ((E\gamma_s)/(\pi a^*(1-\nu)^2))^{1/2} \quad [2]$$

where σ_c is the critical stress for crack propagation, E is the modulus of the material, γ_s is surface energy, 'a' is the radius of the flaw, and ν is Poisson's ratio.

The assumption that no adhesive interface will be completely free of defects or cracks allows for the extension of these equations and theories to the study of adhesives. The defects will serve as stress raisers to initiate crack growth and subsequent failure of the adhesive joint. The energy required to fracture an adhesive joint, known as G or the Griffith's fracture energy per unit area, is most simply expressed as twice the energy required to form the new surfaces, also known as Dupre's work of adhesion.

$$G = w_a = 2\gamma_s \quad [3]$$

Given an adherend of radius a on a thin polymeric coating of thickness t with a bulk modulus of K, the critical stress of removal is

$$\sigma_c = ((2GK) / t)^{1/2} \text{ where } t < a \quad [4]$$

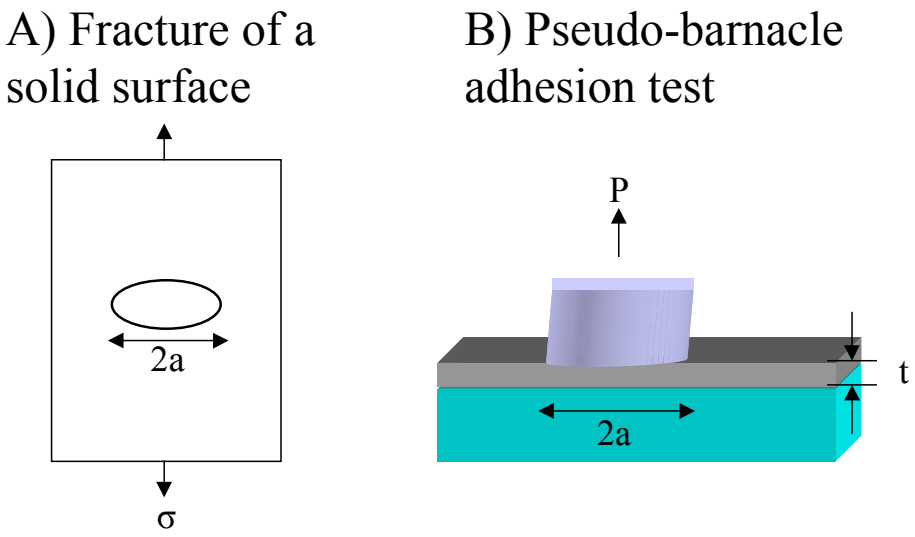

Figure 1-3: Schematic of fracture mechanics theories A) Griffith's fracture of solids B) Critical pull-off tests using pseudobarnacles

Note that the force required to remove an adherend will increase as this coating thickness decreases and will be directly proportional to the square root of the surface energy times the modulus. For the case of a thick elastomeric coating, where thickness is considerably thicker than the radius of the adherend, the coating will show appreciable elongation. This results in failure in a tensile or peel mode rather than by shear [3].

$$\sigma_c = ((2GE) / (\pi a (1-\nu^2)))^{1/2} \quad \text{where } t >> a \text{ and } E = 3K(1-2\nu) \qquad [5]$$

where σ_c is the critical stress for crack propagation, E is the modulus of the material, G is the Griffith's fracture energy per unit area, 'a' is the radius of the flaw. Note that thickness is no longer a parameter in this equation, but that force is still related to the square root of the surface energy times the modulus.

This equation is referred to as the Kendall equation and reported as

$$\mathbf{\sigma_c = ((4w_aE) / (\pi a (1-\nu^2)))^{1/2}} \qquad \mathbf{[6]}$$

where σ_c is the critical stress for crack propagation, E is the modulus of the material, w_a is the work of adhesion, and 'a' is the radius of the flaw.

Surface Energy/Surface Chemistry

Surface energy, as shown above, clearly affects adhesion. The maximum work of adhesion generally increases on the same order of magnitude as the values of γ_C, which is the critical surface tension of the substrate. The wettability of a substrate is determined by the exposed chemical species and their relative packing at the substrate surface and is generally independent of the underlying atoms and molecules in the bulk.

According to the classical treatment by Young, the contact angle θ between a liquid drop and a planar solid surface describes the extent to which the liquid wets or spreads across the surface (Figure 1-4). The term wettability indicated the ability of the liquid to spread across a substrate. When $\theta = 0$, the liquid is said to completely wet the solid, and it spreads spontaneously at a rate depending on the viscosity of the liquid and the regularity of the substrate. Nonzero contact angles are measured for substrates that are not completely wet by liquids. Contact angle is, thus, an inverse measure of a substrate's wettability, and the value of the cosine of θ is a direct measure. There is an empirical linear relation between cosine θ and γ_{LV}, the liquid vapor surface tension, for a wide variety of pure liquids on surfaces. The critical surface tension, γ_C, is defined as the intercept of the cosine θ versus γ_{LV} line with the cosine $\theta = 1$ horizontal line.

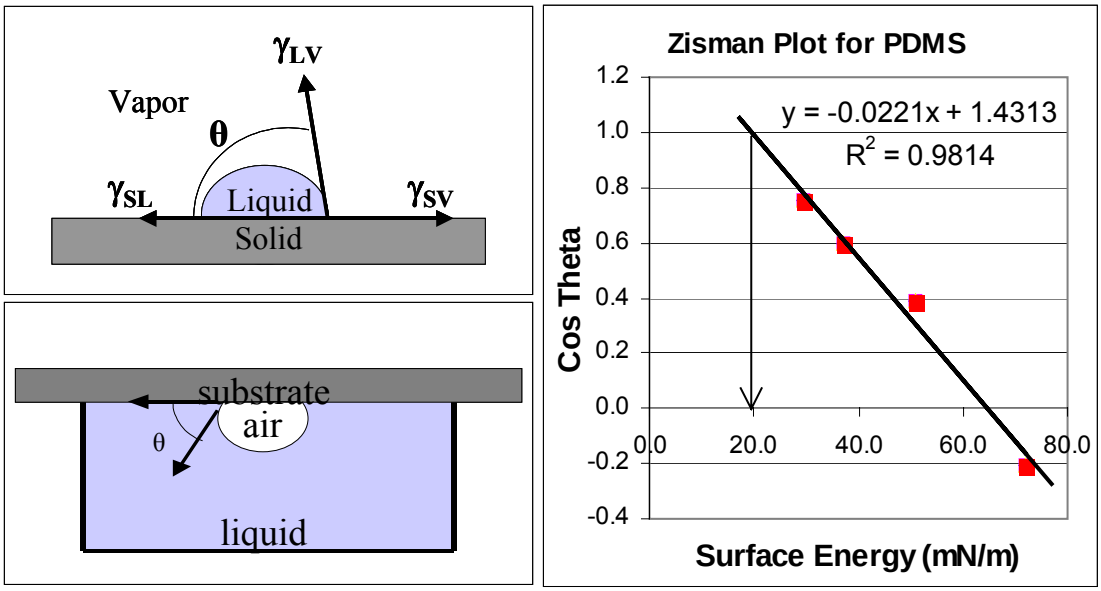

Figure 1-4: Upper left: Schematic of sessile drop; Lower left: schematic of captive air bubble contact angle measurements; Right: Example of Zissman plot to determine surface free energy of PDMSe

Surface energy is important in the context of the Kendall relationship in terms of the work of adhesion and in terms of the contact area of adhesion. Hydrophobic coatings can often not be "wet" by the biological adhesive; therefore, the contact area of adhesion, "a" as described above, is decreased allowing for ease of release. This effect is shown in Figure 1-5 for an algal spore. The adhesive wets a hydrophilic substrate to a greater extent than the hydrophobic substrate. These particular samples were glass substrates modified with self-assembled monolayers (SAMs) based on either –OH or $–CH_3$ to produce hydrophilic or hydrophobic substrates, respectively. The adhesive secreted from the zoospore spreads on the hydrophilic substrate producing a larger effective contact area.

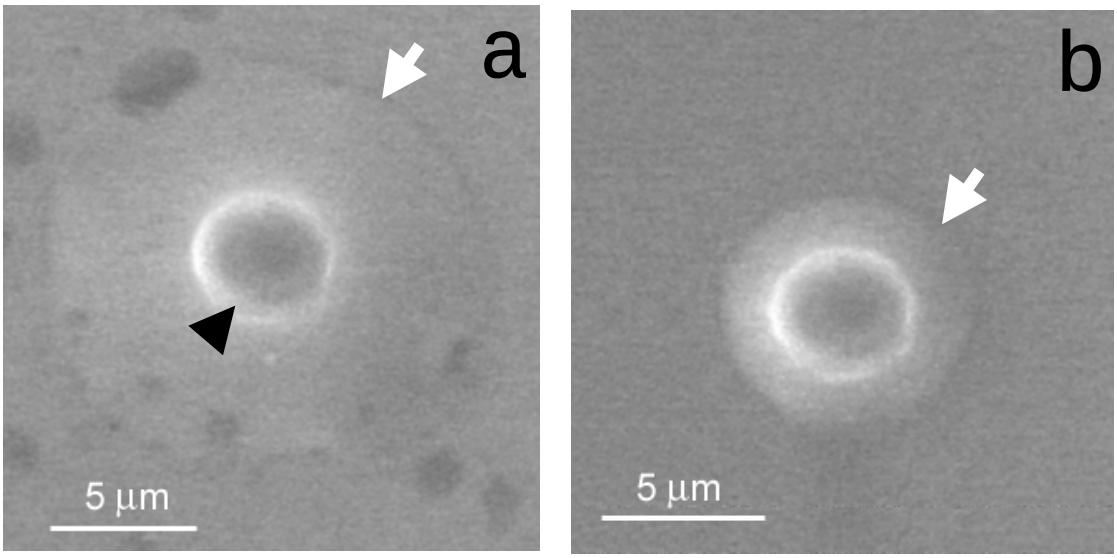

Figure 1-5: Ulva zoospore on a) hydrophilic and b) hydrophobic substrate showing the spreading of the adhesive pad which would relate to the spore's contact area, 'a' in the Kendall equation. Image used by permission of Maureen Callow.

Despite the fact that the work of adhesion generally increases with γ_C, both extremely hydrophobic and hydrophilic surfaces have recently been shown to work well as foul release coatings. This fact may seem counterintuitive given the Kendall relationship shown in equation 5. However, ultra-hydrophilic coatings hold water so closely to the surface that the adhesive is unable to bond to the actual substrate. Even a monolayer of absorbed molecules is capable of converting a high-energy surface to a low-energy surface. Johnson and Dettre demonstrated that the clean surface of bulk water is itself a low-energy surface with a critical surface tension of about 22 dynes/cm [49].

The change in surface energy with the adsorption of a single monolayer is especially important in biofouling research. Hydrophobic coatings, such as silicone, are ideal in deterring adhesion of many marine organisms. However, proteins, lipids, and polysaccharides can strongly adhere to hydrophobic

substrates. There is abundant evidence that biological adhesion is significantly dependent upon proteins absorbed at the joint interfaces. As described above, many marine species will not adhere to coatings unless they have been pre-conditioned with a biofilm layer consisting of proteins, bacteria, and other microorganisms. The extreme localization of surface forces should make clear the importance of intervening films in determining biological adhesion. Once a monolayer of proteins is adhered to a hydrophobic film, the subsequent cascade of biofouling events is inevitable.

Topography

In recent decades, there has been considerable research into cellular responses to topographical cues on both nanometer and micrometer scales [50-56]. This concept is now being employed to develop engineered surface topographies that reduce marine fouling by optimizing mechanical and energetic effects [57-64].

It is reasoned that topography influences bioresponse due to induced changes in surface wettability. The adhesion strength to elastomers is most frequently described by the Kendall relationship as represented in equation 6 [3, 47].

This equation addresses both modulus and wetting behavior of the elastomer by an adhesive material. The work of adhesion is equivalent to twice the interfacial tension and can be determined by measuring contact angles formed at the interface of a liquid adhesive and the solid substrate to which it is bonded. These are dependent upon the differences in surface energies of the adhesive, the substrate, and the roughness of the surface.

It has long been known that surface roughness affects wettability. On a rough surface, an adhesive with sufficiently small interfacial tension will energetically favor wetting the surface and so the liquid will be wicked into the recesses of the topography to minimize liquid-air contact as described by Wenzel [65]. However, an uncured adhesive with sufficiently large interfacial tension will not wet the surface readily and will instead rest upon a composite surface of solid and air as described by Cassie [66-69]. By increasing substrate roughness, one can change the wettability of the substrate such that an adhesive will not wet the recesses of the topography. This will decrease the effective contact area of the adhesive and thus minimize the strength of adhesion.

This analysis accounts for bioadhesion and foul release, but does not account for the observed effect of topography on settlement. It is hypothesized that each of the many marine organisms represented in marine biofouling may have a different mechanism of surface recognition, and this process is not completely understood. It is known that the settlement of *Ulva* zoospores is driven by a complicated set of cues including thigmotactic (texture), phototactic (light), and chemotactic (chemical) cues [70]. The zoospore settlement is enhanced in topographic features on or above the average dimension of the spore body (~5 μm), but is greatly reduced for bioengineered topographies less than half the spore body. At short durations, there was a significant reduction in *Balanus improvisus* accumulation on textured panels with a PDMS elastomeric coating as compared to smooth [61]. Hills and Thomason have shown that the topographical features of naturally occurring structures influence fouling in

marine environments [11]. Surface features are also known to play a significant role in the way that living cells interact with substrates, an effect known as contact guidance [50, 71-79].

Many naturally occurring organisms use their inherent topographical features to manipulate surface energy and prevent fouling. This is evident in sharkskin, the lotus leaf, and even found in the turbulent flow areas of the heart [80-82]. Such biomimetic surfaces have been shown to exhibit substantial drag reduction, as shown in the research by Bechert [80, 81]. As such, it is necessary to investigate topography as a factor affecting biological settlement as well as release.

The research presented in this dissertation is the modification of a silicone elastomer to evaluate the factors discussed in this introduction: topography, elastic modulus, and surface chemistry. Topographic features can be introduced in the elastomer surface by curing it against an etched wafer. Modulus modification can be achieved by addition of additive that can either act as plasticizers or directly alter the network structure of the elastomer by increasing or decreasing the crosslink density. Finally, a change in surface chemistry/energy can be achieved by the introduction of surface graft copolymers. Three polymers were selected to graft to the surface of the silicone elastomer. The justification for their inclusion and their relevance to biofouling research will be discussed in the next chapter. Justification of the silicone elastomer, Silastic T2®, as the starting polymer system will also be described.

CHAPTER 2
JUSTIFICATION OF POLYMER SELECTION

Polydimethylsiloxane

As briefly discussed in chapter 1, silicones are frequently used as foul release (FR) agents. The research on silicones for minimally fouling and foul release substrates is extensive [5, 7, 10, 48, 57, 60, 62, 63, 83-114]. Researchers have analyzed silicones for bulk additives-oils and biocides, modulus modifiers, copolymers, surface texture, and surface modification.

Silicone Nomenclature and Background

Silicone is the generic name for the class of polymers containing alternate silicon and oxygen atoms, as $(\text{-Si-O-Si-O-})_n$ whose properties are determined by the organic groups attached to the silicon atoms. The Si—O bond is known as siloxane bone and thus a more accurate, though less widely used, name for these polymers is polysiloxanes. A variety of polysiloxanes can be synthesized, but the most common is polydimethylsiloxane (PDMS) in which each silicon atom is directly bonded to two methyl groups. Other common groups that may replace the methyl groups on a siloxane repeat unit can include, for example, other alky groups, hydrogen, phenyl, hydroxyl, and vinyl groups. The polysiloxanes endgroups can also be varied to impart reactivity or inertness to the polymer as desired. The endgroups encountered in this dissertation include trimethylsiloxy (TMS), vinyl, hydrogen, silanol, and acetoxy groups.

The presence of these reactive groups in the polymer backbone and polymer endgroups allow for the creation of an elastomeric network by introducing chemical crosslinks between the polysiloxane chains. Crosslinking the linear polysiloxane chains results in the formation of a three-dimensional elastomeric network. Siloxane based elastomers have often also been described simply as silicone, a generic term that permeates and obfuscates the literature, as the exact conditions of network formation are rarely described. These elastomers will have unique physical, chemical, and mechanical properties based on the conditions of network formation. The structure and resultant properties of the elastomers will depend on the nature of the starting polysiloxanes, specifically the number, position, and chemical nature of the reactive organofunctional groups.

Silicone elastomers are often produced from linear polydimethylsiloxanes (PDMS) and should therefore be called polydimethylsiloxane elastomers (PDMSe). The elastomeric network is produced by crosslinking the linear PDMS via either an addition reaction or a condensation reaction.

Condensation cured silicone systems are produced using silanol-terminated polydimethylsiloxanes. One-part systems contain polydimethylsiloxanes with endgroups that are extremely susceptible to hydrolysis to create these silanols at the chain ends. When these end groups are exposed to moisture, a rapid crosslinking reaction takes place. Commonly used endgroups are alkoxy, amine, enoxy, oxime, and the most common acetoxy. In the case of the acetoxy-terminated polymer, acetic acid is produced as a byproduct. The two-part

condensation cured silicones typically have one part that contains linear polydimethylsiloxane with a hydrolysable end group and a second component that contains a multifunctional ethyl silicates crosslinker and a catalyst. In condensation-cured systems, tin compounds are usually employed as that catalyst at a level up to 5000ppm. This group of condensation-cured silicone elastomers includes General Electric's formulation RTV-11® and Dow Corning's formulation RTV-3140®. RTV-3140® is a one-part moisture cured silicone and is silica filled. RTV-11® is a two-part condensation cure silicone and is calcium carbonate filled. Both products use tin based catalysts.

Addition cured silicone systems use platinum rather than tin catalysts, and the catalytic amount of platinum needed for the hydrosilylation reaction is much lower (5-10ppm). In addition reaction, also know as the hydrosilylation reaction, no byproducts are produced. This curing reaction proceeds via the reaction between vinyl terminated polydimethylsiloxanes and poly(dimethyl-co-methyhydride)siloxane copolymers. The silicon hydride reacts with the vinyl groups in the presence of a platinum catalyst to produce an ethylene crosslink. Dow Corning's Silastic® elastomers and Sylgard 184® are crosslinked by this reactivity and contain silica fillers.

It should be noted that each of the formulations discussed above contains fillers. The siloxane elastomer networks produced from chemical crosslinking of linear polydimethyl siloxanes are relatively weak and gum-like, regardless of the mechanism used to produce the siloxane network. It is necessary to use fillers to produce elastomers with reasonable mechanical properties. The addition of

silica fillers can increase the tensile strength of a silicone elastomer network by forty times [115]. The mechanical properties of silicone elastomers can be readily modified by adjusting the effective crosslink density via the addition of fillers, reactive siloxane oils, and plasticizers.

Silicone Elastomers and Marine Biofouling Research

The research on silicone elastomers for biofouling control and biomedical applications is ubiquitous. Akzo-Nobel International Paint currently holds the largest market share for marine coatings. This company first patented a silicone-based coating for marine applications in 1975 [43]. According to their website, International Paint currently has two FR products, Intersleek® 425 for high speed coastal vessels which operate at speeds in excess of 30 knots, and Intersleek® 700 for deep sea high activity scheduled vessels e.g. LNG carriers and container ships. Both Intersleek® products have now been well proven over in-service periods in excess of 60 months. Intersleek® is the only silicone based FR coating on the NavSea qualified use for application on US Naval vessels.

Intersleek® literature states that the commercial success of FR coatings has been limited thus far due to the fact that the majority of the world's fleet, i.e. tankers and barges, do not operate at high enough speeds, and do not have sufficient activity, for the current FR coatings to perform at their best. However, several other companies have or are developing silicone based FR coatings including Hempel, Sigma Kalon Coatings, Wearlon, MicroPhase Coatings, and General Electric.

General Electric initiated research into silicone based FR coatings in the mid-eighties and has published several extensive studies on their performance

[93, 104-114]. General Electric's first commercial silicone based nontoxic FR system was a joint venture with Ameron called Exsil2200®. This material was a hydrosilylation cured silicone elastomer with amorphous silica filler adhered to metal with a durable primer coating. Relatively low biofouling, less than forty percent coverage, was reported for panels submerged for two years at some power plant locations and the Miami Marine Research and Testing Facility [105].

Working closely with many of the ONR sponsored researchers, GE has reported on both addition cured PDMSe with a silica filler and a condensation cured PDMSe with a calcium carbonate filler, RTV-11® [104]. Toughening of FR coatings was evaluated through variation of silicone system, crosslink density, filler type and amount, oil incorporation, and biocide and natural product antifoulant incorporation. The type of silicone oil additive was the primary controlling factor in their barnacle adhesion tests, with methylphenyl siloxane oils achieving the lowest adhesion as opposed to dimethyl siloxane oils. Oil incorporation generally resulted in reduced coverage, but percent reduction relative to the oil-free control was site-dependent. Oil addition, regardless of type, had the additional benefit of shifting the failure mechanism from cohesive failure of the silicone coating to adhesive failure at the barnacle adhesive-substrate interface.

General Electric completely shifted their research from their addition cured silicone elastomers to RTV-11® by the late 1990s. This fact was somewhat disappointing since there has not been a full investigation comparing the two directly in the literature. It is known that RTV-11® silicones, condensation cured

with tin catalysts, typically exhibit lower overall fouling than the addition cured Silastic T2® used in this dissertation. However, GE silicones RTV-11® and other condensation-cured silicones have possible problems with lower bulk modulus (due to use of extending rather than reinforcing filler) and with residual tin catalyst. Callow research on tin catalyst has showed that it may actually act as chemoattractant for *Ulva* zoospores [86].

Non-commercial research on filled and non-filled silicone elastomer formulations has yielded information with respect to fundamental adhesive and cohesive failure mechanisms. However, many of these “model coatings” are not appropriate for field assays as they are not compounded with fillers and are extremely weak. Dr. Kendall performed fundamental research on the fracture mechanics associated with the release of an adherend in the 1970s [47]. Dr. Irwin Singer and Dr. Brady at the Naval Research Labs along with Dr. Manoj Chaudhury at Lehigh University have since made significant contributions to the fundamental research on the foul release mechanisms of silicones based on the Johnson Kendall Roberts theory [116-123]. In this research, pseudobarnacles and silicone hemispheres were placed in contact with substrates to evaluate the effects of coating modulus and lubricity on ease of release.

Many other researchers have evaluated the combination of silicone-based FR coatings and topographical modification. Some of the pioneering work in this field was by Gatenholm [57, 61, 62, 84, 124]. He cured silicone elastomers against stainless steel screens of various mesh sizes to impart a regular topography. These topographies resulted in a short-term decrease in barnacle

settlement. It should be noted that these features were quite large, and Gattenholm's mesh produced a woven appearance in the silicone. The Brennan group has made great strides in understanding the importance of the combined effects of topographical scale and geometry in the control of biofouling [63, 97]. The research here described will show that even at the correct species-specific scale, the geometrical pattern of the topography can drastically affect settlement.

Silicone Elastomers and Bioresponse

The impetus of much of the interest in silicones for control of marine biofouling dates back to some fundamental research about the relationship between surface energetics and bioresponse in the 1970s [125, 126]. Baier showed that the attachment of cells from human blood to a substrate was related to the surface energy of that surface in a reproducible fashion. He noted that there was a minimum of attachment for surfaces with γ_{crit} approximately equal to 25-30 dynes/cm (Figure 2-1). He described this as the "biocompatible range" and surfaces with both higher and lower values of γ_{crit} were said to be in the "bioadhesive range."

The substrates he used, in order of increasing surface energy, were Teflon, Vaseline smeared on glass, silicone, cellulose acetate, and acid washed glass. He discovered that all substrates developed a glycoprotein-based conditioning film within minutes of exposure to both blood and natural seawater. The surface energy of the conditioned bioadhesive substrates shifted the initial values of γ_{crit} towards, but not within, the biocompatible range as he defined it.

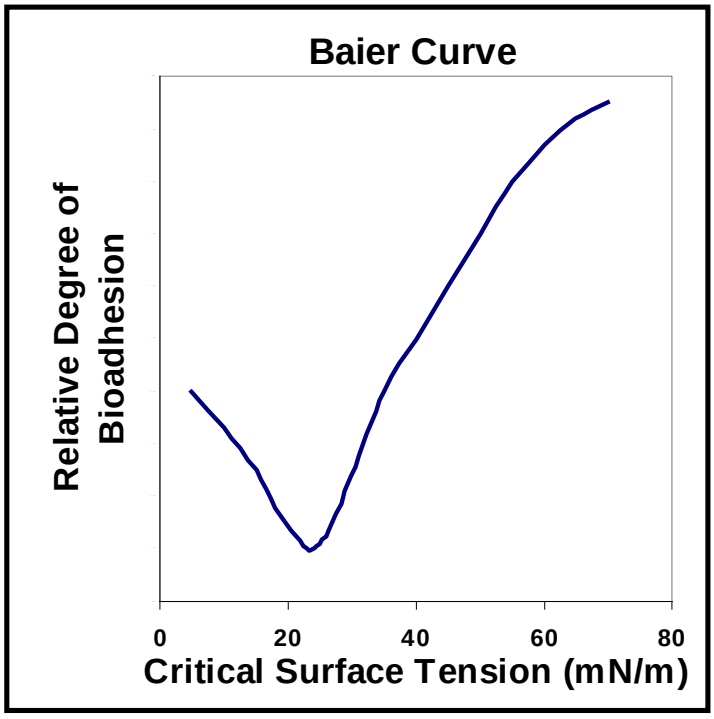

Figure 2-1: Typical Baier curve with generalized term "relative bioadhesion" plotted against substrate surface energy. This trend has been shown to describe behavior across many species.

The extension of Baier's work on the influence of surface chemistry from biomaterials to marine biofouling was first examined by Dexter [127, 128]. He also detected a minimum in marine fouling on polymeric substrates in the range discovered by Baier. He noted that, "since glycoprotein conditioning films have been shown to form on substrates immersed in both seawater and human blood, an influence of critical surface tension on the rate of attachment of microorganisms to substrates immersed in natural seawater should be similar to that observed in blood [127]." By this reasoning, it is important to review the literature for factors affecting bioresponse for both biomedical and biofouling applications.

A series of polymers were selected for this research to surface graft onto PDMSe. The polymers were selected based on their range of surface energies/wettabilities and for their relevance in biofouling applications. The justification for each polymer selection and brief literature review is presented followed by a brief literature review of surface modification of silicone elastomers.

Polymer Surface Grafts

Perfluoropolyether

Fluoropolymers typically exhibit the lowest critical surface tensions of all polymers, <20 dynes/cm. Previous researchers have stated that the surface free energy is probably the most important physico-chemical property of a substratum, because this property results from the molecules available at the surface that are free to interact with other species approaching the surface [14, 129]. The work of adhesion for a substrate/adherend system is typically described as equal to the sum of the surface free energy of the solid substrate and the surface tension of the liquid adhesive minus the interfacial tension between the two.

$$w_{sl} = \gamma_s + \gamma_l - \gamma_{sl} \qquad [7]$$

The weakest adhesive bonds are thus expected for substrates with the lowest surface free energy. Nevertheless, as noted by Baier and others, there is a minima associated with substrates with surface free energies of ~20-25 dynes/cm. These researchers noted the bioadherends actually exhibited higher settlement and adhesion to lower free energy fluorinated substrates, ~18 dynes/cm, than to silicone substrates, ~22 dynes/cm. Thus by about the mid 1990's all research on low energy surfaces for marine fouling research shifted to

focus on silicone elastomers. In these initial studies, no references discussed the effects of bulk modulus or surface roughness on this minimum.

In Baier's work, he states that the minimum is a result of the low interaction parameter between silicones and other "biocompatible" polymers and cites the observation by Johnson, Dettre, and others that the free energy of bulk water is ~22 dynes/cm. However, this observation seems to have been lost from articles that have been published more recently about the Baier minimum. Most researchers have instead focused on the dual low surface energy/low bulk modulus combination of silicones as the reasoning for the minimal bioadhesion.

Brady and Singer published several works on the interrelationship between surface energy and bulk modulus on bioadhesion. Brady observed relative bioadhesion on a series of polymers to further evaluate the Baier phenomenon. He evaluated bioadhesion (bioadherend was not disclosed) for a series of polymers poly(hexafluoropropylene), Teflon, silicone, poly(vinylidene fluoride), polyethylene, polystyrene, and polymethyl methacrylate. He observed the familiar Baier curve (Figure 2-2A), but noted that for the materials that they tested the bulk modulus varied in a similar manner when plotted against the surface energy, known as the Brady curve (Figure 2-2B).

Thus for these samples, the modulus of the material was dominating the effect of surface energy on bioadhesion. A linear relationship for relative bioadhesion with respect to the square root of surface energy times bulk modulus was observed, as expected based on the theories of fracture mechanics described in chapter 1 (Figure 2-2C). This finding supported the theory that it

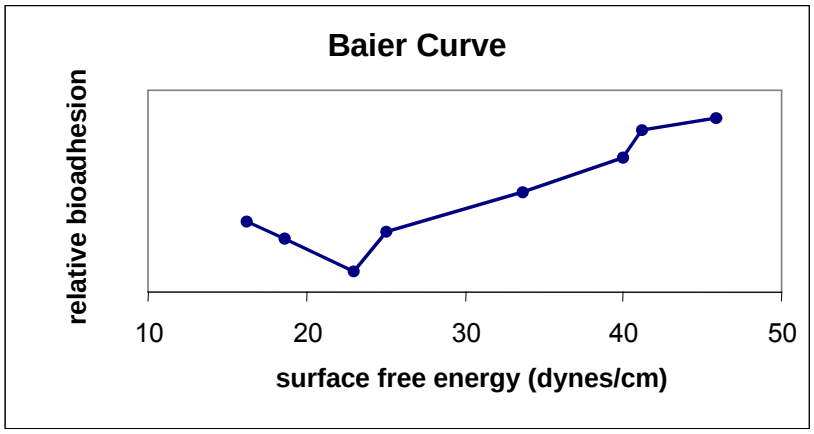

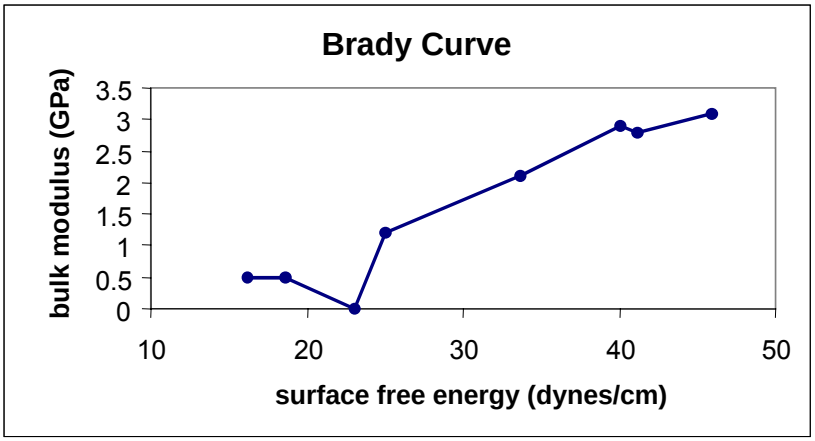

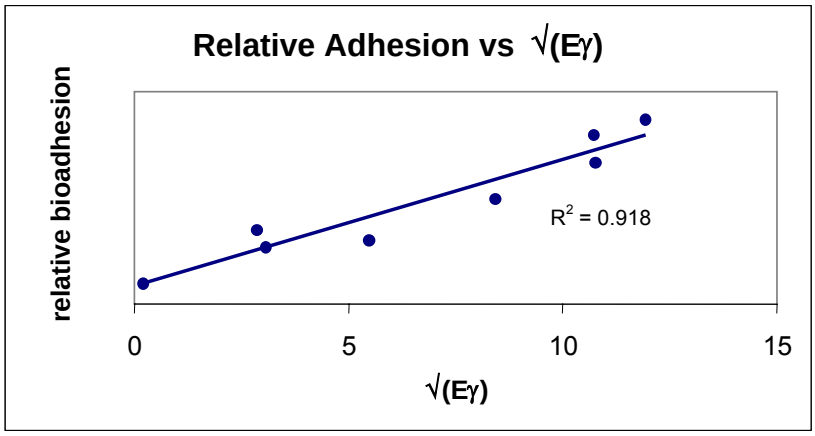

	Relative Bioadhesion	Surface Energy (dynes/cm)	Bulk Modulus (GPa)	√(Eγ) √(GPa *dynes/cm))
PHFP	21	16.2	0.5	2.85
PTFE	16	18.6	0.5	3.05
PDMS	6	23	0.002	0.21
PVDF	18	25	1.2	5.48
PE	30	33.7	2.1	8.41
PS	40	40	2.9	10.77
PMMA	48	41.2	2.8	10.74
Nylon 66	52	45.9	3.1	11.93

Figure 2-2: Data replotted from Brady [5]: Empirical data for Baier and Brady curve and depiction of the linear relationship between bioadhesion and $\sqrt{(E\gamma)}$

was the dual low surface energy/low bulk modulus combination of silicones as the reasoning for the minimal bioadhesion.

Based on these insights of Brady, researchers have once again shifted their focus back to fluoropolymers, more specifically fluoroelastomers with low bulk moduli values. The DeSimone group has produced fluoroelastomers using hydroxyl-terminated perfluoropolyether as a crosslinking reagent in an isocyanato-based polyurethane reaction. These fluoroelastomers have a bulk modulus of 3MPa and a surface energy of 18 dyne/cm and have been produced with topographies generated by the Brennan research group [130]. This elastomer was capable of reproducing our micropatterns to the same if not higher fidelity. Assays were performed on elastomer with respect to settlement and release of the *Ulva* zoospore and performed similarly to PDMSe. This polymer was therefore chosen as one of the polymers to evaluate surface chemistry versus bulk chemistry.

For this research, perfluoropolyether, PFPE (Figure 2-3) was surface grafted to Silastic T2® silicone elastomer. This modification of the substrate would allow for direct comparison of a lower surface energy substrate with a known silicone FR material without significantly altering the inherent low bulk modulus of the PDMSe to investigate the Baier minimum independently of the change in bulk moduli.

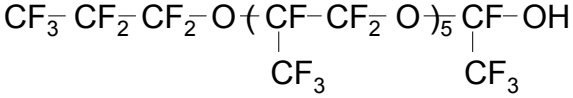

Figure 2-3: Chemical structure of perfluoropolyether studied

Polyethersulfone

Polysulfone, PSf, was selected as a substrate with moderate wettability. Poly (arylene ether sulfones), or polysulfones, are a unique class of engineering thermoplastics with many favorable attributes including high ductility, durability, thermal, hydrolytic and dimensional stability [131-139]. Poly (arylene ether sulfones) are typically amorphous, transparent, tough thermoplastic materials with relatively high modulus and glass transition temperatures in the range of 180–250°C, depending on the structure of the backbone [138]. Common backbone features of polyether sulfones include rigid aromatic groups connected by flexible ether and sulfone linkages. Some typical applications include medical and food service equipment, which may require repeated exposure to heat and steam for sterilization purposes, in electrical wire coatings due their low dielectric constant and in a myriad of membrane applications. Bisphenol-A polysulfone is the most common and economical poly (arylene ether sulfone), and is sold under the trade name UDEL (shown in Figure 2-4).

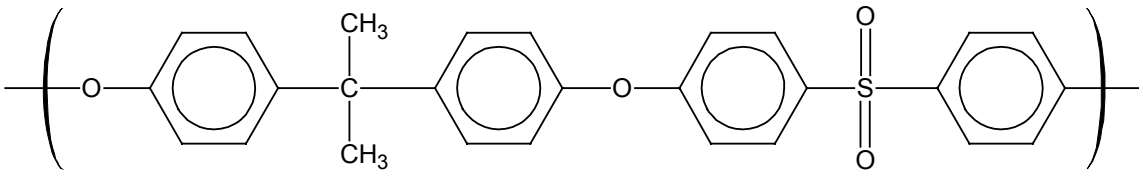

Figure 2-4: Chemical structure of repeat unit of Udel polysulfone

Chemical modification such as sulfonation (Figure 2-5) and chloromethylation provides specific chemical groups along the backbone that make these materials useful as membranes, both proton exchange and ultrafiltration. Sulfonation is powerful and versatile tool for polymer modification

[138]. Noshay and Robeson post-sulfonationed Udel polysulfone with a 2:1 ratio of SO3/triethyl phosphate. This treatment was found to increase the water sorptive properties of the polymer. Effects included an increase in T_g and a decrease in modulus, due to plasticization. This sulfonation also increases the water permeability of polysulfone membranes.

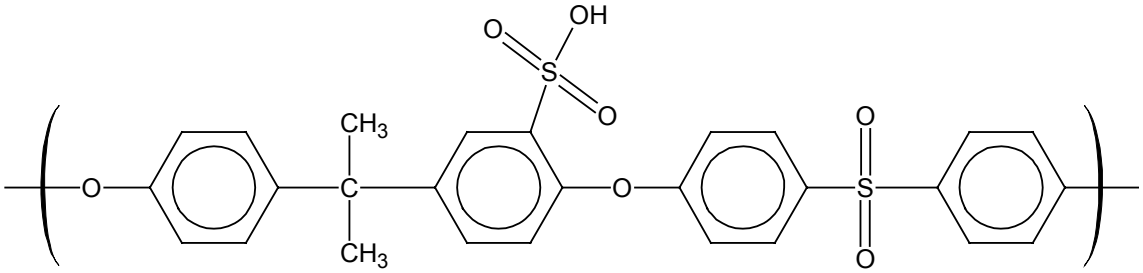

Figure 2-5: Chemical structure of repeat unit of sulfonated polysulfone (based on Udel)

Sulfonated polymers have been utilized as anti-fouling membranes for ultrafiltration for many years. For clarification, filtration refers to the removal of particles, whereas, ultrafiltration refers to the separation of macromolecules, including proteins. Ultrafiltration membranes are used in a variety of applications including desalination, dialysis, cell harvesting, water and sewage treatment, etc. Research in the characterization and reduction of membrane fouling is extensive. Fouling of membranes increases resistance to flow, thus decreasing efficiency. In membrane research, fouling is segregated into various categories: scaling is the deposition and adherence of inorganic matter; organic fouling is the deposition and adherence of organic substances; and biofouling is the adsorption and growth of microorganisms.

Extensive research exists for each subcategory, but only research on membrane biofouling will be here addressed. To fully understand and combat

membrane biofouling, one must take into account the microorganisms, the liquid, and the membrane surface. According to a microbiological approach to membrane biofouling, the process can be divided into four distinct phases [140]. The first stage is the adsorption of macromolecules resulting in a conditioning film. This same conditioning step occurs in marine and biomaterial fouling. The second stage is the primary adhesion by fast adhering cells. This is followed by the colonization and growth of bacteria with subsequent adhesion of a number of different species. These species secrete extracellular polymers (slime) and result in the development of a biofilm. This biofilm is resistant to cleaning and sanitization with chlorine and leads to irreversible blockage of the membrane.

Sulfonated polysulfones are used in these membranes based on their ability to preclude the initial adhesion of microorganisms. One conjecture is that the high affinity for water of the sulfate or sulfonate group increased the hydrophilicity of the surface, thus preventing actual adherence to the membrane itself.

There has been limited research in coatings for marine biofouling control. The reason that PSf was originally included in this study was the ability to modify the chemical structure, especially via sulfonation. This modification was the original impetus for the proposed research. A natural product antifoulant, zosteric acid, derives its antifouling nature from a similar sulfonate group. Much research has been conducted on the potential antifouling and fungicidal effects of zosteric acid, a derivative of eelgrass [104, 141-143].

Zosteric acid (Figure 2-6) is a sulfonated form of cinnimic acid, which has shown potential as a non-toxic fungal inhibitor in species as diverse as *Ulva* and

strawberries. It is reported that the sulfonic acid ester portion of the molecule was required for antifouling activity. In addition to increasing hydrophilicity, some have hypothesized that the zosteric acid may complex with the spore adhesive, thereby reducing its functionality. It was also proposed that since the sulfonic acid group held water so closely that other organisms could not find a suitable surface for attachment.

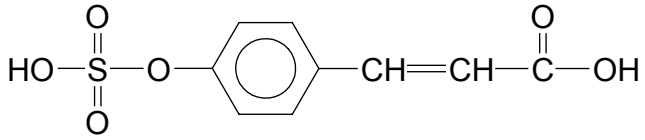

Figure 2-6: Chemical structure of natural product antifoulant, zosteric acid, that is derived from eelgrass

This surface complexation with water has prompted a number of researchers to hypothesize that an ultra-hydrophilic surface may be just as effective in inhibiting biofouling as a hydrophobic surface. This theory has suggested that there may be a downward turn in the Baier curve for substrates more hydrophilic than those previously studied.

It was originally intended that similar surface modifications would be produced on both silicone and polysulfone to probe the combined effects of surface energy, topography, and bulk modulus on bioresponse. The required processing of the modified polysulfones did not allow for the production of substrates suitable for *Ulva* bioassays. The films produced were wavy and lacked transparency due to solvent casting techniques. However, it was still possible to utilize the polysulfone for surface grafting onto the silicone elastomers either through the sulfonated polysulfone species or through end-modified polysulfone.

Polyethylene glycol

Polyethylene glycol and polyethylene oxide are highly hydrophilic polymers that have been extensively researched for their effects on bioresponse. The most research has been conducted on blood compatibility [144-152] and protein adsorption [145, 149, 152-162], but additional research has evaluated bacterial response and marine biofouling [163, 164].

Polyethylene oxide (PEO) is a semi-crystalline, water soluble, thermoplastic polymer with the general chemical formula shown in Figure 2-7. This polymer is commercially available in wide range of molecular weights. Low molecular weight PEO is known as polyethylene glycol (PEG). PEG and PEO are widely known to be highly resistance to protein adsorption. Several theories have been suggested to account for this effect.

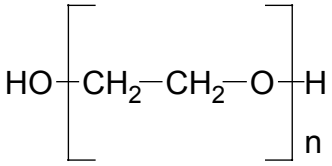

Figure 2-7: Chemical formula of poly(ethylene glycol)

As discussed previously, proteins typically adsorb onto hydrophobic substrates to a greater degree than hydrophilic substrates. The initial theories were based on the low *interfacial free energy* with water, as opposed to the low *surface free energy* encountered with silicones and fluoropolymers. The basic concept is that as the interfacial free energy approaches zero, the driving force for protein adsorption decreases. PEG modified, or PEG-ylated, surfaces are thus considered to be minimally fouling and researchers are currently trying to exploit this property for foul resistant coatings in the marine biofouling industry.

Researchers have investigated many means of PEG-ylating surfaces. Early research involved simple phys-adsorption of the long chain PEO molecules [147]. These surfaces were, however, not very stable, so methods of covalently bonding PEG and PEO were investigated.

Direct coupling methods utilize PEO molecules that have first been derivatized using a reactive coupling agent. End-groups of PEO were derivatized with carboxyl [165], isocyanate [166-169], and silane [154-156, 170] functional groups that were then reacted with specific reactive substrates. Direct coupling requires that the surface have chemically active functional groups that can react with PEO derivatives. This limits the technique unless the substrate itself can be modified to possess the necessary functional groups. In the research presented in this dissertation, PEG-silane is grafted onto a hydrolyzed silicone elastomer.

The Wooley group has recently proposed the use of amphiphillic and highly branched star copolymers based on siloxane, polyethylene glycol, and fluorinated segments [163, 164]. The theory set forward was that utilizing polymers at both end of the hydrophobicity/hydrophilicity spectrum could produce a better minimally fouling substrate by combating both protein adsorption and higher organisms in the biofouling cascade. Additionally, this material may be able to utilize the minimally fouling PEG properties and the foul-release or minimally adhesive properties of low energy surfaces. Initial research with *Ulva* zoospores has been promising, but this is a very expensive polymer system.

As described in this brief review of the literature, the four polymers proposed for this research, PFPE, PSf, and PEG are representative of polymers

used in biofouling research and represent a wide range of wettability. The surface grafting of these polymers onto a silicone elastomer allows for the evaluation of surface energy with fixed low modulus. The additional micropatterning of these substrates allows for the evaluation of the combined effects of surface chemistry and topography.

Modification of Silicone Elastomers

As described above, PDMSe was chosen for this research because it is a low surface energy, low modulus materials with known foul release properties. It was also selected because PDMSe is readily modifiable. Both bulk and surface properties can be addressed. Some techniques described in the literature will affect both the surface and bulk properties, and some techniques allow for the selective alteration of either the bulk or surface.

Bulk modification of silicone elastomers

The crosslink density can be readily altered by changing the number and position of reactive functional groups along the polysiloxane starting material. The PDMSe used in this dissertation is a commercially formulated two-part hydrosilylation cured elastomer with compounded with fumed silica filler. Such formulations may be altered by adjusting the stoichiometric ratio of the reactive compounds. This can be achieved by adding additional reactive compounds [171] or by simply altering the amount of crosslinker added [100]. Gray et al., varied the moduli of a hydrosilylation cured PDMSe by decreasing the amount of the vinyl terminated PDMS and keeping the hydride crosslinker level constant. They found a statistically significant correlation between the modulus and barnacle settlement. This study however ignores the fact that unreacted

crosslinker may affect the surface properties of the elastomer, especially underwater. No surface characterization was reported. The Brennan group has evaluated the addition of vinyl functional polymers of various chain lengths [171]. In the Brennan group studies, additional crosslinker was added to keep the stoichiometric ratio constant. Silicone elastomer formulations can also be altered by appropriate use of filler. Filler size, composition, concentration, and surface treatment are all important factors in determining the mechanical properties of the cured elastomer [108]. Often fumed silica fillers are surface treated with coupling agents that can increase the effective crosslink density of the silicone elastomer network. Other filler choices, such as calcium carbonate do not increase the crosslink density.

In recent years, considerable research has focused on the production of silicone interpenetrating polymer networks (IPN). These materials are produced by swelling a silicone elastomer with a solution containing a second reactive monomer. This monomer becomes trapped in the silicone elastomer network and is then polymerized forming a highly complicated network of two polymers. Several of these IPN systems have been produced with silicone elastomers including polyHEMA [172], n-vinyl pryrrolidone, and polypyrrole [20]. The properties of the resulting materials will depend on the compatibility of the polymer with siloxanes, the processing of the system, and the properties inherent in the secondary polymer. For example, the Brennan group has produced IPNs with conductive polymers as the second phase. The surface and bulk properties of this system could be altered by the application of a voltage [20].

Surface modifications of silicone elastomers

The surface of PDMS elastomers are comprised of closely packed methyl groups, and are thus, relatively chemically inert. The surface must be activated in order to selectively modify the surface without affecting the bulk properties of the PDMSe. Several methods of rendering a silicone elastomer surface reactive have been described in the literature. Most of these techniques essentially degrade the surface of the silicone elastomer and include etching, oxidation, hydrolysis, amination, peroxidation, etc. These activation techniques can be separated into two broad categories; the so-called dry or energy techniques and the wet chemical techniques.

Further, the surface grafting of polymers can be separated into two categories, namely, the direct coupling of previously synthesized polymers or the graft polymerization of monomers on the substrate. The research on graft polymerization onto silicone substrates is extensive, but as the research presented in this dissertation involves the direct coupling method, literature on graft polymerization will not be discussed in detail. In this dissertation, direct coupling of polymers onto a surface activated with a wet chemical technique will be investigated. This is the first example of direct coupling of a polymer to a silicone elastomer that has been activated with wet chemical hydrolysis. Other direct coupling reactions onto silicones in the literature were achieved via activation of the PDMSe surface with plasma, corona, or pulsed laser exposure. Therefore, these techniques will be briefly reviewed.

Exposure of silicone to various energy sources can dramatically alter the elastomers surface properties. Glow discharge plasma and corona are the two

most common techniques for creating a reactive layer on PDMSe. Other techniques include ultraviolet light, gamma irradiation, and pulsed laser exposure. These methods all work by exposing the elastomer substrate to high-energy species, e.g. electrons, ozone, radicals, and ions. The cumulative effect of these species with PDMS is the formation of a reactive, often oxidized or peroxidized, surface. The chemical composition of these surfaces is highly complex and contains radicals, peroxides, silicon hydrides, carboxylic acids, silanols, and silica-like species. The specific compositions will vary based on the energy source, the duration of exposure, and the environment immediately after exposure to the high-energy source.

Several excellent reviews for plasma modification of polymers exist in the literature [151, 173]. Whilst the exact mechanism of surface treatment by plasma is not fully understood, it is the general consensus of the literature that the process described by Owen is most likely correct [174]. His proposed sequence of events in the oxygen plasma modification of silicones accounts for the chemistries and the subsequent hydrophobic recovery seen in treated silicone elastomers. Generally, a thin glassy silica-like (SiO_x) layer is produced on the surface of the elastomer with much higher oxygen content than seen on unmodified PDMSe or within the bulk of the plasma-treated PDMSe, PT-PDMSe. Researchers have reported this layer to be on the order of nanometers for exposure times less than one minute. As the treatment duration increases, this silica-like layer grows and microcracks begin to form. Almost immediately after exposure to this plasma treatment, silicone elastomers will have a very low water

contact angle, <5°. This hydrophilicity will be maintained if the samples are stored in water, however, upon exposure to air, the treated surface will begin to revert to a hydrophobic surface. This phenomenon is known as hydrophobic recovery and is believed to be related to a series of factors, the most important of which is the migration of free PDMS oils from the bulk through the microcracks to the surface. It is also hypothesized that any silanols on the surface of the treated elastomer will try to reorient into the bulk or re-condense with other silanols to minimize the free energy of the system. Some of the problems associated with plasma treatment of silicones include the hydrophobic recovery, surface roughness from microcracks, and increased surface modulus as compared to the bulk.

The two main schemes for coupling polymers to an activated silicone substrate include hydrosilylation and silanation. Hydrosilylation schemes typically involve plasma activation with hydrogen gas rather than oxygen. This imparts some silicon hydride onto the surface of the silane. This functional group can then react with allyl or vinyl-terminated molecules in the presence of platinum catalyst to produce a covalent linkage [175, 176].

An example of silanation of an activated silicone elastomer was by Chaudhury and Whitesides [116]. In their research, silicone substrates were oxidized by oxygen plasma and subsequently reacted with short chain hydrocarbon and fluorohydrocarbon silane terminated molecules. Many research groups have replicated this scheme with various silane-terminated chains [177-180]. Jo and Park and also Delemarche et al. extended this derivatization

scheme to couple silane terminated polyethylene glycol chains [154, 155]. These studies have all used plasma to activate the surface of the PDMSe.

Wet chemical methods can also be used to activate the PDMSe. Perutz et al. hydrolyzed PDMS elastomers in 0.1M HCl for twelve hours [181]. This group also mentioned that aqueous ammonia could be used to hydrolyze PDMSe, but no experimental data was presented. The acid catalyzed hydrolyzed surface had an advancing water contact angle of 121° ± 2° and a receding water contact angle of 71° ± 2° as compared to 118° ± 2° and 90° ± 2° for the unmodified PDMSe. This hysteresis is related to the ability of the silicone surface to rearrange to minimize the surface free energy. In air, the methyl groups on the silicone backbone will be located at the air-polymer interface. These groups will reorient towards the bulk and expose the surface silanols when the surface is exposed to water. This dramatic hysteresis is not seen in plasma treated PDMSe because the silica-like layer is glassy and minimizes the ability of the chains to reorient. The hydrolyzed substrates in this experiment were produced to evaluate the contact adhesion between two pieces of hydrolyzed silicone elastomer.

A second group conducted a similar study in which the PDMSe substrates were activated by plasma exposure and wet chemical techniques [182]. The wet chemical treatments included boiling the PDMSe in 0.5 M HCl for 10 minutes, soaking the PDMSe in piranha solution for 5 minutes or 30% hydrogen peroxide for 1 hour. They reported that the “contact angle” did not change very much for the wet chemical techniques; so further analyses were not performed. The

method of determining contact angle was not reported nor was the procedure for samples handling. If these samples were stored in air for any duration before testing condensation of the surface silanols leading to complete hydrophobic recovery may have occurred. Also, it may be possible that the surface silanols were merely buried below the surface at the polymer-air interface if the contact angle determination was made by simple sessile drop technique. A third hypothesis is that the duration of treatment was insufficient to create a silanol-rich surface. Another group activated a silicone elastomer surface by soaking in sodium hydroxide solutions (2-10 M) for up to a day, resulting in surface silanols as verified with XPS and Raman spectroscopy [183]. The presence of surface silanols on PDMSe is usually difficult to characterize due to the transient nature and surface rearrangement. Silane functionalized molecules have been used to derivatize the silanols to confirm their existence [184].

Some other methods for producing surface modified silicone elastomers exploit the reactivity of the pre-elastomers. Chaudhury et al. reacted an allyl-terminated perfluoropolyether with the hydride groups present in the PDMS-co-PMHS via hydrosilylation during the curing process [185]. The extremely hydrophobic nature of the PFPE allows it to migrate to the surface. Brook, Sheardown, et al. used a similar scheme to produce PEG modified silicone elastomers [162]. In this study, silane-terminated PEG was co-reacted with the hydroxyl-terminated PDMS used in condensation cured silicone elastomers. A second novel method of preparing PEG modified PDMS elastomers was recently published by the same group [186]. They produced cured PDMS elastomer

substrates and then exposed them to PMHS and triflic acid. A unique property of silicones is that in the presence of an acid catalyst, two different silicone homopolymers can be equilibrated to produce a copolymer. Therefore, exposure of the cured silicone elastomer to the PMHS with an acid catalyst in a non-solvent will allow for the introduction of silicon hydride groups into the elastomer surface. The silicon hydride groups were then available to react via hydrosilylation with an allyl-terminated PEG. This is an exciting study that may lead to increased research in wet chemical methods for silicone elastomer modifications. The research presented in this dissertation is another example of wet chemical modification of a silicone elastomer.

The following chapter will detail the characterization and bulk modifications of a commercially available hydrosilylation cured silicone elastomer. Bulk modifications were achieved by addition of vinyl terminated polydimethylsiloxane polymers to affect the crosslink density and trimethylsiloxy terminated polydimethylsiloxane polymers that act as plasticizers. The bulk modifications were achieved without changing the surface energy of the silicone elastomer. The bulk modifications were subsequently coupled with topographical modifications. Chapter four details the bioresponse of *Ulva* zoospores to that silicone elastomer modified with respect to bulk PDMS additives and topographical features.

Chapter five details the surface activation of the silicone elastomer with KOH and HCl soaks. The substrates hydrolyzed via acid catalysis were then subsequently coupled with polyethylene glycol, polysulfone, or

perfluoropolyether. These surface grafts affect the surface without altering the bulk modulus. The surface modifications were then subsequently coupled with topographical modifications. The surface modified substrates are then assayed for algal bioresponse as described in Chapter six. These substrates are also assayed with diatoms and *Ulva* zoospores with respect to the surface chemistry and topographical features.

CHAPTER 3
SILICONE ELASTOMER CHARACTERIZATION

Introduction

Silicones are an interesting class of polymers known for their unique combination of low surface energy and low bulk modulus. The polyorganosiloxane repeat unit consists of alternating silicon and oxygen atoms with two R groups on each silicon atom, as seen in Figure 3-1. As indicated by its name polydimethylsiloxane has two methyl groups attached to each silicon atom in the repeat structure.

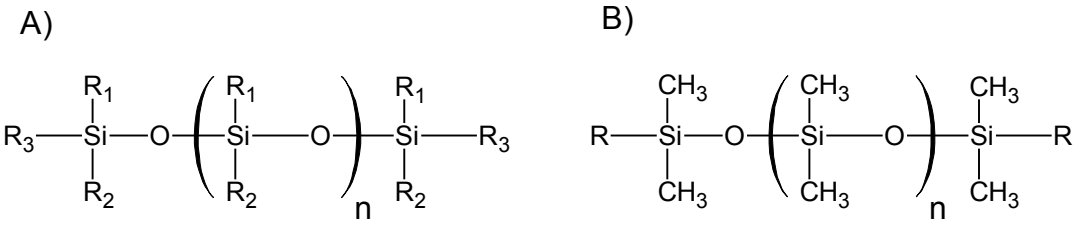

R_1, R_2, R_3, and R = CH_3, H, phenyl, CH_2-CH_3, CH=CH_2

Figure 3-1: Structure of A) general siloxane repeat unit and B) structure of polydimethylsiloxane, PDMS

Polydimethylsiloxane chains exhibit great flexibility due to the low rotational barriers associated with the Si-O bonds, 4kJ/mol as opposed to other polymers for example polyethylene 16kJ/mol [187]. Crosslinked PDMS produces elastomers that are gum-like at room temperature. Crosslinked silicone elastomers often require reinforcing fillers to overcome their poor mechanical

properties. Filled PDMS elastomers (PDMSe) have extremely low T_g and modulus, -127°C and 1MPa, respectively.

The polymer chains are readily able to adapt to the lowest possible energetic conformation. The methyl groups of the PDMS backbone will orient towards the air/polymer interface, effectively burying the more hydrophilic siloxane bonds. The highly hydrophobic nature of the methyl groups renders this polymer one of the most hydrophobic. However, after a short time in water, the molecules can effectively rearrange and reverse this orientation. This leads to a hysteresis in advancing and receding contact angle for PDMSe.

PDMSe are effective foul release coatings both in terms of minimization of fouling and ease of release during cleaning operations. Laboratory contrived and field immersion tests have shown that foul release coatings with critical surface tensions between 20 and 25 mN/m had greatest ease of release [188].

Dow Corning's Silastic T2® PDMSe was selected for this research from the various commercially available silicone elastomers and is currently under consideration by the Office of Naval Research, as the standard by which all other silicone based foul release coatings will be measured. The basic components of Dow Corning's Silastic T2® resin are listed in Tables 3-1 and 3-2. It is a platinum catalyzed hydrosilylation cures PDMS elastomer that was selected for the following reasons

- Low modulus, 1.3 MPa
- Low critical surface energy, 22.0 dynes/cm
- Low catalyst concentration (5 ppm)
- Optically transparent
- Readily adhered to glass
- Modifiable properties such as chemistry, modulus, and topography

Table 3-1: Silastic T2® base resin (as received from Dow Corning Corporation)

	Component	Structure
Base resin		
	Polydimethyl siloxane, dimethylvinyl terminated	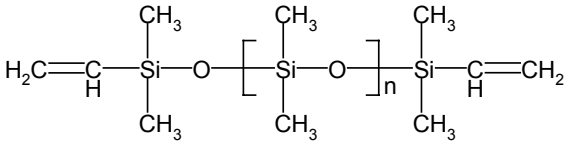
	Dimethyl, methylvinyl siloxane, dimethylvinyl terminated	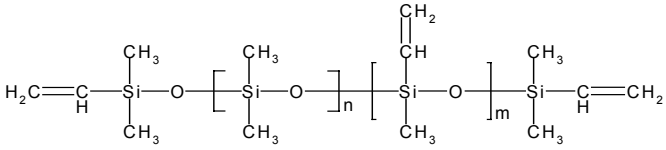
	Surface treated silica	SiO_2, with trimethyl, methyl-vinyl and dimethylvinyl groups on surface.

Table 3-2: Silastic T2® curing agent (as received from Dow Corning Corporation)

	Component	Structure
Curing agent		
	Polydimethyl siloxane, dimethylvinyl terminated	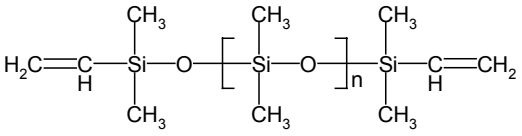
	Dimethyl, methylhydrogen siloxane	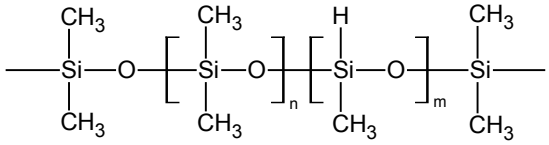
	Tetramethyl, tetravinyl cyclotetrasiloxane	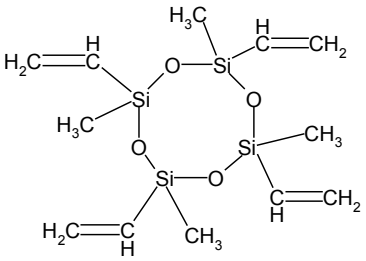
	Surface treated silica	SiO_2, with trimethyl, dimethylvinyl, and methyl-hydrogen groups on surface.

Materials and Methods

Characterization of Silastic T2® Components

Filler extraction and characterization

In order to evaluate the Silastic T2® filler and to obtain pure Silastic® base resin and curing agent for subsequent analyses, the filler had to be removed via extraction. The following procedure was adapted from A. Lee Smith's reference book on the analysis of silicones [189]. Approximately 2g of each Silastic® component was placed into a separate 50ml centrifuge tube. Approximately 20ml of aqueous NH_3 (ammonium hydroxide water solution, <3N NH_4OH) was added followed by 20ml of toluene. The mixture was mixed via vortex mixer until a stable suspension was achieved, typically 1 minute for the curing agent and 10 minutes for the more viscous base resin. The tubes were centrifuged in a Beckman J2 centrifuge at 10,000 rmp for thirty minutes. The siloxane component should become solvated in the toluene layer, and the silica particles separated at the toluene ammonia interface. If this separation was not achieved, centrifugation was repeated and checked at 15-minute intervals. Once the separation was achieved, the toluene/siloxane layer was withdrawn via pipette with care to avoid disturbing the silica layer. The toluene was removed via rotovap to yield unfilled siloxane polymer for further analysis. The silica layer was withdrawn via pipette and placed in an evaporating dish to dry.

Thermal analysis

Thermogravimetic analysis (TGA) on the Silastic® components and cured elastomer was performed using a TG/DTA 320 Seiko apparatus. Approximately

12 mg of the sample and an alumina reference were heated from 30 to 1000 °C at a rate of 10 °C/min under air or argon.

Scanning electron microscopy (SEM)

The filler extracted from the Silastic® components and the residual filler from thermal analysis were analyzed by SEM. The silica was placed onto a piece of double-sided tape on an aluminum SEM stub using a laboratory spatula. The mounted samples was then coated with Au/Pd for 3 minutes and imaged on a Jeol 6400 SEM equipped with an Oxford ISIS image capture system.

Characterization of Silastic T2® Components:

Hydride-Vinyl Stoichiometry

In order to determine the stoichiometric ratio of the vinyl to hydride in the Silastic T2® base resin and curing agent, several tests for functionality were performed.

Fourier transform infrared spectroscopy (FTIR)

Transmission Fourier-transform infrared (FTIR) spectroscopy was performed with a Nicolet 20SX spectrometer using 64 scans at a 4 cm^{-1} resolution. A background spectrum was taken before each sample for subtraction.

Iodometric titration (Wij's test)

Iodometric titration was performed to quantify the percent vinyl content of the Silastic T2® components [189]. Wij's solution, a 0.22 N solution of iodine monochloride in glacial acetic acid, was purchased from Fisher Scientific and used as received.

To perform this test, approximately 0.5 grams of the Silastic T2® base and curing agent as well as several vinyl terminated polydimethylsiloxane polymers were each dissolved in 20ml of chloroform in individual Erlenmeyer flasks. 20ml of chloroform was also added to an empty flask as a blank for the titration. 25 mL of the Wij's solution was pipetted into each of the flasks, which were subsequently placed in the dark for one hour. After 1 hour, the samples were titrated with a 0.1 N sodium thiosulfate solution using ~2 mL of 10g/L starch solution as an indicator. Percent vinyl content was calculated by standardizing the titrations with the vinyl-terminated polydimethylsiloxane oils obtained from Gelest, Inc.

Nuclear magnetic resonance spectroscopy (NMR)

Approximately 25mg of each unfilled Silastic T2® base resin and curing agent were dissolved in 0.5ml of deuterated chloroform and injected into 5mm NMR tubes through 0.2 μm PTFE syringe filters. Proton nuclear magnetic resonance (1H NMR) 200 MHz spectra were obtained with a Varian XL-Series NMR superconducting spectrometer system at the UF Brain Institute with the assistance of Dr. Jim Rocca. Tetramethyl silane was used as an internal reference material.

Molecular Weight Determinations

Gel permeation chromatography (GPC) was used to determine molecular weight. The pure polymer was dissolved in toluene to a concentration of 30mg/ml and tested on GPC with light scattering. Several silicone oils of known molecular weight were also evaluated under the same conditions. Monodisperse

polystyrene was used for calibration. The experiments were performed with GPC combined with multi-angle light scattering (MALS) was performed to measure the molecular weight of the Silastic® components. Experiments were performed using an 18 angle Wyatt Dawn EOS™ MALS detector and a Waters 600E system controller equipped with a Waters 966 Photo Diode Array, a Waters 410 Differential Refractometer, and a Waters 717 autosampler.

Characterization of Silastic T2® PDMS Elastomers

Preparation of silicone elastomer samples

The silicone elastomer was prepared by mixing the Silastic T2® base resin and curing agent in a 10:1 ratio, respectively. The amount of silicone elastomer prepared depended on the sample type and the number of samples to be prepared on a given day. Typically, batches were prepared containing approximately 120 grams of the base resin that was weighed out into a 1000 ml polypropylene tricorner beaker. To this, approximately 12 grams of the curing agent was added. The components were mixed together by hand using a stainless steel scupula for approximately 3-5 minutes, and the mixture was degassed thoroughly in a vacuum chamber for ~15 minutes. The elastomer was typically cured between two smooth glass plates that had been treated with hexamethyldisilazane (HMDS) to minimize adhesion to produce a freestanding film or backed to a glass microscope slide that had been treated with a coupling agent.

Preparation of silicone elastomer coated glass slides

For bioassays and other surface characterization techniques, the silicone elastomer was coated on a glass microscope slide. A coupling agent was

required to maintain proper adherence of the silicone elastomer to a glass substrate. Allyltriethoxysilane coupling agent solution was prepared by addition of 2 drops of glacial acetic acid to 30ml of 90 proof ethanol in a 150 ml polypropylene graduated container. To this acidified ethanol, 0.17ml of allyltriethoxysilane was added. A 10 mm octagonal Teflon coated stir bar was added; the container was capped and placed onto a magnetic stir plate. The ATS solution was allowed to stir for at least 5 minutes, which allowed for the hydrolysis of the silanes.

Meanwhile, a glass microscope slide was cleaned by passing through a very clean Bunsen burner flame. Each slide was grasped using self-closing forceps and passed through the flame four times on each side. The duration of contact with the flame was approximately one second per pass. The slide was then placed onto a kimwipe® on a level surface. The slide was then coated liberally with the ATS solution deposited from a narrow stem polyethylene transfer pipette. The liquid coated slides were left undisturbed for 2-3 minutes to allow for the reaction of the silanes with the glass. The slides were then rinsed on both sides with ethanol squirted from a wash bottle. The slides were placed treated side up on an kimwipe® covered metal tray and oven-dried at ~120°C for at least 20 minutes [190].

The 10:1 mixture of the Silastic T2® components prepared as described above was poured onto ATS-treated glass slides that were placed on a large glass plate. The glass plate was first cleaned with ethanol, inspected for scratches or defects, and treated with hexamethyldisilazane (HMDS). The

HMDS treatment was performed by applying approximately 0.5 ml of HMDS to the glass with a transfer pipette or syringe and wiping over the entire surface with a kimwipe®. A second glass plate treated in the same manner was lowered onto the first. Pressure was applied by hand to assure that the top plate was in contact with each of the four appropriately sized spacers (1700μm) located at the corners of the bottom plate in order to achieve a constant thickness and a smooth surface. The silicone elastomer was allowed to cure either at room temperature or at an elevated temperature.

After the silicone elastomer was cured, the two glass plates were pried apart using a large metal screwdriver as a fulcrum. The silicone coated glass microscope slides were carefully removed from the glass plate using with a small polyethylene wedge and small quantities of ethanol to aid in the removal process. The slides and silicone elastomer were removed as one large sheet of silicone elastomer. The individual silicone elastomer coated glass slides were carefully cut out using a clean razor blade. Any excess silicone elastomer was trimmed from the edges of the glass slides with the razor blade. The silicone elastomer coated glass slides were rinsed with ethanol and visually inspected imperfections on the surface and for adhesion to the glass microscope. The slide thickness was measured using digital calipers and recorded. The silicone coated glass slides were then placed into individually labeled polypropylene bags or 50-ml centrifuge tubes for storage.

Curing conditions

Approximately 1 gram of the Silastic T2® base resin was mixed with ~0.1 grams of the curing agent. The mixture was degassed for less than ten minutes and the uncured mixture was placed on the lower platen of the rheometer. Cure profiles were collected on a Paar Physica parallel plate rheometer model MC200 with 5% strain at 1Hz. The effect of cure temperature on cure of the Silastic T2® elastomer was evaluated by heating the platens of the parallel plate rheometer during measurement. The effect of the addition of vinyl-terminated additives on cure was evaluated by mixing these additives into the base resin prior to the addition of the curing agent. The functional additive cure profile study was performed at 80°C.

Mechanical testing

The bulk mechanical properties of the cured Silastic T2® elastomer were determined via tensile testing. Freestanding films of the silicone elastomer were prepared by mixing the Silastic T2® components in a 70-gram to 7-gram ratio as above. The mixture is degassed and poured onto a 7 in^2 glass plate with 1 mm thick glass microscope slides affixed with double-sided tape in each corner. The glass plate was first cleaned with ethanol, inspected for scratches or defects, and treated with hexamethyldisilazane (HMDS). The HMDS treatment was performed by applying approximately 0.5 ml of HMDS to the glass with a transfer pipette or syringe and wiping over the entire surface with a kimwipe®. A second glass plate treated in the same manner was lowered onto the first. Pressure was applied by hand to assure that the top plate was in contact with each of the four

glass spacers. The silicone elastomer was cured either at room temperature or in a 50° C or 80° C oven. The cured sheet of silicone elastomer was removed from the glass plates post cure and stored between two kimwipes® prior to testing.

Tensile specimens were cut from the cured freestanding silicone elastomer films using an ASTM D1822-68 type L dogbone die. Samples were approximately 1 mm thick with total length of 63.5 mm. Each was individually measured to account for thickness variability in calculations. The grip separation for the samples was set at 25.4 mm and the width of the testing portion was set at 3.1 mm.

Tensile measurements were made according to ASTM D412-97 on an Instron model 1122 equipped with the TestWorks 3.07 software for analysis. Seven replicate dogbone specimens were tested per sample set at a rate of 2 inch/min. Modulus measurements were calculated from the linear portion of the stress-strain plot below 90% strain and compared. The strain was measured with a MTS lx1500 laser extensometer rather than via crosshead displacement to minimize the data distortion due to grip slippage at high strains.

It was necessary to develop spring clamps to affix the requisite retroreflective tape at the gage lengths of the PDMSe dogbones, because the MTS Systems brand retroreflective tape would not stick (Figure 3-2). The spring clamp was fashioned from a small spring removed from a pen. The tape was carefully folded over the first two loops of the spring. The spring was wound tighter at the spring ends. The PDMSe dogbone was grasped at both ends and

placed in the center of the spring. While holding the dogbone stationary, the spring was twisted such that the PDMSe dogbone was repositioned in the tighter coils of the spring near the retroreflective tape. The spring was only tightened until distortion was noted in the PDMSe and then loosened one-half twist. This allowed for attachment of the extensometer laser targets without inducing stress raisers in the tensile testing of the elastomer.

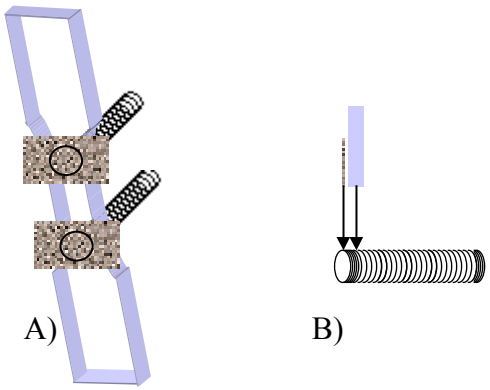

Figure 3-2: A) Schematic of spring clamps on a dogbone affixing retroreflective tape. B) The retroreflective tape was place under the first loop of a 4 mm wide, 30 mm long spring. The silicone elastomer was placed several loops behind the tape.

Surface energy and contact angle determination

Initial studies of the surface energy on the PDMSe formulations were evaluated using sessile drop contact angles obtained on a digital contact angle apparatus created in-house by the Brennan group (Figure 3-3). Five drops each of nanopure water, n-propanol, methylene iodide, acetonitrile, and dimethylformamide were measured for each sample set with two replicate specimens per set. Each drop was approximately 2 µL and was dispensed from a 20 µL syringe. An image of each drop was acquired with a digital camera, and the contact angle, θ, of the drop on the surface was analyzed using UTHSCSA

ImageTool for Windows version 3.0. An inverse Zisman plot, which relates cos θ and (solvent surface energy)$^{-1/2}$, was prepared for each sample set to determine the surface energy.

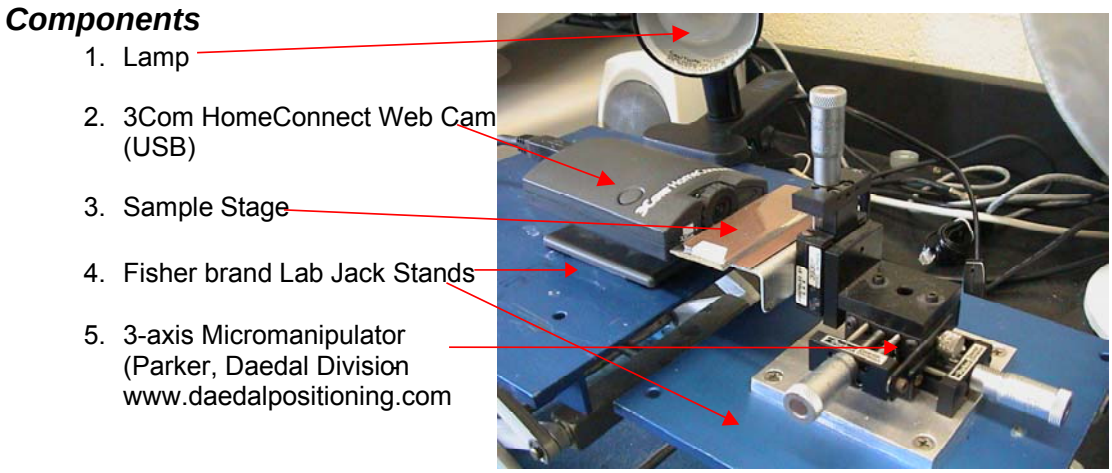

Figure 3-3: Digital contact angle setup

Subsequent studies involving contact angle determination were carried out on a Ramé Hart Model 500 automated goniometer with computerized pump (Figure 3-4). The solvent reservoir was a 200-ml Erlenmeyer flask. One end of the tubing was placed through the parafilm covering this reservoir with the other end connected to a syringe tip just above the sample stage. Tubing from the syringe pump was flushed out each day that samples were tested. Nanopure water filled the tubing when the system was not in use. The tubing was emptied by cycling the syringe pump with the tubing end out of the liquid in the reservoir, but inside the flask as to avoid contamination. The tubing end was then placed into a new reservoir filled with 200 proof ethanol. Ethanol, followed by air, was cycled through the tubing. Meanwhile, the water reservoir was emptied, rinsed with ethanol, rinsed five times with and then filled with fresh nano pure water. The tubing end was placed into the fresh nanopure water reservoir and flushed

with fresh nanopure water, flushed with air, and flushed for third time with nanopure water. The syringe tip was changed and testing for water contact angles was commenced. This cleaning process took approximately thirty minutes. A similar procedure was carried out when solvent was changed. Separate tubing was used for dissimilar, i.e. immiscible, solvent types.

Components

1. Light source with dimmer
2. CCD camera and image acquisition software
3. Precision 3-axis sample stage with fine and course vertical adjustments mounted on 20" base rail
4. Syringe pump

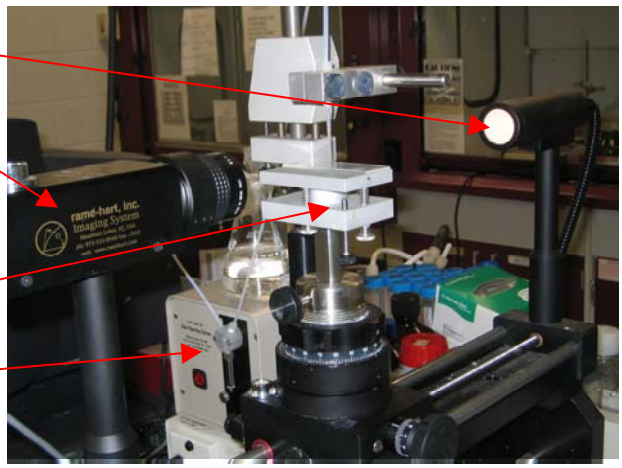

Figure 3-4: Ramé Hart Model 500 automated goniometer

The silicone elastomer coated glass slides were placed onto the sample stage. The stage was leveled, the clean tip was lowered to ~1 mm above the substrate, and the slide and tip were bought into focus. Five drops each of nanopure water, n-propanol, methylene iodide, acetonitrile, and dimethylformamide were measured for each sample set with two replicate specimens per set. Each drop was approximately 5 µL and was dispensed via syringe pump from a polypropylene microliter syringe tip. The syringe tips were replaced with every solvent change or if contaminated by inadvertent contact with a sample. Images were acquired using the Ramé Hart DropImage Advanced software and were later analyzed with software available from FirstTenAngstroms. An inverse Zisman plot, which relates cos θ and (solvent

surface energy)$^{-1/2}$, was prepared for each sample set to determine the surface energy.

Captive air bubble determinations were also carried out in water using the Ramé Hart system with a j-type needle. A polymethylmethacrylate box was constructed using pieces of PMMA sheet joined together with a mixture of PMMA in dichloromethane. The box was approximately 0.5 inches tall, 2.5 inches wide, and 1.25 inches deep. The box was cleaned with ethanol and then rinsed five times with nanopure water. It was then filled with nanopure water, place onto the sample stage, and the silicone elastomer coated glass slide was inverted and placed onto the water filled box. A stainless steel j-type needle was used instead of the polypropylene syringe tip. The end of the syringe pump tubing was located above the liquid in the reservoir, but inside the flask as to avoid contamination. The PMMA box and the j-needle were cleaned with ethanol and repeated rinsing with nanopure water, and the box was re-filled with fresh nanopure water with each sample set. The bubbles deposited onto the substrate were ~8 μl. Smaller bubbles tended to remain on the j-needle. Images were acquired using the Ramé Hart DropImage Advanced software and were later analyzed with software available from FirstTenAngstroms.

After contact angle images are acquired, the contact angle is measured with software available from FirstTenAngstroms. The baseline is shown in blue and the yellow lines show the fit to the sessile drop for the contact angle measurements for a water drop on PDMSe (Figure 3-5). For sessile drops with

contact angles less than 90°, the spherical fit mode was used, and the non-spherical fit mode was used to measure contact angle greater than 90°.

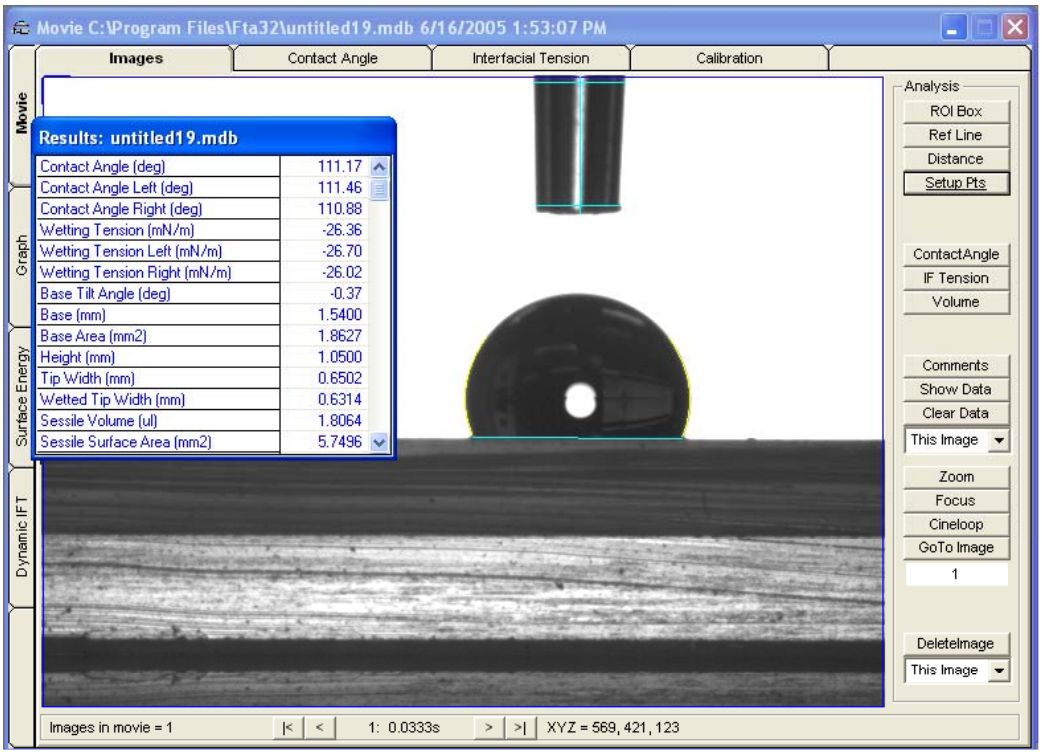

Figure 3-5: FirstTenAngstroms software. Sessile drop measurement of water on PDMSe. Contact angle fit selected is non-spherical, which is required for all drops with greater than 80° contact angles.

Results and Discussion

Filler Extraction and Characterization

Silicone elastomers have very poor tensile strength without the aid of reinforcing filler. The most commonly used reinforcing fillers include carbon black, fumed silica, and in situ precipitated silica [191]. Calcium carbonate is often used in RTV silicones as an extending rather than reinforcing filler. Fumed silica is the reinforcing filler used in Silastic T2®.

Fumed silica is produced by burning silicon tetrachloride ($SiCl_4$) with hydrogen and oxygen at a temperature of about 1000 °C [192]. This technique produces agglomerates of very small silica particles the diameter of which typically vary between approximately 5 to 20 nm. Due to the small particle size, the surface area is enormously high, several hundred square meters per gram silica, producing a very high reinforcing effect.

Filler extraction

A reasonably clean separation of the filler from the Silastic® prepolymers can be achieved with a 1:1 mixture of solvent, such as toluene, and a non-solvent, aqueous NH_3 [189]. As described by A. Lee Smith and others, ammonia disrupts the hydrogen bonding between the siloxane and the silica filler. The siloxane components become solvated in the toluene, which is immiscible with the ammonia. The silica filler becomes separated at the toluene-ammonia interface.

The base resin is considerable more viscous than the curing agent. The silica filler can be separated from the base resin to obtain the unfilled siloxanes. However, some siloxane appears to remain adhered the surface of the silica filler particle in the base resin system. The silica layer separated between the toluene and ammonia appears thick and somewhat gelatinous as compared to the filler layer from the curing agent. Even with repeated washing with the toluene and ammonia, this gelatinous nature is maintained in contrast to the curing agent silica layer that appears white and fluffy at the interface. It is undetermined why the curing agent-filler separation was achieved more readily than the base resin-

filler separation. Several contributing factors are proposed. The base resin is considerably more viscous than the curing agent and contains higher molecular weight polysiloxanes based on GPC data. Based on thermal analysis data, there is more silica filler in the base resin than in the curing agent. The silica fillers in both Silastic® components are surface modified to possess trimethylsilyl and dimethylvinyl groups according to their respective MSDSs. The silica particles in the curing agent were also treated to contain dimethylhydrogen groups.

Thermal analysis

Thermogravimetric analysis (TGA) is a common technique for studying thermal decomposition and for determining the filler content in plastic materials [189, 193]. Approximately 12 mg of each of the Silastic T2® components were thermally degraded by heating from 30 to 1000 °C at a rate of 10 °C/min under air. The major degradation of the high molecular weight vinyl terminated polydimethylsiloxane polymers present in both the base and curing agent occurred at approximately 500°C. The thermogram also clearly demonstrated the degradation of the lower molar mass PDMS-co-PMHS present only in the curing agent at a lower temperature (Figure 3-6). The mass of the residual white ash was used to estimate the % silica filler content [189, 193].

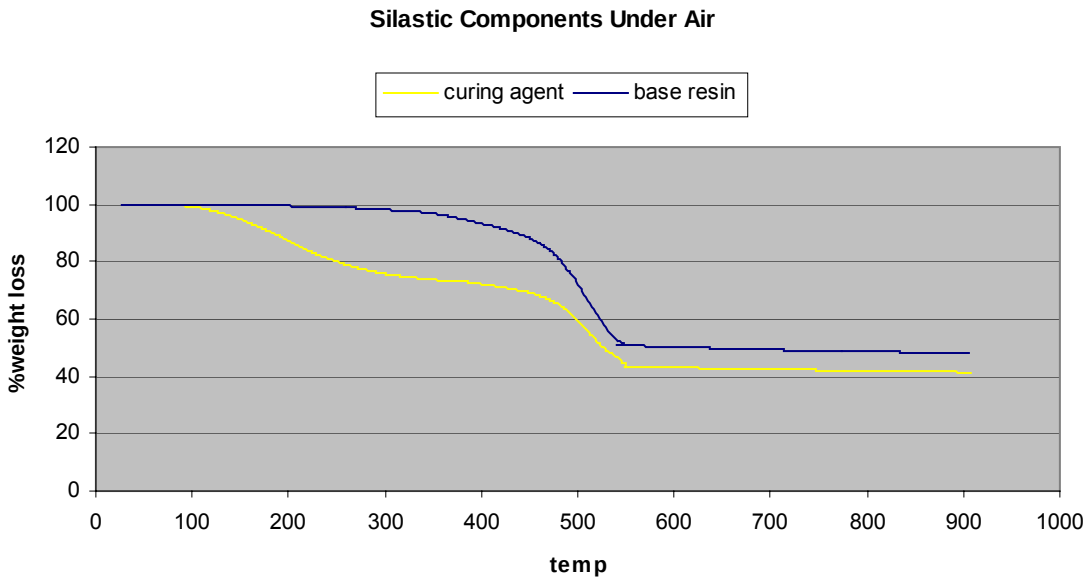

Figure 3-6: TGA data for Silastic T2® base (blue) and curing agent (yellow). ~12 mg of the sample and an alumina reference were heated from 30 to 1000 °C at a rate of 10 °C/min under air.

From this analysis, the filler content was estimated at 48% ± 6% and 41% ± 4% for the base resin and curing agent respectively. Degradation of filled silicone polymers in air typically results in a high estimation of the filler content, because the silicone that is directly bonded to the silica filler typically chars resulting in some silicon carbides and other non-silica species. The test was repeated in an inert atmosphere and resulted in similar silica content for the base resin (47% ± 7%) but a much lower content for the curing agent (18% ± 3%) as seen in Figure 3-7. It appears that a similar weight loss was detected for the low molar mass hydride based siloxanes, but significantly more of the high molar mass siloxane was detected.

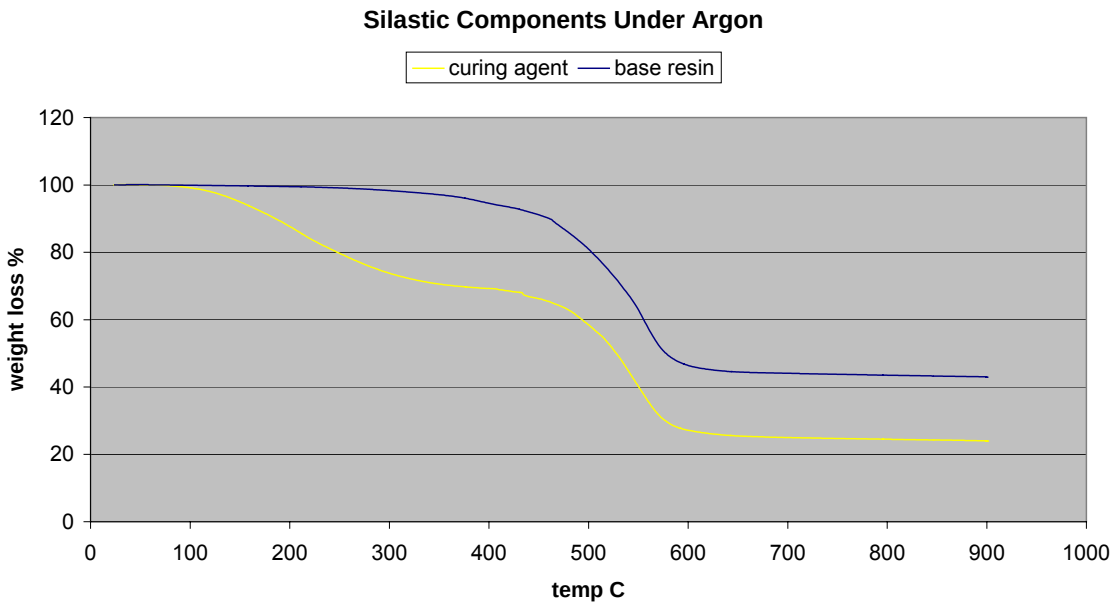

Figure 3-7: TGA results for Silastic T2® base (blue) and curing agent (yellow) degraded under argon. ~12 mg of the sample and an alumina reference were heated from 30 to 1000 °C at a rate of 10 °C/min under argon atmosphere.

SEM was utilized to further characterize the silica fillers obtained from these degradation experiments. The filler looked similar for the thermally degraded base resin samples regardless of degradation atmosphere. This was not unexpected as there was no statistical difference in the residual mass values obtained for the base resin degraded in air or argon. The curing agent that was degraded under argon yielded far less sample than that degraded under air as also detected by the difference in residual mass reported (18% and 41% respectively). The representative image shows the relative abundance (Figure 3-8). For all images, the silica pieces are considerably larger than expected.

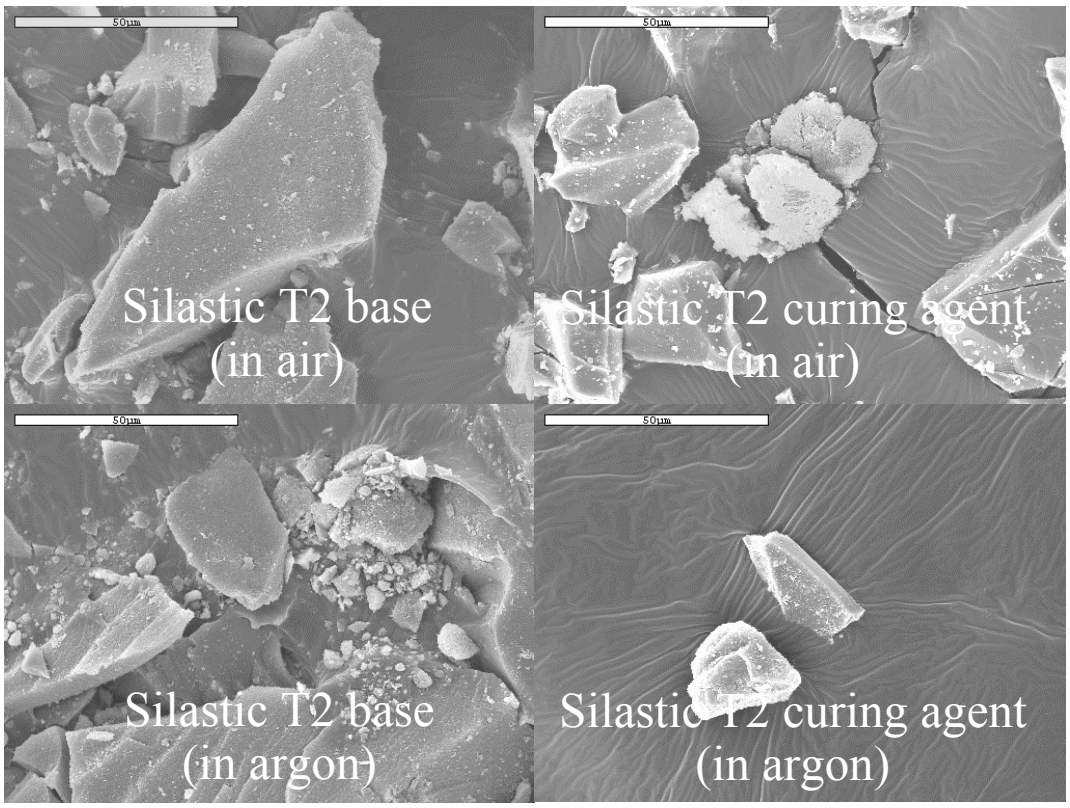

Figure 3-8: SEM of residual silica filler after thermal degradation in air and argon. Scale bar is 50μm.

SEM was also performed on the filler obtained from the filler extraction experiment. Since this method releases the hydrogen bonded PDMS from the silica filler, the particles obtained were much finer upon visual inspection of the micrographs (Figure 3-9).

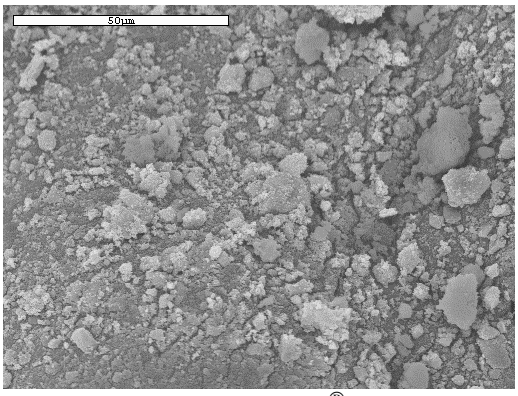

Figure 3-9: SEM of silica filler from Silastic T2® curing agent obtained from filler extraction method. Scale bar is 50μm.

An approximately 12mg piece of the cured Silastic T2® PDMSe was also evaluated using this thermal analysis technique under argon (Figure 3-10). The residual mass after degradation of the silicone elastomer was 42%. This is consistent with the findings from the two components, which yielded 47% and 18% residual mass when degraded under argon.

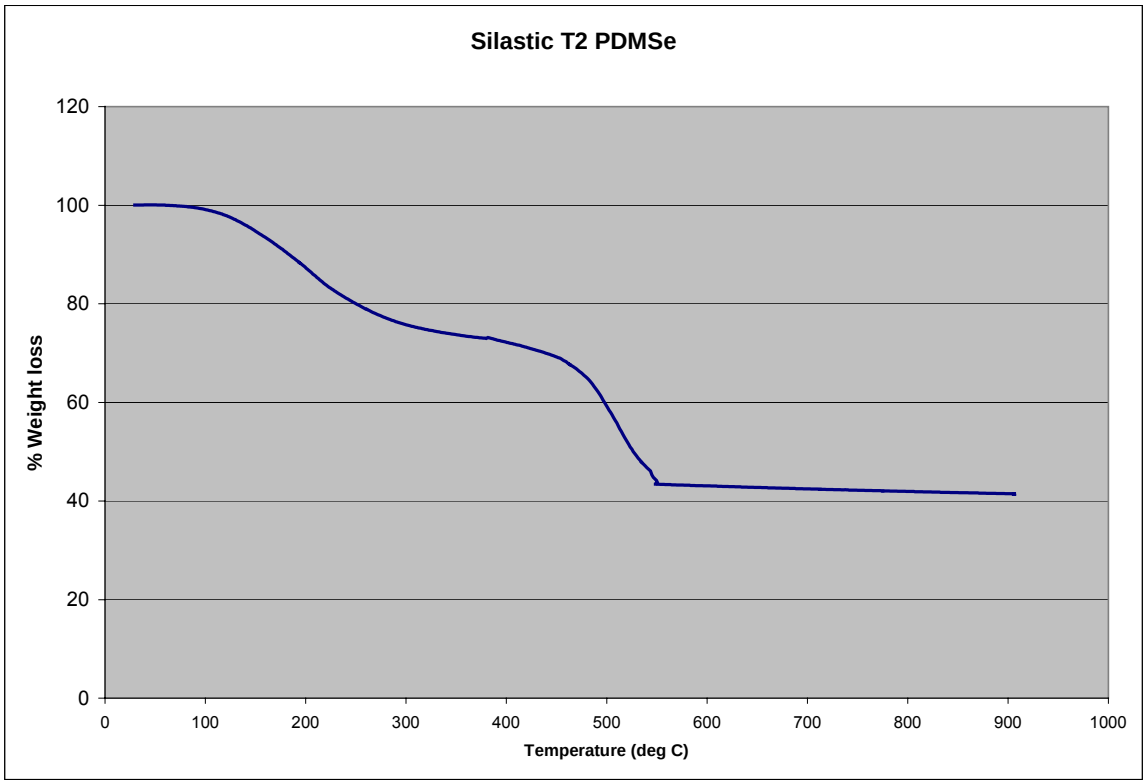

Figure 3-10: TG/DTA data from the thermal degradation of Silastic T2® silicone elastomer under argon. ~12 mg of the sample and an alumina reference were heated from 30 to 1000 °C at a rate of 10 °C/min under argon atmosphere.

Hydride-Vinyl Stoichiometry

Quantification of the hydride vinyl ratio allows for a deeper understanding of the curing process. As shown in Figure 3-11, these two structures are responsible for the formation of the ethylene crosslinking bond. The vinyl groups are found both in chain ends and along the chain backbone in both the base

resin and the curing agent components. The hydride functionality is present as a poly(dimethyl-co-methyl hydride siloxane) in the crosslinking agent and is found in stoichiometric excess to the vinyl. It is presumed that all the vinyl groups will be reacted with the degree of excess of hydride functionality affecting the crosslinking density. In order to determine the stoichiometric ratio of the vinyl to hydride, several tests for functionality were performed.

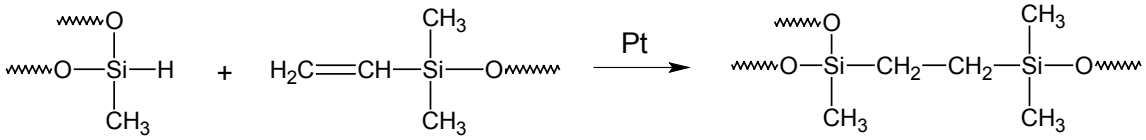

Figure 3-11: Reaction scheme for crosslinking in Silastic T2® via hydrosilylation of silicon hydride present in crosslinking agent and vinyl groups present in both the base resin and crosslinking agent. The platinum catalyst is present in the base resin.

Spectroscopic techniques performed on the Silastic® components include FTIR and NMR. An iodometric titration was performed that allows for the quantification of vinyl groups. Finally, molecular weight determinations were carried out with GPC.

Fourier transform infrared spectroscopy (FTIR)

FTIR spectroscopy utilizes the vibration of atoms in molecules to determine the chemical structure and bonding. Certain functional groups have characteristic vibrational frequencies. Some of the characteristic frequencies expected in the polysiloxanes used in this research are listed in Table 3-3.

FTIR was performed on the base resin, curing agent, and several reference polysiloxanes. FTIR can be used to quantify functional groups that are present as more than 5% of the sample. Filler extraction was performed on the Silastic T2® components prior to analysis with FTIR. Shown are the FTIR plots for

Silastic T2® base resin (Figure 3-12), Silastic T2® curing agent (Figure 3-14), vinyl terminated polydimethylsiloxanes (Figure 3-13) obtained from Gelest, Inc and poly(dimethyl-co-methyl hydride siloxanes) (Figure 3-15) obtained from Gelest, Inc. FTIR was performed to ascertain the quantity of silicon hydride and vinyl groups present in these polymers. A semi-quantitative FTIR analysis was attempted on the Silastic® base resin and curing agent after filler extraction.

Table 3-3: Characteristic Frequencies for FTIR [190]

Chemical Structure	Characteristic Frequencies	Notes
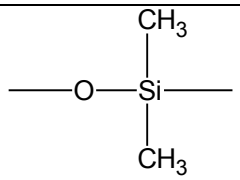	1260, 860 (weak), 800	The Si-CH_3 group is recognized by a strong band at 1260 with one or more strong bands in the range of 865-750cm^{-1}
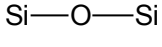	1130-1000	As chains become longer, bands become broader and more complex, showing 2 or more overlapping bands
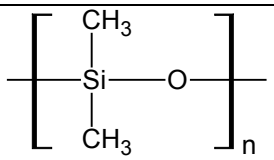	1090, 1020	Long poly(dimethyl siloxane) chains show two very strong, distinct bands at 1090 and 1020cm^{-1}
	1600, 1410, ca 1010, ca 960	If other alkenyl and aryl groups are absent, this functional group can also be identified by the CH peaks at 3060 and 3020cm^{-1}
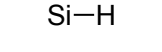	2280-2080, 950-	Generates a very strong band in the range 2280-2080cm^{-1} where there is very little interference from other bands.

FTIR was determined to be an unacceptable technique for the quantification of the vinyl content in the Silastic® components. This is due in part to both the low concentration of the vinyl species and the lack of a resolvable peak. The vinyl groups are present only as endgroups on high molecular weight polydimethylsiloxane polymers. The FTIR spectrum for the base resin does not

show any detectable peaks characteristic of vinyl groups. A vinyl-terminated polydimethylsiloxane with 10% vinyl content was run for comparative purposes. In this spectrum, the only evidence of the vinyl groups is a small peak appears at 3057 cm^{-1} and another even smaller peak at 1600 cm^{-1}. The other differences between these two spectra include peak broadening in the siloxane region between 1000 and 1100 cm^{-1} for the base resin. This peak broadening is due to the higher molecular weight. The reported molecular weight for the vinyl-terminated polydimethylsiloxane with 10% vinyl content is 500 g/mole.

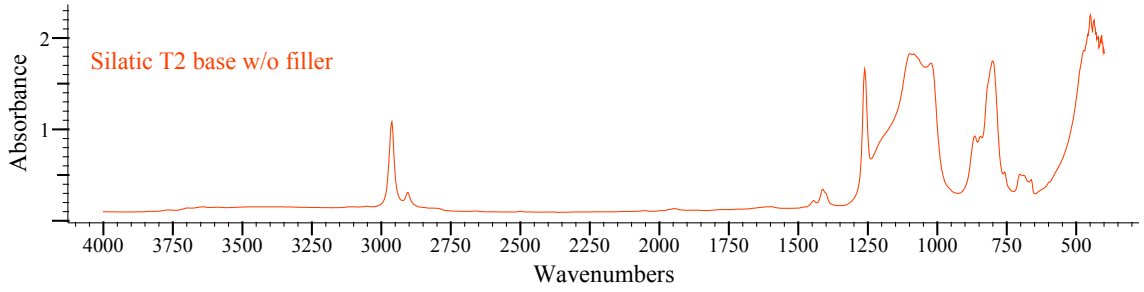

Figure 3-12: FTIR absorbance spectrum for Silastic T2® base without filler obtained with a Nicolet 20SX spectrometer using 64 scans at a 4 cm^{-1} resolution. A background spectrum was taken before each sample for subtraction.

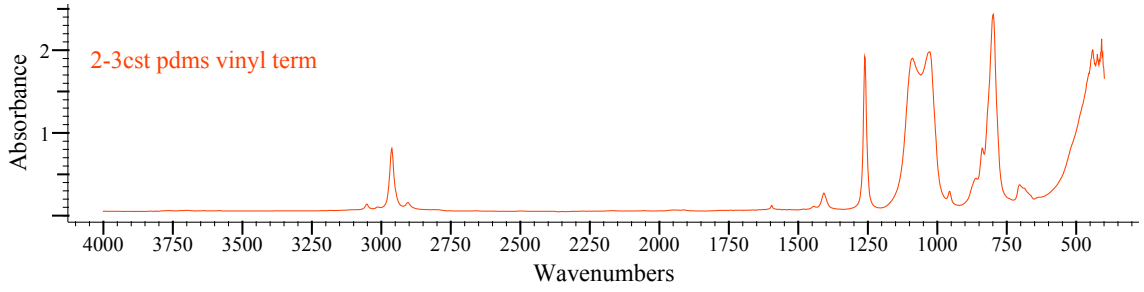

Figure 3-13: FTIR absorbance spectrum for vinyl-terminated PDMS oil. This polymer was reported by Gelest to have a molecular weight of 500g/mole, 2-3 cSt viscosity, and 10% vinyl content. The spectrum was obtained with a Nicolet 20SX spectrometer using 64 scans at a 4 cm^{-1} resolution. A background spectrum was taken before each sample for subtraction.

The curing agent contains silicon hydride functional groups in the form of a methyl hydride siloxane copolymer as opposed to the vinyl groups that are present only as chain ends. It is a reasonable assumption that the hydride content of the curing agent is considerably higher than the vinyl content. Additionally the hydride peak, located at 2200 cm^{-1}, is easy to identify due to lack of interference with other peaks. FTIR analysis of the hydride content of the Silastic T2® curing agent was performed and compared with poly(methyl hydride siloxane) and several poly(methyl hydride-co-dimethyl siloxane) polymers obtained from Gelest, Inc. (Figure 3-14 and 3-15).

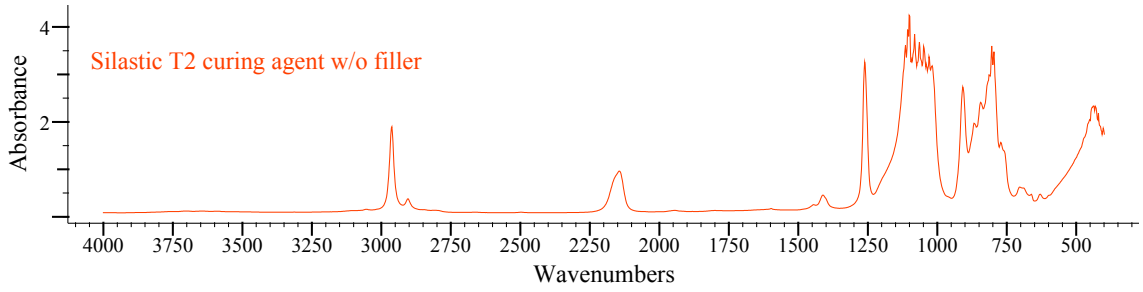

Figure 3-14: FTIR spectrum of Silastic T2® curing agent without filler. The spectrum was obtained with a Nicolet 20SX spectrometer using 64 scans at a 4 cm^{-1} resolution. A background spectrum was taken before each sample for subtraction.

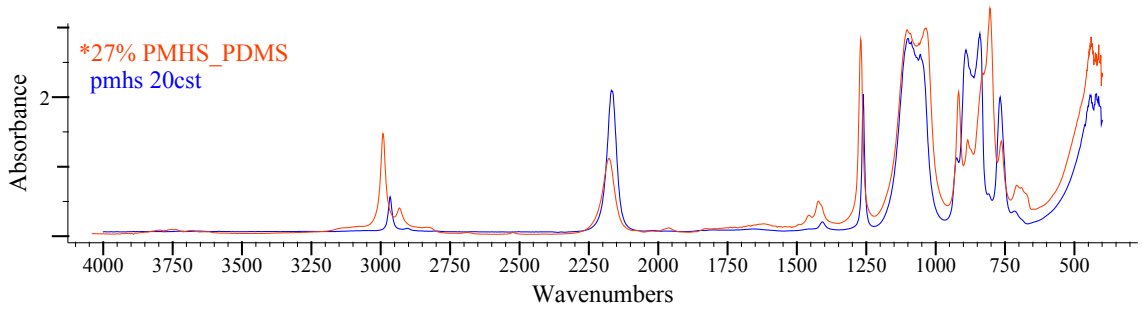

Figure 3-15: FTIR spectrum of poly(methyl hydride siloxane) homopolymer and poly(methyl hydride-co-dimethyl siloxane) copolymer. The spectrum was obtained with a Nicolet 20SX spectrometer using 64 scans at a 4 cm^{-1} resolution. A background spectrum was taken before each sample for subtraction.

A series of PDMS-co-PMHS polymers were evaluated for comparison. The FTIR spectra were converted to absorbance and normalized between 0 and 1 using BioRad software. The peak heights were measured for the silicon hydride peak at 2160 cm^{-1} and for the Si-CH_3 groups at 1261 cm^{-1} and the relative ratio was calculated. The data obtained are summarized in Table 3-4. The ratio of the two peak heights were plotted against the value for mole% SiH reported by Gelest, Inc. A linear relationship was obtained with a strong correlation (R^2 = 0.9768). The relationship molar % MHS = 97.595 (Abs_{2160}/Abs_{1261}) + 3.067 was used to calculate the hydride content of the curing agent. The curing agent was found to contain 30% silicon-hydride by this method.

Table 3-4: FTIR absorbance values for Si-H and Si-CH_3 in PDMS, PDMS-co-PMHS, PMHS, and Silastic T2® curing agent

Product	Mole% MHS	Abs_{2160}	Abs_{1260}	Abs_{2160}/A_{1260}
DMS-T15	0	0.008	0.466	0.017
HMS-301	27.5	0.256	0.9	0.284
HMS-501	52.5	0.336	0.862	0.390
HMS-991	100	0.716	0.697	1.027
Curing agent	?	0.211	0.764	0.276

Wij's test

As discussed in the previous section, there is not a readily identifiable peak for the determination of vinyl functionality, and the concentration of vinyl groups in the Silastic® is very low. The most reliable test for vinyl groups is an iodometric titration known as Wij's test [189]. Approximately 0.5 grams of Silastic T2® base, curing agent, and two vinyl terminated polymers with 10% and 0.2% vinyl content were each dissolved in 20ml of chloroform in individual Erlenmeyer flasks. 20ml of chloroform was also added to an empty flask as a blank for the

titration. 25 mL of the Wij's solution, iodine monochloride, was pipetted into each of the flasks. The flasks were allowed to react in a darkened area for one hour, at which point the samples were titrated with a 0.1 N sodium thiosulfate solution using ~2 mL of 10g/L starch solution as an indicator.

The %vinyl content was calculated using the equation

$$\%\text{Vinyl Content} = ((B - S) * N * 1.84) / W$$

where B and S represent the volumes of sodium thiosulfate required for the titration of the blank and sample respectively, N is the normality of the sodium thiosulfate, and W is the weight, in g, of the sample taken. The factor 1.84 was determined by standardizing the titrations with 10%, 0.2%, and 0% vinyl-terminated polydimethylsiloxanes. The Silastic T2® base was found to contain 0.5% ± 0.1% vinyl groups, and the curing agent was found to contain 11% ± 0.5% vinyl groups. The high percentage of vinyl groups in the curing agent was attributed to the tetramethyl-tetravinyl cyclotetrasiloxane additive.

Nuclear magnetic resonance spectroscopy (NMR)

Due to the higher sensitivity of the technique, NMR was used to verify the vinyl content of the Silastic T2® components. Proton NMR integration ranges for species expected in Silastic T2® are listed in Table 3-5, and the NMR spectra are shown in Figure 3-16 and 3-17. The NMR data from the Silastic T2® base resin showed a very large singlet peak associated with dimethyl siloxane groups in the range of –0.7 to 0.8 and small triplet centered at 6.0 as anticipated for the vinyl. There were also peaks present for water and an unknown aliphatic impurity and for the chloroform solvent.

Table 3-5: NMR integration ranges for pertinent species in Silastic® components [193]

Integration Range	Chemical Species	Structure
-0.7 – 0.8	Dimethyl siloxane	$-Si(CH_2)_2O-$
4.2 – 5.2	Methylhydrogen	$-SiHCH_2O-$
6.0 – 6.2	Dimethylvinyl	$-Si-CH=CH_2$

Based on the NMR data, the % vinyl content was determined to be 0.537%, which agrees very well with the Wij's test titrations. It is not possible to estimate the molecular weight of the vinyl functional polymers, since both vinyl terminated PDMS and vinyl terminated dimethyl-co-methyl vinyl siloxane polymers are both present.

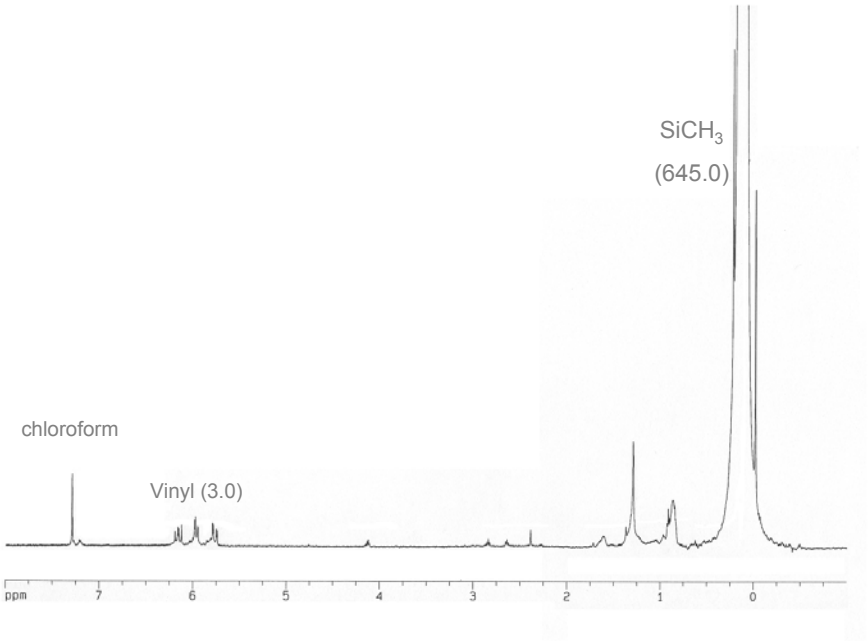

Figure 3-16: Proton NMR spectrum for 50 mg/ml Silastic T2® base resin in d-chloroform obtained obtained with a Varian 200 MHz XL-Series spectrometer system at the UF Brain Institute with the assistance of Dr. Jim Rocca.

The NMR data for the curing agent was less straightforward due to the presence of three very different chemical molecules (Figure 3-17). The vinyl portion of the NMR spectrum was complex as compared to the vinyl portion of

the Silastic® base resin. This is attributed to the presence of the cyclic vinyl siloxane species. There were also several types of methyl groups present as expected from the methyl-hydride siloxane copolymer, dimethyl siloxane polymer, and tetramethyl-tetra-vinyl cyclic siloxane. There was also significantly more of the greasy aliphatic unknown impurity. The main point of interest from the curing agent NMR data is that the hydride exceeds the vinyl content in the curing agent by at least a three-to-one ratio.

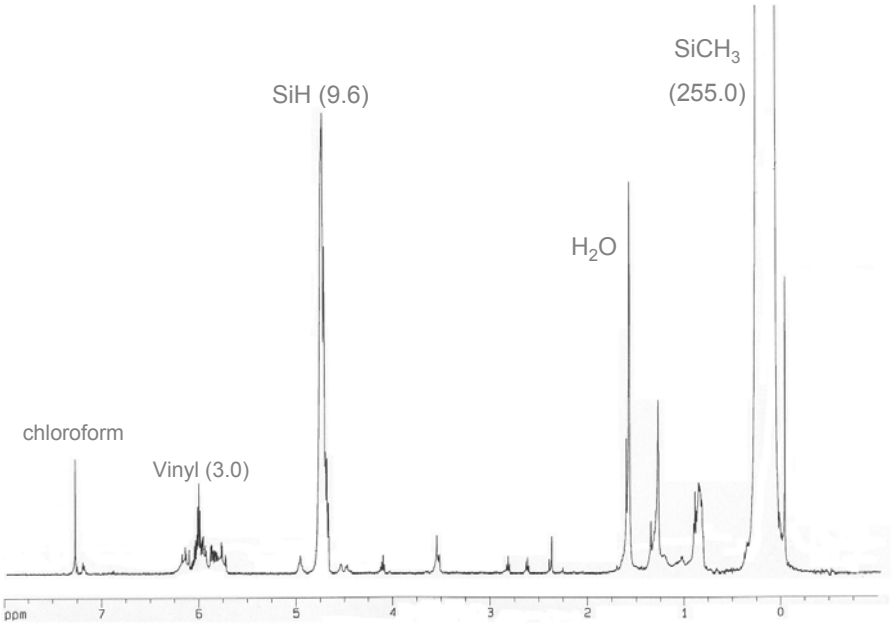

Figure 3-17: Proton NMR spectrum for 50 mg/ml Silastic T2® base resin in d-chloroform obtained obtained with a Varian 200 MHz XL-Series spectrometer system at the UF Brain Institute with the assistance of Dr. Jim Rocca.

Molecular Weight Determinations

The pure polymer was dissolved in toluene to a concentration of 30mg/ml and characterized by gel permeation chromatography (Figure 3-18). Several silicone oils of known molecular weight were also evaluated under the same conditions. Monodisperse polystyrene was used for calibration.

Table 3-6: Gel permeation chromatography data for polydimethylsiloxanes obtained from Gelest, Inc. and Silastic T2® base resin and curing agent

Sample	Reported Viscosity (cSt)	Reported Molecular weight (g/mol)	GPC values for Mn and Mw (g/mol)
DMS-T15	50	3,780	3.7E+03
			4.7E+03
DMS-T25	500	17,250	1.9E+04
			2.7E+04
DMS-T35	5000	49,350	4.7E+04
			6.0E+04
DMS-V00	0.7	186	1.4E+02
			1.4E+02
DMS-V03	2-3	500	5.3E+02
			7.6E+02
DMS-V31	1000	28,000	2.6E+04
			3.4E+04
DMS-V41	10000	67,700	5.9E+04
			7.7E+04
Base	Unknown	Unknown	3.7E+03
			4.7E+03
CA	Unknown	Unknown	1.9E+04
			2.7E+04

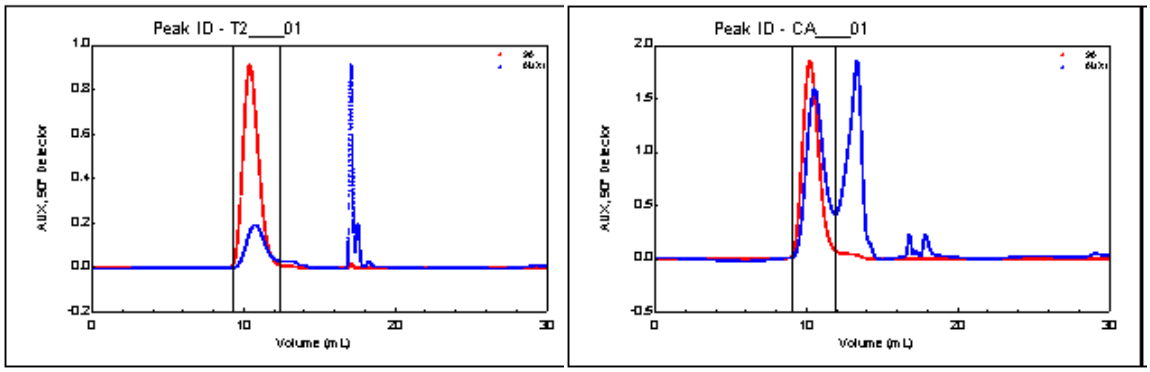

Figure 3-18: GPC elution peaks for a) Silastic T2® base resin and b) Silastic T2® curing agent. Experiments were performed with 30mg/ml samples in toluene and evaluated using gel permeation chromatography with light scattering.

Molecular weight data obtained from GPC of silicone oils of known molecular weight obtained from Gelest agreed fairly well with their reported

values (Table 3-6). The molecular weight of the Silastic T2® base resin was determined to be 200,700 g/mol. The first peak of the curing agent was presumed to be the vinyl functional portion, and the molecular weight was determined to be 81,610 g/mol. The second peak was presumed to be the lower molecular weight PMHS-co-PDMS.

Characterization of Silastic T2® PDMS Elastomers

Rheometer cure profiles

Cure profiles were collected on a Paar Physica parallel plate rheometer model MC200 with 5% strain, at a frequency of 1Hz, and various cure temperatures and times. The initial study involved the effects of cure temperature. Cure profiles were measured at 25, 34, and 80°C. A sample was considered cured when the value of the storage modulus plateaus.

There was very little difference between the storage moduli values for the cured PDMSe regardless of cure temperature (Figure 3-19). The value for the silicone elastomer cured at 25°C was 9.45 ± 0.3 GPa as compared to 8.72 ± 0.1 GPa for the silicone elastomer cured at 80°C. The elastomer cured at an intermediate temperature had a storage modulus of 8.59 ± 0.4 GPa. There is not a linear trend with respect to modulus of the cured elastomer and the cure temperature. This was verified with tensile measurements for Silastic T2® cured under various conditions as well.

There was an anticipated increase in curing time with decreased cure temperature. For an 8 by 8 inch area of 1 mm thick silicone cured between two glass plates that are each greater than 10 mm thick the following conditions for

cure are used; 2 hours at 80°C, 6 hours at 50°C, and 24 hours at 25°C. For the rheometer data, there was an almost immediate increase in storage modulus to a stable value indicates curing is much faster than that experienced in the actual lab setting. The relatively fast cure rate exhibited in the rheometer was attributed to greater heat transfer of metal plates, smaller sample size, and shear forces.

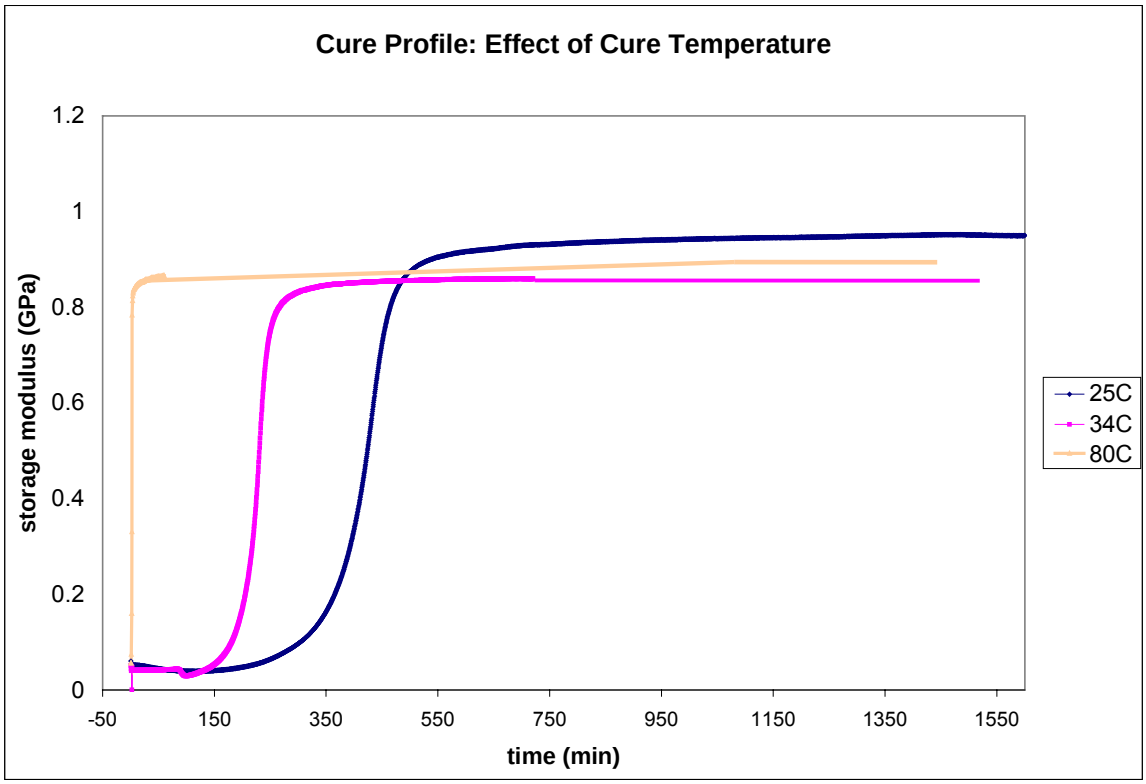

Figure 3-19: Rheometer data for Silastic T2® elastomer cured at 25, 34, and 80°C collected on a Paar Physica parallel plate rheometer model MC200 with 5% strain, at a frequency of 1Hz

The addition of vinyl terminated polydimethyl siloxane polymers and oligomers were evaluated as modulus modifiers for the Silastic T2® system. The vinyl terminated PDMS, 28kg/mol and 500g/mol, were added to the Silastic® base resin (15% by weight). The low molecular weight polysiloxanes contains 12% vinyl groups and the high molecular weight polysiloxanes contained 0.2% vinyl groups. Additional curing agent, above the recommended 10%, was added

to compensate for the increase in vinyl groups to minimize the possibility of uncrosslinked polymer in the cured elastomer (Table 3-7). The modified and unmodified PDMSe was monitored at 80°C with 5% strain and at a frequency of 1Hz (Figure 3-20).

Table 3-7: Formulations tested to evaluate the effect of the addition of vinyl terminated PDMS oils

Sample additive	MW of Additive (g/mol)	Base Resin (g)	Additive Added (g)	Curing Agent Added (g)
None	N/A	1	0	0.1
15% DMS-V03	500	1	0.15	0.28
15% DMS-V31	28,000	1	0.15	0.103

The low molecular weight functional PDMS increased both the modulus (41% relative to unmodified PDMSe) and dramatically increased the time required for cure (~2000% relative to unmodified PDMSe). This is related to the drastic increase in crosslink density accompanying the inclusion of these small chains into the elastomer network. Low molar mass vinyl terminated polydimethylsiloxanes are sometimes included in silicone elastomer formulations to inhibit the cure and thus increase the pot-life of the uncured silicone. The addition of the higher molecular weight polymer decreased the storage modulus slightly (18%) and slightly increased the time required for cure (19%). The change in modulus and cure time relative to the unmodified PDMSe was also verified in the preparation of samples for tensile measurements (Figure 3-22).

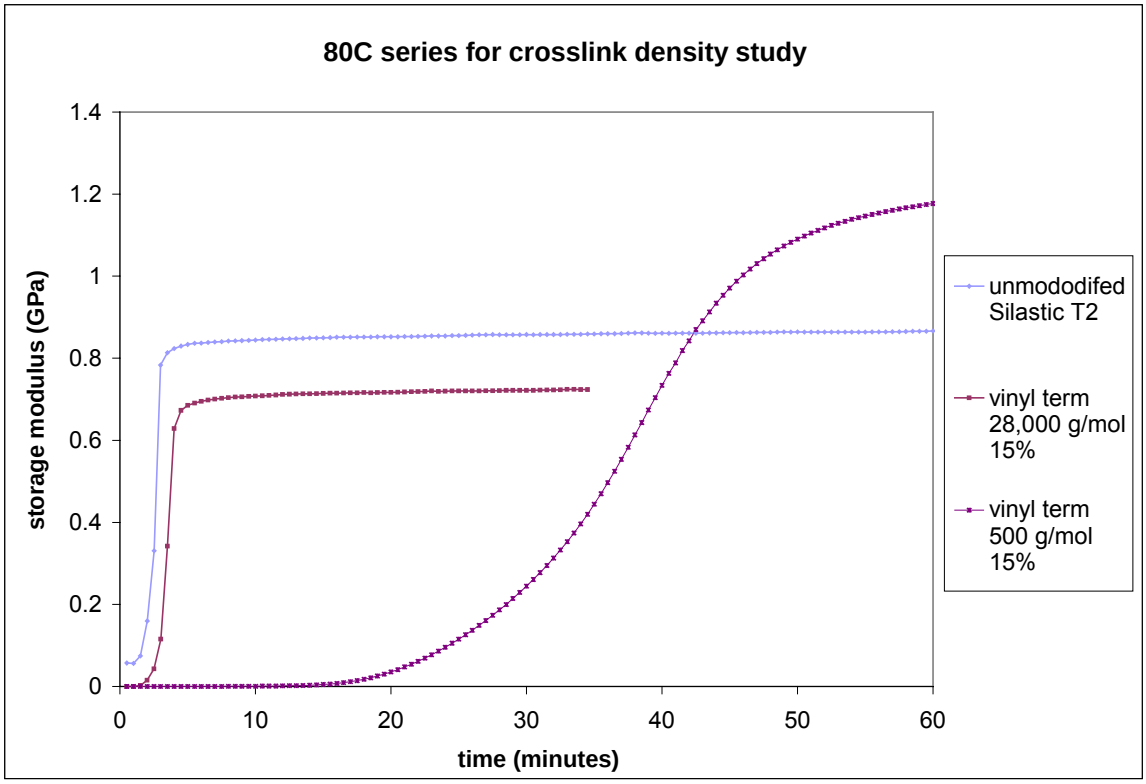

Figure 3-20: Rheometer cure profile data for crosslink density study. All elastomers cured at 80°C. Unmodified Silastic T2®, Silastic® with 15% vinyl terminated PDMS 28kg/mol, and Silastic® with 15% vinyl terminated PDMS 500g/mol.

Mechanical testing

The bulk mechanical properties of the cured Silastic T2® elastomer were determined via tensile testing. A representative stress-strain plot for the unmodified PDMSe is shown in Figure 3-21. Filled silicone elastomers exhibit two distinct linear regions in the stress strain plot. The initial linear region is for strains less than 90% and the modulus calculated from this region is thus called the low strain modulus. At higher strains, the silica filler agglomerates in the elastomer begin the break apart. The newly exposed silanols on the silica filler will serve to increase the effective crosslink density. Thus the modulus calculated from the high strain region of the stress strain plot will be greater than

the low strain modulus. In general, the low strain modulus is more important for the present research. The forces that a silicone-based foul release coating will experience will most likely not result in a >90% strain of that coating.

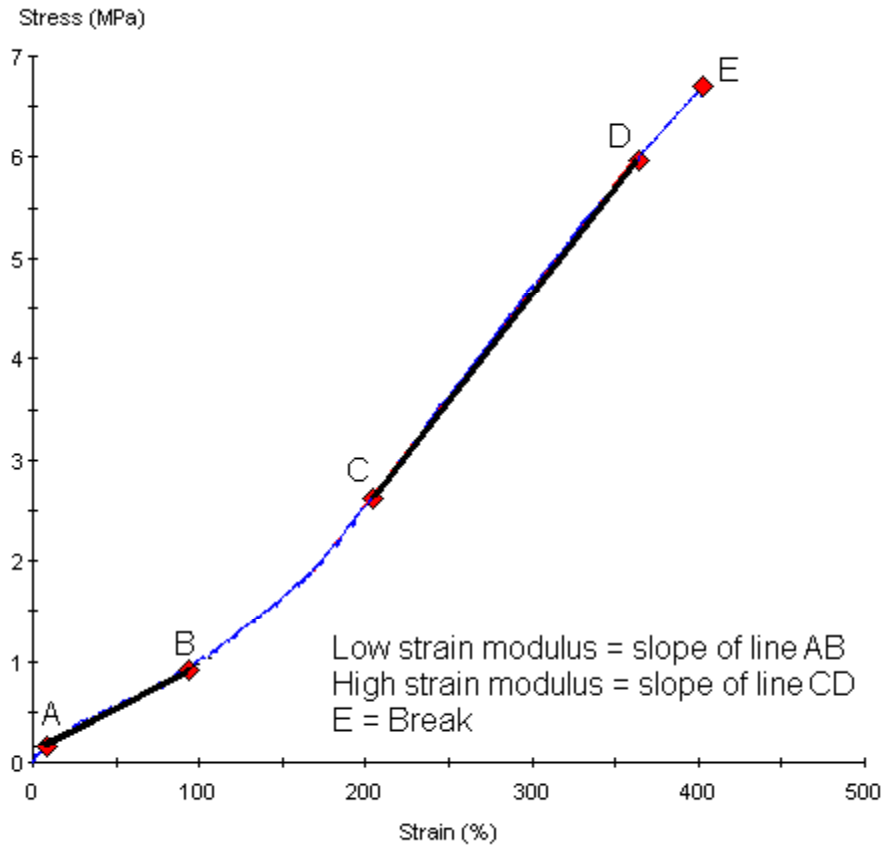

Figure 3-21: Representative stress-strain plot for unmodified PDMSe cured at room temperature.

The effect of cure temperature was evaluated. There was no statistically significant trend in modulus with cure temperature (Figure 3-22). The Silastic® PDMS elastomer was modified with the addition of either vinyl or trimethylsiloxy terminated PDMS oligomers as discussed above. The modulus values for several formulations are shown in Figure 3-23. The intention of the vinyl terminated PDMS oligomers was to affect a change in the bulk modulus by variation of the crosslink density. Using functional polydimethyl siloxane

oligomers, the moduli of the PDMS elastomer were varied over an order of magnitude. At least five dogbones were measured for each sample set.

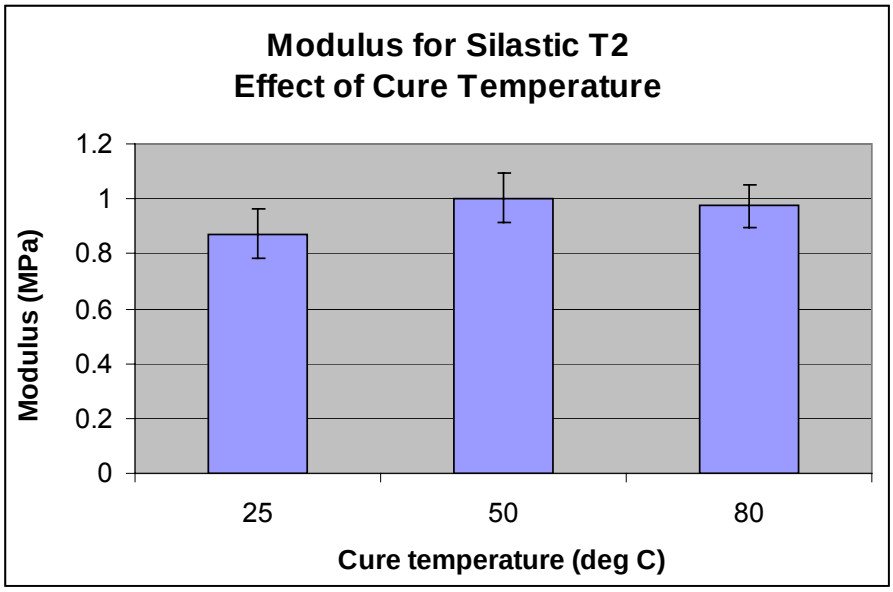

Figure 3-22: Modulus values for silicone elastomers cured at various temperatures. Modulus measurements were taken from the initial linear portion (>90% strain) of the stress-strain plot from tensile measurements made according to ASTM D12-97

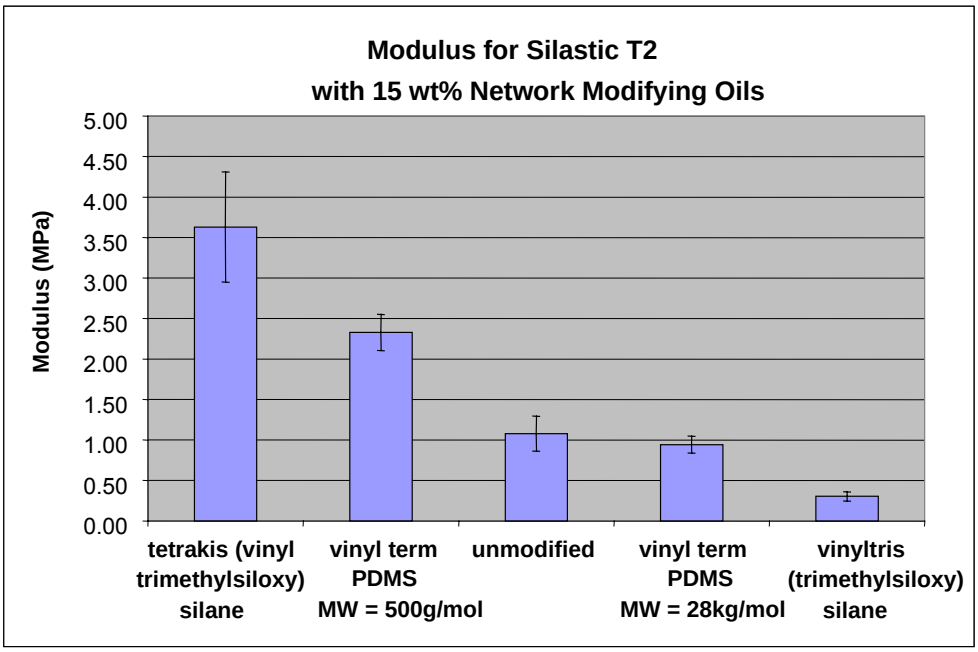

Figure 3-23: Modulus values for silicone elastomers formulated with vinyl functional oils. Modulus measurements were taken from the initial linear portion (>90% strain) of the stress-strain plot from tensile measurements made according to ASTM D12-97

Wade Wilkerson evaluated the vinyl functional modulus-modified samples I prepared for their effect on bioresponse with respect to contact guidance of porcine vascular endothelial cells on 5, 10, and 20μm wide channels [171, 194]. This work was published in his master's thesis. Other Brennan group research has shown that there is a correlation between endothelial cell contact guidance and spore settlement density. The range of moduli values produced did not have as strong an effect on contact guidance as the range of topographical dimensions. Figure 3-24 shows the main effects of this study that combined PDMSe modulus and surface topography. Channel width had the greatest effect on cell alignment.

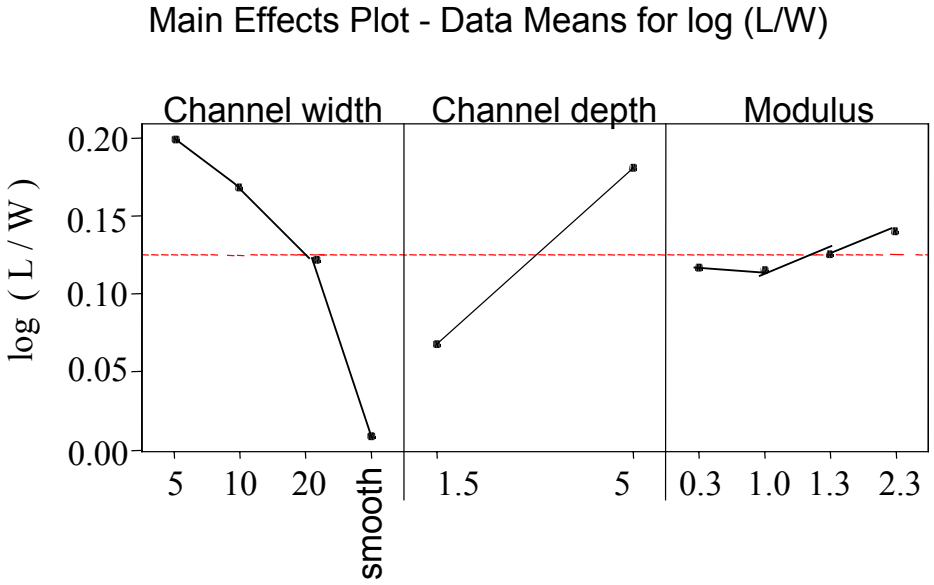

Figure 3-24: Main effects plot for endothelial cell contact guidance for alignment of cells in channels separated by 5μm ridges. Channels width and channel depth have a stronger effect on response than the moduli range evaluated.

TMS terminated PDMS oils are free oils that act as plasticizers and also increase the surface lubricity. The effect of the addition of these oils was evaluated on modulus and surface energy. There was very little change in bulk modulus with the addition of the non-functional oils (Figure 2-25). The effect of the addition of the non-functional oils on bioresponse was evaluated with respect to *Ulva* spores and will be presented in Chapter 4.

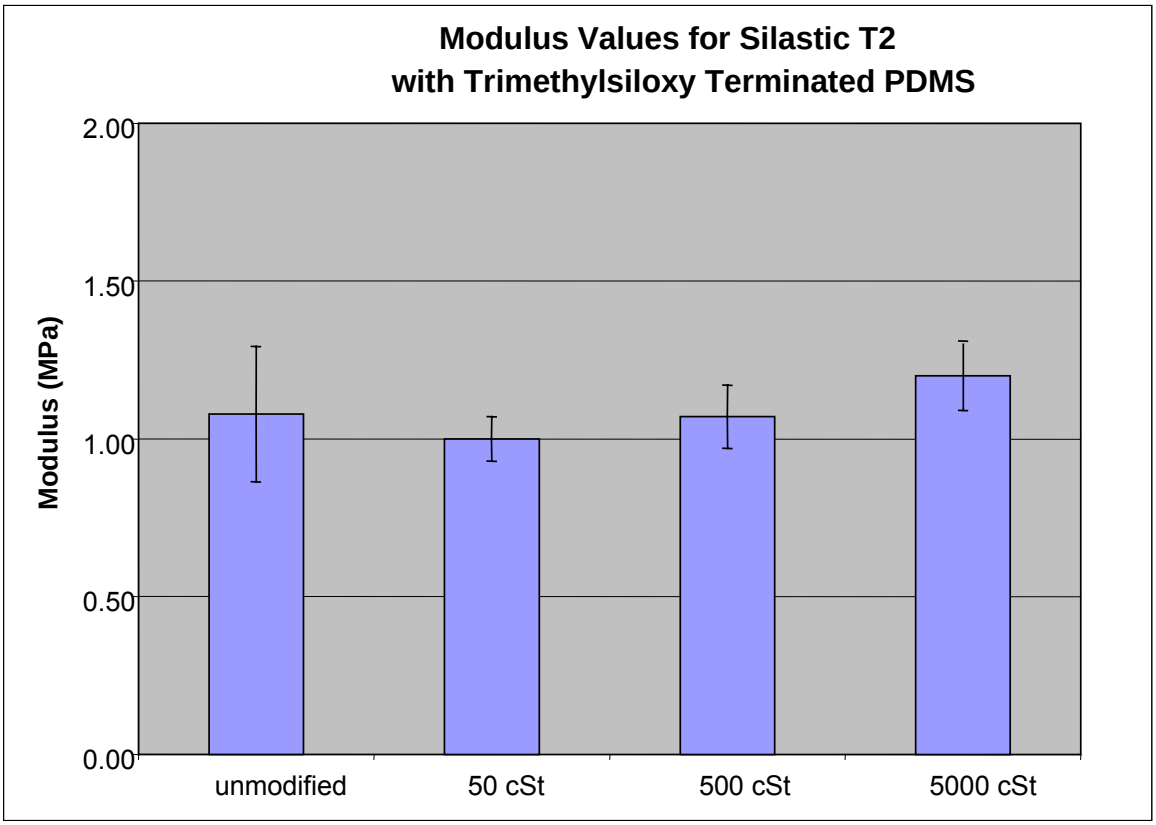

Figure 3-25: Modulus values for silicone elastomers formulated with 15% non-functional oils. Modulus measurements were taken from the initial linear portion (>90% strain) of the stress-strain plot from tensile measurements made according to ASTM D12-97

Surface energy

Initial studies on the surface characterization of the PDMSe with bulk additives were performed in on a digital goniometer setup built in house [98, 171, 195], subsequent studies were performed on a Ramé Hart model 500 automated

goniometer. Representative images of solvent sessile drops on unmodified PDMSe are shown in Figure 3-26. Contact angles were measured from such images and used to create a modified Zisman plot to calculate surface energy (Figure 3-27 and 3-28).

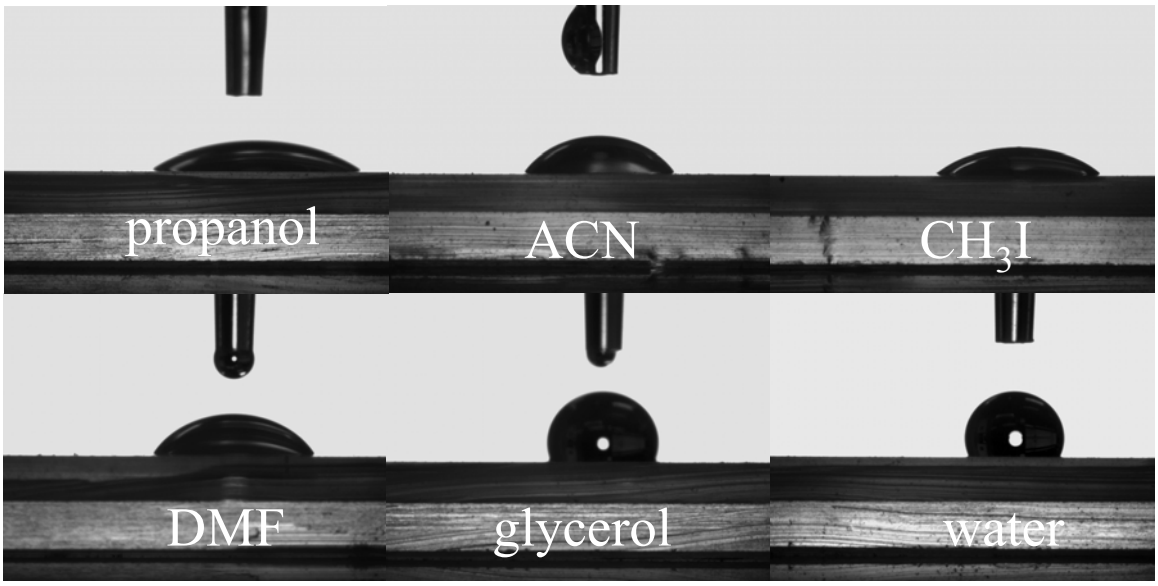

Figure 3-26: Representative images of contact angle of various solvents used for surface energy analysis on PDMSe with Ramé Hart goniometer.

As discussed in the introductory chapter, a Zisman plot of cos θ versus γ_{lv} can be used to calculate the surface energy of a solid from contact angle measurements, as described by Young's equation.

$$\gamma_{sv} - \gamma_{sl} = \gamma_{lv} \cos \theta$$

where γ_{sv}, γ_{sl}, and γ_{lv} are the surface tensions for the surface-vapor, surface-liquid, and liquid-vapor interfaces, respectively, and θ is the contact angle. A cos θ value of one is achieved when the liquid completely wets the solid resulting in a zero contact angle. This critical surface tension can be calculated determined by extrapolating a linear regression line from the data of multiple liquids on a Zisman plot.

On low surface energy materials, nonlinearity occurs for liquids with surface tensions greater than 50 dynes/cm. Good proposed a modified Zisman plot of cos θ versus $1/\gamma_{lv}^{1/2}$ for calculation of critical surface tension of low surface energy materials [196]. The surface energy of the silicone elastomer substrate is thus calculated from extrapolating a linear regression line from the data of multiple liquids on an inverse Zisman plot. The liquids used for this calculation were water, dimethyl formamide, acetonitrile, methylene iodide and propanol. At least ten drops were measured for each liquid on each samples set.

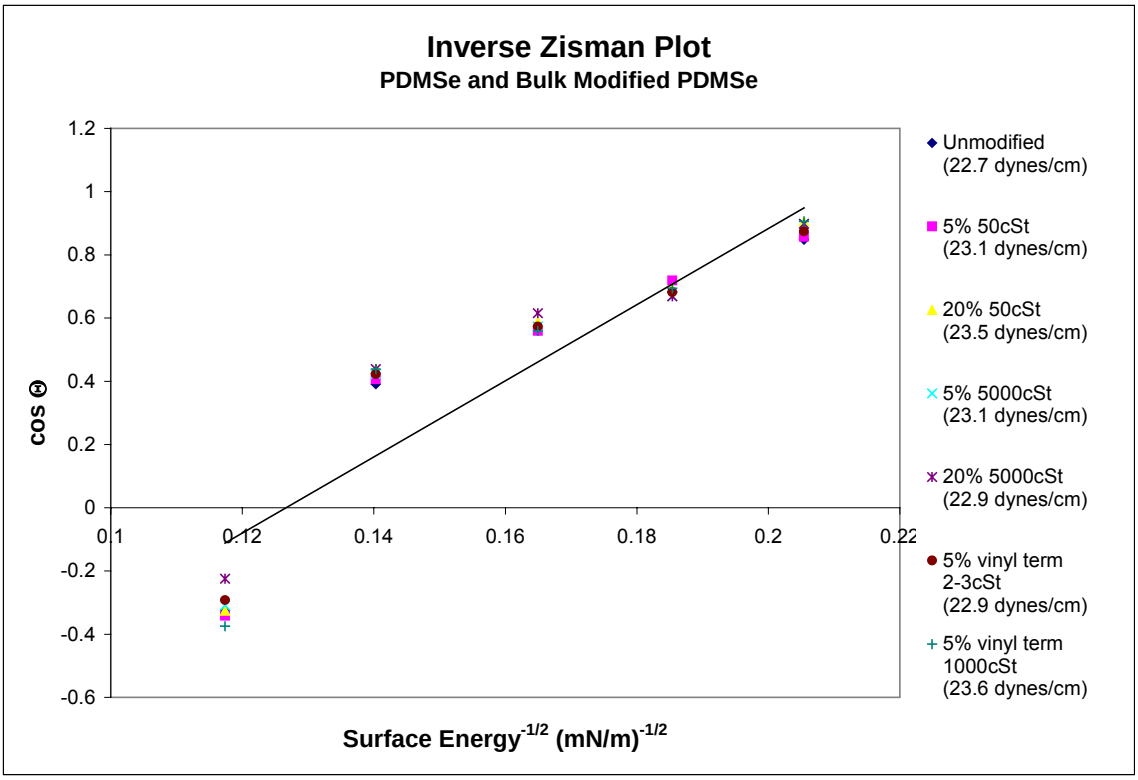

Figure 3-27: Representative inverse Zisman plot for Silastic T2® and PDMSe with bulk additives. Calculated surface energy is listed in the figure legend and in the following figure. Trend line is for unmodified PDMSe.

For all Silastic T2® coatings tested, the surface energy as determined by inverse Zisman plot, was approximately 23 dynes/cm regardless of bulk additive (Figure 3-28).

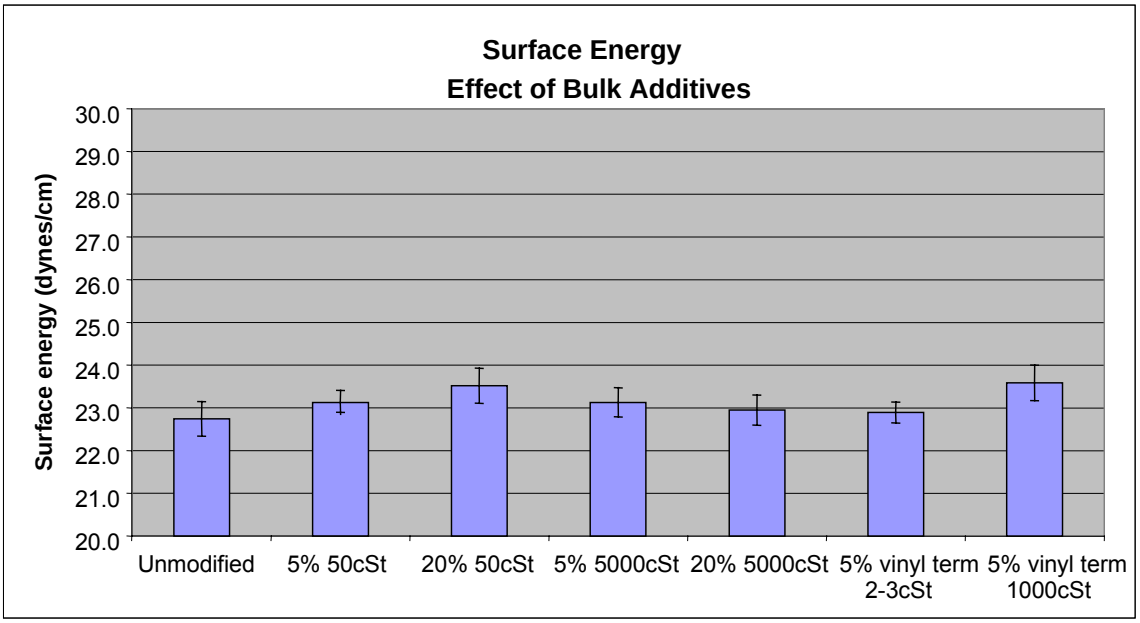

Figure 3-28: Calculated values for surface energy of PDMSe and PDMSe with bulk additives.

Conclusions

Silastic T2® components were evaluated with respect to molecular weight, chemical structure, and stoichiometric ratio. The base resin contains vinyl terminated PDMS, poly(methyl vinyl) siloxane, platinum catalyst, and silane treated fillers. In order to more fully characterize base resin component, it would be necessary to separate the vinyl terminated PDMS and the PMVS and ascertain their individual molecular weight distributions and vinyl content. It was determined that the base resin had very little vinyl content, 0.5% as verified by iodometric titration and NMR, but the molecular weight measurement of ~200kg/mol was not verified by a secondary technique.

The Silastic® curing agent was considerably more difficult to characterize given the presence of both vinyl and hydride functionalized polymers. The curing agent contains 50% less silica filler than does the base resin. The curing agent contains 30% silicon-hydride in the form of PDMS-co-PMHS and a vinyl terminated PDMS. The vinyl terminated PDMS could not be characterized fully, as the material also contained tetramethyl, tetravinyl cyclotetrasiloxane. The two polymers should be separated and then characterized to get a better understanding of the composition.

The cured silicone elastomers were evaluated for surface energy and bulk modulus. PDMS based additives could be included in formulations to affect the bulk modulus or surface lubricity without affecting the surface energy. The bulk modulus of the unmodified PDMSe was determined to be approximately 1.3 MPa and could increase threefold or decreased by an order of magnitude. The surface energy of the PDMSe was maintained at approximately 23 dynes/cm regardless of bulk additive. This allowed for the evaluation of changes in modulus independently of surface energy. The bioresponse of porcine vascular endothelial cells with respect to the modulus modified samples and topography by the Brennan group. Topography was found to dominate bulk modulus for the range evaluated. Samples modified with the non-functional PDMS oils were also evaluated for bioresponse with *Ulva* zoospores as reported in the following chapter.

CHAPTER 4
BIOASSAYS WITH RESPECT TO OIL ADDITION AND TOPOGRAPHICAL MODIFICATION

Background

Ulva (syn. *Enteromorpha*) is the most common green macroalga. In 1753, Linnaeus originally classified *Ulva* and *Enteromorpha* as species within the same genus. Ten years later, Adanson reported that *Enteromorpha* was an autonomous genus and the two algae have been recognized as two separate geneses since that time. Recently, it was determined that *Ulva* and *Enteromorpha* are in fact synonymous despite the obvious morphological differences (*Ulva* thallus is lettuce-like and *Enteromorpha* tubular).

Ulva is the largest macroalgal contributor to the biofouling problem. This is due to the fact that *Ulva* is an opportunistic settler and is very fast growing thus it is able to rapidly colonize substrates. Additionally, *Ulva* is highly tolerant a wide variety of environmental factors (pH, salinity, temperature, antifouling methods such as heavy metal toxins). The problematic tin used in antifouling paints was originally added as a booster biocide for *Ulva* algae, which was the only biologic species that was resistant to copper biocides.

Fouling occurs via the settlement of motile zoospores that are released from the fronds of the mature plant material (Figure 4-1). These zoospores are asexual, quadriflagellate, pear-shaped cells. They are approximately 5-7μm in length and 5μm in diameter at widest point.

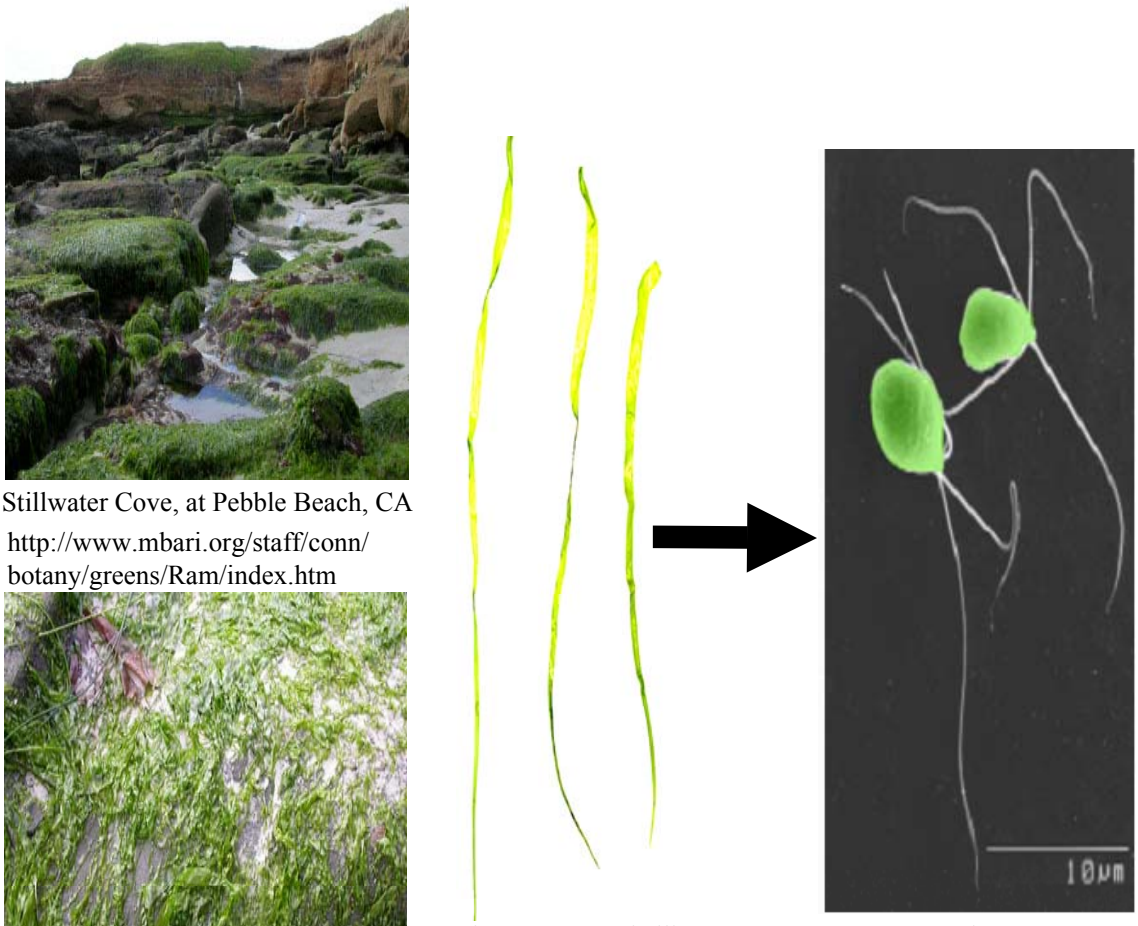

Stillwater Cove, at Pebble Beach, CA
http://www.mbari.org/staff/conn/botany/greens/Ram/index.htm

Three separate thalli of Enteromorpha

Enteromorpha zoospores (false colored image)

Figure 4-1: *Ulva* of various forms. Images obtained from and used by permission of the Monterey Bay Oceananographic Research group and the Callow group.

A variety of cues are involved in the selection of a settlement location, including phototactic, thigmotactic, and chemotactic cues [70]. The zoospores show highly selective settlement behavior with respect to surface roughness. The selectivity of the spore settlement was shown not to be a simple energy

driven process but rather biologically driven by comparing settlement of zoospores to polystyrene beads of the same dimension [97].

Once an individual spore settles on a substrate, it secretes a glycoprotein adhesive [197]. Evidence suggests that the size of the adhesive plate is controlled by surface chemistry/energy (Figure 4-2B). The adhesive itself is a hydrophilic, gel-like material that rapidly cures to tether the spore to the surface. It is proposed that the strength of this adhesion is controlled by the factors included in the JKR equation.

Ulva zoospore settlement data can vary significantly from study to study, due to variability between spore batches. This may be related to season and when the spores were collected in relation to the tidal cycle.

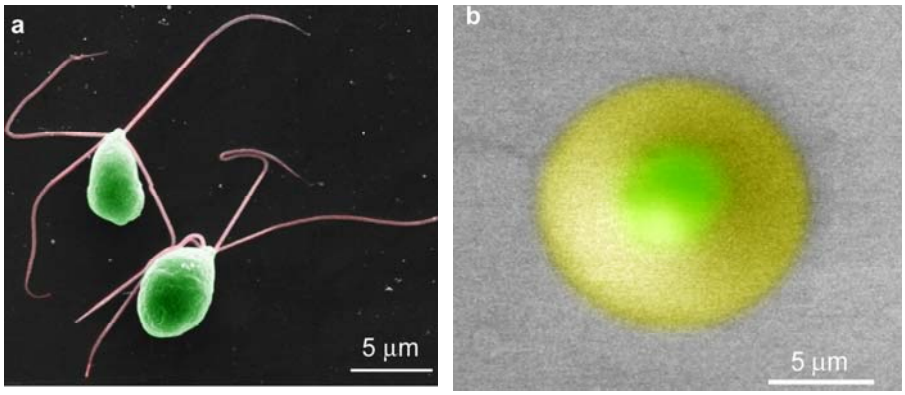

Figure 4-2: A) motile *Ulva* zoospores B) settled zoospore with adhesive pad. Images obtained from and used by permission of the Callow group.

One major problem with silicone based foul release coatings is the accumulation of 'slimes'. These slimes are aesthetically unpleasing and do not release at operating speeds as high as 430 knots [90]. Diatoms are a major component of these slimes, and in general, fouling diatoms adhere more strongly to hydrophobic substrates. The three most common diatoms are *Amphora coffeaeformis*, Craspedostauros *australis*, and *Navicula perminuta*.

Diatoms are unicellular algae with an ornamental silica shell that encases the protoplast. Diatoms adhere to surfaces through the production of sticky extracellular polymeric substances (EPS). This EPS also allows for 'gliding' motility of a settled diatom. The attached cells can divide rapidly to produce a compact biofilm, which may achieve 500 mm in thickness [8].

Material and Methods

PDMSe Coated Glass Microscope Slides

Smooth PDMSe slides were prepared as discussed in Chapter 3. Silicone coated microscope slides were prepared by mixing 10 parts of the Silastic T2® base resin with 1 part of the curing agent. Trimethyl siloxane terminated PDMS of ~4000 or 50,000 g/mol (Table 4-1) was incorporated during the mixing, prior to degassing the silicone. The oils were added at a level of 5 or 20% by weight with respect to the base resin. The mixture was degassed and poured over glass microscope slides that had been treated with allyltriethoxysilane, ATS, coupling agent.

The silicone was cured at room temperature for twenty-four hours between two glass plates with spacers to achieve a silicone thickness of ~700-1000μm. After cure, the PDMSe coated microscope slides prepared in this manner were then removed from the glass plates and excess silicone was trimmed away from the edges. Samples were evaluated for thickness, surface defects, and for adhesion to the glass microscope slide. The samples were placed in individual, labeled polypropylene bags and either kept in house for analysis or shipped to the University of Birmingham, UK for bioassay.

Table 4-1: TMS-terminated oil additives

Name	Structure	Viscosity (cSt)	Molecular Weight (g/mol)
Polydimethyl siloxane, trimethyl siloxy terminated	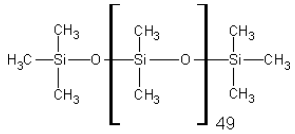	50	3,800
Polydimethyl siloxane, trimethyl siloxy terminated	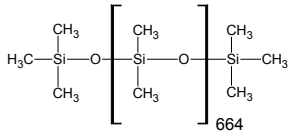	5,000	49,400

Patterned PDMSe coated glass microscope slides

Patterned PDMSe coated slides were prepared by curing the silicone against an epoxy mold or silicon wafer rather than against smooth glass. Details of the preparation and use of said epoxy molds are as follows.

The patterns evaluated in this initial research were conceptualized and created in 2D form in software programs such as AutoCAD. These renderings were submitted to Mitronics Inc. to create a photoresist mask of chrome on glass. The patterns were etched into silicon wafers Chuck Seegert with the assistance of Al Ogden using standard photoresist technology. The silicon wafers were provided to me directly for this research.

The original patterns evaluated for this research were fabricated in 2000. These first generation patterns were designed to elucidate the effect of critical spacing of simple topographic features. The patterns selected were channels of various spacings separated by fixed 5μm wide ridges. There were three channel lengths originally proposed as depicted in Figure 4-3 in addition to 5μm wide

square pillars. Only the continuous ridges (a) and pillars (d) are evaluated in this research.

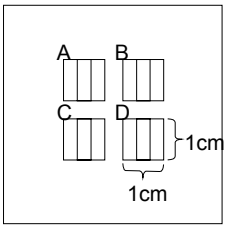

	Feature Width μm	Feature Length μm	Feature Spacing μm
A	5	10,000	5,10,20
B	5	800	5,10,20
C	5	60	5,10,20
D	5	5	5,10,20

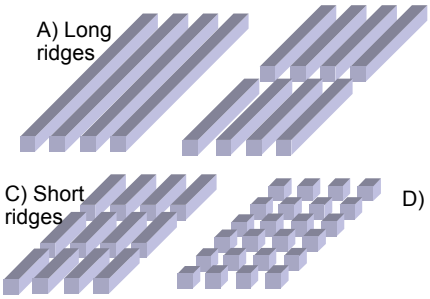

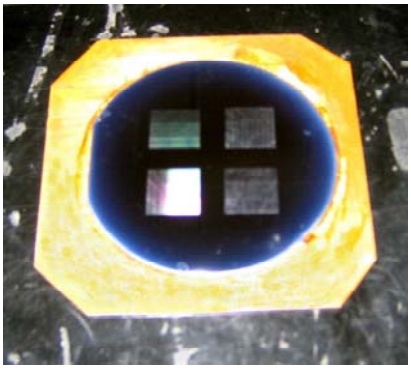

Figure 4-3: Description and image of channel/pillars wafers

The original chrome mask was designed in such a way that the etched silicon wafer was a positive replica of the desired pattern. Thus, it was necessary to replicate the wafer in a secondary material that would replicate the pattern with high fidelity, release from the silicon wafer, and finally not react with or transfer material to the curing silicone. Two materials, polystyrene and polyurethanes, have been identified that meet these criterion. Polystyrene was used for wafer replication of channel and pillar patterned samples generated between 2000 and 2004.

To fabricate the pattern negative in polystyrene, a 15wt% solution of polystyrene in chloroform was prepared. This solution was pipetted slowly onto a clean, hexamethyldisilazane treated wafer that had been placed on a level stage inside a fume hood. The solvent was allowed to evaporate for ~36hours. The PS film was released from the wafer by placing the wafer in contact with a small

piece of dry ice. The PS film was then epoxied to a glass plate. This PS film was subsequently replicated with Silastic T2® to produce the desired patterns. Typically, the PDMSe replicates generated off the PS negatives were then used in the production of a master epoxy mold.

The silicone elastomer replicates were placed pattern-side down onto a clean HMDS treated 4" by 4" glass plate. This glass plate was then placed onto an 8" by 8" glass plate. Four microscope slides were stacked together and used as spacers in each corner of the larger glass plate. Freshly mixed Silastic T2® was poured on top of the small glass plate / patterns. A second 8" by 8" glass plate was then slowly lowered onto the silicone-covered plate. The silicone elastomer was the cured at 80°C for 1 hour. Once the silicone elastomer was cured, the glass plates were carefully separated from the PDMSe, leaving a patterned PDMSe well.

29.1 grams of Epon 828 resin and 8.2 grams of Jeffamine D230 were thoroughly mixed and degassed. Meanwhile, the PDMSe well was placed pattern-side up onto a clean glass plate, such that no air bubbles were present between the glass and the silicone elastomer. This was facilitated by placing the plate and silicone elastomer well into a heated vacuum oven for 30 minutes at 30 inHg. A second glass plate was treated with a thermoset mold release agent called Stoner. A thin coat of this material was sprayed onto the clean glass plate, which was then placed into an 80°C oven for 30 minutes or until the coating was fully dry.

Once the epoxy was degassed, it was poured into the patterned silicone elastomer well. The Stoner-treated glass plated was slowly lowered onto the uncured epoxy in the silicone elastomer well. The well was then placed into an oven at 60°C for 4 hours. Once the epoxy was cured and cooled, it was removed from the silicone elastomer well. One PDMSe well can typically produce 2-3 epoxy molds. The epoxy molds can produce >5 repeated replications of PDMSe.

There were many drawbacks in using the polystyrene as the negative replication step. First, the process was very time consuming. Second, the polystyrene films often had inherent problems such as bubbles or sticking to the wafer. Additionally, the final product often had a wavy appearance due to the process of epoxying the PS film to the glass. Finally, this process was repeated frequently because the PS replicates do not stand up to repeated replications with PDMSe and degrade with time as evidenced by cracking.

Once the epoxy molds were prepared, patterned silicone coated microscope slides were prepared by mixing 10 parts of the Silastic T2® base resin with 1 part of the curing agent. Zero, five, or twenty percent by weigth of the trimethyl siloxane terminated PDMS (Table 4-1) was incorporated during the mixing, prior to degassing the silicone. The mixture was degassed and poured over the epoxy mold that was located on a 7 sq-inch with spacers in each corner to achieve a silicone thickness of ~700-1000μm. ATS treated glass microscope slides were taped to a second glass plate, which was slowly lowered onto the first plate. Pressure was applied evenly by hand to assure intimate contact of the top glass plate with the spacers. The silicone elastomer was cured at room

temperature for twenty-four hours against the epoxy mold between these glass plates. After cure, the PDMSe coated microscope slides prepared in this manner were then removed from the glass plates and excess silicone elastomer was trimmed away from the edges. Samples were evaluated for thickness, surface defects, and for adhesion to the glass microscope slide. The samples were placed in individual, labeled polypropylene bags and either kept in house for analysis or shipped to the University of Birmingham, UK for bioassay.

Ulva Assays

Ulva assays were performed by the Callow group at the University of Birmingham, UK. Samples were prepared at the University of Florida and then shipped to the Callow group for further evaluation. The procedure followed by the Callow group for the *Ulva* assays is reported in the literature and briefly described here for clarity [63, 97, 198, 199].

Ulva zoospores were obtained from fertile plants of *Ulva linza* that were collected by Maureen Callow and John Finlay from Wembury beach, UK ($50^{o}18'$ N; $4^{o}02'$ W). The plants are washed thoroughly in sterile seawater, wrapped in adsorbent paper, and transported to the University of Birmingham laboratory in a cooler. The following day individual algal fronds were transferred into glass tubes containing 3-5ml of sterile seawater. Zoospores were retrieved from the tubes, checked microscopically, placed in a suspension of artificial seawater, and diluted to a concentration of 2×10^{6} ml^{-1}.

Zoospore settlement assays

PDMSe coated slides were equilibrated by immersion in sterile artificial seawater (Instant Ocean™) for twenty-four hours and then rinsed in sterile

seawater. Slides (6 replicates) were placed in individual compartments of quadriperm polystyrene culture dishes (Fisher) to which 10 ml of spore suspension was added. Dishes were then incubated in the dark at 20^{o}C for 60 min.

The samples were washed to remove unattached spores by passing backwards and forwards 10 times through a beaker of seawater. Three replicate slides from each treatment were then fixed in 2% glutaraldehyde in seawater and processed as described in Callow *et al*. (1997) [200]. The remaining three replicates were placed in a flow apparatus as described in the following section before fixing.

Attached spores were counted at 1 mm intervals along the unpatterned portion of the replicate slides. On the patterned surfaces, attached spores were counted at 0.5 mm intervals down two tracks of the long axis (10,000 μm) of each section of the patterned areas. Thirty counts were made for each of three replicates. Images of spores, on each of 3 replicate samples, were recorded in 30 fields of view using a 25x objective with a Zeiss Kontron 3000 image analysis system attached to a Zeiss epifluorescence microscope via a video camera as described in Callow *et al.* (2002) [97].

Zoospore shear strength assays

Slides settled with spores were exposed to shear in a specially designed flow cell apparatus [198], modified by fitting a higher capacity pump (1.12 kW (1.5 hp) 3-phase Baldor thermoplastic centrifugal pump (McMaster-Carr, Chicago, IL, USA) capable of delivering 281 L min^{-1} at 9 m head). The apparatus

holds six 1-inch by 3-inch microscope slides. The flow cell had a variable bedding system that allowed for height adjustment such that the coatings were flush with the surrounding channel wall.

Turbulent flow was created in a 60 cm long low aspect ratio section of channel preceding the slides. Seawater was flowed through the testing portion of the flow cell at a rate up to 4.9 m s^{-1} to generate wall shear stresses up to 56 Pa. The exposure of slides to flow was standardized at 5 min. Wall shear stresses were determined from streamwise pressure drop measurements using the Reynolds-averaged Navier-Stokes equation [198]. Control experiments conducted on uncoated slides have previously established that there are no streamwise differences in the removal of cells in the flow chamber [199].

Spore density on exposed slides was determined via image analysis as described in the previous section.

Percentage spore removal data were calculated from the mean number of spores remaining attached to the surface after exposure to turbulent flow compared with the mean number before the slides were subjected to flow. Data are expressed as percentage removal; 95% confidence limits were calculated from arc sine transformed data. This treatment is typical for statistical analysis for calculated percentage-type data and allows for a more appropriate estimation of the error associated with the calculated value. Spore settlement data are presented for the mean number of spores adhered and the 95% confidence limits (x=90).

Sporeling growth assays

Ulva zoospores were settled using standard methods as above. Six replicates of each treatment were settled with spores. Zoospores were settled in individual dishes containing 10 ml of zoospore suspension in the dark at ~20^{o}C. Unsettled spores were removed by washing and observed for symptoms of toxicity. Sporelings were cultured in enriched seawater medium in individual (10 ml) wells in polystyrene dishes under illuminated conditions. The medium was refreshed every 2 days and the sporelings cultured for 10 days.

The sporelings were scraped off and collected from half of each slide. The chlorophyll is extracted from the sporelings into dimethyl sulfoxide and the amount of chlorophyll$_a$ is determined spectrophotometrically. A direct proportionality has been shown between the quantity of chlorophyll$_a$ and the biomass of sporelings present. Biomass was measured in this manner on one half of the slide before exposure to flow and from the other half after flow in the water channel.

Sporeling strength of attachment assays

The slides with biomass remaining on half of the area were exposed to a shear stress of 53 Pa in the water channel. The biomass remaining after exposure was analyzed for chlorophyll$_a$ content as described above.

Diatom Assays

Diatom assays were performed by the Callow group at the University of Birmingham, UK. Samples were prepared at the University of Florida and then shipped to the Callow group for further evaluation. The procedure followed by

the Callow group for the diatom assays is reported in the literature and briefly described here for clarity [90, 199].

Diatom settlement assays

Per the protocol discussed in Holland et al 2004 [90], *Amphora* diatom cells were cultured for three days in natural seawater supplemented with nutrients to form Guillard's F/2 medium [201]. *Amphora* cells were cultured in F/2 medium. Cells were washed 3 times in artificial sea water (TM) to remove traces of medium and secondary metabolites before dilution with sea water to give a suspension of cells with chlorophyll$_{\underline{a}}$ content of approximately 0.3 μg/ml.

Six replicates were used for each treatment. Cells were settled in individual dishes containing 10 ml of suspension in natural daylight at ~20 °C. After 5 h the slides were gently washed in seawater to remove cells that had not properly attached. Three replicate slides were fixed in 2.5% glutaraldehyde in sea water, desalted by washing first in 50:50 seawater/distilled water, followed by distilled water, and dried before counting. The density of cells attached to the surface was counted on each slide using an image analysis system attached to a fluorescent microscope. Counts were made for 15 fields of view (each 0.4 mm^2) on each slide with a Zeiss Kontron 3000 image analysis system attached to a Zeiss epifluorescence microscope via a video camera.

Diatom shear strength assays

The remaining three replicates were used to evaluate the strength of diatom attachment as detailed below. Slides settled with *Amphora* were then exposed to shear in a water flow cell. Glass standards were included. The water channel

exposes cells to shear stresses that are approximate to those typically experience by ship hulls [198]. Slides were placed in the flow cell apparatus described above to expose attached diatoms to turbulent flow for 5 min at a range of wall shear stresses up to the maximum of 53 Pa. The maximum shear stress generated by this method does not necessarily remove the most tenaciously adhered diatom species; thus additional studies were also performed via water jet, which produces compressive as well as shear stresses on the slide surface [104, 199, 202].

The number of cells remaining attached was compared with unexposed control slides (used to determine settlement as above). The number of cells in 15 fields of view (each 0.4 mm^2) was counted on each slide using with a Zeiss Kontron 3000 image analysis system attached to a Zeiss epifluorescence microscope via a video camera. Data are expressed as percentage removal with 95% confidence limits.

Statistics

Data were analyzed using the Fusion Pro (D.O.E. Fusion^{TM}) Design of Experiments software package. This program allowed for the data analysis to determine and model the significant factors within the design. A factorial multi-level experimental design was analyzed at a 95% confidence level to determine statistically significant variables and at lower confidence levels to ascertain trends with respect to oil viscosity (2 levels), oil amount (3 levels), topography type (2 levels), topography depth (2 levels), and topography spacing (4 levels) on various spore density measurements. All comparisons described in the text as statistically significant are significant at a 95% confidence level.

Results and Discussion

Assays with Respect to Oil Modification: Smooth

The values of liquid surface tension reported by the manufacturer of the TMS terminated polydimethylsiloxane oils (20.8 –21.3 dynes/cm) are lower than the surface tension of the PDMSe (23 dynes/cm). This causes these oils to migrate to and spread over the surface. This is noted most for the highest oil loading of the highest viscosity oil (20% 5000 cSt). An oily layer was visible on the samples when they were removed from the storage bags. This phenomenon also resulted in the infilling of the micropatterns. The 20% 5000 cSt oil-laden patterned PDMSe substrates could not be evaluated for bioresponse as the patterns were completely filled with oil and could not be distinguished from flat. The surface properties of these samples, reported in Hoipkemeier-Wilson et al. are summarized in the following table (Table 4-2).

Table 4-2: Surface properties of oil-laden and unmodified PDMSe substrates [63]

Oil Additive		Dynamic Contact Angle			Static Contact Angle	
Viscosity (cSt)	Loading Level	θ_{adv} (°)	θ_{rec} (°)	$\Delta\theta$ (°)	Water contact angle (°)	Surface energy (dynes/cm)
No Oil	0%	115.1 ± 3.8	68.7 ± 2.2	46.4 ± 1.7	112 ± 3	21.5 ± 1.8
50	5%	113.9 ± 1.8	77.5 ± 1.8	36.4 ± 0.3	106 ± 4	22.8 ± 1.2
50	20%	100.5 ± 1.3	65.1 ± 2.1	35.4 ± 1.6	106 ± 3	22.5 ± 0.9
5000	5%	106.1 ± 0.7	71.6 ± 2.2	34.5 ± 2.1	106 ± 4	23.3 ± 1.4
5000	20%	100.9 ± 1.1	91.8 ± 2.4	9.1 ± 1.3	100 ± 2	21.7 ± 1.2

Ulva zoospore settlement characteristics

The presence of unbound oils has been shown to affect biological adhesion [93]. A full study was launched for unpatterned silicone samples with the addition of PDMS oils of varying viscosities and percentages. The composition and

number of slides shipped for this study are listed in Table 4-3. Retain were kept in-house for each formulation for characterization. An acid-washed glass slide was included in this study as a control.

Table 4-3: Smooth PDMSe slides shipped for zoospore assay with respect to oil addition. Retains were kept in house for analyses performed in chapter 3.

Number of Slides	Formulation	Topography	Date Shipped
14	Unmodified	None	3/01
20	5% 50cSt PDMS oil	None	3/01
17	20% 50cSt PDMS oil	None	3/01
21	5% 5000cSt PDMS oil	None	3/01
18	20% 5000cSt PDMS oil	None	3/01

The mean number of spores settled on a standard acid-washed glass slide was approximately twice that to the elastomer-coated slides with and without added oils (Figure 4-4). There were more spores settled on the PDMSe substrates with oil than on the unmodified PDMSe, although this difference was not significant for the lowest loading of the 50 cSt oil-modified, unpatterned PDMSe coatings. There was significantly more settlement on the substrate laden with 5% 5000 cSt oil compared to the unmodified PDMSe and to the 50 cSt oil-laden surfaces. The 20% 5000 cSt oil-laden PDMSe had the highest settlement of the PDMSe substrates and was nearly twice that seen on the unmodified PDMSe. Many spores attached to this high molecular weight oil-laden substrates were described by the Callow group as partially ‘embedded’ in the oily surface layer.

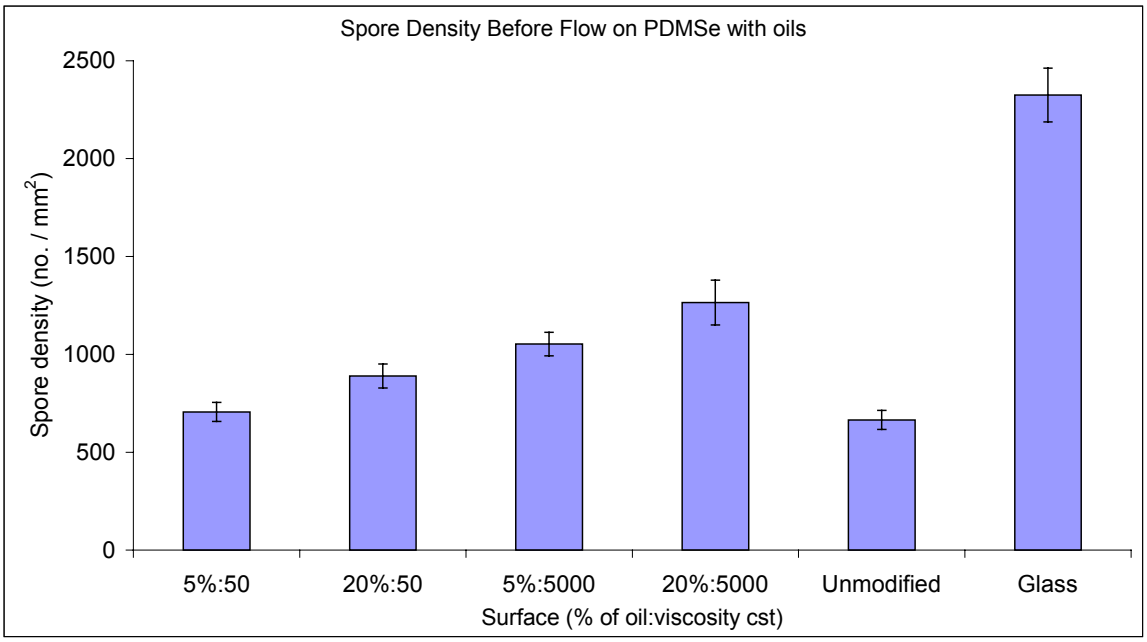

Figure 4-4: *Ulva* zoospore settlement density on oil laden smooth PDMSe slides. Each data point is the mean of 90 counts, 30 from each of 3 replicates. Error bars show 95% confidence limits.

Ulva zoospore release characteristics

The mean spore density remaining attached to smooth PDMSe surfaces after exposure to water flow (56 Pa) was at least 60% less than the mean spore density remaining attached to glass. The values for the control PDMSe and for the oil-laden substrates were similar (Figure 4-5). There was no statistically significant difference between the mean spore densities after flow for the 50 cSt oil-laden samples regardless of oil loading level. There was a statistically significant difference between the two oil-loading levels for the 5000 cSt oil-laden samples. The 5% 5000 cSt oil-laden sample had the highest spore density after flow and was nearly twice that reported for the unmodified PDMSe.

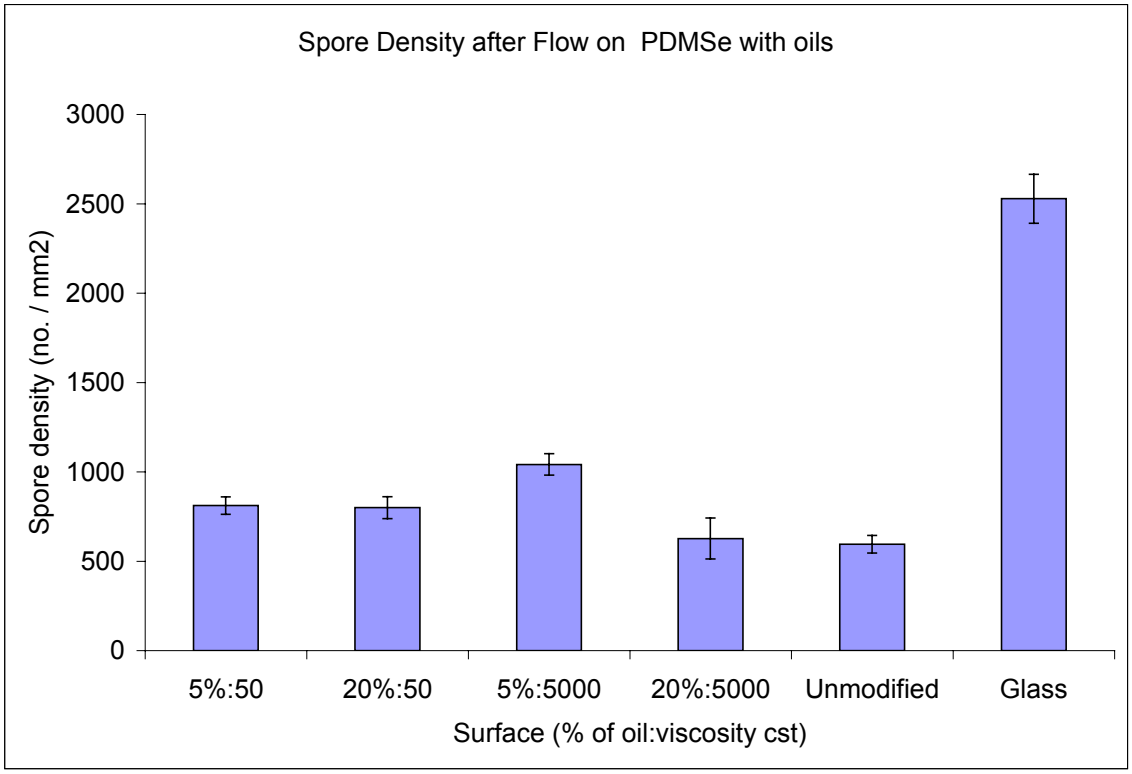

Figure 4-5: *Ulva* zoospore density after exposure to flow channel (56 Pa) on oil-laden smooth PDMSe slides. Each data point is the mean of 90 counts, 30 from each of 3 replicates. Error bars show 95% confidence limits.

The highest percent removal (50%) was from the 20% 5000 cSt substrate, which was also the PDMSe substrate with the highest initial settlement and spores 'embedded' in the oily surface layer (Figure 4-6). There was only 1% removal from the lower loading of this same oil (5% 5000 cSt oil). There was virtually no removal from the 5% 50 cSt oil-laden PDMSe or from the glass control slides. There was approximately ten percent removal from the unmodified PDMSe and the PDMSe substrates loaded with 20% 50 cSt. The percent removal from these two substrates were not statistically different from each other.

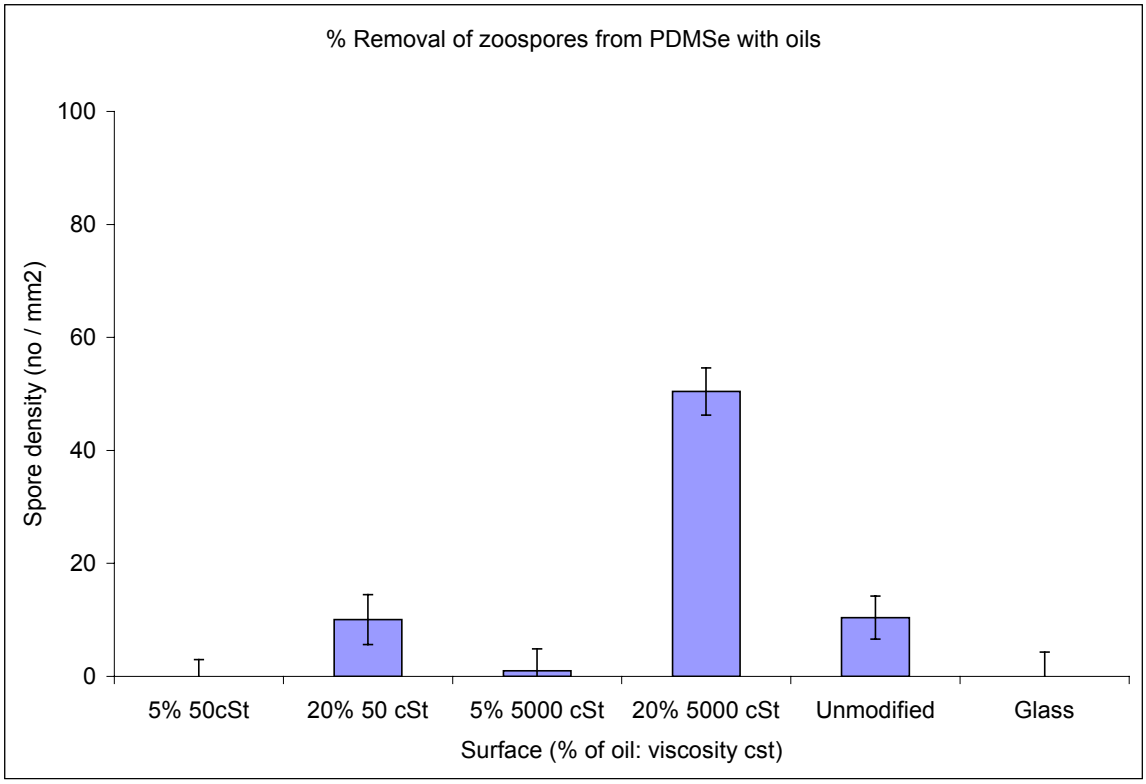

Figure 4-6: Calculated percent removal data for *Ulva* zoospores removed after exposure to flow channel (56 Pa) on oil-laden smooth PDMSe slides. No data point indicates 0% removal. Each point represents the mean percentage removal of *Ulva* zoospores from 90 observations from 3 replicate slides. Bars represent 95 % confidence limits derived from arcsine transformed data.

Amphora **diatom settlement characteristics**

Amphora is a unicellular alga, approx 15 um long and commonly found in algal slimes. Unlike *Enteromorpha* spores it is capable of a gliding movement on surfaces and consequently its attachment strength tends to be weaker. The data presented here is for an identical set of oil-laden samples as those tested with *Ulva* zoospores. As discussed above, the oils migrate to and spread over the surface of the PDMSe, forming a thin boundary layer that may deter the settlement, weaken the attachment, or facilitate detachment by slippage.

Settlement was similar on all PDMSe samples. This was not unexpected. Ulva zoospores respond to active settlement cues, but the settlement of *Amphora* cells is a passive process driven primarily by gravity. Once in contact with the surface, the diatom cells are able to change their position and orientation in order to facilitate attachment and motility. Thus the same number of cells will contact the substrates, but the number forming an initial attachment may differ. The rinsing procedure removes cells that had not formed an initial attachment. The fact that the settlement density was significantly higher (greater than 10%) on the PDMSe substrates as compared to glass indicates that cells adhere more readily to PDMSe (Figure 4-7).

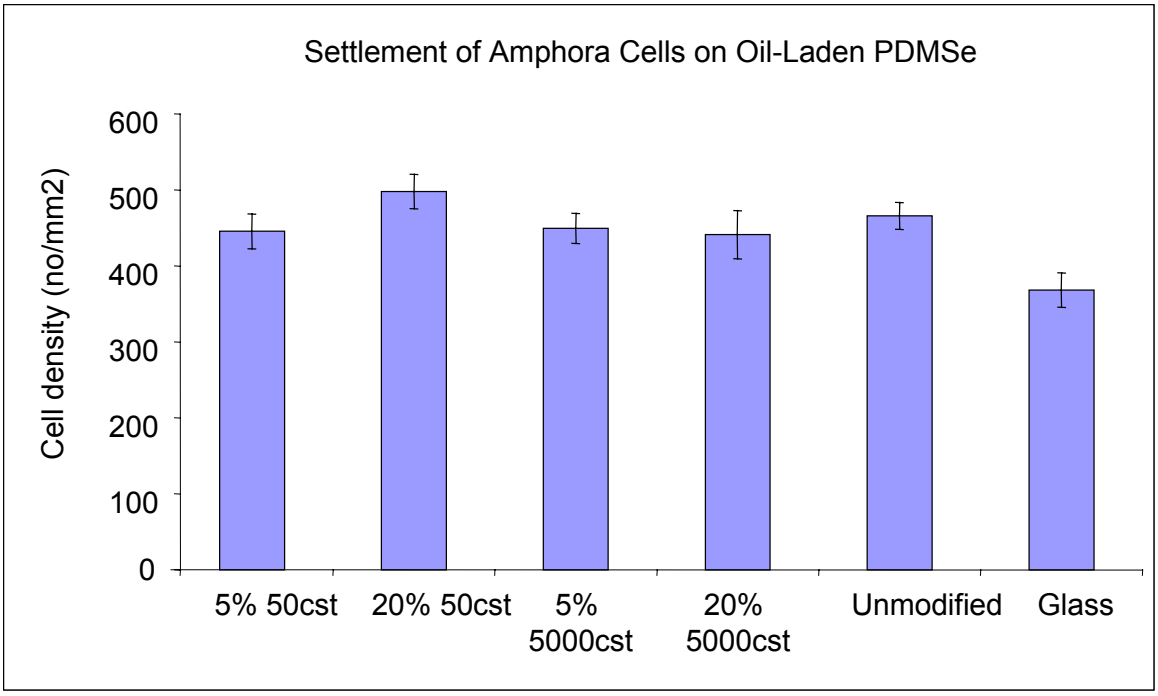

Figure 4-7: *Amphora* diatom settlement density on oil-laden smooth PDMSe slides. Each data point is the mean of 45 counts, 15 from each of 3 replicates. Error bars show 95% confidence limits.

Amphora diatom release characteristics

Slides settled with *Amphora* were then exposed to shear in a water channel (53 Pa). Glass standards were included for comparison. Percent removal data showed little difference between the oil-laden substrates tested, but there was statistically significantly greater removal from the unmodified PDMSe (Figure 4-8). This unmodified PDMSe had the greatest amount of removal was from unmodified PDMSe. The glass substrates had less removal than unmodified PDMSe but greater removal than from any of the oil-laden PDMSe substrates. The incorporation of oils into the PDMSe increased retention of the cells to the PDMSe by 10–20%.

It was noted by the Callow group that the cells were still motile on all surfaces and that physical entrapment of the cells within the oil did not appear to be occurring. The thin layer of oil on surface of the oil-laden PDMSe minimizes the surface rearrangement of PDMSe in water. This explains the increase of attachment to the oil-laden substrates, because *Amphora* diatoms typically adhere more strongly to hydrophobic surfaces.

These results contrast those for *Ulva* zoospore adhesion in which the removal of spores was greater from the highest oil containing coating (20 % of 5000 cSt). Other studies have also confirmed that the attachment strengths of the two algae are very different, and that they tend to favor very different types of substrates. Additionally, it has previously been shown the incorporation of oils in PDMS coatings has been shown to decrease barnacle oyster adhesion strength, but had no effect on tubeworms.

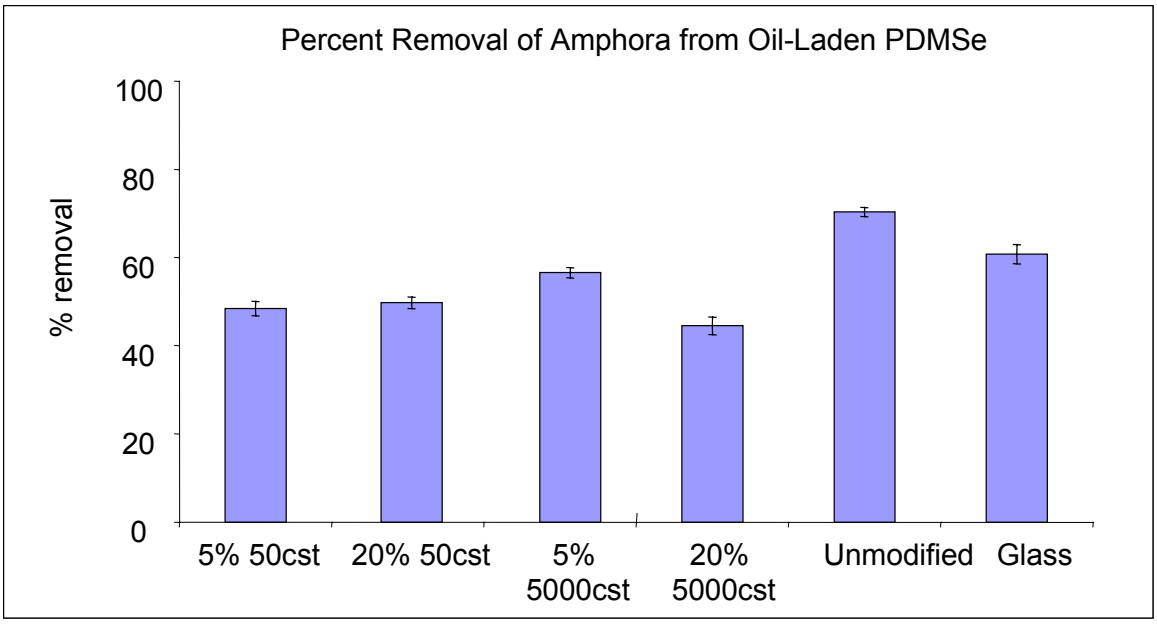

Figure 4-8: Calculated percent removal of *Amphora* diatoms after exposure to flow channel (53 Pa) on oil-laden smooth PDMSe slides. Each point represents the mean percentage removal of *Amphora* diatoms from 45 observations from 3 replicate slides. Bars represent 95 % confidence limits derived from arcsine transformed data.

Sporeling assays

The two previous studies evaluated the effect of oil incorporation on the settlement and attachment strengths of two algae, *Ulva* and *Amphora*. This study analyzes the long-term effects of oil incorporation on the germination and growth of *Ulva* sporelings. To investigate growth and attachment strength of sporelings, six replicate slides of each treatment were settled with spores: biomass was measured on one half of the slide before exposure to flow, and from the other half after flow in the water channel. Biomass was evaluated by measurement of chlorophyll$_a$ content. Standard leaching and settlement methods were used. Sporeling detachment was examined using the water channel that produces a fully developed turbulent flow. All experiments were run at maximum velocity to produce a wall shear stress of 53 Pa.

Growth of sporelings was similar on all the coatings. Settlement of zoospores has previously been shown to increase with increasing oil content and viscosity. Due to competition, individual sporeling biomass tends to increase as sporeling density decreases, consequently lower spore settlement does not necessarily mean lower biomass. The even growth on all surfaces indicates that the oils did not affect the growth of sporelings (Figure 4-9).

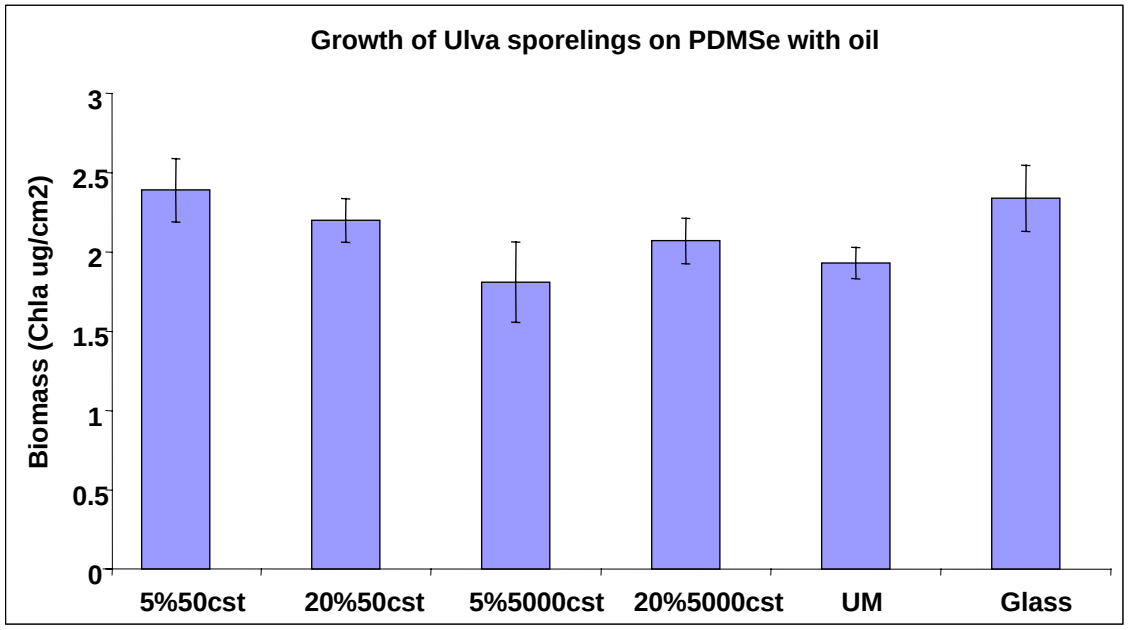

Figure 4-9: Quantification of *Ulva* sporelings on oil-laden smooth PDMSe slides as determined by biomass method. Each data point is the mean 3 replicates. Error bars show 95% confidence limits.

Sporeling attachment strength was similar on the PDMSe and on all the oil-laden PDMSe surfaces and was much lower than on glass. The incorporation of oil did affect the degree of removal, with all oil-laden samples exhibiting greater release than the unmodified PDSMe (Figure 4-10). However, only the 5% 5000 cSt substrate exhibited a statistically significant increase relative to the unmodified. Previously, the 20% 5000 cSt oil incorporation increased percent release 40% of Ulva zoospores relative to unmodified. This dramatic release

was not seen for the sporelings. This may be due to the fact that the rhizoids (roots) of the sporelings could push aside the oily layer and contact the PDMSe.

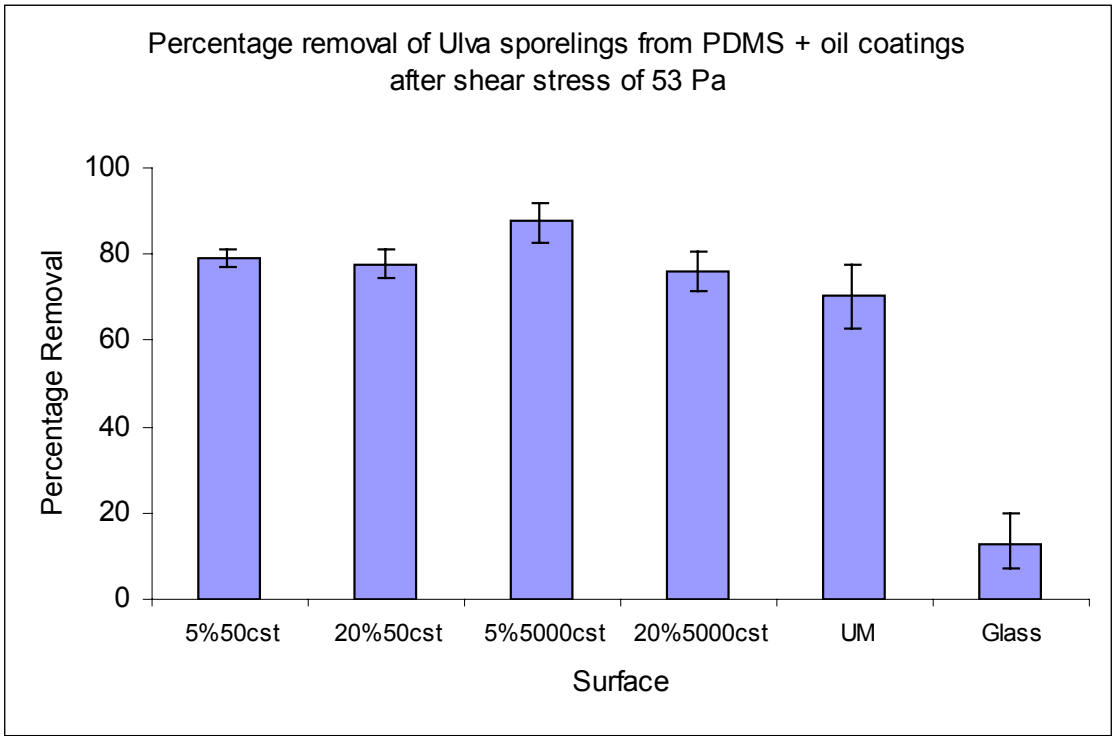

Figure 4-10: Quantification of % removal of *Ulva* sporelings after exposure to flow (53 Pa) from oil-laden smooth PDMSe slides as determined by biomass method. Each point represents the mean percentage removal 3 replicate slides. Bars represent 95 % confidence limits derived from arcsine transformed data.

Assays with Respect to Oil Modification: 5μm Channels and Pillars with 5, 10, and 20μm spacing

***Ulva* zoospore settlement characteristics**

A study was launched to ascertain the effects of the combination of topography and oil additive factors. An initial group of slides were shipped in September of 2001, but due to high variation in sample thickness, the slides were deemed unusable for flow cell experiments. In March and April of 2002, a large number of these patterned slides were shipped (Table 4-4).

Table 4-4: Slides shipped for zoospore assay with respect to oil addition and topography

Number of Slides	Formulation	Topography	Date Shipped
24	Unmodified	None	3/02-4/02
12	Unmodified	5μm ridge pattern, 1.5μm deep	3/02-4/02
12	Unmodified	5μm ridge pattern, 5μm deep	3/02-4/02
24	5% 50cSt PDMS oil	None	3/02-4/02
12	5% 50cSt PDMS oil	5μm ridge pattern, 1.5μm deep	3/02-4/02
12	5% 50cSt PDMS oil	5μm ridge pattern, 5μm deep	3/02-4/02
24	20% 50cSt PDMS oil	None	3/02-4/02
12	20% 50cSt PDMS oil	5μm ridge pattern, 1.5μm deep	3/02-4/02
12	20% 50cSt PDMS oil	5μm ridge pattern, 5μm deep	3/02-4/02
24	5% 5000cSt PDMS oil	None	3/02-4/02
12	5% 5000cSt PDMS oil	5μm ridge pattern, 1.5μm deep	3/02-4/02
12	5% 5000cSt PDMS oil	5μm ridge pattern, 5μm deep	3/02-4/02
24	20% 5000cSt PDMS oil	None	3/02-4/02
12	20% 5000cSt PDMS oil	5μm ridge pattern, 1.5μm deep	3/02-4/02
12	20% 5000cSt PDMS oil	5μm ridge pattern, 5μm deep	3/02-4/02

Patterned samples were prepared as described with the pattern layout as shown in the schematic in Figure 4-11. The substrates were conditioned and evaluated as described above, and both settlement and release data were assessed. The 20% 5000 cSt oil patterned samples were not evaluated because the patterned areas could not be located microscopically due to infilling by oil.

The results of this study were published in Hoipkemeier-Wilson, et al in Biofouling in 2004 [63].

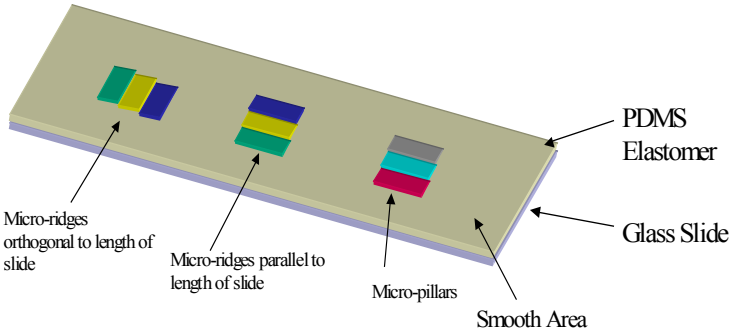

Key	Feature Width [um]	Valley Width [um]
	5	5
	5	10
	5	20
	5	5
	5	10
	5	20

Figure 4-11: Schematic of the initial topography study for channels and pillars.

Ulva zoospore settlement characteristics

The spore settlement density on the oil-laden patterned PDMSe slides are summarized in the following table and figures (table 4-5). Spore density counts were made on the flat area between the patterned areas on patterned slides as contrasted with counts from a smooth, completely unpatterned, PDMSe slide.

Table 4-5: Spore settlement density values for on oil laden patterned PDMSe slides. Each value is the mean of 90 counts, 30 from each of 3 replicates with standard error at 95% confidence limits.

Pattern area	Unmodified	5% 50cSt	20% 50cSt	5% 5000cSt
Smooth slide	562 ± 32	592 ± 35	615 ± 30	675 ± 40
Flat on patterned slide	482 ± 41	532 ± 39	538 ± 29	577 ± 34
5μm x 5μm channel	1740 ± 84	800 ± 68	761 ± 51	903 ± 108
5μm x 10μm channel	932 ± 58	562 ± 49	625 ± 40	1034 ± 148
5μm x 20μm channel	725 ± 60	490 ± 37	605 ± 38	772 ± 115
5μm x 5μm pillar	872 ± 72	467 ± 47	554 ± 28	610 ± 64
5μm x 10μm pillar	528 ± 50	442 ± 35	522 ± 38	522 ± 49
5μm x 20μm pillar	525 ± 42	435 ± 37	535 ± 33	504 ± 58
Smooth slide	562 ± 32	592 ± 35	615 ± 30	675 ± 40
Flat on patterned slide	498 ± 45	446 ± 59	557 ± 55	500 ± 43
1.5μm x 5μm channel	875 ± 80	608 ± 64	632 ± 55	498 ± 52
1.5μm x 10μm channel	558 ± 58	470 ± 54	456 ± 43	506 ± 48
1.5μm x 20μm channel	478 ± 58	412 ± 59	475 ± 34	528 ± 52
1.5μm x 5μm pillar	700 ± 70	468 ± 54	470 ± 48	494 ± 56
1.5μm x 10μm pillar	492 ± 50	438 ± 52	446 ± 47	534 ± 54
1.5μm x 20μm pillar	488 ± 55	464 ± 59	425 ± 44	534 ± 61

In general, the addition of oils to PDMS reduced settlement of *Ulva* spores. By averaging the spore density values for a given formulation over all topographies, the 5% 50cSt oil had the lowest settlement (515 ± 49) and the unmodified PDMSe had the greatest (689 ± 55). This trend was seen for most of the patterned slides, but not for the smooth slides. Overall, the 50 cSt oil reduced settlement more than the 5000 cSt oil (617 ± 64), but there appeared to be no benefit of increasing the concentration of the 50 cSt oil above 5% (515 ± 49 increased to 552 ± 40).

In general, the presence of channels promoted spore attachment (260% increase in spore settlement for 5μm deep, 5 μm wide channels in PDMSe relative to flat), although the effect was reduced by the addition of oils (~50% increase in spore settlement for 5μm deep, 5 μm wide channels in oil-laden PDMSe substrates relative to flat). In general there was lower settlement on the 1.5μm deep features as compared to 5 μm features. For example, the 5μm deep, 5μm wide channel increased spore settlement by 260%, but the increase in spore settlement density for the 1.5μm deep, 5 μm wide channel was 76%. These differences became less significant on the surfaces with oil especially on the surface with pillars.

The spore settlement density was not statistically different for the flat portions on the 5 μm deep versus the flat portions on the 1.5 μm deep patterned slides (Figure 4-12). The spore settlement density was slightly higher for the smooth unpatterned slides than for the flat area of the patterned slides (Figure 4-12).

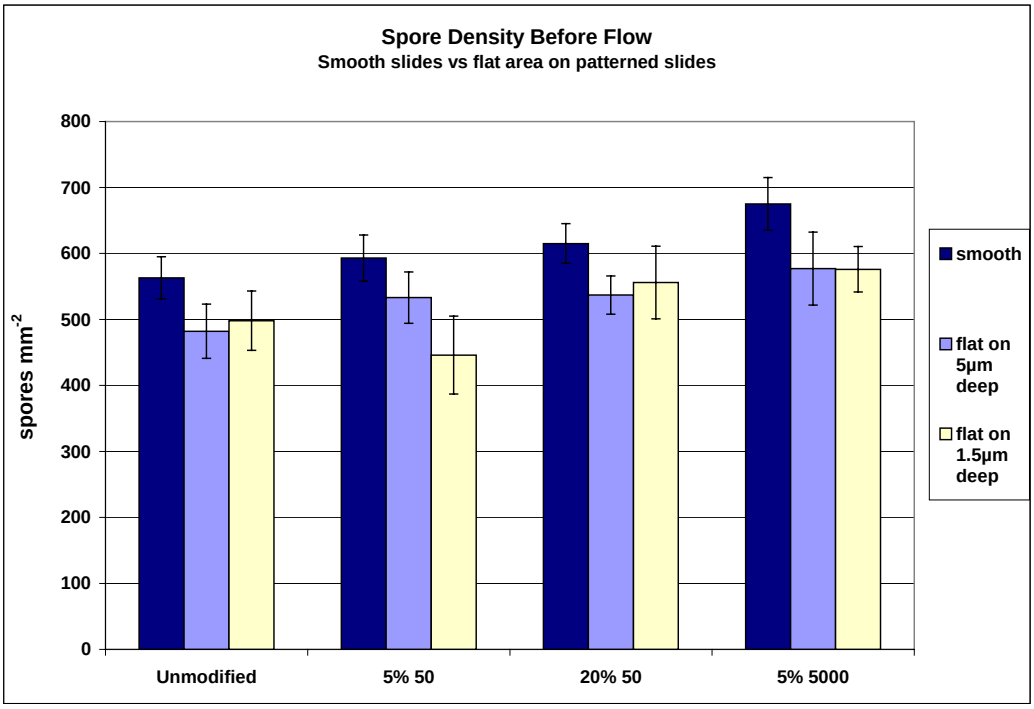

Figure 4-12: *Ulva* zoospore settlement density on oil laden patterned PDMSe slides. Each data point is the mean of 90 counts, 30 from each of 3 replicates. Error bars show 95% confidence limits.

Significantly greater numbers (>2x) of spores attached to the unmodified PDMSe surfaces with channels 5 μm wide compared to the surrounding flat PDMSe. Moreover, significantly greater numbers of spores attached to the PDMSe surfaces with the deeper (5 μm) channels compared to the shallower (1.5 μm) channels, the difference being particularly marked for the channels that were 5 μm wide (Figure 4-13). As stated before, the 5μm deep, 5μm wide channel increased spore settlement relative to flat by 260%, but the increase in spore settlement density relative to flat for the 1.5μm deep, 5 μm wide channel was only 76%. Figure 4-13 shows the spore settlement density data for the 5μm and 1.5 μm deep patterns in the unmodified PDMSe substrates. The effect oil oils on these patterns is depicted in the plots in Figure 4-14.

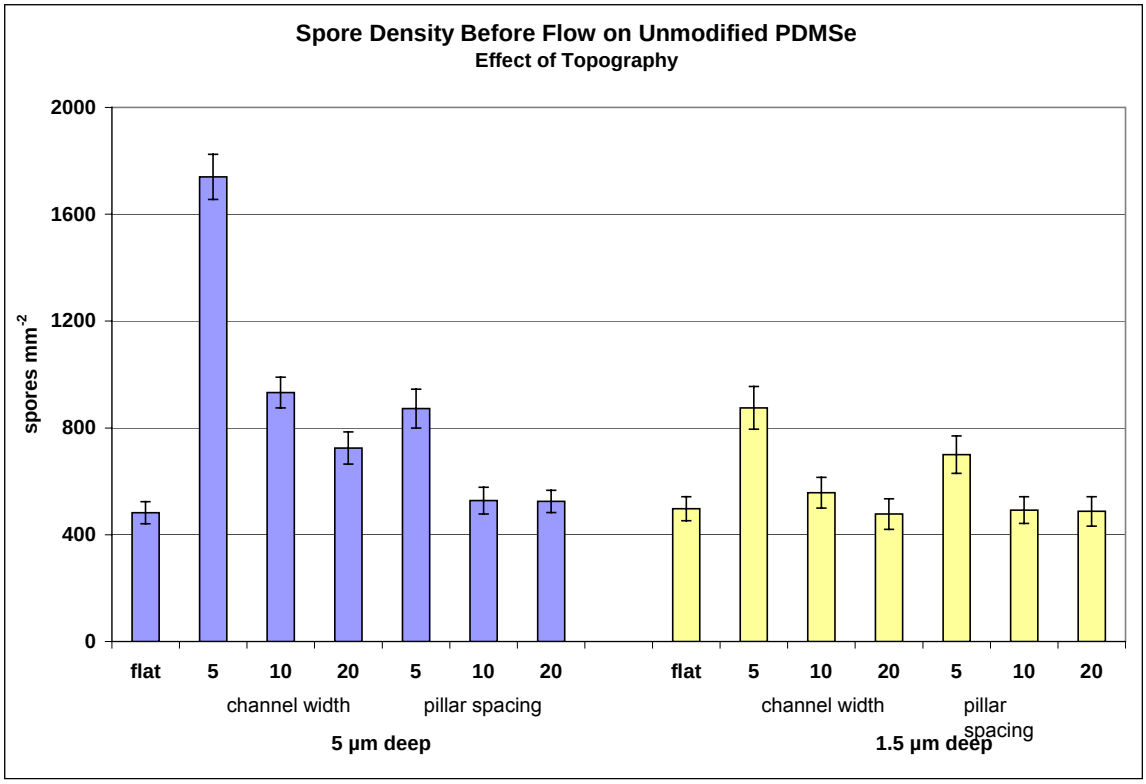

Figure 4-13: *Ulva* zoospore settlement density on unmodified smooth PDMSe slides: effect of topography. Each data point is the mean of 90 counts, 30 from each of 3 replicates. Error bars show 95% confidence limits.

The addition of oils to PDMSe reduced settlement of *Ulva* spores in the 5-µm deep channels (Figure 4-14). There were significantly fewer spores settled in the 5-µm deep channels when the concentration of the 50 cSt oil was increased from 5 to 20% but for the shallower channels (1.5 µm deep), there was only a slight benefit of increasing the concentration of the 50 cSt oil above 5%. In general, the presence of channels promoted spore attachment, although the effect was reduced by the addition of oils. Furthermore, there was generally lower settlement on the 1.5 µm deep features as compared to 5 µm features, but the differences became less pronounced on the surfaces with oil especially on the surface with pillars (Figure 4-14 and 4-15).

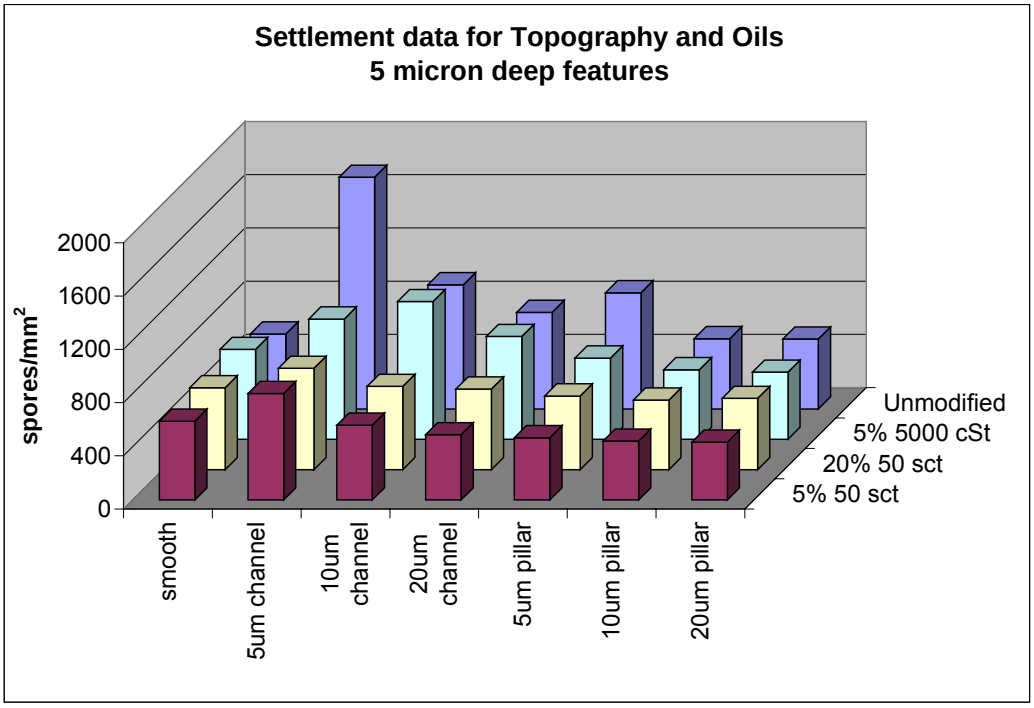

Figure 4-14: *Ulva* zoospore settlement density on oil laden 5μm deep patterned PDMSe slides. Each data point is the mean of 90 counts, 30 from each of 3 replicates.

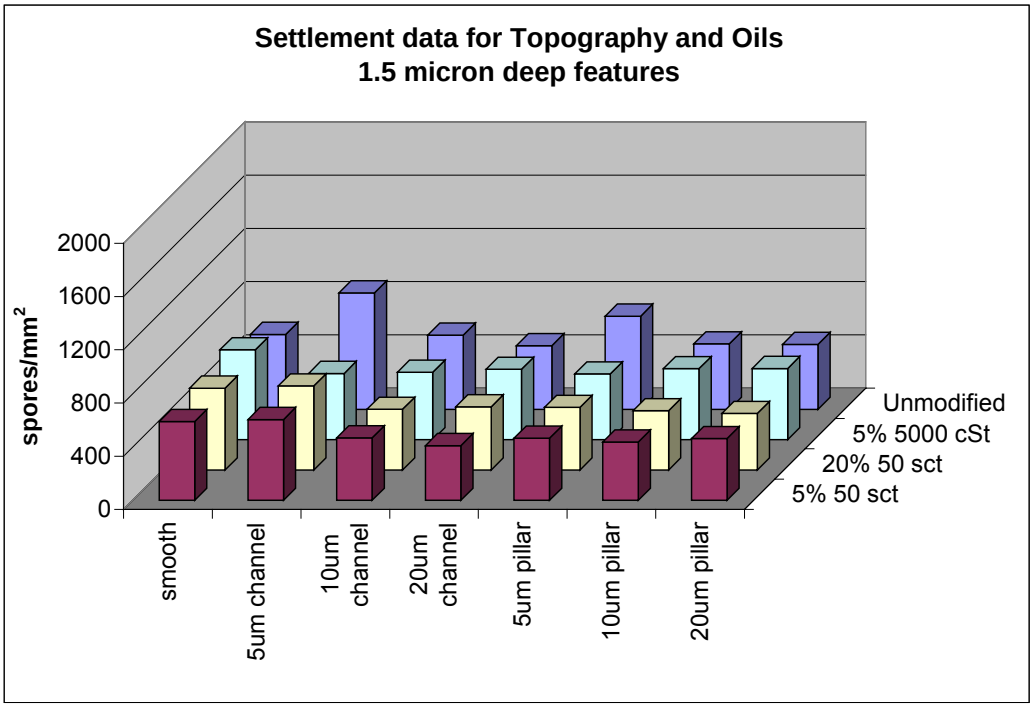

Figure 4-15: *Ulva* zoospore settlement density on oil laden 1.5 μm deep patterned PDMSe slides. Each data point is the mean of 90 counts, 30 from each of 3 replicates.

For all formulations, except the 5% 5000 cSt oil-modified 1.5 μm deep pattern, there was a significant increase in spore settlement for the 5 μm wide channels (Figure 4-14 and 4-15). For all feature widths, except for the 10 and 20 μm pillars, there was lower settlement with 1.5 μm features compared to 5 μm features (Figure 4-14 and 4-15).

Ulva zoospore release characteristics

Overall, the density of settled spores was significantly reduced by turbulent flow at a wall shear stress of 56 Pa, on all PDMSe surfaces. The data expressed as percentage removal are summarized in the following tables and figures.

Table 4-6: Calculated percent removal data of Ulva zoospore after exposure to flow from oil laden patterned PDMSe slides. Each value is the mean of 90 counts, 30 from each of 3 replicates with standard error at 95% confidence limits derived from arcsine transformed data.

Pattern area	Unmodified	5% 50cSt	20% 50cSt	5% 5000cSt
Flat on patterned slide	66.7±2.2	70.4±3.2	66.2±3.0	78.1±1.7
5μm x 5μm channel	31.4±3.1	36.3±4.0	39.7±3.8	40.3±2.2
5μm x 10μm channel	50.1±3.5	45.4±3.3	46.8±2.9	47.5±1.5
5μm x 20μm channel	48.8±2.0	48.3±2.1	46.1±1.6	48.7±1.7
5μm x 5μm pillar	67.9±4.0	51.8±5.3	65.0±3.0	46.6±3.7
5μm x 10μm pillar	60.4±3.7	49.0±2.2	51.4±2.7	51.3±3.6
5μm x 20μm pillar	62.1±3.7	51.7±3.1	56.0±3.6	59.6±3.8
Flat on patterned slide	57.0±3.7	60.3±2.9	55.7±4.9	55.4±3.5
1.5μm x 5μm channel	55.9±3.3	58.0±3.2	58.7±2.6	48.9±2.3
1.5μm x 10μm channel	51.9±2.3	52.5±3.4	51.1±1.5	45.2±2.4
1.5μm x 20μm channel	53.1±1.3	54.7±1.8	51.6±3.6	45.5±2.8
1.5μm x 5μm pillar	51.9±4.4	63.5±3.0	59.5±2.2	57.3±3.2
1.5μm x 10μm pillar	49.0±3.6	58.5±2.3	57.9±2.1	58.0±1.7
1.5μm x 20μm pillar	51.6±3.5	60.9±2.3	58.8±1.8	57.3±1.9

The orientation of the channels parallel with the flow predictably increased spore removal under shear flow conditions compared to channels oriented orthogonal to the direction of the flow (Figure 4-16). The orientation of channels

parallel to flow resulted in a 34% increase the percent removal relative to those oriented orthogonal to flow. This relative change with respect to flow cell orientation was minimized for the 5% 5000cSt oil-laden samples. This is explained by the fact that this formulation had the greatest amount of feature infilling. Thus, these spores had the highest profile in the flow cell. The 20% 50 cSt oil-laden samples had the greatest change with respect to orientation followed by 5% 50 cSt and unmodified samples. Further studies always oriented channels parallel to flow.

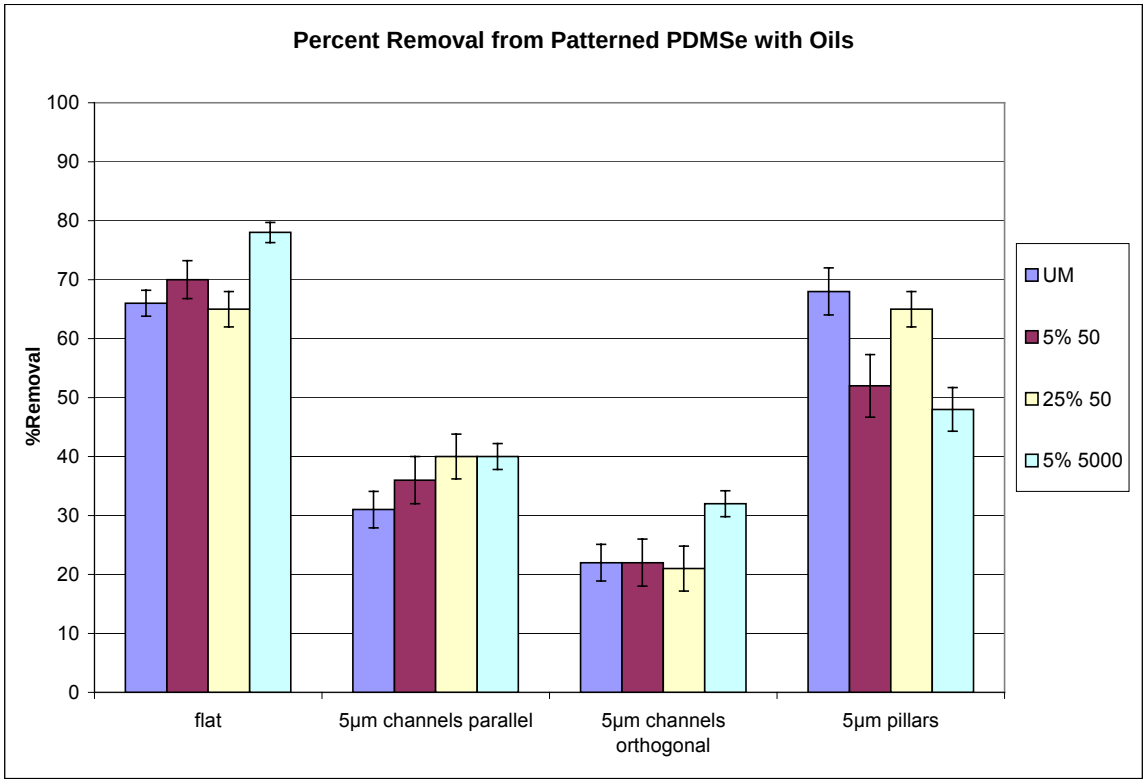

Figure 4-16: Calculated percent removal data for *Ulva* zoospores removed after exposure to flow channel on oil-laden patterned PDMSe slides. Each point represents the mean percentage removal of *Ulva* zoospores from 90 observations from 3 replicate slides. Bars represent 95 % confidence limits derived from arcsine transformed data.

The topography type was the most significant variable for percent removal and spore density after exposure to flow. The presence of pillars as opposed to

channels decreased the spore density after flow and increased the overall percent removal.

While the spore settlement density was not statistically different for the unpatterned slides and for the flat portions on the 5 μm deep versus 1.5 μm deep patterned slides, the adhesion characterized by the mean spore density after flow was significantly less on the flat portions on the 5 μm deep slides (Figure 4-16). Additionally, the percent release data indicate that spores release substantially more readily from the flat areas of patterned slides than unpatterned slides. This may indicate that particularly tenacious spores will seek out the patterned area leaving the weaker spores to the flat portion.

Ulva Zoospore Settlement Assays with Respect to Topography: 5-μm Channels and Pillars with 1, 3, and 5-μm Spacings

A preliminary experiment was launched in May of 2002 to look at a design incorporating 1-5 micron spaced channels and pillars. Our primary objective was to determine if these dimensions could deter spore settlement. Flow cell studies were not performed.

The designs are shown in Figure 4-17. The depth of these patterns was roughly 1.5μm. The first is a series of 5-micron ridges separated by 1, 3, or 5 micron ridges. The second pattern was 5-micron pillars with the spacing varied from 1 to 3 to 5 microns. One each of these patterns was sent to the Callows to be evaluated for spore settlement. A batch of 4 slides patterned with 2-micron ridges spaced by 2-micron channels was also assayed at this time, and the results are discussed in the following section.

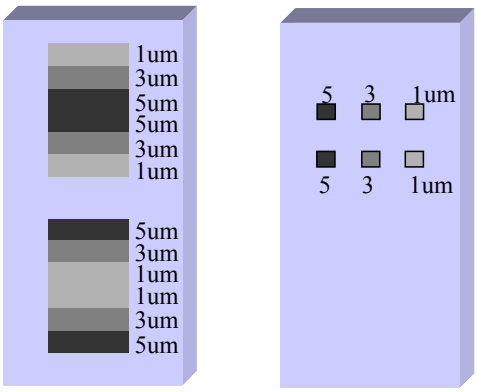

Figure 4-17: Schematic of new designs to evaluate smaller spacings and smaller features.

The patterns were gradients of texture with the spacing of the channels providing the method of developing the gradient. Manoj Chaudhury's recent study involving chemical gradients was the basis for this proposed study. It was intended that a gradient could be created by variation of surface area for a given surface chemistry as based on theories of wetting on topographically modified surfaces (I.e. Wentzel, Cassie and Baxter). However for this pilot study, the patterns were not perfectly aligned to produce the desired effect. Additionally, the fidelity of the pillar pattern decreased with decreasing spacing. The assay was still performed so that we could ascertain the possible effects of these dimensions on spore settlement. The spore settlement counts are not statistically significant due to the problems with these patterns and the lack of replicates.

However, there appeared to be no difference in the number of spores that settle on the patterned areas compared to the flat area within each subset of surfaces (Figure 4-18). Settlement on the flat and patterned areas of the pillar slide was less than those areas on the channel-patterned slide. The depth of these channels was <1.5 μm deep. The validity of this study was called into

question given the fact that the 5μm channels did not show the dramatic increase in zoospore density seen in previous studies.

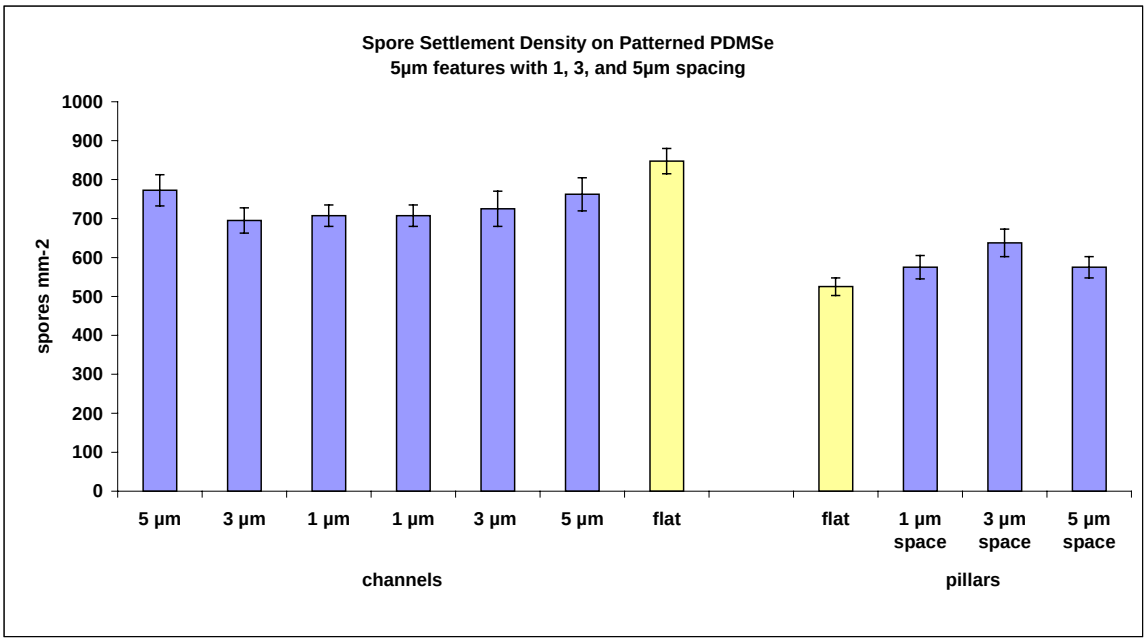

Figure 4-18: Spore settlement density for 5 μm channel and pillar designs with smaller spacings. Each data point is the mean of 30 counts from a single replicate. Error bars show 95% confidence limits.

Per the visual assessment of the Callow group, the majority of the spores settled on the 1μm wide channel pattern appeared to settle on the tops of the 5μm wide ridges adjacent to the channels, whereas the spores settled in the 5 and 3μm wide channels. For the 5 and 3μm spaced pillars, the majority of the spores settled between the pillars, whereas the settlement location was random for spores on the 1μm spaced pillars.

When the channel width or pillar spacing decreases and becomes too narrow for spores to penetrate, the spores settle on top of the feature but still attempt to locate the depressed area. This positioning may actually occur after

initial settlement as the spore goes through ‘space-filling’ movements during the secretion of its adhesive [200].

This pilot experiment did not prompt a full study since there was not an apparent difference in spore settlement density for the patterned areas compared to the flat area for these dimensions. This effect may be due to the shallow depth of these patterns. It was also proposed that the spore cannot detect a difference between flat surfaces and features with spacing less than half that of the spore diameter.

Ulva Zoospore Settlement Assays with Respect to Topography: 2-micron Channels and Pillars

A study with 2-micron channels was launched to evaluate features that were less than half the diameter of the average spore body. Three separate assays were performed on slides modified with 2-micron channels separated by 2-micron ridges. The pattern depth was approximately 1.5 microns. A total of 15 slides with three replicate patterns per slide were assayed.

The net result of the experiments was that there was not a significant difference in either spore settlement or release for the 2μm pattern as compared to the flat area (Figure 4-19). In the previous study, as the channel spacing decreased for 3μm to 1 μm in the previous study, the spores simply settled on top of the 5 μm ridges between the 1μm channels. For this study, both the channels and the ridges between these channels were less than the spore body. All larger features and spacings in previous studies had yielded a consistent increase in spore settlement with topographies of this geometry.

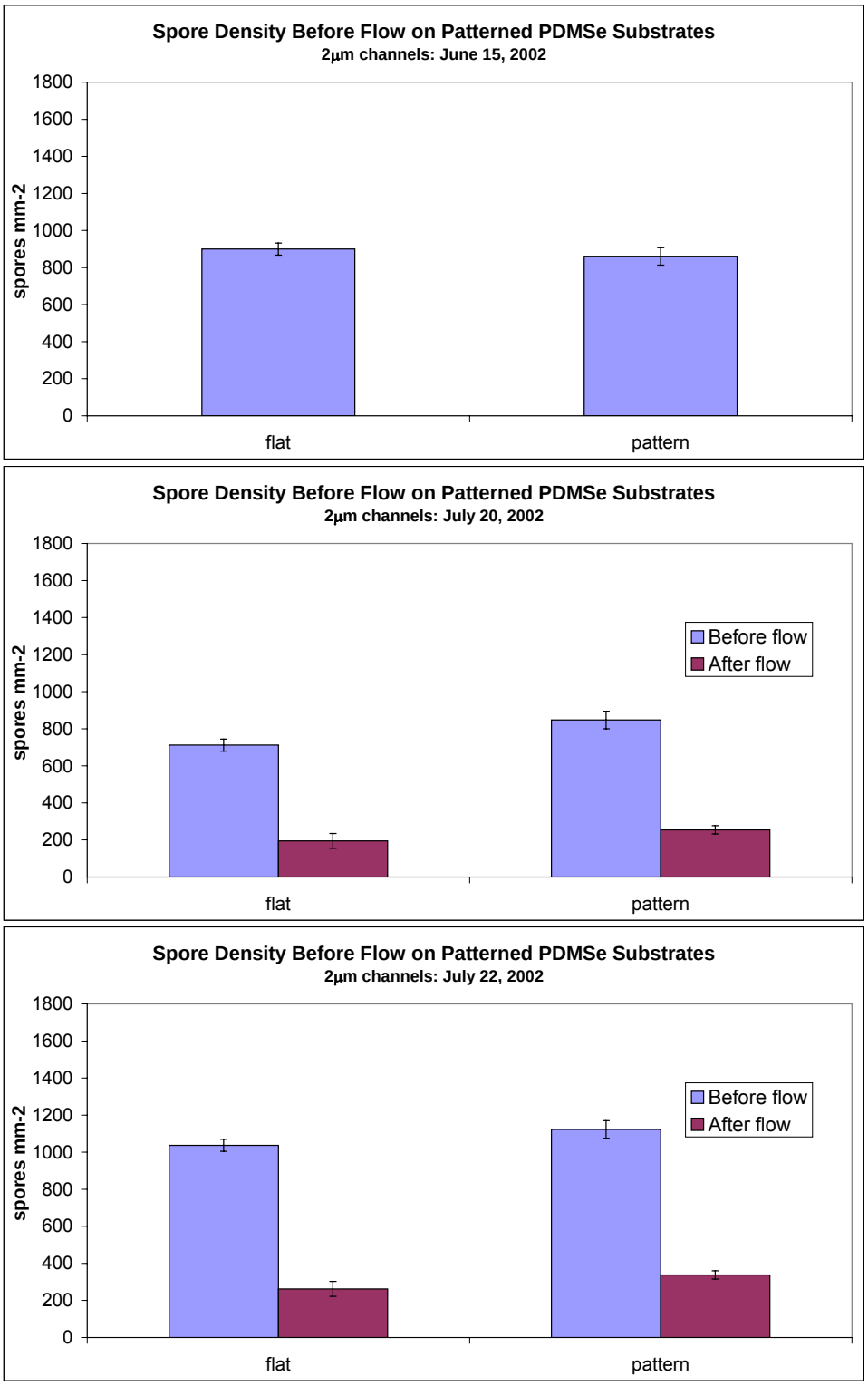

Figure 4-19: Spore density before and after exposure to flow for 2 μm channels in unmodified PDMSe. Each data point is the mean of 90 counts, 30 from each of 3 replicates. Error bars show 95% confidence limits.

The fact that there was not a statistically significant difference in spore settlement density or spore density after exposure to flow indicated the possibility that 2 microns is a critical topographical dimension for *Ulva* spores. The best results for topographical modification of PDMSe with these geometries thus far was obtaining values similar to that seen on flat. Future studies in the Brennan group examined different geometries to produce patterned substrates that could perform better than flat substrates.

Conclusions

The effects of oil addition and topographical modifications in PDMSe were evaluated for bioresponse with respect to the algae *Ulva* and *Amphora*. The PDMS oils were not effective in minimizing fouling or maximizing foul release, in fact oils of increasing viscosity were found to significantly increase the number of spores settled before flow and attached after flow directly.

For the oil-laden topography study, with the exception of some of the oil-laden pillars, flat substrates typically exhibited the lowest settlement and highest percent removal values. Based on the pilot studies with the 2 μm features this effect appears to be due to the scale of topography chosen in this analysis.

Future studies will take advantage of the fact that the topographical feature size must be less than the critical dimension required for the organism. For *Ulva* spores, this critical size is smaller than that of the spore body. This dimension will initiate an energetically unstable condition for settlement.

CHAPTER 5
SURFACE MODIFICATION OF SILICONE ELASTOMERS

Introduction

Surface Modification of Silicone Elastomers

The surface of a PDMS elastomer is considered to be relatively inert or non-reactive due to the closely packed methyl groups at the surface. Surface modification of PDMSe therefore requires some sort of surface activation. Some chemical treatments employed for surface activation of PDMS elastomers have included etching, surface oxidation, and hydrosilylation [203]. Surface modification of the activated PDMSe by other polymers has been achieved through simple physadsorption, covalent coupling, and graft copolymerizations. Additional research has focused on bulk modifications, such as block copolymerizations in which one of the polymers will migrate toward the surface. This has also been achieved with the use of surfactants.

The research here presented involves a wet chemical activation of the PDMSe surface rather than for example a plasma treatment, which is more common. Short durations of argon plasma exposure can produce Si-H groups at the surface of PDMSe [175]. Via hydrosilylation, any vinyl-functionalized molecule can subsequently be covalently bonded to the surface. Argon plasma treatment followed by exposure to ambient air leads to the formation of Si-OH and Si-CH_2OH groups on the surface of the silicone elastomer [174]. Oxidized silicone can then be reacted with a suitable silane based coupling agent. Long

plasma exposure times lead to the formation of a silica-like layer. Coupling agent can also bond to this silica layer. These plasma treatments produce a very disorganized surface of various hydroxyl and carboxylic groups. The treatment can also produce a significant increase in the surface modulus of the PDMSe and can impose a significant change in the roughness of the surface. For these reasons, a wet chemical based hydrolysis of the PDMSe is proposed for this research. The acid and base catalyzed surface hydrolysis of PDMSe has been documented (Figure 5-1). This should lead to a significantly simpler surface composed of primarily surface silanols. Ideally this process will affect neither the

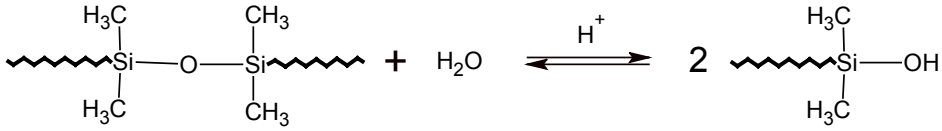

modulus nor the roughness of the surface.

Figure 5-1: Proposed hydrolysis of PDMSe

Silane Based Coupling Agents

Coupling agents are compounds that possess the ability to bond simultaneously to organic and inorganic materials. They have the generalized form R-$(CH_2)_n$—Si–X_3. Where R is an organofunctional group, $(CH_2)_n$ is described as a linker or chain extender, Si is a silicon atom, and X is a hydrolysable group such as a halogen, an amine, or an alkoxy group such as –OCH_2CH_3 or –OCH_3. Coupling agents are typically used to increase adhesion e.g. polymers bonded to glass or silica fillers or the ATS coupling agent used to adhere the silicone elastomer to the glass microscope slides. But as seen in this

research, the R group described above can be a polymer itself. These silane-derivatized polymers can be coupled directly to a substrate.

Reactions of these sorts of silanes involve 4 critical steps (Figure 5-2);

1) Hydrolysis of the alkoxysilane
2) Condensation
3) Hydrogen bonding to surface
4) Covalent bond formation

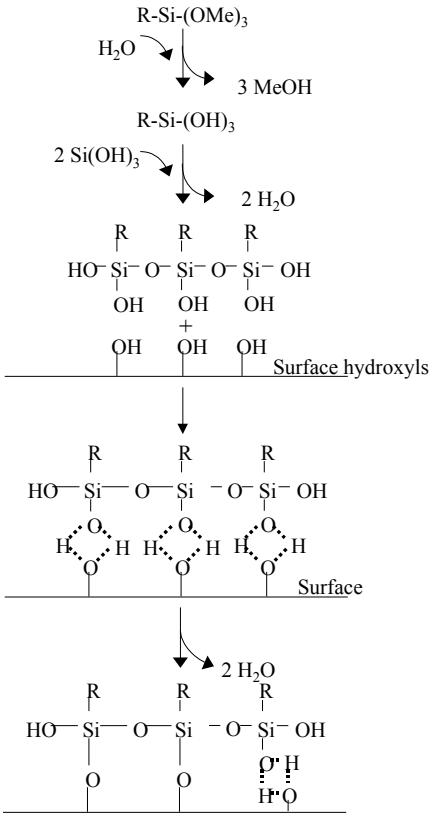

Figure 5-2:Reaction pathway for surface modification by silane coupling agents

It is necessary that the substrate possess hydroxyl groups in order to bond with the alkoxysilane. This is the predominant reason for the surface activation of the PDMSe. The acid catalyzed hydrolysis will produce a number of surface-active hydroxyls.

Materials and Methods

Silicone Surface Treatments

PDMSe coated glass microscope slides

Silicone coated microscope slides were prepared as described above. Briefly, 10 parts of the Silastic T2® base resin were thoroughly mixed with 1 part of the curing agent. The mixture was degassed and poured over glass microscope slides that had been treated with allyltriethoxysilane, ATS, coupling agent. The silicone was cured at room temperature for twenty-four hours between two glass plated with spacers to achieve a silicone thickness of ~700-1000μm.

To prepared the patterned slides, the degassed silicone mixture is also poured onto an etched and HMDS treated silicon wafer, which is covered by a top plated to achieve a silicone thickness of ~200-600μm. Once cured, this freestanding silicone replicate is trimmed and suctioned pattern side down to a clean glass plate. Microscope slides are treated with the ATS and taped to a separate glass plate. More silicone is mixed, and degassed, and poured onto the backside of the silicone replicates. The glass plate with the treated glass slides is slowly lowered onto the uncured silicone such that the slides line up with the patterned silicone as desired. Spacers are located in the corners of the bottom glass plated to achieve a total silicone thickness of ~700-1000μm. The silicone is then cured at room temperature for twenty-four hours.

After cure, the silicone coated microscope slides prepared in this manner were then removed from the glass plates and excess silicone was trimmed away from the edges of the microscope slides.

Hydrolysis of PDMSe

In order to determine the optimal hydrolysis conditions, 1 and 3 molar solutions of both KOH and HCl were prepared with nanopure water. Silicone slides were washed with ethanol, dried under a nitrogen stream, and placed onto glass incubation racks in glass containers. The containers were subsequently filled with either the acid or base. Individual slides were removed at predetermined intervals and evaluated with captive air bubble water contact angle and ATR.

For the samples prepared for *Ulva* bioassays, 3M HCl was used. The HCl was prepared fresh for each batch of slides. Individual slides were cleaned by soaking in ethanol, wiping with a chem-wipe, and then dried under a nitrogen stream. Slides were placed into incubation dishes, which were then filled with HCl. The dishes were placed briefly in a liquid N_2 trapped vacuum oven to remove air bubbles trapped at the silicone surface. The slides remained in the HCl for 4hours, at which point the silicone became as or more hydrophilic than the glass it was backed to as evidenced by lifting a slide out of the aqueous HCl and observing the runoff.

The slides were then rinsed with nanopure water and placed immediately into a 50mL centrifuge tube filled with nanopure water. Slides prepared in this manner were designated PDMSe-OH or hydrolyzed PDMSe. Slides, which would receive subsequent silane treatment, were washed in nanopure water and

then with 95% ethanol (aq) and placed onto a chem-wipe into a disposable petri dish and immediately covered with a layer of the appropriate silane treatment.

Silane treatments

Poly(ethylene glycol). Monomethoxy poly(ethylene glycol) trimethylsilyl ether (m-PEG-silane) (CAS: 132068-85-0) was originally received from Biolink Life Sciences, Inc. This product was discontinued in September of 2004 after which it was obtained from Nektar Therapeutics (formerly Shearwater Corporation). The product, an off-white powder, was stored in the freezer with desiccant and used without further purification. This material from both suppliers had a reported molecular weight of 5,000g/mol.

A 5mg/ml solution of the m-PEG-silane was produced in a 95% aqueous ethanol with a pH of ~4. Approximately 60-mL of 90-proof ethanol was acidified by the addition of 7 drops of glacial acetic acid and the pH was monitored. This acidified ethanol was reserved for the production of the various silane solutions. The m-PEG-silane was weighed out into a 15ml centrifuge tube. One drop of nanopure water was added followed by the necessary amount of acidified ethanol. The addition of the water drop greatly enhanced the rate of dissolution of the m-PEG-silane in the acidified ethanol. This solution was allowed to react with stirring for 2 hours, during which time the silicone slides were being hydrolyzed.

When the time for hydrolysis was complete, silicone slides were removed from the HCl wash, rinsed with water and ethanol, and then placed onto a chem-wipe in individual disposable petri dishes. The m-PEG-silane solution was pipetted onto the surface of the hydrolyzed PDMSe such that the surface was

completely covered. The petri dish lid was then placed onto the petri dish. This kept the humidity high inside the petri dish so that the silane solution would not evaporate. Evaporation during an aqueous ethanol deposition leads to uneven coverage and can lead to multilayer deposition as the concentration increases unevenly across the surface. In the case of mild evaporation, more solution was added to the surface.

The slide was left undisturbed for 1 hour, after which the slide was rinsed with copious amounts of ethanol to remove any silane that was not hydrogen bonded to the surface. The slide was dried in a stream of nitrogen and placed in an 80°C oven to cure for 20 minutes. The slide was then placed in a 50ml centrifuge tube for shipping. Slides were typically produced the day before shipping to the Callow group in England for bioassay with respect to *Ulva* spores. The centrifuge tubes were filled with nano-pure water just before shipping. A replicate was kept in-house under the same storage conditions and tested for water contact angle the same day the other samples were bioassayed.

Polysulfone. Udel polysulfone was obtained from Solvay Advanced Polymers. The polysulfone was sulfonated in order to achieve functional groups that could be coupled to the hydrolyzed PDMSe substrates. This form of deposition led to a greater than monolayer coverage of the polysulfone. Therefore, in late 2004, α,ω-hydroxyl terminated polysulfone was obtained from Polysciences, Inc. This polymer was then end derivatized to obtain α,ω-silane terminated polysulfone. The methods for the sulfonation of Udel and its coupling to the PDMSe-OH with

GPS and the derivatization reaction of the PSf-OH and its deposition on PDMSe will be briefly described.

Sulfonation of Polysulfone. Approximately 3 grams of dried Udel polysulfone polysulfone was weighed out and transferred to a clean dry 100ml three-neck round bottom flask. To this approximately 30ml of distilled 1,1,2-trichloroethane was added. Once the polysulfone was fully dissolved the solution was bubbled with argon for ten minutes. The required amounts of chlorotrimethylsilane and chlororsulfonic acid were calculated based on the desired stoichiometry of the reaction. The molar equivalents of chlorosulfonic acid to polysulfone repeat unit was varied between 0.5 to 3.5. Chlorotrimethylsilane was always added in slight molar excess to the chlorosulfonic acid. This was added slowly via syringe and allowed to fully distribute throughout the polysulfone mixture. The chlorosulfonic acid was then diluted with trichloroethane and added over twenty minutes via addition funnel.

After the desired reaction time, the reaction was bubbled with argon until no further evolution of HCl gas was detected visually. The polymer solution was slowly poured into stirred methanol to allow for precipitation of the polymer and removal of the CTMS. The majority of the methanol was decanted and additional methanol was added. This slurry was stirred thoroughly and the poured through a polypropylene mesh to collect the polymer precipitate. The polymer was dried in air overnight and then in a 75°C oven for 4 hours. Sulfonated polysulfone prepared in this manner was designated s-PSf. The s-PSf was then dissolved to a 5-wt% concentration in dimethylformamide (DMF).

Grafting of Sulfonated Polysulfone. The s-PSf was grafted onto the surface via a glycidoxypropyltriethoxysilane-coupling agent (GPS) received from Gelest, Inc. The GPS solution was prepared using the acidified ethanol prepared in the PEG-silane section. To this acidified ethanol, 0.17ml of neat glycidoxypropyltriethoxysilane was added. The GPS solution was allowed to stir for at least 5 minutes, which allowed for the hydrolysis of the silanes.

Hydrolyzed silicone slides were removed from the HCl wash, rinsed with water and ethanol, and then placed onto a chem-wipe in individual disposable petri dishes. The GPS solution was pipetted onto the surface of the PDMSe-OH such that the surface was completely covered. The petri dish lid was then placed onto the petri dish. The slide was left undisturbed for 20 minutes, after which the slide was rinsed with copious amounts of ethanol to remove any silane that was not hydrogen bonded to the surface. The slide was dried in a stream of nitrogen and placed in an 80°C oven to cure for 20 minutes.

After reaction with the GPS coupling agent, the slides were dipped into a 5-wt% solution of s-PSf in DMF for 20 minutes. Any unreacted s-PSf was rinsed away with excess DMF and finally with ethanol and dried in a nitrogen stream. The slide was then placed in a 50ml centrifuge tube and filled with nano-pure water just before shipping. A replicate was kept in-house under the same storage conditions and tested for water contact angle the same day the other samples were bioassayed.

Silane derivatization of Polysulfone (OH-terminated). Hydroxyl terminated polysulfone was derivatized with isocyanatopropyltriethoxysilane (ICPES) using

urethane chemistry. The catalyst used was 1,4 diazabicyclo[2.2.2]octane rather that the more common tin catalyst due to concerns with toxicity for the *Ulva* bioassays. 2 g of PSf-OH and 20mg (0.12 molar equivalents) of the tertiary amine catalyst, DABCO were dissolved in 20ml of 1,1,2-trichloroethane in a sealed 50ml round bottom flask. To this was added 0.5g (1.2 molar equivalents) of ICPES slowly via syringe. The reaction was allowed to proceed at room temperature for 72 hours. The silane-terminated polymer was precipitated into stirred methanol and excess methanol was removed via Buchner filtration. The catalyst is soluble in methanol and was thus removed. The polymer, PSf-silane, was then oven dried prior to further use.

The resulting off-white powder was used to produce a 5mg/ml solution. The powder was not completely soluble in ethanol, although it had increased solubility as compared to PSf-OH. It is important to have the polymer silane completely dissolved in order to obtain a consistent surface treatment. Thus the PSf-silane was dissolved in a 70:30 mixture of the acidified ethanol and 1,1,2-trichloroethane. This combination of solvents yielded a clear solution with a yellowish tint.

A PDMSe-OH slide was removed from the HCl wash, rinsed with water and ethanol, and then placed onto a chem-wipe in a disposable petri dish. The PSf-silane solution was pipetted onto the surface of the hydrolyzed PDMSe such that the surface was completely covered. The petri dish lid was then placed onto the petri dish. The slide was left undisturbed for 1 hour, after which the slide was rinsed with trichloroethane followed by ethanol to remove any silane that was not

hydrogen bonded to the surface. The slide was dried in a stream of nitrogen and placed in an 80°C oven to cure for 20 minutes. The slide was then placed in a 50ml centrifuge tube and filled with nano-pure water just before shipping. A replicate was kept in-house under the same storage conditions and tested for water contact angle the same day the other samples were bioassayed.

Perfluoropolyether, PFPE. Monofunctionalized perfluoropolyether alcohol, m-PFPE-OH was initially obtained as a sample from a research group at the University of North Carolina. Their research involved using this hydroxyl terminated polymer as a crosslinking reagent in an isocyanato-based polyurethane reaction. Using similar chemistry scheme, this monofunctional alcohol was reacted with ICPES in the presence of a catalytic amount of DABCO, resulting in a monotriethoxysilane terminated PFPE, mPFPE-silane.

When more material was required, I was referred to DuPont. In addition to samples of the m-PFPE-OH, they also offered samples of m-PFPE-silane. The commercial names are Krytox alcohol and Krytox-silylamide. Both treatments resulted in sufficient surface treatment, but the silyl amide functionalized polyether resulted in a higher degree of surface functionalization with fewer processing steps. Thus it was used once it became available. The methods for the derivatization reaction of the PFPE-OH and its deposition on PDMSe will be briefly described as well as two methods for the deposition of the PFPE-silyl amide.

Silane derivatization of Perfluoropolyether. The monofunctional perfluoropolyether alcohol was derivatized in the flowing scheme. Approximately

2 grams of PFPE-OH and 2 mg of the tertiary amine catalyst DABCO were dissolved in 10 ml of 1,1,2-trichlorotrifluorethane in a sealed 50 ml round bottom flask. To this was added 0.5g of ICPES slowly via syringe. The reaction was allowed to proceed for 3 days.

To the PFPE-silane in trichlorotrifluoroethane solution, 95% ethanol and acetic acid were added to obtain a 2.5wt% mixture of the PFPE-silane. This was then deposited on the surface of a hydrolyzed PDMSe slide. After sufficient time was allowed for the surface condensation reactions, the excess PFPE-silane was rinsed with trichlorotrifluoroethane and subsequently with ethanol.

Alternately, the isocyanatopropyltriethoxysilane was deposited onto the surface of the hydrolyzed PDMSe slide as per the procedure for deposition of GPS described above. Once the coupling agent was fully cured to the surface of the PDMSe-OH, a mixture of 10wt% PFPE-OH in trichlorotrifluoroethane with DABCO was deposited on to the surface. The reaction was allowed to procede for one hour. Any nonreacted polymer was rinsed off with trichlorotrifluoroethane and subsequently with ethanol.

Deposition of Perfluoropolyether-silyl amide.

The Krytox-silyl amide was a viscous liquid that was deposited directly onto the hydrolyzed PDMSe slide via transfer pipette. These slides were placed into a 50°C vacuum oven, and the reaction was allowed to proceed under gentle vacuum for one hour. This bulk deposition process resulted in a very thick viscous layer of the PFPE on the slides. Thus the slides were immersed in trichlorotrifluoroethane to remove any non-reacted polymer.

The trichlorotrifluoroethane was found to swell the PDMSe on the slide. The slides were removed from the solvent and rinsed with ethanol and dried thoroughly under an argon stream. From subsequent bioassays using slides produced by this technique, it was determined that there was some toxicity not found in previous samples. It was not clear whether this was due to residual solvent or to the silyl amide functionality.

Due to the similarity of the isocyantopropyltriethoxysilane derivatized PFPE and the PFPE-silyl amide structures, it was assumed that this toxicity was related to the residual solvent. Thus subsequent slides were treated in a manner similar to the treatment of the original slides. The PFPE-silyl amide was deposited from a 2.5 wt% aqueous alcohol solution. The viscous liquid was not completely soluble in ethanol. Thus the PFPE-silane was dissolved in a 70:30 mixture of the acidified ethanol and trichlorotrifluoroethane. This combination of solvents yielded a clear solution with a yellowish tint.

A PDMSe-OH slide was removed from the HCl wash, rinsed with water and ethanol, and then placed onto a chem-wipe in a disposable petri dish. The PFPE-silane solution was pipetted onto the surface of the hydrolyzed PDMSe such that the surface was completely covered. The petri dish lid was then placed onto the petri dish. The slide was left undisturbed for 1 hour, after which the slide was rinsed with trichloroethane followed by ethanol to remove any silane that was not hydrogen bonded to the surface. The slide was dried in a stream of nitrogen and placed in an 80°C oven to cure for 20 minutes. The slide was then placed in a 50ml centrifuge tube and filled with nano-pure water just before

shipping. A replicate was kept in-house under the same storage conditions and tested for water contact angle the same day the other samples were bioassayed.

Surface Characterization

Captive air bubble and sessile drop contact angle determination

Wettability was measured with an automated Ramé-Hart model 500 digital goniometer with a j-type needle. For captive air bubble measurement, silicone coated glass microscope slides were inverted onto a PMMA chamber filled with nano-pure water (17Ω). A j-type needle driven by a computer controlled syringe pump was used to inject 8 μl air bubbles onto the specimen surfaces. Images were acquired using the Ramé Hart DropImage Advanced software and were later analyzed with software available from FirstTenAngstroms.

To assess the state of the materials used for bioassays, replicate samples were prepared and kept in-house for testing on the day of *Ulva* analysis. Sessile drop time-lapsed analysis was also performed to visualize the rearrangement of the siloxane surface. A 10 μl drop was placed on a substrate and an image was acquired of said drop every minute for the first ten minutes, and then every five minutes thereafter for one hour.

Dynamic contact angle

Dynamic contact angles were taken on a Cahn dynamic contact analyzer using the Wilhelmy plate technique. Briefly, Wilhelmy plate contact angles are taken by advancing and withdrawing a thin film into a liquid. The force on the film is measured and correlated to the film displacement. Surface grafted PDMSe

were examined in nanopure water, DMF, formamide, and acetonitrile in clean polypropylene beakers.

Smooth films of were cast in between glass plates to achieve a thickness of 1 mm. Individual specimens were achieved by cutting the films into squares approximately 25 mm wide and 25 mm long.

PDMSe squares were placed into an Erlenmeyer flask, which was subsequently filled with 3M HCl. A Teflon coated stir bar was added and the squares were swirled in the HCl for 4 hours, allowing for even hydrolysis of all sides of the samples. The acid was decanted into a waste bottle, and the flask was filled with nanopure water and swirled. Five samples were placed in one of three evaporating dishes that were each filled with one of the silane treatments and covered. The dishes were swirled every 15 minutes to ensure that all sides received even treatment. The silane deposition step proceeded for 1hour. The squares were then rinsed with ethanol and cured at 80°C.

Five specimens were examined for each sample set. The perimeter of the advancing cross-section was measured for each specimen, using the formula 2*(width + thickness). Samples were lowered into the solvent at a rate of 50 μm/sec to a depth of 8 mm. The sample remained in the solvent for a dwell time of five minutes and was withdrawn at the same rate with a five-minute hold out of the solvent. The samples were cycled in this manner two additional times. Advancing and receding contact angles were calculated from the three cycles on two separate replicates using the Cahn DCA4A software package.

Fourier transform attenuated total reflectance spectroscopy

FTIR-ATR spectroscopy was collected on a Nicolet 20SX spectrometer using 64 scans at a 4 cm-1 resolution. A background spectrum was taken before each sample and subtracted from the acquired sample scans.

MicroATR spectroscopy was performed using a Nicolet Magna 706 FTIR Spectrometer and a SiO crystal using 64 scans at a 4 cm_{-1} resolution. Background was collected prior to scanning each sample. All spectra were corrected for water and carbon dioxide absorption and processed using Nicolet OmnicESP™ software. Spectra were further processed with BioRad Know-It-All spectroscopy software which correlated peak values with chemical structure to obtain peak assignments.

X-ray photoelectron spectroscopy

X-ray photoelectron spectroscopy (XPS) data was collected on a Kratos XSAM 300 spectrometer. Data were collected using an Al Kα x-ray source ($h\upsilon$ = 1486.6 eV) operated at 12 kV and 9 mA in FRR (fixed retardance ratio) mode with analyzer chamber pressure at ~10^{-7} torr. Peak quantification was performed on medium resolution elemental spectra with CasaXPS software version 2.2.24. All sample analyzed by XPS were Soxhlet extracted in chloroform prior to surface treatment to minimize contamination of the XPS chamber.

Bulk mechanical testing

The bulk mechanical properties of the surface grafted and hydrolyzed PDMSe were determined via tensile testing. Tensile specimens were cut from cured freestanding silicone films using an ASTM D1822-68 type L dogbone die,

resulting in a 1-inch gauge length. Samples were ~1 mm thick and each was individually measured to account for thickness variability in calculations.

Dogbones were placed into an Erlenmeyer flask, which was subsequently filled with 3M HCl. A Teflon coated stir bar was added and the dogbones were swirled in the HCl for 4 hours. The stirring kept the dogbones from sticking to each other thus ensuring even hydrolysis of all sides of the dogbones. The acid was decanted into a waste bottle, and the flask was filled with nanopure water and swirled. The dogbones were place into evaporating dishes such that the testing portion of the dogbone was raised above the glass. The wells of the dishes were each filled with one of the silane treatments. The dishes were covered and occasionally swirled as the silane deposition step proceeded for 1hour. The dogbones were then rinsed with ethanol and the surface treatment was cured at 80°C.

Tensile measurements were made according to ASTM D412-97 on an Instron model 1122 equipped with the TestWorks 3.07 software for analysis. The dogbones were tested at a rate of 2 inch/min.

Results and Discussion

Surface Treatments and Characterization

Surface hydrolysis

Several experiments were performed to determine optimal surface hydrolysis treatment. 1 Molar and 3 Molar KOH were initially evaluated. These treatments resulted in a dramatic increase in surface hydroxyls with the greatest hydroxyl content (note broad peak at ~3400 cm^{-1} in Figure 5-3) for the 6-hour treatment, but with an accompanying increase in surface roughness as

evidenced by a frosted appearance. The slides appeared frosted after as little as two hours exposure to the base treatments. For greater treatment time a reduction in surface hydroxyls was seen by ATR.

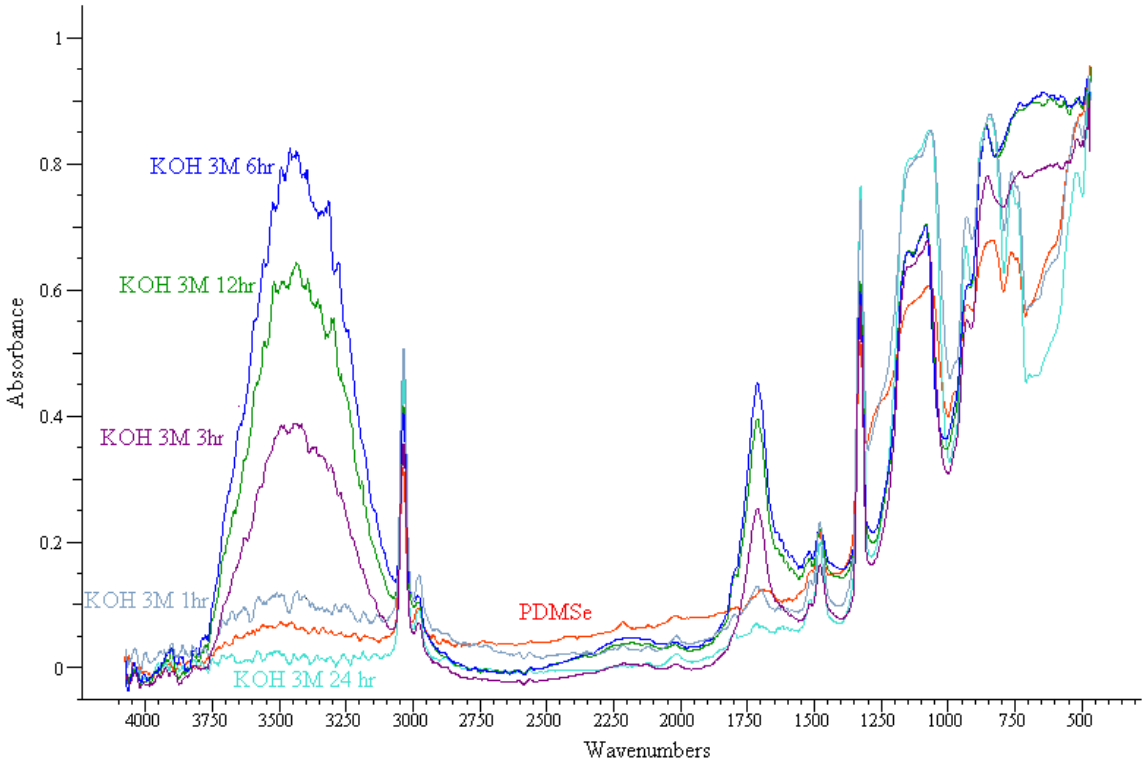

Figure 5-3: ATR spectrum for base catalyzed hydrolysis of PDMSe. Treatment was 3M KOH and various treatment durations are shown. Unmodified PDMSe is shown in blue.

This reduction in surface hydroxyls at treatment durations greater than 6 hours could not be verified by contact angle due to the roughness of the samples.

This resulting roughness of this treatment would be detrimental for slides with engineered microtopographies; thus, this method was not further evaluated. The roughness of these samples is such that they behave as hydrophobic substrates regardless of the hydroxyl content (Figure 5-4). This is problematic for biological studies since wettability is a primary concern.

Figure 5-4: Representative images of captive air bubble contact angle in water for hydrolyzed PDMSe treated with KOH. Contact angles for hydrolyzed PDMSe were similar to PDMSe due to surface roughness.

1 and 3 Molar HCl washes were also evaluated. The twelve-hour treatment resulted in the greatest concentration of surface hydroxyls as measured by ATR. There was no difference between the 1, 3, and 6 hour treatment durations.

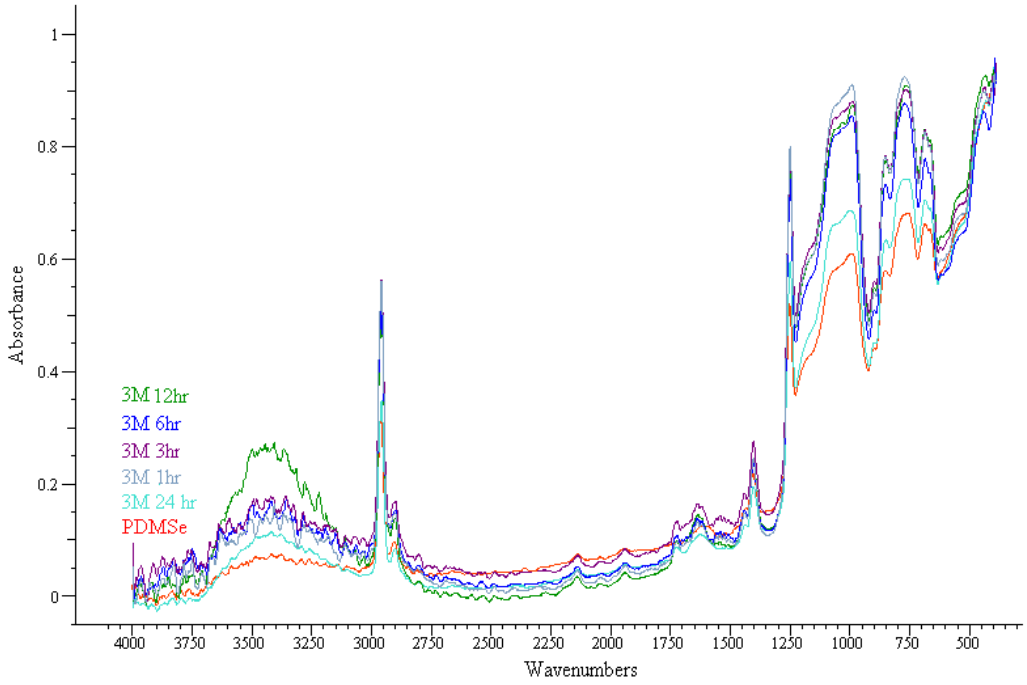

Figure 5-5: ATR spectrum for acid catalyzed hydrolysis of PDMSe. Treatment was 3M HCl and various treatment durations are shown. Unmodified PDMSe is shown in blue.

Acid catalyzed hydrolysis, in contrast to the base catalyzed hydrolysis, resulted in lower hydroxyl content as evidenced by ATR but resulted in far

greater wettability (Figures 5-5 and 5-6 respectively). Therefore, 3 M HCl soaks for 3-4 hours durations were used for producing PDMSe-OH substrates for the silane treatments as this treatment resulted in the best combination of hydrophilicity and hydroxyl content.

Figure 5-6: Representative captive air bubble contact angle in water for hydrolyzed PDMSe treated with HCl. All greater treatment times resulted in completely spherical bubbles (i.e. water contact angle were less than 5°)

Dynamic contact angle data was collected for the samples hydrolyzed via acid catalysis to determine the change in both the advancing and receding contact angles. The difference between advancing and receding contact angles is known as hysteresis and in these samples is attributed to the ability of silicones to readily achieve surface rearrangement. The PDMSe-OH in water presents the higher energy hydroxyl groups. These groups are buried by low energy methyl groups in air and also by the Si-O-Si backbone that has lower surface energy than the hydroxyls. Hysteresis is evident even in the unmodified PDMSe, where the rearrangement exposes either the methyl groups or the siloxane backbone in air or water respectively.

A quick measure of hysteresis is to compare the sessile drop contact angle to the captive air bubble contact angle in water. A more precise measurement uses dynamic contact angle techniques such as the Wilhelmy plate to determine

the advancing and receding contact angles. In this method, a specimen is slowly lowered at a constant rate into a liquid of known surface tension, i.e. water. As the specimen is lowered, the liquid wets the surface as it would for a sessile drop placed on the surface. The attached liquid increases the mass of the specimen, and this increase is proportional to the surface energy of the liquid. The downward force is measured with a microbalance throughout the experiment and is converted into cos θ by the equation, cosθ = Force / (Surface tension * Wetted perimeter), where the wetted perimeter is 2*(width + thickness). The specimen is then withdrawn from the liquid at the same fixed rate. Since this surface is already wetted, the receding contact angle is measured. In air, the hydrolyzed PDMSe appears hydrophobic, but upon exposure to water, the material regains its hydrophilicity.

Table 5-1: Advancing and receding water contact angle data for unmodified PDMSe and PDMSe-OH as hydrolyzed by 4-hour soak in 3M HCl.

Sample	Advancing water contact angle (°)	Receding water contact angle (°)
PDMSe	109.2° $\pm$ 8°	70.6° $\pm$ 1°
PDMSe-OH	77.3° $\pm$ 2°	34.9° $\pm$ 1°

The hydrolysis was stable if the samples were kept in water. Samples stored in water maintain hydrophilicity for months. Whereas, a PDMSe substrate that was hydrolyzed and then stored in air had advancing and receding water contact angles that were indistinguishable from unmodified PDMSe indicating that complete hydrophobic recovery can occur.

Tensile measurements were obtained for PDMSe that was hydrolyzed in 3M HCl for 4 hours. Samples were tested after acid treatment and at 160 days aging in water (Figure 5-7).

Fresh samples generated modulus values that were very similar to those obtained for unmodified PDMSe, but the aged PDMSe-OH had a 15% higher low strain modulus value.

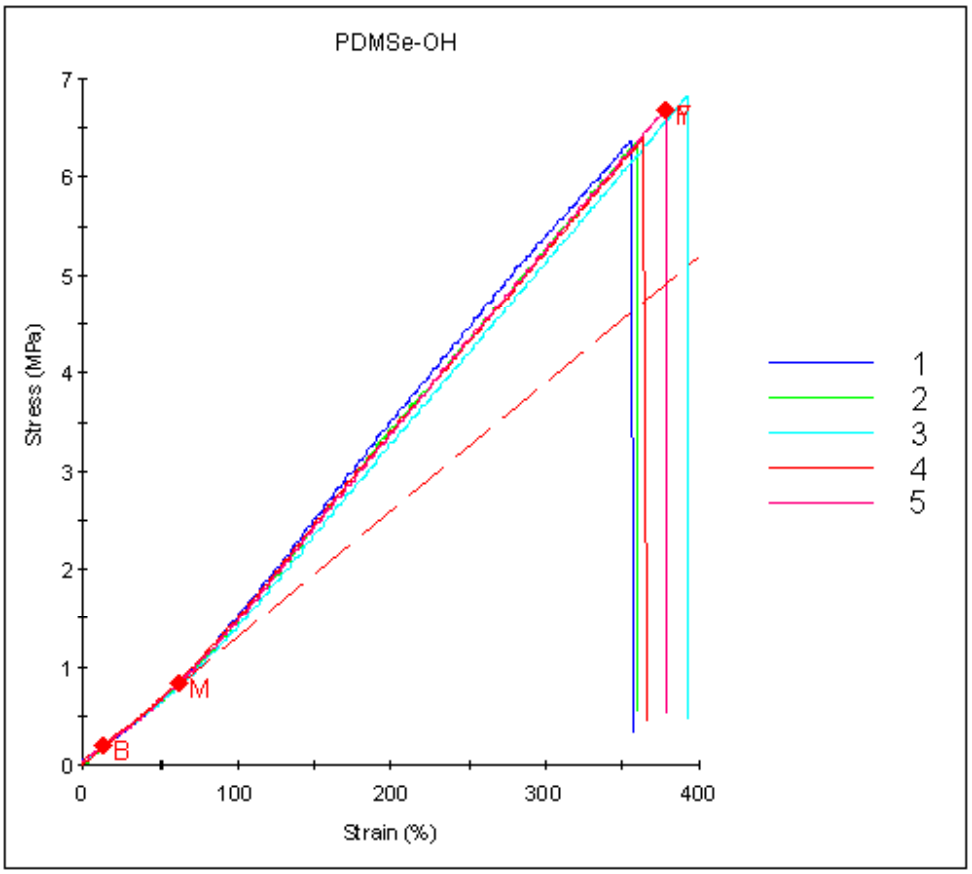

Figure 5-7: Representative stress-strain plot for 5 specimens of hydrolyzed PDMSe

The hydrolysis treatments used produce samples that are rich in surface hydroxyl groups capable of reacting with silane treatments. Additionally, the hydrolyzed samples are stable for long periods of time if stored in water. At short

storage times, there is no difference in bulk modulus as compared to unmodified PDMSe.

mPEG-silane

m-PEG-silane was used as received. The molecular weight was 5,099 g/mol according to the product specification sheet. The material was analyzed with FTIR (Figure 5-8).

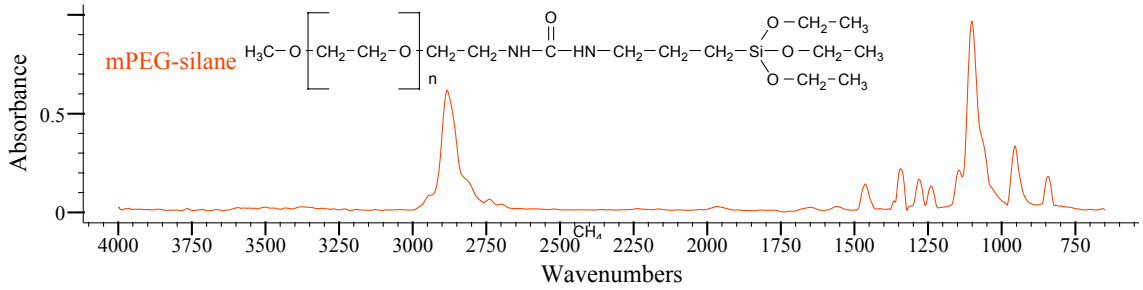

Figure 5-8: FTIR spectrum of mPEG-silane

Table 5-1: Peak assignments for mPEG-silane

Functional Group	Bonding type	Peak Assignment	Mode
Alkanes R-CH3	CH	2972-2952	Asymmetric stretch
	CH	2882-2862	Symmetric stretch
	CH	1475-1435	Asymmetric deformation
	CH	1380-1375	Symmetric deformation
Alkanes R'-CH2-R"	CH	2936-2916	Asymmetric stretch
	CH	2863-2843	Symmetric stretch
	CH	1485-1445	deformation
Amides -CO-NH-C	N-H	3320-3270	Stretch
	C=O	1680-1630	Stretch
	CNH	1570-1515	Combo of C-N stretch and N-H bend
	CNH	1305-1200	Combo of C-N stretch and N-H bend
Ethers CH2-O-CH2	C-O-C	1150-1060	Asymmetric stretch
Organosilicon Si-O-C	Si-O-C	1100-1000	Stretch
	Si-O-C	990-945	Stretch
Ureas R-NH-CO-NH-R	NH	3360-3320	Stretch
	C=O	1670-1615	Stretch
	NH	1585-1535	DEF
	N-C-N	1360-1320	ASY_STR

In order to determine the surface grafting capabilities of this material, a glass microscope slide was treated with the mPEG-silane. A glass microscope slide (FisherFinest Cat No. 12-544-1) was passed briefly through a very clean flame to remove organic contaminants. XPS and sessile drop contact angle data were obtained for the "clean glass" slide.

The sessile drop contact angle for the "clean glass" slide was 36° ± 2° (Figure 5-9). The XPS data showed that adventitious carbon was detected on the "clean glass" slide, as two carbon peaks were present. Fisher does not report any information on the glass type, e.g. borosilicate, soda-lime-silicate, etc. However, the XPS data is consistent with soda-lime-silica glass: SiO_2, Na_2O, CaO, MgO, and Al_2O_3.

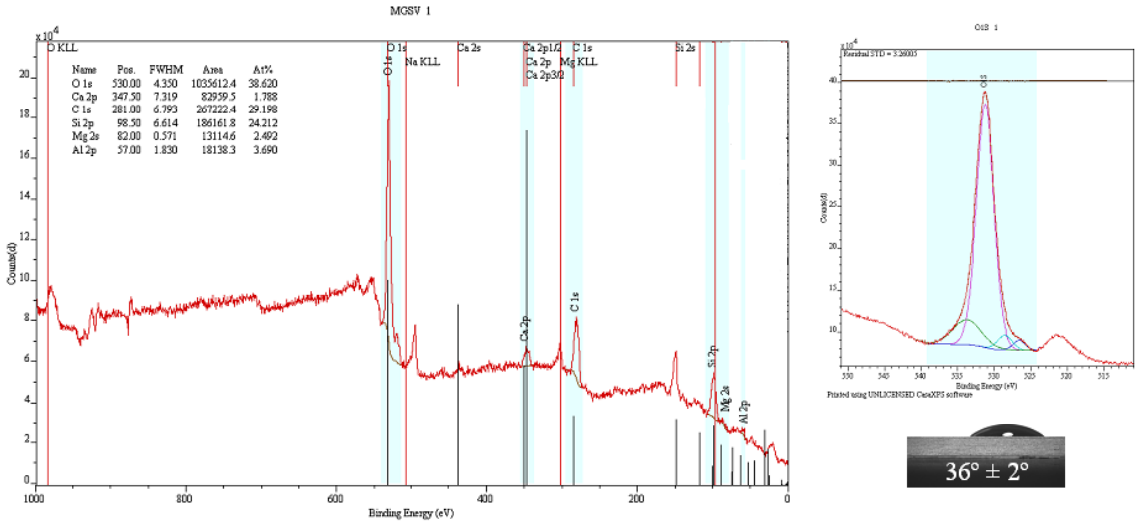

Figure 5-9: XPS spectrum for clean glass microscope slide. Inset is oxygen region from elemental scan. Sessile drop water contact angle is also shown.

Oxide compositions could not be fully quantified, because XPS analysis did not show sodium peak. The XPS spectrum was run from 0-1000eV, and the sodium peak is expected at 1072.0eV. It is known, however, that sodium is

present as evidenced by an Auger peak at ~500eV. Additionally, oxygen data shows several peaks, including the major component SiO_2 (79%) and 3 other prominent oxide peaks (Figure 5-9).

A second glass microscope slide was passed through a very clean flame to remove organic contaminants and was then treated with 5mg/ml PEG-silane in aqueous ethanol. The mean contact angle was reduced from 36° ± 2° to 25° ± 5° (Figure 5-10 inset).

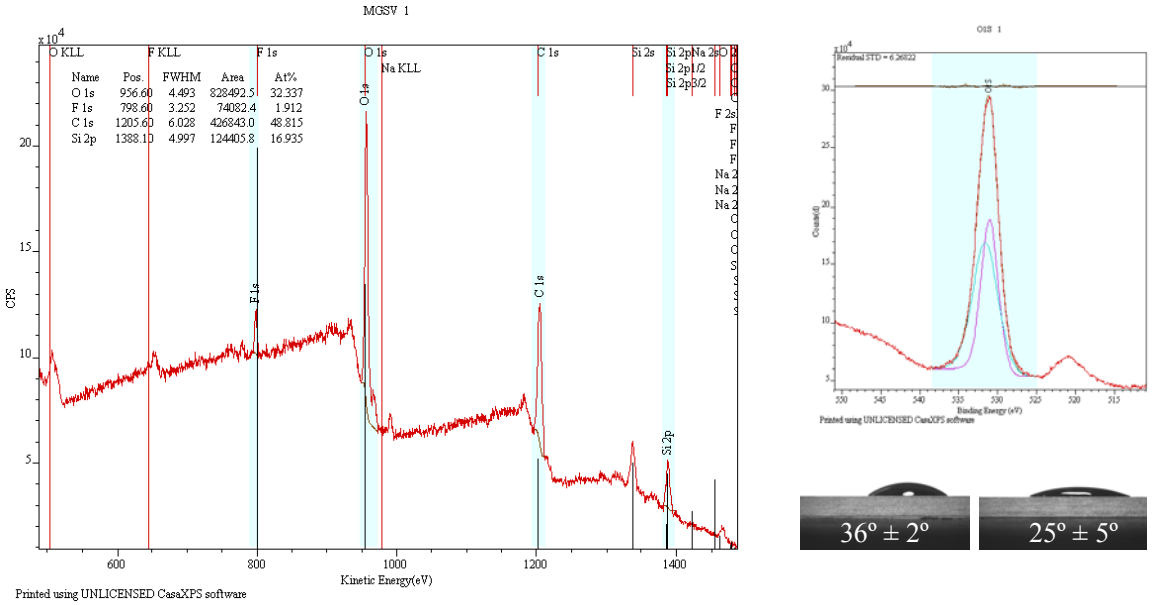

Figure 5-10: XPS spectrum for glass microscope slide treated with mPEG-silane. Inset is oxygen region from elemental scan. Sessile drop water contact angles for "clean glass" and PEG treated glass are also shown.

The resulting XPS showed a reduction in several of the peaks seen in the "clean glass" spectrum (Figure 5-10). Only silicon and faint sodium peaks were still present from glass. Additionally, the carbon peak changes from 2 peaks for the adventitious carbon on the glass to one peak for the PEG hydrocarbon backbone for the silane treated glass. The oxygen region changes from 4

distinct oxide peaks for the glass to two peaks for the PEG-glass. These two peaks were attributed to SiO_2 and PEG and were of roughly equal intensity.

PDMSe-g-PEG

Characterization of the PEG-silane grafted onto PDMSe is very difficult. In air or under vacuum the surface of the PDMSe-g-PEG is almost completely composed of the silicone component due to surface rearrangement. Upon immersion in water, the PEG groups quickly reorient to the surface. This fact makes this grafted surface very difficult to characterize. Since the silicone dominates the surface in vacuum and in air, it is not possible to obtain good XPS or FTIR data descriptions of the surface. Additionally, sessile drop measurements, as typically used to determine surface energy, yield surface energy data that approximates that of PDMSe. Therefore the most convincing data of the PEG grafting is the measurement of the captive air bubble water contact angle which is significantly different from both the unmodified PDMSe and the PDMSe-OH (Figure 5-11).

Figure 5-11: Captive air bubble in water for unmodified PDMSe, PDMSe-g-PEG, and PDMSe-OH.

The reorientation of the surface in water with time can be detected by placing a sessile drop on the dry (silicone rich) surface of the PDMSe-g-PEG. A

steady decrease in this contact angle is detected as the surface reorients to become rich in the hydrophilic PEG groups (Figure 5-12). Evaporation of the drop does occur in this time frame, so a similar sized sessile drop was placed on unmodified PDMSe so as to directly compare. The contact angle on the PDMSe-g-PEG obtains a minimum value, 11°, that is much lower than either the captive air bubble measurement, 42.3°, or receding angle as determined by DCA, 43.1°. This may be attributed to the competing mechanism of evaporation. This time-lapse experiment showed that the PDMSe-g-PEG achieved the expected value of ~40° at thirty minutes.

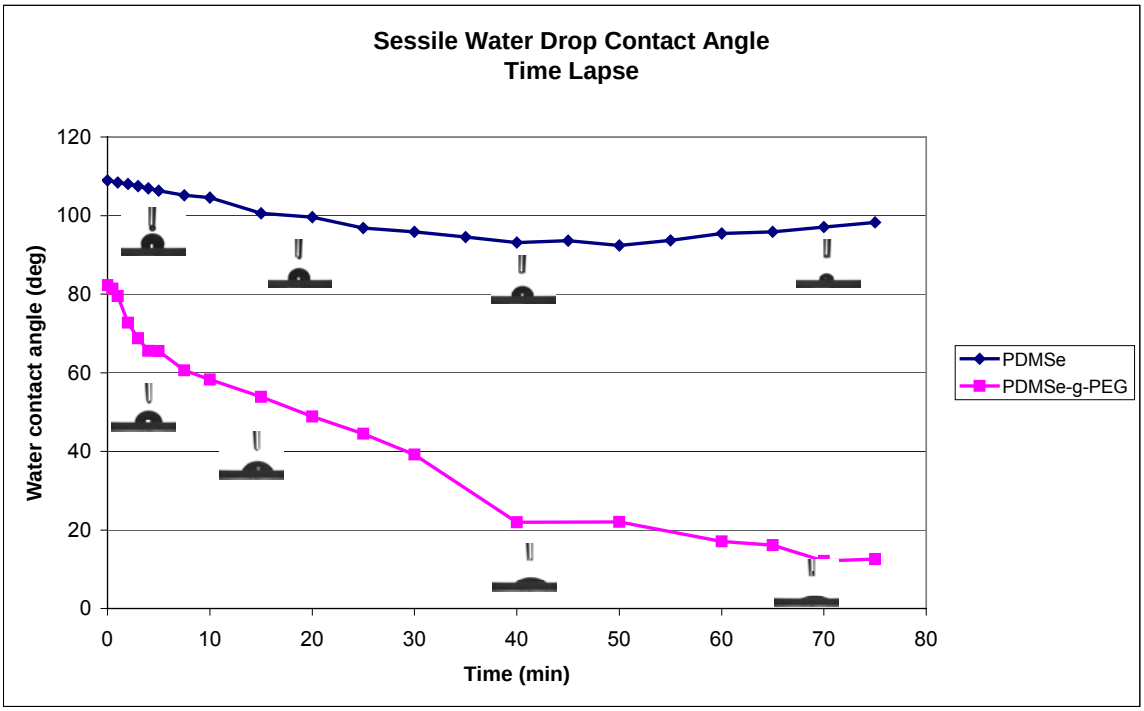

Figure 5-12: Plot of sessile drop contact angle for a single drop placed on either PDMSe or PDMSe-g-PEG as a function of time.

Dynamic contact angle measurements were also obtained to verify the advancing and receding contact angles and also in an attempt to determine the surface energy of the PEG in both the dry and wet states. The advancing

contact angle in water as determined by DCA was 110°, and the receding angle was 43.1°.

The dynamic contact angles were also obtained for PDMSe-g-PEG in formamide and n-n-dimethylformamide, whose surface tensions are 58.0 dynes/cm and 36.76 dynes/cm respectively. The hysteresis of each of these substrates decreases with decreasing surface tension of testing liquid indicating less reorganization with lower surface tension liquids. This indicates that the siloxane component remains at the surface, thus this procedure is not useful to determine the actually surface energy of the PEG rich surface.

Table 5-2: Advancing and receding data for unmodified PDMSe and PDMSe-g-PEG in water, formamide, and dimethylformamide

	Water		Formamide		DMF	
	Adv	Rec	Adv	Rec	Adv	Rec
PDMSe	109.2 ± 12	70.6 ± 1	96 ± 3	64 ± 1	56.2 ± 4	49 ± 1
PDMSe-g-PEG	110.6 ± 8	43.1 ± 1	61.7 ± 3	43 ± 2	46.2 ± 2	38.2 ± 1

PSf-silane

The initial polysulfone treatment used the sulfonation of polysulfone to create reactive groups along the polymer backbone. These reactive groups could then be coupled to the surface hydroxyls with the use of an appropriate coupling agent. As will be discussed in more detail in chapter 6, this method of grafting the PSf to the surface results in a thicker than desired coating that was problematic for the *Ulva* assays. The thicker coating resulted in an increased surface modulus and a distortion of the topographies. This problem was eventually eliminated by derivatizing a hydroxyl-terminated polysulfone with an

isocyanatopropyl trimethoxy silane. The PSf-silane treatment resulted in a thinner coating with a similar surface energy.

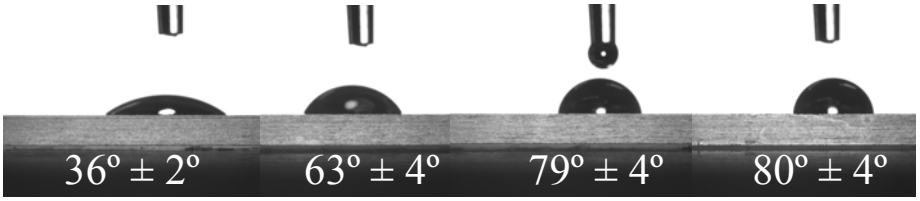

Figure 5-13: Sessile drop water contact angle from left: "clean glass slide," PSf-OH treated glass slide, PSf-silane treated glass slide, and sulfonated polysulfone treated glass microscope slide, coupled with GPS

This point is illustrated by using the various polysulfone treatments to modify glass slides. The modified slides were then evaluated with XPS and contact angle. The contact angle for the PSf-silane and the s-PSf + GPS treated glass slides were not statistically different (79° ± 4° and 80° ± 4°, respectively as seen in Figure 5-13).

Polysulfone is a carbon rich polymer (> 70%) with less than 10% theoretical sulfur content. The clean glass slide had a composition including 29.2% C, 38.6% O, and 24.2% Si. The PSf-OH treated glass slide had an slight increase in carbon and a decrease in oxygen, but the silicon content remained the same. Using the PSf-silane treatment increased the carbon content to 51% and decreased the silicon content. The s-PSf coupled with GPS exhibited the highest carbon content (75.5%) and the lowest silicon content (5.0%). Given that the contact angle for these last two treatments is identical, the difference in the XPS data can be attributed to coating thickness.

PDMSe-g-PSf

The initial polysulfone treatment utilized a glycidoxylpropl triethoxysilane coupling agent that was reacted with the hydrolyzed PDMSe. The sulfonated

polysulfone was then coupled to the GPS through the sulfate in the sulfonated backbone. The polymer was sulfonated with chlorosulfonic acid. This sulfonation reaction was evidenced by a dramatic change in the solubility of the polymer. The coupling with the GPS on the PDMSe surface was evidenced by XPS (Figure 5-14).

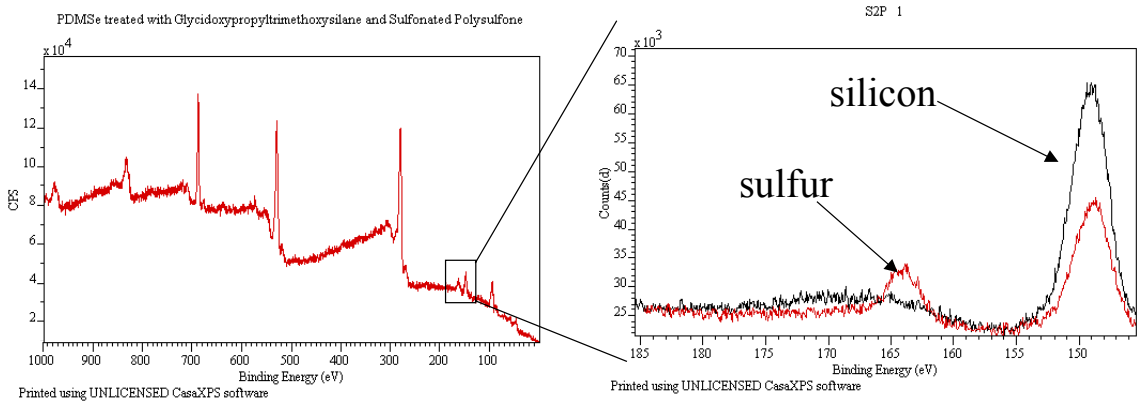

Figure 5-14: XPS spectrum for s-PSf grafted on GPS modified PDMSe-OH. Inset shows environmental spectrum for sulfur. Black is GPS-PDMSe-OH and red is s-PSf coupled to GPS modified PDMSe-OH

The black detailing in the inset shows the GPS treated PDMSe-OH and the red shows the substrate after reaction with the s-PSf. As discussed above, changing the protocol from grafting via GPS and s-PSf to grafting with a silane terminated polysulfone produces similar contact angles with a reduction in the thickness of the polysulfone layer.

The polysulfone grafted PDMSe samples were evaluated for water wettability and dynamic contact angle behavior. The polysulfone showed high hysteresis even in low surface tension solvents, unlike the unmodified PDMSe and the PDMSe-g-PEG which showed a reduction in hysteresis with increasing solvent surface tension. In addition to the data shown, the polysulfone modified

PDMSe showed a zero contact angle, perfect wetting, for the solvent acetonitrile with a surface tension of 39 dynes/cm.

Table 5-3: Advancing and receding data for unmodified PDMSe and PDMSe-g-PSf in water, formamide, and acetonitrile

	Water		Formamide	
	Adv	Rec	Adv	Rec
PDMSe	109° ± 7°	71° ± 1°	96° ± 3°	64° ± 1°
PDMSe-g-PSf	102° ± 9°	62° ± 1°	98° ± 1°	52° ± 1°

mPFPE-silane

The FTIR data for the mPFPE-OH and the mPFPE-silane show vastly different structures (Figure 5-15). Full peak assignments for both polymers are shown in tables 5-3.

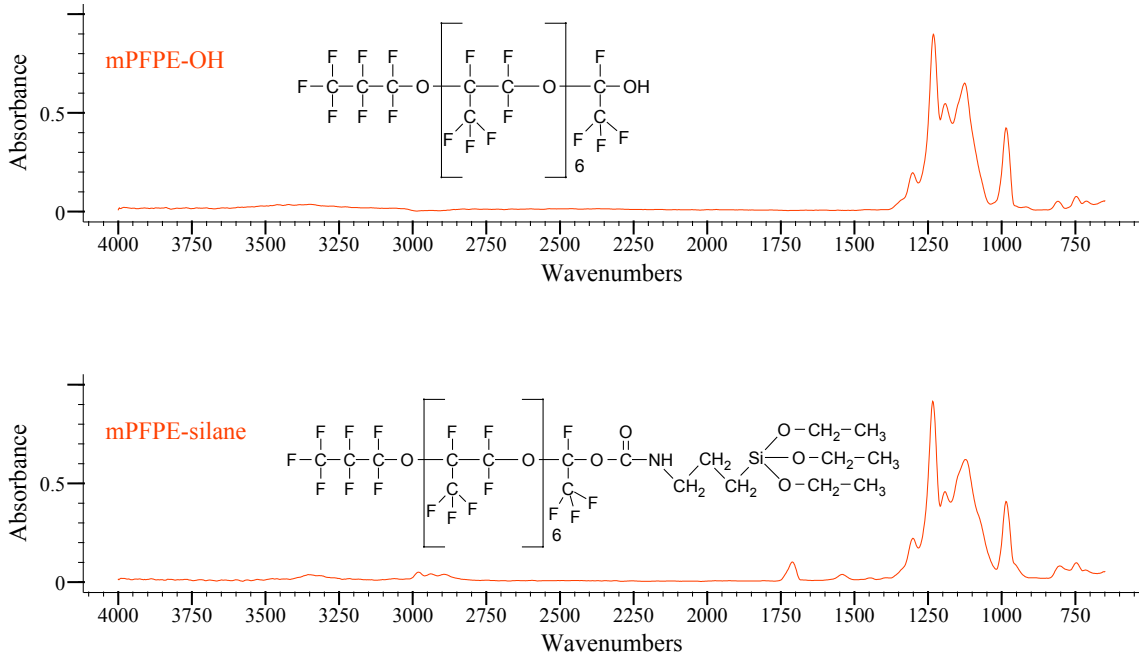

Figure 5-15: FTIR spectra for mPFPE-OH (top) and mPFPE-silane (bottom)

Most notable is the addition of multiple peaks in the range of 2980-2860 cm^{-1} that is indicative of the alkanes present in the propyl trimethoxy silane and the NH peak from the urethane linkage at 1700 cm^{-1}. Additionally, the broad but weak peak for the –OH in the mPFPE-OH has become considerably more narrow and shifted to a shorter wavelength and is thus attributed to the N-H stretch.

Table 5-4: FTIR peak assignments for mPFPE-silane and mPFPE-OH

Functional Group	Bonding type	Peak Assignment	Mode	mPFPE -silane	mPFPE-OH
Alcohols (R)3C-OH	OH	3400-3200	Stretch		X
	OH	1410-1310	Stretch		X
	C-O	1210-1100	Deformation		X
Alkanes R-CH3	CH	2972-2952	Asymmetric stretch	X	
	CH	2882-2862	Symmetric stretch	X	
	CH	1475-1435	Asymmetric deformation	X	
	CH	1380-1375	Symmetric deformation	X	
Alkanes R'-CH2-R"	CH	2936-2916	Asymmetric stretch	X	
	CH	2863-2843	Symmetric stretch	X	
	CH	1485-1445	Deformation	X	
Amides -CO-NH-C	N-H	3320-3270	Stretch	X	
	C=O	1680-1630	Stretch	X	
	CNH	1570-1515	Combo of C-N stretch and N-H bend	X	
	CNH	1305-1200	Combo	X	
Halogens C-F	C-F	1400-1000	Stretch	X	X
Halogens CF3	C-F	1350-1120	Stretch	X	X
	C-F	780-680	Unknown	X	X
Halogens CF-CF3	C-F	1365-1325	Stretch	X	X
	C-F	745-730	Unknown	X	X
Halogens CF2	C-F	1280-1120	Stretch	X	X
Organosilicon Si-O-C	Si-O-C	1100-1000	Stretch	X	X
	Si-O-C	990-945	Stretch	X	See text
Urethanes R-NHCOO-R	NH	3440-3400	Asymmetric stretch	X	
	C=O	1740-1680	Stretch	X	
	CHN	1540-1530	Deformation	X	
	C-N & C-O	1265-1200	Stretch	X	
	C-O	1090-1040	Stretch	X	

There was a sharp peak in both spectra at 980 cm^{-1}, which corresponds to the positioning expected for Si-O-C. This is expected in the mPFPE-silane, but

not in the mPFPE-OH. The origin of this peak for the PFPE-OH is unclear, but it is unlikely trimethoxysilane, since none of the other peaks are present e.g. alkyl peaks.

The mPFPE-silane and m-PFPE-OH were both used to treat glass slides using the procedure established for the surface grafting on the hydrolyzed silicone, and sessile drop contact angles were measured (Figure 5-16).

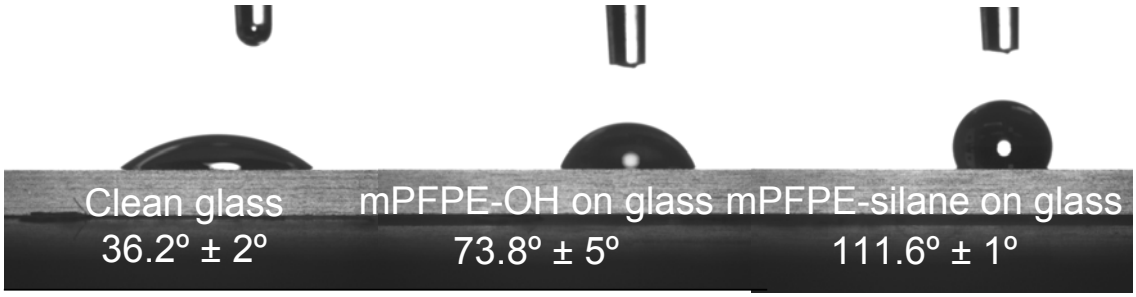

Figure 5-16: Sessile drop water contact angles on glass for untreated clean glass and glass treated with mPFPE-OH or mPFPE-silane

The mPFPE-OH treatment is a physadsorption process rather than a covalent linkage. This treatment resulted in surface with nearly twice the contact angle of the “clean glass” microscope slide. The PFPE-silane treated glass had nearly four times the water contact angle. These surfaces were also evaluated with XPS to better quantify these results. The mPFPE-OH treated glass microscope slide showed a slight increase in the fluorine content (2.1%), whereas the percent fluorine content for the mPFPE-silane treated glass was 21.1%. It is interesting to note that the dramatic increase in contact angle occurred with only 2% increase in fluorine content. In addition to the 21% increase in fluorine content for the PFPE-silane treated glass, there was also a strong secondary carbon peak that was indicative of the C-F bond. The theoretical composition for a surface that is composed entirely of mPFPE-silane

would be 24.3% C, 13.2% O, 2.1% Si, 1.1% N, and 54% F. The treated glass slide compositions was 45.0% C, 16.6% O, 14.8% Si, 2.4% N, and 21.1% F. There is still quite a significant amount of silicon detected from the glass, indicating an incomplete coating, but it is significantly better than the PFPE-OH treated slide that had 29.5% Si.

PDMSe-g-PFPE

The PFPE modification of the PDMSe produced a surface with a lower surface energy that was therefore much easier to characterize than the PDMSe-g-PEG. Sessile, captive, and dynamic contact angles were measured for PDMSe-g-PFPE. X-ray photoelectron spectroscopy measurements were obtained for the surface grafted PDMSe.

The XPS composition data shown is for unmodified PDMSe and hydrolyzed PDMSe that has been treated with ICPES that was then reacted with hydroxyl terminated PFPE, and also for hydrolyzed PDMSe that was treated with the PFPE-silane obtained from DuPont (Table 5-4 and Figure 5-17).

Table 5-5: XPS composition data for unmodified PDMSe, PFPE-OH coupled with ICPES to PDMSe, and PDMSe-g-PFPE

Element	Binding Energy (eV)	%Atomic Composition PDMSe	%Atomic Composition PDMSe-ICPES-PFPE-OH	%Atomic Composition PDMSe-g-PFPE
Carbon (1s)	287	42.3	56.3	54.3
Oxygen (1s)	531	35.5	17.2	13.8
Silicon (2p)	102 (149*)	21.1	7.0	4.7
Nitrogen (1s)	402	Trace	4.5	1.2
Fluorine (1s)	686	1.0	14.6	25.9
Sulfur (2p)	165	Trace	Trace	Trace
Chlorine (2p)	199	Trace	Trace	Trace

The theoretical composition for a surface that is composed entirely of mPFPE-silane would be 24.3% C, 13.2% O, 2.1% Si, 1.1% N, and 54% F. It is clear that these compositions were not obtained, but the excess carbon may be ascribed to adventitious carbon from the environment.

The ICPES coupled PFPE showed that there was a significant amount of PFPE grafted to the surface. However, the increased nitrogen content relative to the PFPE-silane indicated that there might also be some unreacted ICPES on the surface. The PFPE-silane treated surface exhibited ~5% silicon, indicating a good surface coverage. This combined with the large increase in the fluorine peak for the silane terminated PFPE justifies the use of this treatment as opposed to the separate coupling agent step.

The surface of the PDMSe-g-PFPE shows very little surface rearrangement as measured by hysteresis between the advancing and receding contact angles measured by DCA for three solvents (Table 5-5). Thus sessile drop measurements were representative of the fluorinated surface, and surface energy could be calculated from an inverse Zisman plot. The surface energy calculated from sessile drop contact angle for a series six solvents was 23.6 dynes/cm for the unmodified PDMSe and 16.24 dynes/cm for the PDMSe-g-PFPE (Figure 5-18).

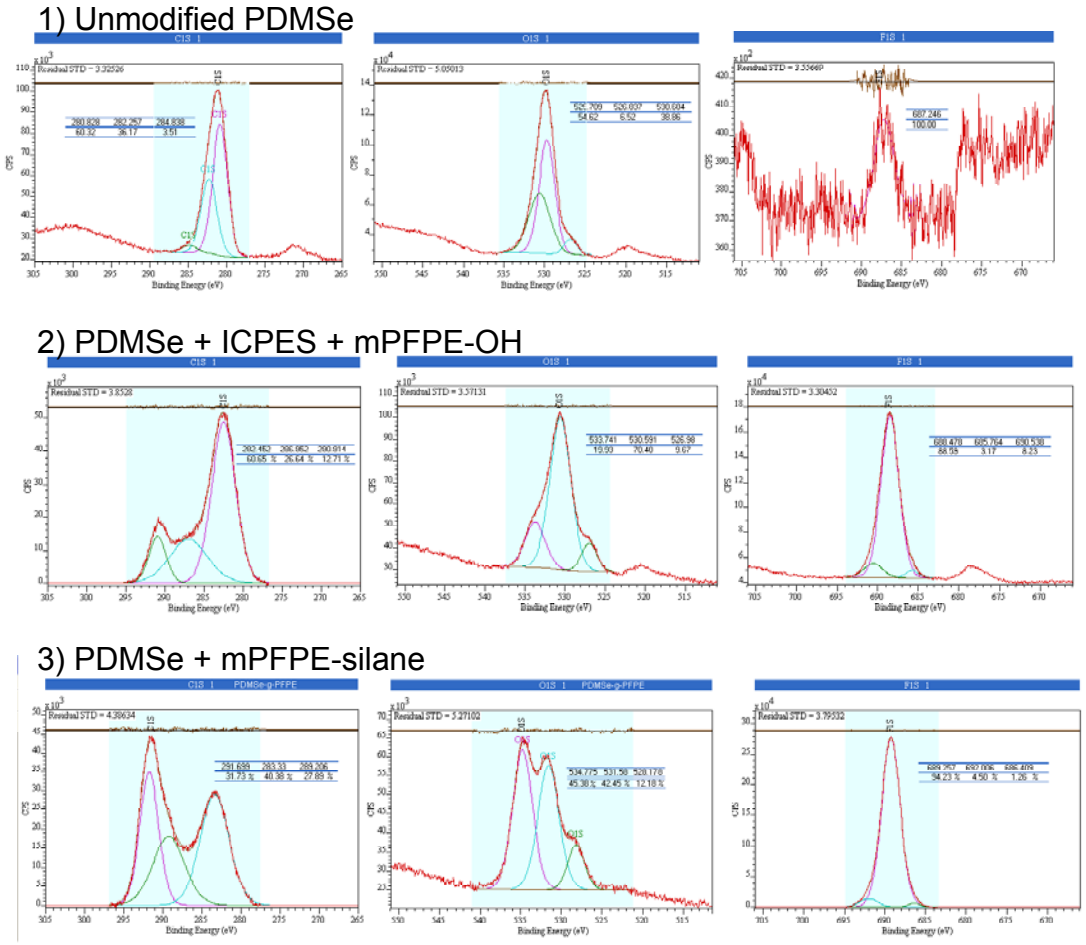

Figure 5-17: XPS elemental data for UM and fluorinated PDMSe. Spectra shown are carbon, oxygen, and fluorine

Table 5-6: Dynamic contact angle data for unmodified PDMSe and PDMSe-g-PFPE

	Water		Formamide		DMF	
	Adv	Rec	Adv	Rec	Adv	Rec
PDMSe	109° ± 12°	71° ± 1	96° ± 3°	64° ± 1°	56° ± 4°	49° ± 1°
PDMSe-g-PFPE	95° ± 2	88° ± 1°	86° ± 1°	84° ± 1°	56° ± 2°	57° ± 1°

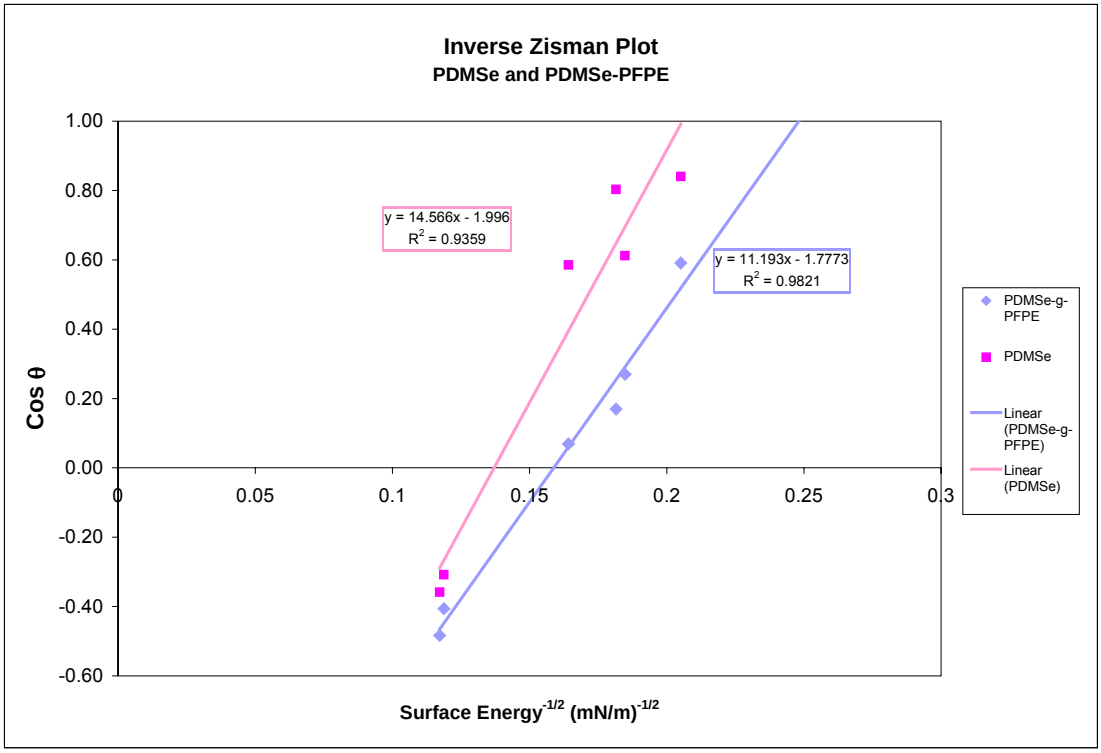

Figure 5-18: Zisman plot for unmodified PDMSe and PDMSe-g-PFPE

All Silane Graft Treatments

The following data are presented together to show the characterization of the various modifications of the PDMSe relative to one another. The surface treatments have produced a range of captive air bubble contact angle measurements from 95° to 30°. The plot below shows samples prepared at different times to show the reproducibility of the surface treatments (Figure 5-19). The samples shown below are from the last batch of samples evaluated for bioresponse in Chapter 6. Representative images of the captive air bubble water contact angle are also shown (Figure 5-20). The sample data in the following chapter will be ordered from hydrophobic to hydrophilic as determined by these values.

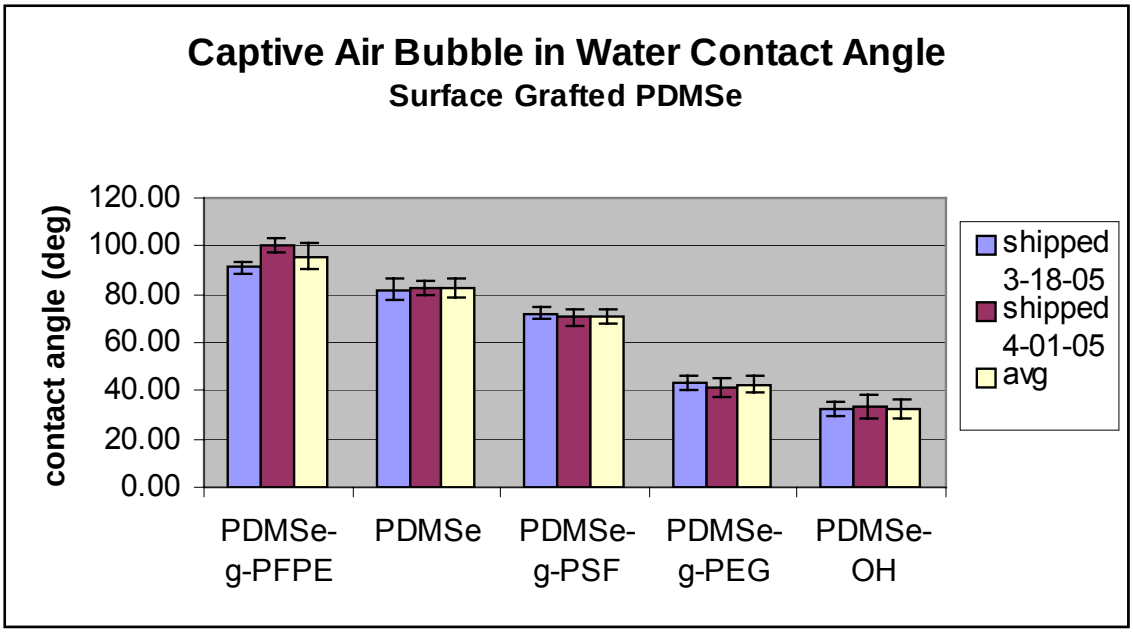

Figure 5-19: Captive air bubble contact angle measurement for all chemical modifications of PDMSe

Figure 5-20: Representative images for captive air bubble contact angles on all chemical modifications of PDMSe

Figure 5-21 shows representative FTIR spectrum for the various chemical modifications of PDMSe. These spectra are representative of some of the sample areas that actually show a change in the FTIR spectrum relative to unmodified PDMSe. Typically the graft coating is such that the spectrum for surface grafted coating is identical to the spectrum for unmodified PDMSe due to the thickness of the graft layer. Most of these spectra shown are from regions of multiple layer deposition. This is typical at the small area that is held by the tweezers, as this area is not rinsed as well as the rest of the slide.

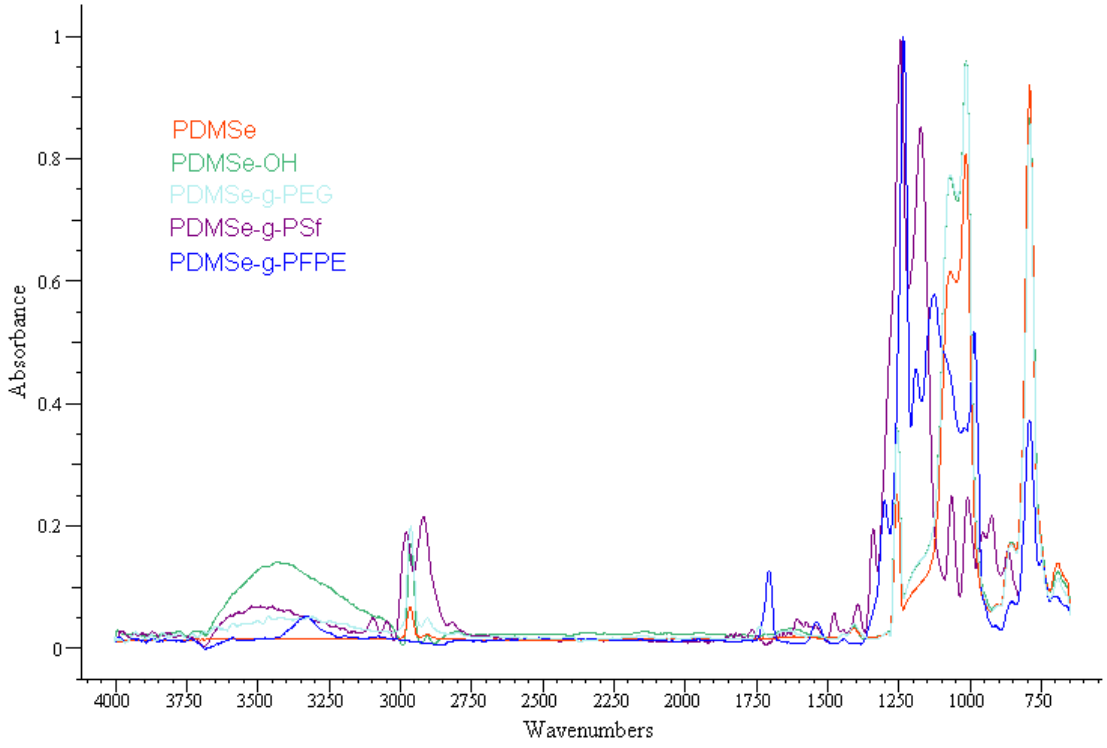

Figure 5-21: FTIR spectra of unmodified PDMSe and all surface chemical modification of PDMSe

One of the main goals of this research was to produce surface modified PDMSe without dramatically changing the bulk mechanical properties. The bulk modulus, as calculated from the initial linear portion of the stress strain plot, for unmodified PDMSe and all chemical surface treatments are shown in Figure 5-22. The lowest modulus values were obtained for the PDMSe-g-PFPE. This data point also had the greatest variability, which may be related to the surface lubricity associated with these samples. There was a slight decrease in the bulk modulus for all surface modification, but they were not statistically different from each other.

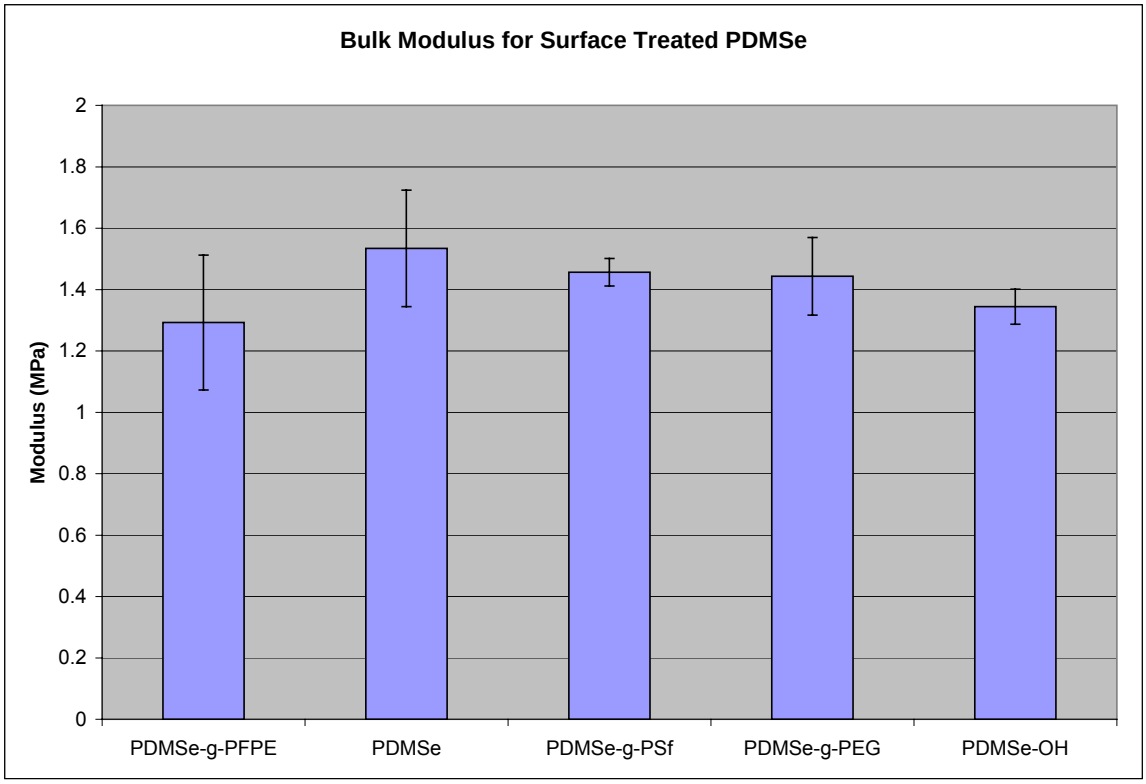

Figure 5-22: Bulk modulus for unmodified PDMSe and all surface chemical modifications of PDMSe.

Conclusions

PDMSe and glass microscope slides were surface grafted with various silane terminated polymers; mPEG-silane, mPFPE-silane, and PSf-silane. Samples were also evaluated that had been treated with either an isocyanatopropyltriethoxysilane or a glycidoxypropyltriethoxysilane and then subsequently coupled to hydroxyl terminated PFPE or sulfonated polysulfone. These surface grafts were evaluated with respect to changes in water contact angle, chemical composition, and bulk modulus. The surface grafting was verified and grafting procedures were continually improved. The data for the finalized grafting procedure produced surface modified PDMSe with a range of captive air bubble water contact angles ranging from 95°- 30° and moduli values

ranging from 1.2 – 1.6 MPa. These surface modified elastomers will be used in the following chapter to determine bioresponse with respect to the alga *Ulva* and the diatom *Navicula*.

CHAPTER 6
BIOASSAYS WITH RESPECT TO SURFACE GRAFTING AND TOPOGRAPHICAL MODIFICATION

Introduction

Natural surfaces have developed many mechanisms to deal with the problem of fouling. There are so called self-cleaning surfaces like the lotus leaf [82]. This plant takes advantage of the dual property of hydrophobicity and microspicules. This roughness imparts an ultrahydrophobocity. When water drops roll across this surface, any particles that have settled on the surface will have a greater affinity for the water and will be thus swept away.

Another organism that exhibits a minimally fouling surface is the skin of fast moving sharks, such as the Mako or Galapagos. This skin is composed of diamond shaped scales, or denticles, that each contains a regular repeating surface topography. Several researchers have noted the hydrodynamic advantage that this topography imparts to the shark [80, 81]. A similarly scaled pattern was even applied to airplane wings and racing boats to decrease drag and therefore increase fuel efficiency. A study was launched by the Brennan group to determine what the biofouling properties of a sharkskin mimic.

The natural sharkskin topography is on the order of 100μm. Due to the research in chapter 4, the Brennan sharkskin mimic possessed a similar repeat structure but on the scale of 2μm (Figure 6-1). The sharklet, meaning “little shark,” exhibited strong antifouling activity with respect to *Ulva* spores (up to an

85% reduction in zoospore settlement density). The sharklet is a novel biomimetic engineered surface topography. The pattern consists of diamond packed ribs that are 2μm wide, spaced 2μm apart and have lengths ranging from 4 to 16μm.

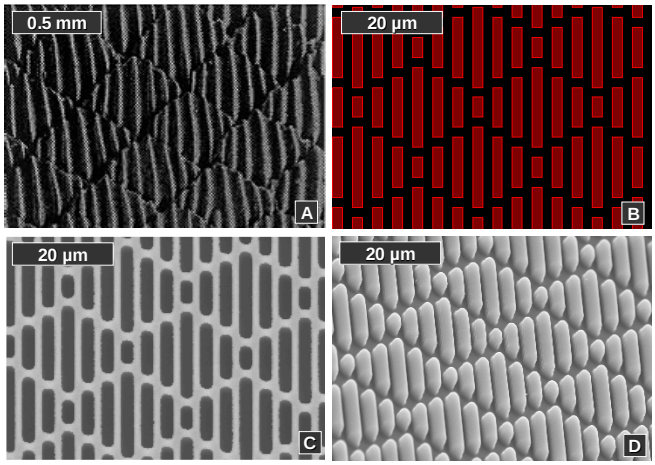

Figure 6-1: A) Photograph of Galapagos sharkskin; B) AutoCAD® drawing of sharkskin mimic called sharklet (designed by Jim Schumacher); C) SEM of the patterned silicon wafer; D) SEM of silicone sharklet replicate. SEM images also by Jim Schumacher [45]

A pilot experiment to evaluate *Ulva* settlement on the sharklet at various depths was performed in June 2003. Sharklet samples in 2003 were prepared by Michelle Carman and wafers were designed, optimized, and prepared by Jim Schumacher. Any data here included is meant to explain the progress of topography studies from my work as described in chapter 4 and to provide justification for the use of sharklet samples with surface chemistry studies.

In a preliminary experiment, it was noted that the settlement data for various replicates of a 5-μm deep sharklet varied drastically. SEM analysis of the samples after exposure to *Ulva* indicated that the variability is attributed mostly to the poor fidelity of pattern replication (Figure 6-2). This study, as well as those presented in this chapter, shows both the importance of pattern fidelity at this

aspect ratio and geometry and the need for multiple replicates for a given surface treatment. For high fidelity sharklet samples shipped in October of 2003, zoospore settlement on the shark pattern was reduced ~86% compared to the flat PDMSe. These results provided the first definitive demonstration that engineered microtopographies are capable of inhibiting algal settlement.

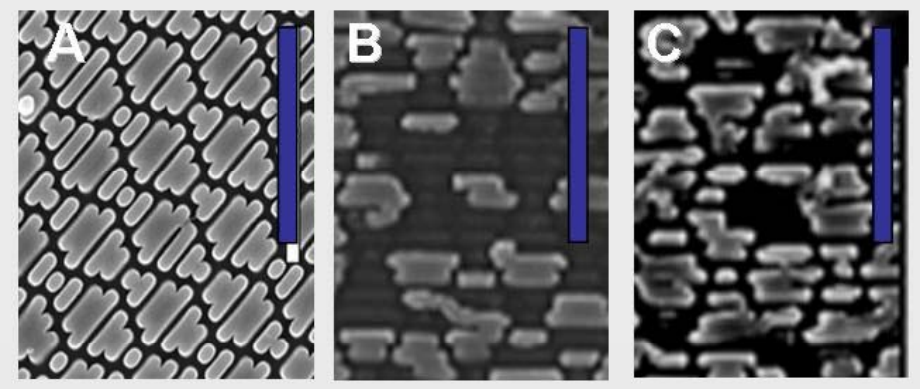

Figure 6-2: SEM images of 5-μm deep sharklet after exposure to *Ulva*. Pattern fidelity varied widely among samples A, B and C. Sample A showed a ~40% reduction in spore settlement relative to smooth, sample B showed a ~35% increase in spore settlement relative to smooth, and sample C showed an ~ 18% reduction in settlement relative to smooth. Scale bars represent 20 μm.

Spore removal is typically very poor for high fidelity sharklet topographies. The few spores that do settle are 'wedged' into the area between the adjacent patterns, providing a mechanical interlocking mechanism for spore adhesion, thereby making settled spores more difficult to remove (Figure 6-3).

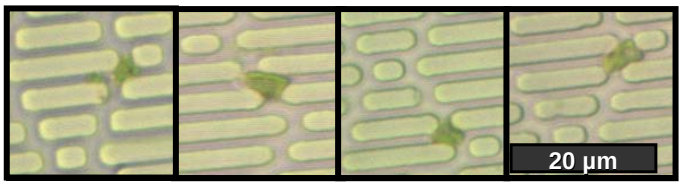

Figure 6-3: Images of spores settled in sharklet topographies.

The reduction in spore settlement was far greater than that expected from the critical spacing alone. Thus, it was suggested that both geometry and dimensions are important factors in using topography to control bioresponse.

Experiments using high fidelity sharklets, channels, and pillars at 2μm width and 2μm spacings were evaluated (Figure 6-4). Feature geometry was found to have a significance influence on both *Ulva* settlement and release, with the sharklet inciting a negative thigmotactic spore settlement response, the pillars exhibited a positive thigmotactic response, and the channels showed little change in spore settlement density as compared to smooth. This study verified the data presented in Chapter 4 that channels of this dimension (2 μm) do not enhance or decrease spore settlement. Feature geometry as well as feature dimensions affect the bioresponse of *Ulva* zoospores to surfaces.

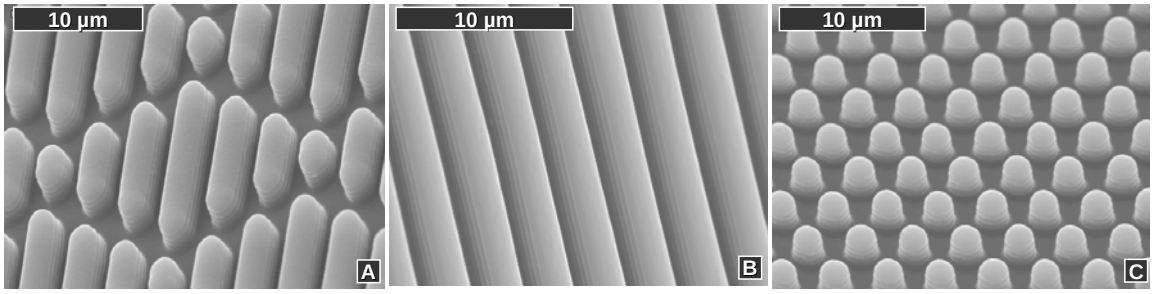

Figure 6-4: SEM micrographs of shark, channel, and pillar micropatterns replicated in PDMSe. Images by Jim Schumacher.

In evaluating the dual response to chemistry and topography, the 2 μm sharklet and 5μm channel patterns were evaluated. The 5 μm channels were selected rather than the 2 μm channels, because this feature size and geometry has elicited the strongest thigmotactic response from *Ulva* zoospores. This allowed evaluation of topographies to which spores exhibited a strong positive

and a strong negative thigmotactic settlement response as well as a topographical cue for release data.

Materials and Methods

Silicone Slides

Smooth silicone slides were prepared as discussed in Chapter 3. No bulk additives were incorporated for these studies. Patterned PDMSe coated slides were prepared by curing the silicone against a polyurethane mold (channels) or silicon wafer (sharklets).

The patterns evaluated in the surface chemistry study include the 5-μm channels from chapter 4 and the sharklet topography discussed above. Silicon wafers of the channel and sharklet topographies were provided by Jim Schumacher (University of Florida).

The photoresist mask for the channel topography was fabricated in 2000 and was designed in such a way that the etched silicon wafer was a positive replica of the desired pattern. It is necessary to replicate the wafer in a secondary material that would replicate the pattern with high fidelity, release from the silicon wafer, and finally not react with or transfer material to the curing silicone. Channel patterned samples produced in 2005 were replicated using a polyurethane rather than the solvent cast polystyrene.

The polyurethane produced a more durable replicate that could be used to directly replicate the silicone, without the need for an epoxy mold production step. The polyurethane negative was prepared by mixing 10:1 of the base to curing agent. The uncured PU was degassed and poured directly onto a clean silicon wafer. The wafer was subsequently placed back into the vacuum oven to

remove trapped air bubbles from inside the patterned areas. The setup time for this material is <1hour, so these steps must be performed quickly. The PU is allowed to cure overnight. This PU replicate allows for direct replication of silicone with out the need for an epoxy mold. This system is still not completely ideal, as the PU replicates are tacky and tend to attract dust. They cannot be easily cleaned, as they swell in most common cleaning solvents.

PDMSe Coated Glass Microscope Slides

Silicone coated microscope slides were prepared by mixing 10 parts of the Silastic T2® base resin with 1 part of the curing agent. The mixture was degassed and poured over glass microscope slides that had been treated with allyltriethoxysilane, ATS, coupling agent. The silicone was cured at room temperature for twenty-four hours between two glass plated with spacers to achieve a silicone thickness of ~700-1000μm.

To prepare the patterned slides, the degassed silicone mixture is also poured onto an etched and HMDS treated silicon wafer or the PU mold, which is covered by a top plate to achieve a silicone thickness of ~200-600μm. Once cured, this freestanding silicone replicate is trimmed and suctioned pattern side down to a clean glass plate. Microscope slides are treated with the ATS and taped to a separate glass plate. More silicone is mixed, and degassed, and poured onto the backside of the silicone replicates. The glass plate with the treated glass slides is slowly lowered onto the uncured silicone such that the slides line up with the patterned silicone as desired. Spacers are located in the

corners of the bottom glass plate to achieve a total silicone thickness of ~700-1000μm. The silicone is then cured at room temperature for twenty-four hours.

After cure, the silicone coated microscope slides prepared in this manner were then removed from the glass plates and excess silicone was trimmed away from the edges.

Surface Treatment of Smooth and Patterned PDMSe

Individual slides were cleaned with ethanol and then soaked in a container filled with 3M HCl for 4 hours. The slides were then rinsed with nanopure water and then with 95% ethanol (aq) and placed onto a chem-wipe into a disposable petri dish and immediately covered with a layer of the appropriate silane treatment. Silane treatments and characterization thereof are described more fully in chapter 5. The silane solutions were pipetted onto the surface of the hydrolyzed PDMSe such that the surface was completely covered. The petri dish lid was then placed onto the petri dish, to keep the humidity level high to discourage evaporation.

The slide was left undisturbed for 1 hour, after which the slide was rinsed with copious amounts of ethanol to remove any silane that was not hydrogen bonded to the surface. The slide was dried in a stream of nitrogen and placed in an 80°C oven to cure for 20 minutes. The slide was then placed in a 50ml centrifuge tube for shipping. Slides were typically produced the day before shipping to the Callow group in England for bioassay with respect to *Ulva* spores. The centrifuge tubes were filled with nano-pure water just before shipping. A

replicate was kept in-house under the same storage conditions and tested for water contact angle the same day the other samples were bioassayed.

***Ulva* Assays**

Ulva assays were performed by the Callow group at the University of Birmingham, UK. Samples were prepared at the University of Florida and then shipped to the Callow group for further evaluation. The procedure followed by the Callow group for the *Ulva* assays is reported in the literature and briefly described here for clarity [63, 97, 198, 199].

Ulva zoospores were obtained from fertile plants of *Ulva linza* and were placed in a suspension of artificial seawater that was diluted to a concentration of 2×10^6 ml^{-1} (see chapter 5 for complete discussion).

Zoospore settlement assays

PDMSe coated slides were equilibrated by immersion in sterile artificial seawater (Instant Ocean) for 24 h and then rinsed in sterile seawater. Slides were placed in individual compartments of quadriperm polystyrene culture dishes to which 10 ml of spore suspension was added. Dishes were incubated in the dark at 20^{o}C for 60 min.

The samples were washed to remove unattached spores by passing backwards and forwards 10 times through a beaker of seawater. Three replicate slides from each treatment were fixed in 2% glutaraldehyde in seawater and processed as described in Callow *et al*. (1997) [200]. The remaining three replicates were placed in a flow apparatus as described below before fixing.

Attached spores were counted at 1 mm intervals along the unpatterned portion of the replicate slides. On the patterned surfaces, attached spores were

counted at 0.5 mm intervals down two tracks of the long axis (10,000 μm) of each section of the patterned areas. Thirty counts were made for each of three replicates. Images of spores, on each of 3 replicate samples, were recorded in 30 fields of view using a x25 objective with a Zeiss Kontron 3000 image analysis system attached to a Zeiss epifluorescence microscope via a video camera as described in Callow *et al.* (2002) [97].

Zoospore shear strength assays

Slides settled with spores were exposed to shear in a specially designed flow cell apparatus [198], modified by fitting a higher capacity pump (1.12 kW (1.5 hp) 3-phase Baldor thermoplastic centrifugal pump (McMaster-Carr, Chicago, IL, USA) capable of delivering 281 L min^{-1} at 9 m head). The apparatus holds 6 1-inch by 3-inch microscope slides. A variable bedding system allowed the height of the coating surface to be adjusted so that it was flush with the surrounding channel wall.

Turbulent flow was created in a 60 cm long low aspect ratio section of channel preceding the slides. Flows of sea water (Instant Ocean) up to 4.9 m s^{-1} generate wall shear stresses up to 56 Pa. Exposure of slides to flow was standardized at 5 min. Wall shear stresses were determined from streamwise pressure drop measurements using the Reynolds-averaged Navier-Stokes equation [198].

Spore density on exposed slides was determined as described above. Control experiments conducted on uncoated slides have previously established

that there are no streamwise differences in the removal of cells in the flow chamber [199].

Percentage spore removal data were calculated from the mean number of spores remaining attached to the surface after exposure to turbulent flow compared with the mean number before the slides were subjected to flow. Data are expressed as percentage removal; 95% confidence limits were calculated from arc-sine transformed data. Spore settlement data are presented for the mean number of spores adhered and the 95% confidence limits (x=90).

Sporeling Growth Assays

Ulva zoospores were settled using standard methods as above. Six replicates of each treatment were settled with spores. Zoospores were settled in individual dishes containing 10 ml of zoospore suspension in the dark at ~20^{o}C. Unsettled spores were removed by washing and observed for symptoms of toxicity. Sporelings were cultured in enriched seawater medium in individual (10 ml) wells in polystyrene dishes under illuminated conditions. The medium was refreshed every 2 days and the sporelings cultured for 10 days.

The sporelings were scraped off and collected from half of each slide. The chlorophyll was extracted from the sporelings into dimethyl sulfoxide and the amount of chlorophyll$_a$ was determined spectrophotometrically. A direct proportionality has been shown between the quantity of chlorophyll$_a$ and the biomass of sporelings present.

Biomass was measured on one half of the slide before exposure to flow, and from the other half after flow in the water channel.

Strength of attachment of sporelings

The slides with biomass remaining on half of the area were exposed to a shear stress of 53 Pa in the water channel. The biomass remaining after exposure was analyzed for chlorophyll$_a$ content as described above.

Diatom Assays

Navicula assays were performed by the Callow group at the University of Birmingham, UK. Samples were prepared at the University of Florida and then shipped to the Callow group for further evaluation. The procedure followed by the Callow group for the *Ulva* assays is reported in the literature and briefly described here for clarity [90, 198, 199]

Diatom Settlement Assays

Per the protocol discussed in Holland et al 2004, *Navicula* diatom cells were cultured for three days in natural seawater supplemented with nutrients to form Guillard's F/2 medium [90, 201]. *Navicula* cells were cultured in F/2 medium. Cells were washed 3 times in artificial sea water (TM) to remove traces of medium and secondary metabolites before dilution with sea water to give a suspension of cells with chlorophyll$_a$ content of approximately 0.3 μg ml^{-1}.

Six replicates were used for each treatment. Cells were settled in individual dishes containing 10 ml of suspension in natural daylight at ~20 ^{o}C. After five hours, the slides were gently washed in seawater to remove unattached cells. Three replicate slides were fixed in 2.5% glutaraldehyde in sea water, desalted by washing first in 50:50 seawater/distilled water, followed by distilled water, and dried before counting. The density of cells attached to the surface was quantified on each slide using an image analysis system attached to a fluorescent

microscope. Counts were made for 15 fields of view (each 0.4 mm^2) on each slide.

Diatom Shear Strength Assays

The remaining three replicates were used to evaluate the strength of diatom attachment. Slides settled with *Navicula* were exposed to shear in a water flow cell. Glass standards were included. The water channel exposes cells to shear stresses that are approximate to those typically experience by ship hulls [198]. Slides were placed in the flow cell apparatus described above to expose attached diatoms to turbulent flow for 5 min at a range of wall shear stresses up to the maximum of 53 Pa. The maximum shear stress generated by this method does not necessarily remove the most tenaciously adhered diatom species; thus additional studies were also performed via water jet, which produces compressive as well as shear stresses on the slide surface [199, 202].

The number of cells remaining attached was compared with unexposed control slides (used to determine settlement as above). The number of cells in 15 fields of view (each 0.4 mm^2) were counted on each slide using an image analysis. Data are expressed as percentage removal with 95% confidence limits.

Statistics

Data were analyzed using the Fusion Pro (D.O.E. FusionTM) Design of Experiments software package. This program allows for the data analysis of designed experiments to determine and model the significant factors within the design. A factorial multi-level experimental design was analyzed at a 95% confidence level to determine statistically significant variables and at lower confidence levels to ascertain trends with respect to topography type (3 levels),

and substrate wettability (5 levels) on various spore density measurements. All comparisons described in the text as statistically significant are significant at a 95% confidence level.

Results and Discussion

The surface chemistry study is divided into four separate groups based on the particular shipment/spore batch. It is not possible to directly compare between spore batches due to seasonal variation, but a great deal of information was gained with each progressive study.

Pilot Experiment for *Ulva* Zoospore Settlement on PDMSe: Effect of Surface Chemistry and Topography Modifications

The full zoospore settlement and release assays are highly work-intensive. Therefore, when a new study is proposed, a simplified pilot experiment is conducted with fewer specimens per sample group to determine if a full study is warranted. A pilot experiment for the combined effects of surface chemistry and topography was performed in August of 2004. The patterned slides included a 1cm^2 area of the 2 μm sharklet discussed above and a 1cm^2 area of the 5 μm channels that were fully evaluated in Chapter 4. Flat area in between the patterns was used for the “flat” data reported. Completely smooth slides were also shipped for sporeling assays.

As in most o the previous pilot experiments, the samples were rushed and had not been fully evaluated prior to shipment. Pattern fidelity was poor; in fact the sharklets exhibited a strange edge effect that was originally attributed to the surface chemistry, but later was determined to be a problem with the wafer

replication step. This experiment was dubbed the gothic sharklet study because the pattern configuration was unexpected (Figure 6-5).

Table 6-1: Slides shipped for zoospore assay: pilot experiment to analyze bioresponse with respect to surface chemistry modifications and topography

Number of Slides	Formulation	Topography	Date Shipped
2	Unmodified PDMSe	None	8/04
2	Unmodified PDMSe	2 μm sharklet & 5 μm channel	8/04
2	PDMSe + mPEG-silane	None	8/04
2	PDMSe + mPEG-silane	2 μm sharklet & 5 μm channel	8/04
2	PDMSe + GPS + s-PSf	None	8/04
2	PDMSe + GPS + s-PSf	2 μm sharklet & 5 μm channel	8/04
2	PDMSe + ICPES + mPFPE-OH	None	8/04
2	PDMSe + mPFPE-OH derivatized with ICPES	2 μm sharklet & 5 μm channel	8/04

It was impossible to compare the differences in spore density attributed to surface chemistry from the sharklet patterns due to the fidelity problems. The fidelity of the sharklet replication was worst on the PEG samples. This resulted in abnormally high spore settlement counts for the PEG sharklet. Typically a > 50% reduction had been shown for high fidelity sharklets replicated with the PDMSe. For this study, the reduction in spore density for unmodified PDMSe was not statistically significant. As discussed in the introduction for this chapter, we have shown previously that the antifouling effects of the sharklet require high pattern fidelity. The problem was identified and eliminated for future studies.

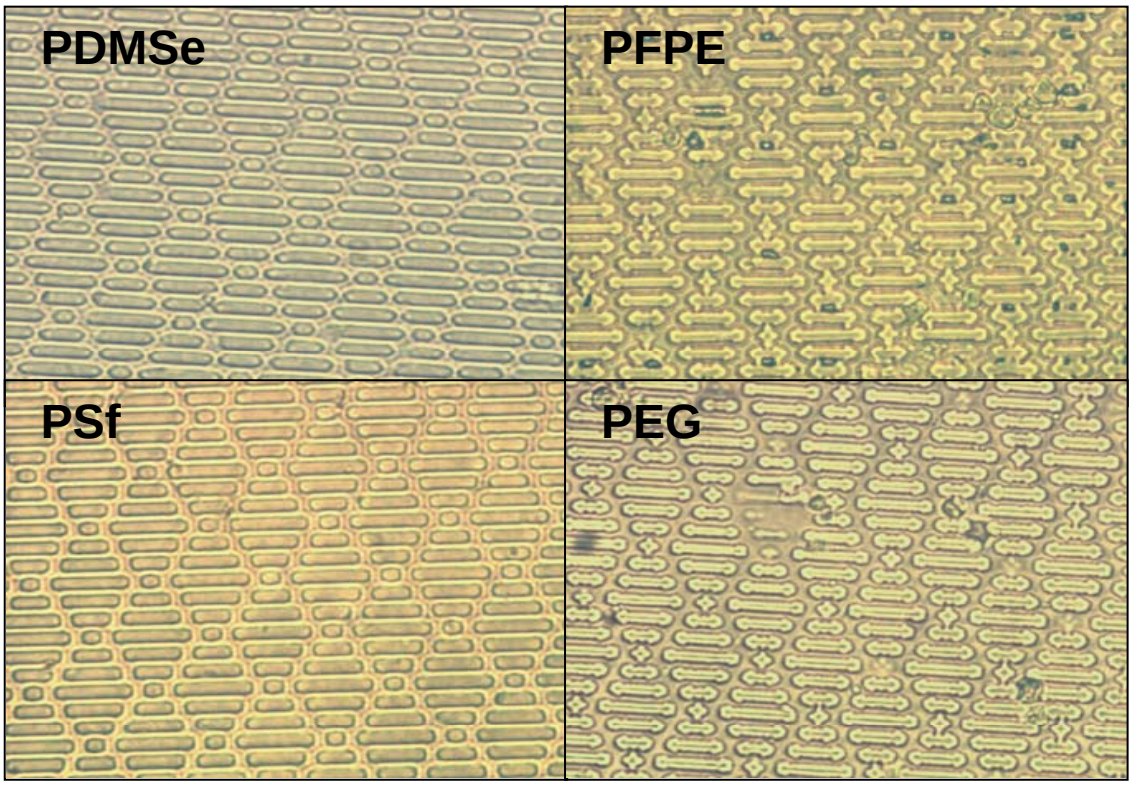

Figure 6-5: Optical microscope images of surface modified samples from pilot experiment. The two specimens on the left are good replicates of the sharklet design, and the two on the right are “gothic sharklets.”

An additional problem with the study was that the area of the sharklet pattern was too small for the given assay. In future studies, separate slides were shipped for smooth, sharklet, and channel features. The channel data and the results for the flat portions are useful for comparisons between the surface chemistries (Figure 6-6), as fidelity is not as great a concern for the 5 μm channel as compared to the 2 μm sharklets.

There was some increase, although not always statistically significant, for the spore settlement density in channels relative to smooth. There was a general trend of increasing spore settlement with increasing hydrophilicity. PDMSe-OH samples were not evaluated in this initial experiment, and no release data were obtained.

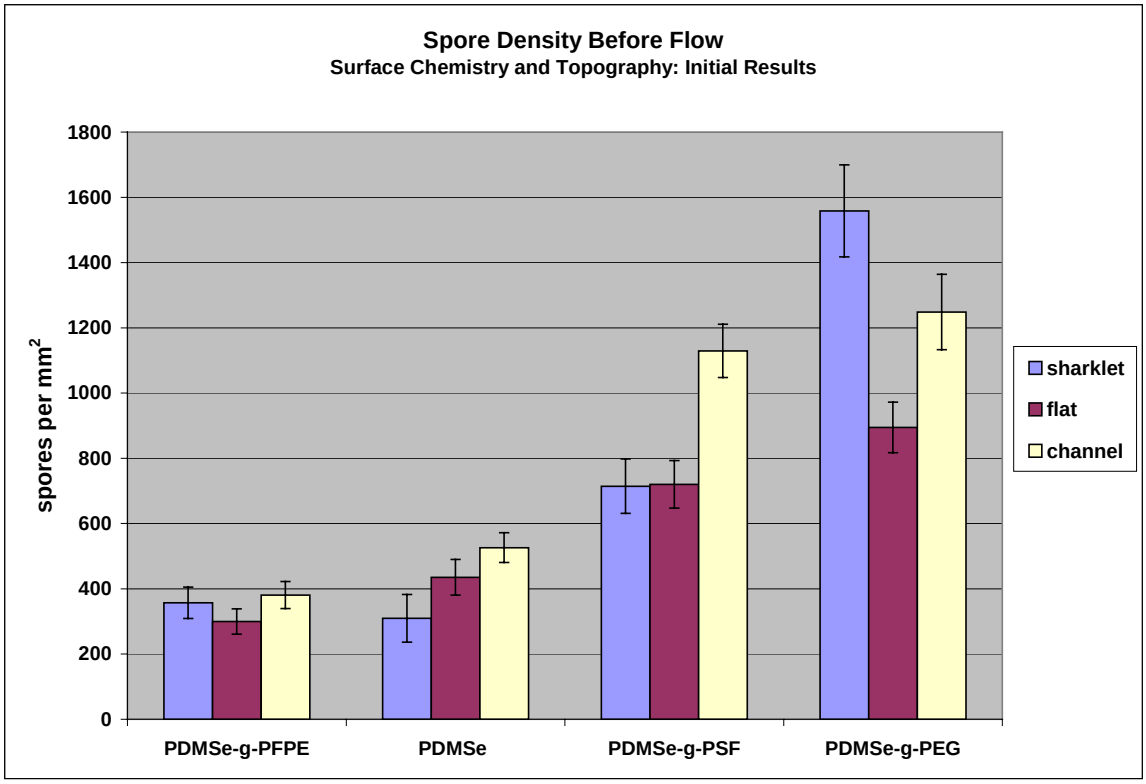

Figure 6-6: Spore settlement density counts for pilot surface chemistry and topography study. Substrates are ranked by increasing hydrophilicity. Each bar is the mean of 60 counts, 30 from each of 2 replicates. Bars show 95% confidence limits.

For the pilot study, two batches of samples were shipped. One batch was evaluated with zoospores assays as described above, and the other was reserved for sporelings assays (Figure 6-7). The smooth slides produced for the sporeling assay were produced at a later date, and the preparation of the PFPE modified samples was different.

This first batch was prepared using m-PFPE-OH that had been derivatized with isocyanatopropyltriethoxysilane catalyzed with DABCO as discussed in chapter 5. Only a small quantity had been prepared. When the second set of samples were requested on short notice, the PFPE slides were prepared by first reacting the ICPES with the silicone surface and then coupling the PFPE-OH.

The data for the two PFPE sample sets were vastly different, with the second set exhibiting extreme affinity for spores. The reaction time required for the urethane reaction with a DABCO catalyst is substantially longer than the time allowed for in the preparation of the smooth slides. The slides were then shipped in water to the Callow group in England.

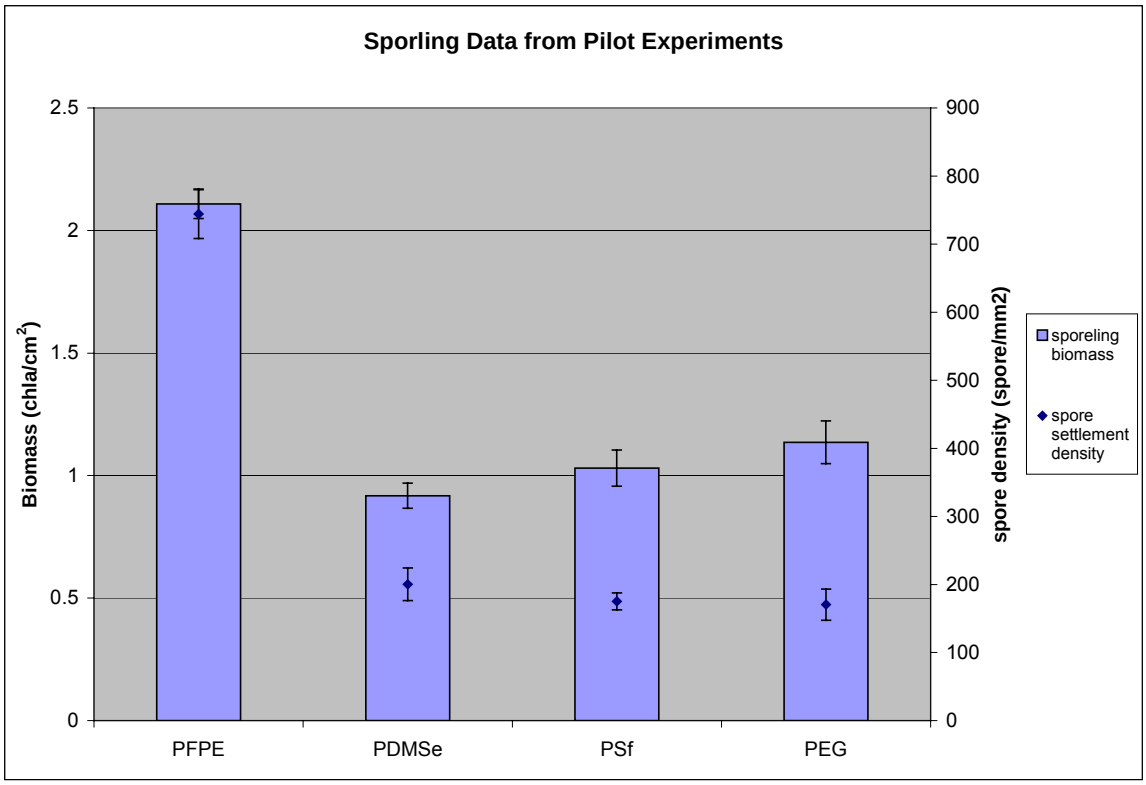

Figure 6-7: Spore settlement data are depicted as points and sporeling growth data at 8 days are reported as columns for surface modified samples in the pilot experiment. The PFPE sample was most likely degraded via hydrolysis at the coupling agent junction. Each bar is the mean of 90 counts, 30 from each of 6 replicates. Bars show 95% confidence limits.

There was PFPE coupled to the surface at the time of shipment, as evidenced by XPS (Figure 5-17 and Table 5-7). However, it is likely that the urethane bond was hydrolyzed leaving a very high-energy surface rather than the low surface energy fluorinated surface that was expected. The spore density on this surface was greater than all others evaluated.

The problem was identified and eliminated by obtaining mPFPE-silane rather than mPFPE-OH for future studies. Also, for subsequent studies, retains were prepared and stored in identical conditions as those shipped for assay. The samples could thus be tested on the same date as the spore assays to better explain the actual surface conditions experienced by the zoospores.

Despite the identified problems, this study did contribute several positive findings. The sporeling assay yielded little information, except the fact that there was no toxicity associated with any of the substrates. Additionally, there was no toxicity associated with the leachates of any of the substrates as determined in a separate assay. This finding allowed for continuation of the study. The spore settlement density appears to increase with increasing hydrophilicity. The spore settlement density on the channel micropatterned and smooth surface grafted PDMSe were all significantly different than unmodified PDMSe. The PFPE modified PDMSe had the lowest spore settlement density overall. This sample, however, had the highest settlement in the sporeling assay.

Ulva Sporeling Growth on Smooth PDMSe: Effect of Surface Chemistry

The pilot experiment was quite promising despite the problems with pattern fidelity. The spurious results for the PFPE modified samples in the sporeling data called the reproducibility of the surface treatments into question. Thus the next series of assays evaluated *Ulva* sporeling growth and attachment strengths for a large number of replicates to determine the reproducibility of the surface treatments.

Table 6-2: Slides shipped for sporeling assays: reproducibility of surface chemistry modifications

Number of Slides	Formulation	Topography	Date Shipped
7	Unmodified PDMSe	None	9/04
7	Unmodified PDMSe	None	11/04
7	PDMSe-OH	None	9/04
7	PDMSe-OH	None	11/04
7	PDMSe + mPEG-silane	None	9/04
7	PDMSe + mPEG-silane	None	11/04
7	PDMSe + GPS + s-PSf	None	9/04
7	PDMSe + GPS + s-PSf	None	11/04
14	PDMSe + mPFPE-silane	None	9/04
7	PDMSe + mPFPE-silane	None	11/04

The samples shipped in September were the first batch of samples produced using the m-PFPE-silane from DuPont. The technical advisors at DuPont suggested bulk deposition at 50°C under a gentle vacuum rather than deposition from an aqueous alcohol solution. The material is a highly viscous liquid. The attempt at bulk deposition left a thick viscous layer, and the excess non-reacted m-PFPE-silane did not rinse away easily.

Thus the slides were immersed in an appropriate solvent for fluoropolyethers. The solvent swelled the PDMSe and some solvent was trapped in the PDMSe. When the slides were shipped this solvent came to the surface and exhibited toxicity to the spores (Figure 6-8). The problem was identified and eliminated by returning to the aqueous alcohol deposition method.

Sporeling growth data varied between the two experiments. In the first experiment (Figure 6-9), the PEG modified PDMSe exhibited the lowest sporeling

growth and the PSf modified PDMSe had the greatest spore growth. The unmodified PDMSe and the PDMSe had similar sporeling growth response and did not vary significantly from the glass. The PFPE modified PDMSe and the unmodified PDMSe had similar sporeling growth and both had significantly less biomass than the glass.

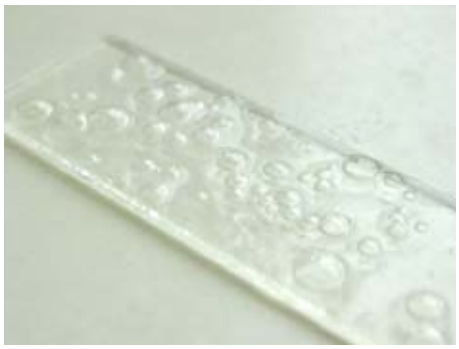

Figure 6-8: PFPE-modified surface showing details of air-bubbles on a slide removed from water. Photograph obtained from the Callow group.

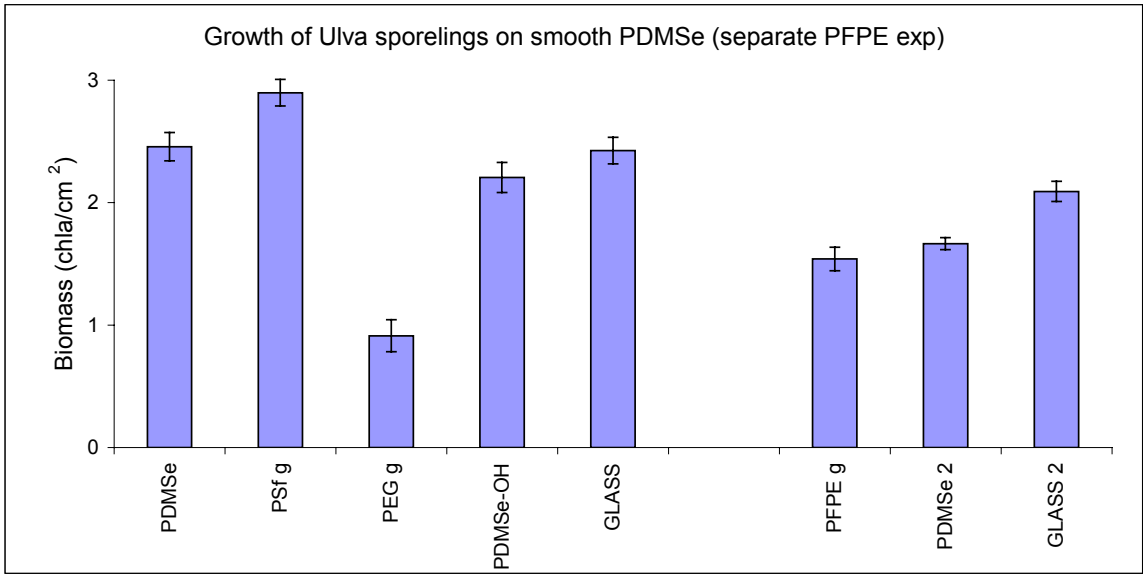

Figure 6-9: Sporeling growth data at 8 days for surface modified PDMSe samples. The original PFPE sample exhibited toxicity, so a separate experiment was run. Each bar is the mean 6 replicates. Bars show 95% confidence limits.

The growth data for the second study is not shown here graphically, but the glass had the highest biomass. The PEG modified silane had 11% less biomass

than glass, but had 17% more biomass than any of the other treatments, which were not statistically different than each other.

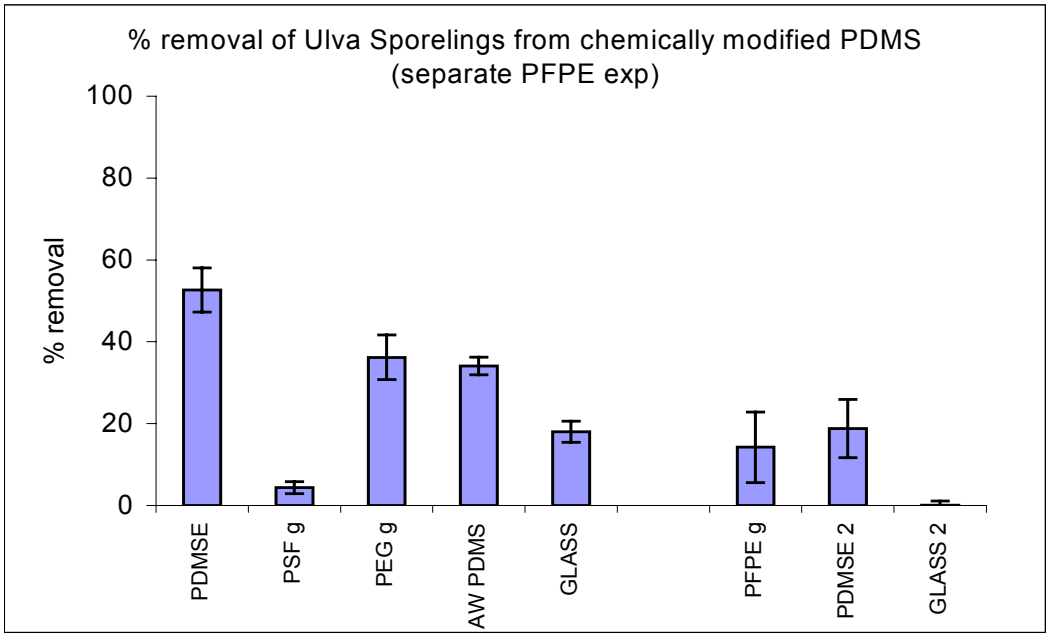

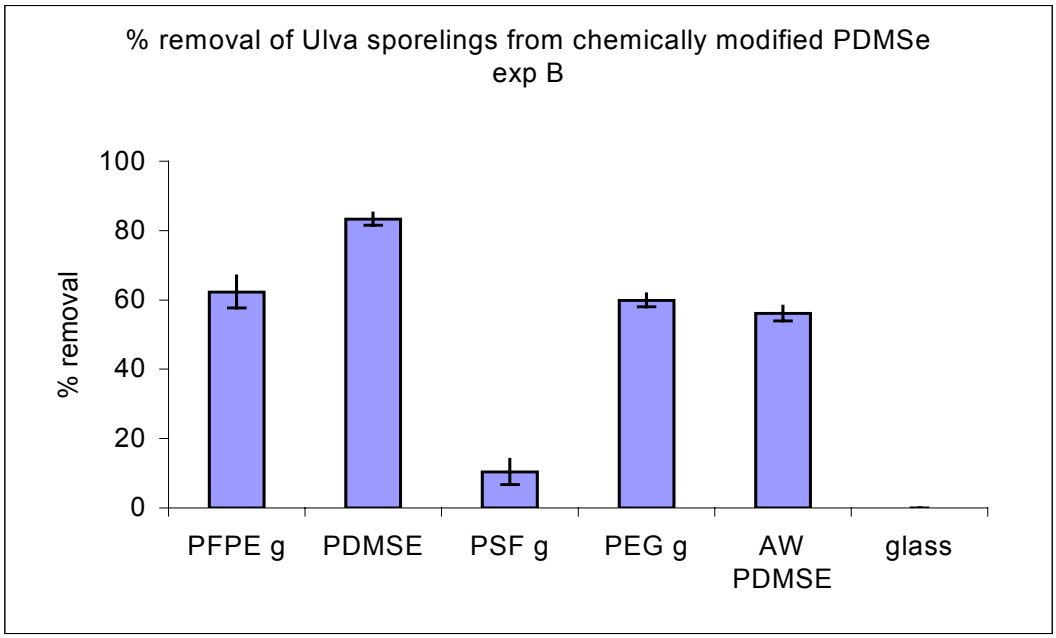

Figure 6-10: Percent removal of *Ulva* sporelings from surface modified PDMS coatings after exposure to shear stress of 53 Pa in water channel. Bars show the standard error of the mean derived from arcsine transformed data from six replicate slides.

The percent release data for these two studies (Figure 6-16 top and bottom) were more consistent than the growth data, for example the sporelings had the lowest retention on the unmodified PDMSe. In both studies, the sporelings had the highest adhesion to PSf, even higher than that on glass standards in the first study and performing only slightly better than glass in the second study. The growth of the sporelings on the PSf modified samples was greatest in the pilot study as well. It was not clear at that time what caused this high growth and adhesion.

This result was later attributed to the thickness of the coating on the PSf modified samples. For all other sample types only a single molecular layer of the polymer was grafted to the surface, because the only reactive site for coupling these polymers to the surface was at the end of the polymer chain. The PEG and PFPE both had molecular weights at or under 5kg/mol, but the PSf had a molecular weight greater than 30kg/mol. A single layer of PEG, PFPE, and PSf would be 0.3, 5, and 20nm thick, respectively, as estimated by a simple non-tethered model of the theoretical radius of gyration of the polymers and assuming no perturbation of the structure upon adsorption to the surface.

Therefore, even if one assumed that only one molecular layer of the polysulfone were tethered to the surface, it would still be thicker than the other surface graft types. However, the mechanism for the deposition of this polysulfone coating involved utilizing groups present along the backbone rather than at the polymer chain ends for coupling. This could result in a considerably

more complex and thicker surface coating. Since the bulk modulus of polysulfone is ~3 GPa, this thick coating would impart a higher surface modulus.

For both studies, the highest percent removal of sporelings was from the PDMSe coatings. PEG and hydrolyzed coatings exhibited statistically similar release properties relative to each other and demonstrated ~25% lower percent release values relative to unmodified PDMSe. PFPE modified samples exhibited less release than PDMSe and values that were not statistically different from either PDMSe-OH or PEG modified PDMSe. These two studies verified that chemically modified surfaces could be reproduced and were therefore ready for a full settlement and release assay with the *Ulva* zoospores.

Modification of PDMSe by Chemistry and Topography: Sharklet Patterns

Since the surface treatments were reproducible, a full study of the chemically modified sharklet micropatterns was launched. As discovered in the first chemistry/topography study, it is important the fidelity is high and that a large area of the sharklet is produced. The one inch square sharklet area was centered on the slide, and the flat areas at either end of the slide were also evaluated.

Table 6-3: Slides shipped for zoospore assay: full experiment to analyze bioresponse with respect to surface chemistry modifications and topography

Number of Slides	Formulation	Topography	Date Shipped
6	Unmodified PDMSe	sharklet	9/04
6	PDMSe-OH	sharklet	9/04
6	PDMSe + mPEG-silane	sharklet	9/04
6	PDMSe + GPS + s-PSf	sharklet	9/04
6	PDMSe + GPS + s-PSf	sharklet	10/04
6	PDMSe + mPFPE-silane	sharklet	9/04

The fidelity of the sharklet micropatterns was very good, but there were problems associated with the initial shipment of the polysulfone modified PDMSe. The thickness of the coating was such that the ribs of the sharklets were clumping together and appeared distorted (Figure 6-11). This, as well as the high adhesion of the *Ulva* sporelings in the previous study, was attributed to the high molecular weight of the PSf and the mechanism of deposition. This problem was identified and was eventually eliminated by purchasing hydroxyl-terminated polysulfone that could be derivatized. In the short term, samples were prepared with a shorter duration of exposure to the s-PSf solution to obtain sharklets that did not appear distorted. The settlement and release assays were performed as soon as the new PSf modified samples were shipped.

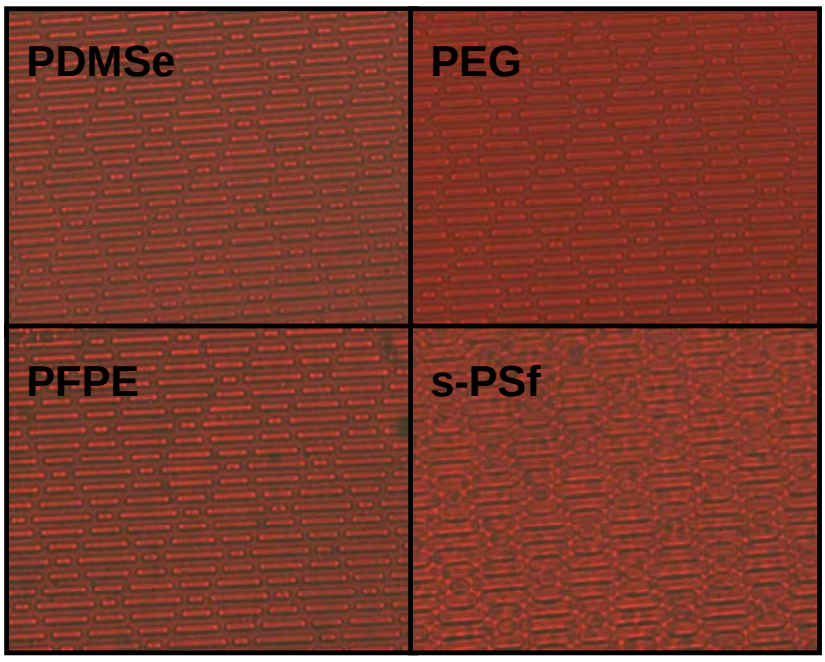

Figure 6-11: Optical microscope images of surface grafted PDMSe samples for *Ulva* bioassays.

The spore settlement data for the flat portions of the chemically modified are shown in Figure 6-12. The polysulfone settlement data, as in previous studies, seems higher than that which would be expected based on the wettability alone. These samples were still prepared with the sulfonated polysulfone coupled to the surface with GPS, which is hypothesized to have a higher surface modulus. The surface modulus was not quantified, so this hypothesis can neither be validated nor rejected.

It is interesting to note that for the flat slides the spore density data after exposure to flow follows the general shape of the Baier curve. The spore settlement density also shows a similar trend, with the exception of the polysulfone peak. The PDMSe has the lowest spore density values both before and after exposure to flow. There is a significant increase in spore density for the more hydrophobic (21%) and the more hydrophilic coatings (>50%). The Baier curve, as discussed in the introduction, is the trend of relative bioadhesion with surface energy for a series of dissimilar polymers. The term bioadhesion, in the context of Baier's work, referred to the number of cells remaining attached to the surface after exposure to flow. The spore density counts after exposure to flow would thus be directly analogous and followed the same trend note by Baier.

Brady and others hypothesized that the Baier minimum at PDMSe was related to the low modulus of this polymer relative to the other polymers assayed in his study. The substrates in the present research all have similar bulk moduli values, and yet, a statistically significant minimum still exists at PDMSe as

predicted by Baier. It is important to note that this trend was seen on the flat portions of the slide but not for patterned area of the slide.

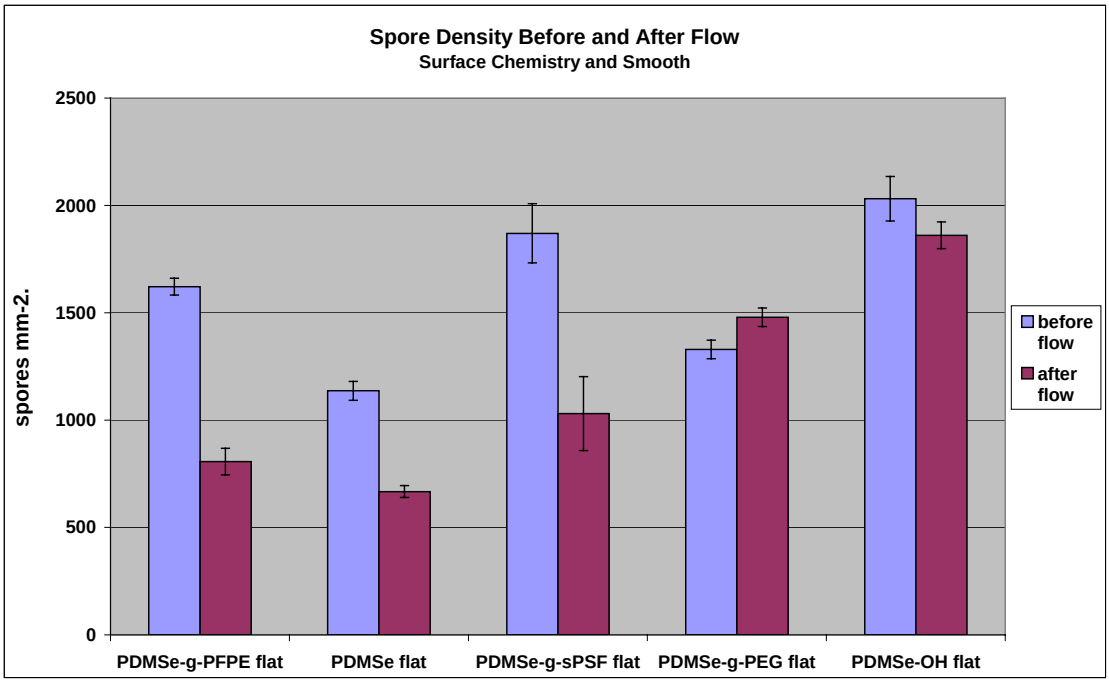

Figure 6-12: Number of spores attached to the surface of flat and sharklet patterned areas of modified PDMSe. Each bar is the mean of 90 counts, 30 from each of 3 replicates. Bars show 95% confidence limits.

The trends with respect to surface chemistry seen in the flat data are not exhibited on the sharklet micropatterns (flat data is shown as points on sharklet plot: Figure 6–13). This is curious as these respective data points are collected from the same slides, and the surface chemical treatment is continuous across the slides. There is still a minimum associated with the PDMSe sharklet slide. The highly hydrophilic PDMSe-OH slide had the second lowest spore density after flow for the sharklet slides, but the highest spore count on the flat slides. Apart from this data point, the Baier trend was followed.

On the PDMSe and PDMSe-OH slides there was a significant reduction in spore settlement for the sharklet relative to smooth. There was a slight reduction

in spore settlement for sharklet relative to smooth for the PEG and PFPE surface treatments, but no reduction for the polysulfone coating. There were no visible differences in the shape or dimensions of the sharklet patterns on these various surfaces.

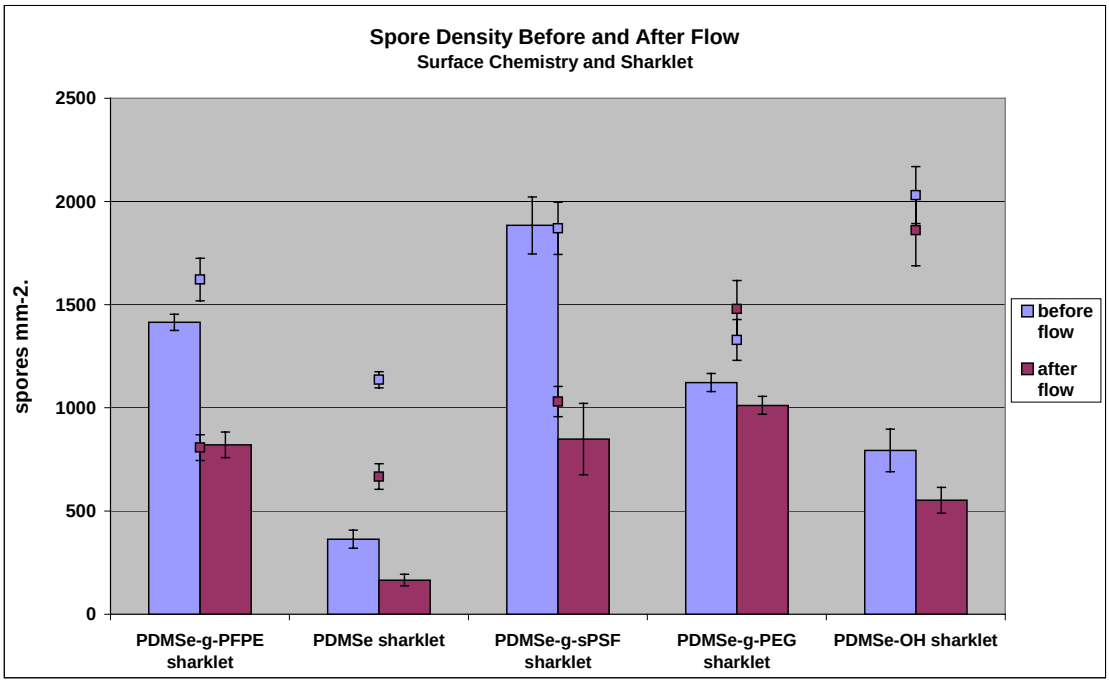

Figure 6-13: Spore density after exposure to flow. Each bar is the mean of 90 counts, 30 from each of 3 replicates. Bars show 95% confidence limits.

The overall spore settlement for this experiment was quite high. The spores were also very large relative to the size of the micropatterns. This experiment was the last experiment performed before the end of the 2004 season. After this point, further collection of spores was not possible due to cold weather.

There was almost no removal of spores from the flat areas of either the PDMSe-OH or the PDMSe-g-PEG; likewise for the PDMSe-g-PEG sharklet.

This was also the first experiment with the sharklet in which there was any significant removal from the sharklet micropattern (Figure 6-14). As discussed in

the introduction, the spores settled on the sharklet typically wedge themselves into the pattern and stick tenaciously. It is possible that this variation is due to the lateness in the spore season. The spores, as shown in images, are quite large and appeared to be settled atop the pattern, rather than within (Figure 6-15). The settlement of the spores on top of the pattern is less stable and led to the result that more spores were removed from the sharklet areas of the slides than from the flat for all coatings except the PFPE modified. On this coating there was still a significant release from the sharklets.

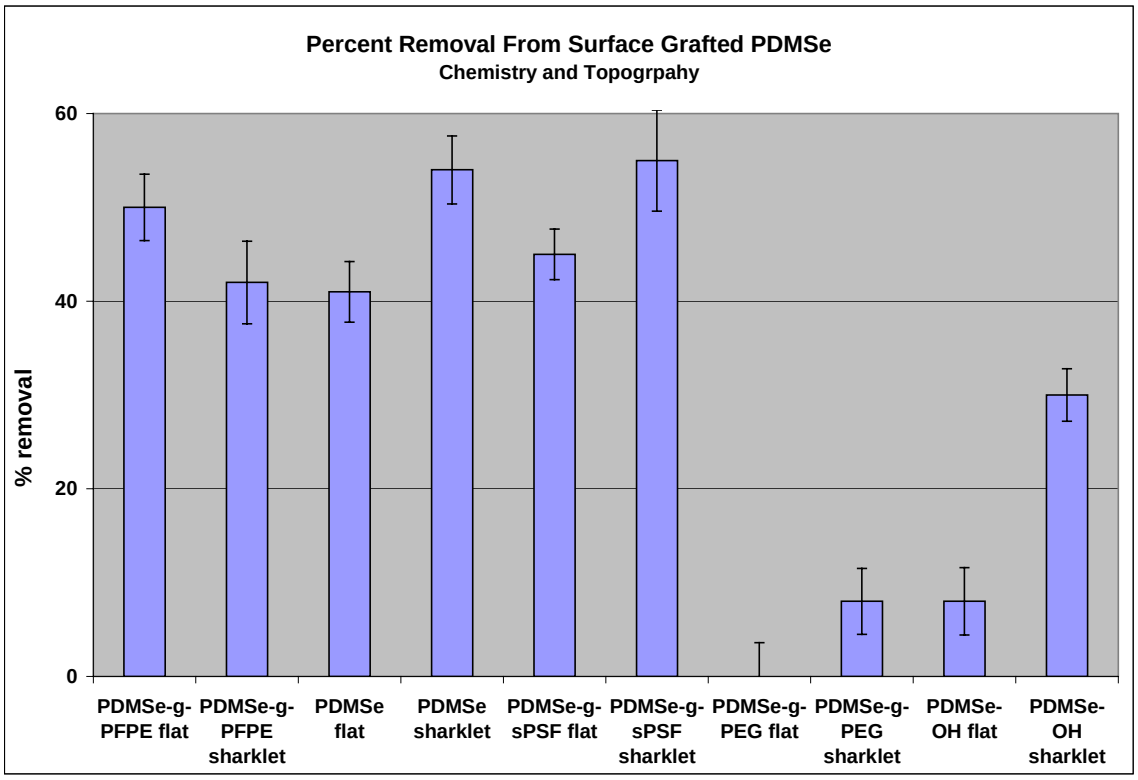

Figure 6-14: Percent removal after exposure to flow. Each point represents the mean percentage removal of *Ulva* zoospores from 90 observations of controls and 90 observations of treatments from 3 replicate slides. Bars represent 95 % confidence limits derived from arcsine transformed data.

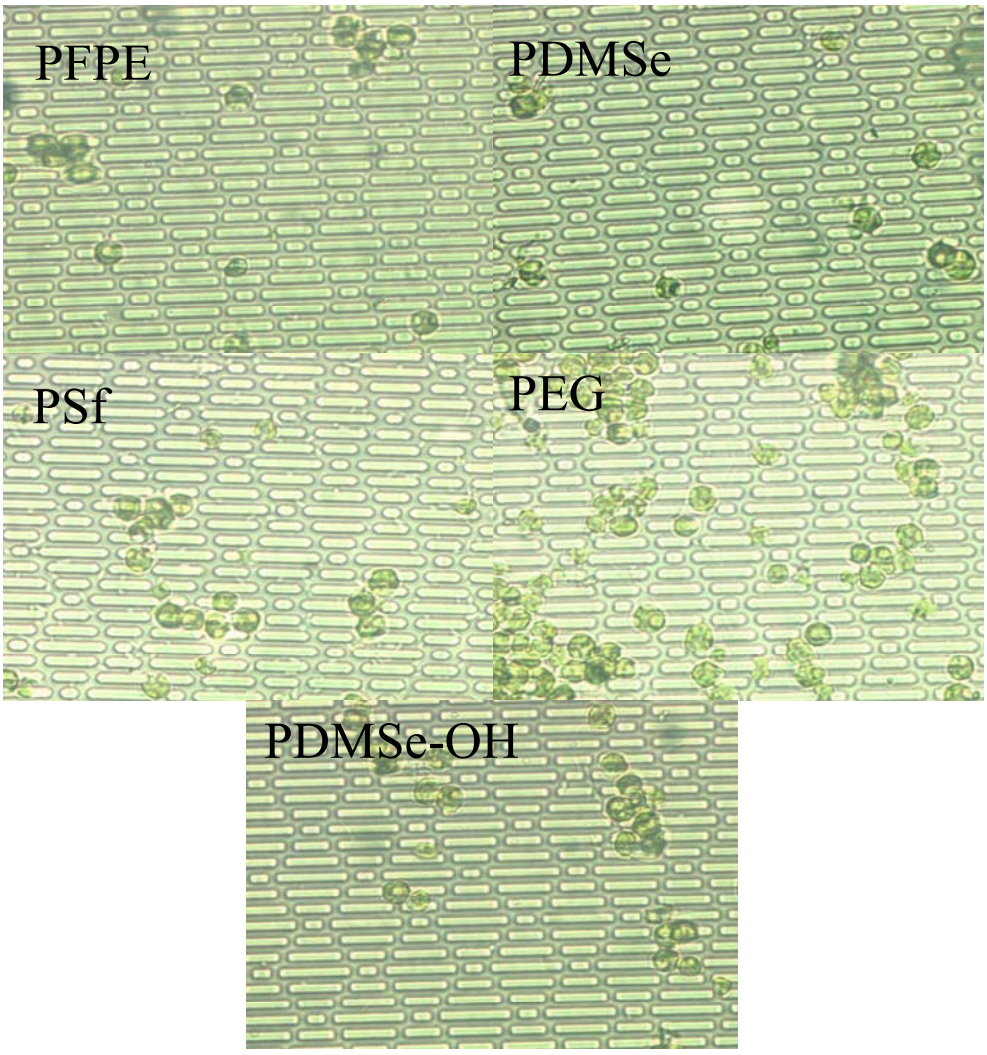

Figure 6-15: Images of zoospores on chemically treated PDMSe sharklets

Modification of PDMSe by Chemistry and Topography: Sharklet and Channel patterns

Due to the anomalous findings and the size of the spores, it was necessary to repeat this study with a second spore batch. A second full study was performed at the start of the new spore season in the spring of 2005. The smooth surface modified PDMSe samples were assayed with respect to spores, sporelings, and diatoms. Patterned and chemically modified samples were assayed with respect to spores.

Ulva sporeling growth and removal data

Table 6-4: Slides shipped for sporeling assay: analysis of bioresponse with respect to surface chemistry modifications

Number of Slides	Formulation	Topography	Date Shipped
6	Unmodified PDMSe	Smooth	3/05
6	PDMSe-OH	Smooth	3/05
6	PDMSe + mPEG-silane	Smooth	3/05
6	PDMSe + GPS + s-PSf	Smooth	3/05
6	PDMSe + GPS + s-PSf	Smooth	3/05

The sporeling assays were highly successful and clearly slowed the effect of surface chemistry on *Ulva* sporeling growth. The growth of *Ulva* sporelings was greater on the hydrophobic than hydrophilic coatings (Figure 6-16) with the lowest settlement on glass standards. All PDMSe based coatings exhibited significantly higher settlement than that found on the glass standard. There was a trend of increasing settlement with increasing hydrophobicity. Spore settlement counts were not performed for this assay, but this trend most likely reflects a higher spore settlement on these coatings. Previous studies have often shown that the spores prefer to settle on hydrophobic rather than hydrophilic surfaces.

Sporeling removal was considerably greater from the hydrophobic coatings than from the hydrophilic coatings or the glass standard (Figure 6-17). There was no release from the glass standard and little release was detected from the hydrophilic coatings. The greatest release was from the unmodified PDMSe, but this value was not statistically different from the PFPE modified PDMSe.

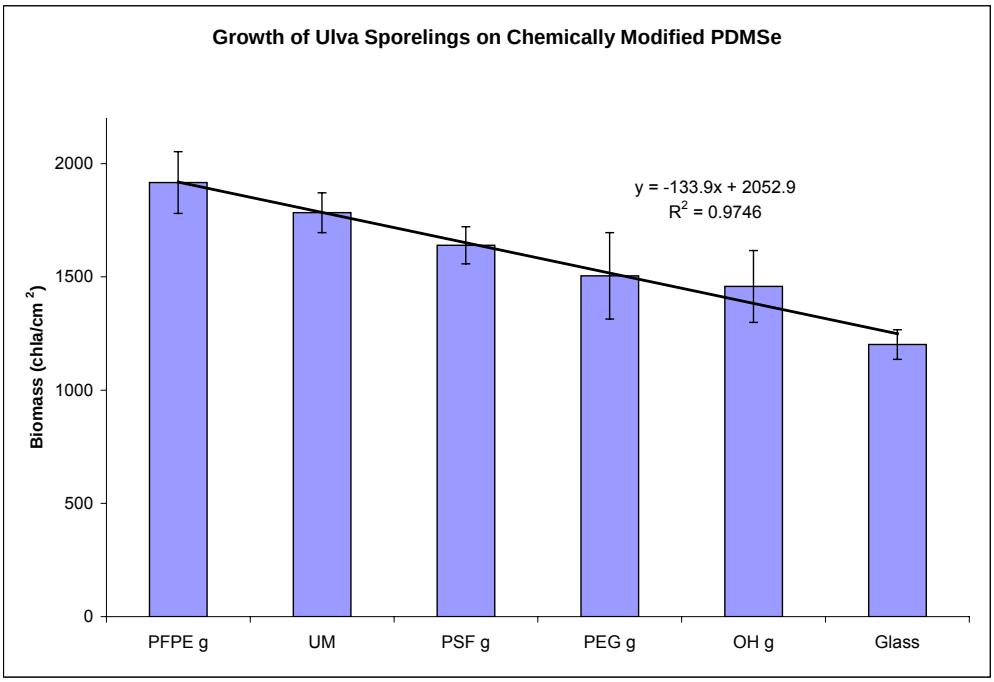

Figure 6-16: Growth of *Ulva* sporelings on surface-modified PDMSE coatings after 9 days. Each point is the mean biomass from 3 replicate slides. Bars show standard error of the mean.

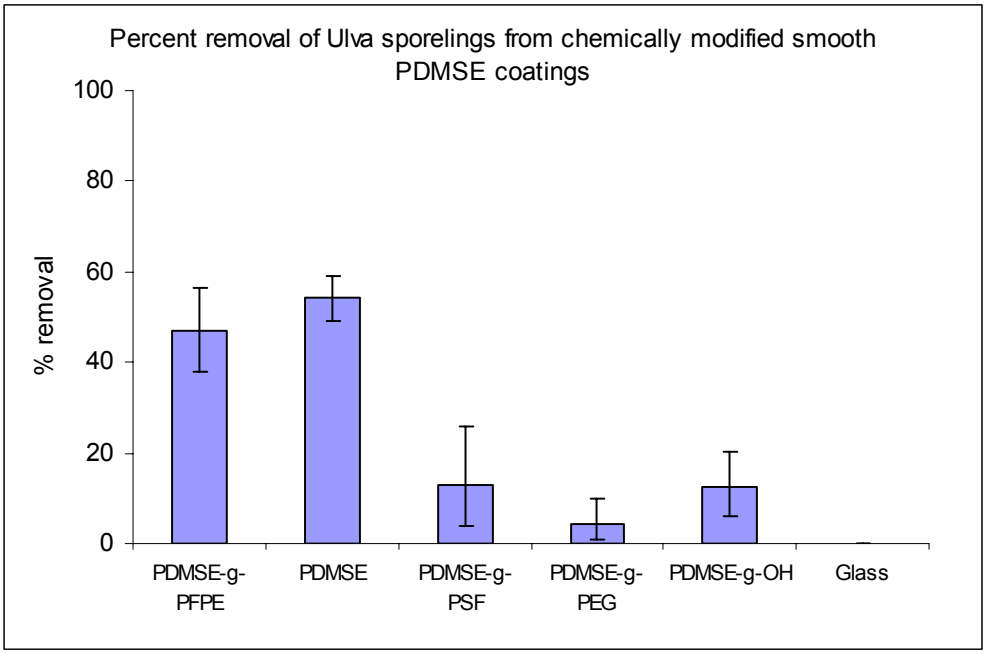

Figure 6-17: Detachment of *Ulva* sporelings plotted as % removal after 9 days growth. Coatings were exposed to a surface pressure of 57 kPa from the water jet. Each point represents the mean percentage removal from 3 replicate slides. Bars represent standard error of the mean derived from arcsine transformed data.

These data suggest good correlation of sporeling data and surface wettability as indicated by an R^2 value of 0.9746. Previous studies from various researchers have indicated that settlement and growth of *Ulva* algae are greater on hydrophobic coatings, but that the release of *Ulva* is also greatest on hydrophobic coatings.

Diatom settlement and release data

Table 6-5: Slides shipped for diatom assay: analysis of bioresponse with respect to surface chemistry modifications

Number of Slides	Formulation	Topography	Date Shipped
6	Unmodified PDMSe	Smooth	4/05
6	PDMSe-OH	Smooth	4/05
6	PDMSe + mPEG-silane	Smooth	4/05
6	PDMSe + GPS + s-PSf	Smooth	4/05
6	PDMSe + GPS + s-PSf	Smooth	4/05

The number of attached diatoms was substantial on all surfaces (Figure 6-18). It has been determined that diatoms settle under the influence of gravity and cannot ‘select’ where they land, as directly opposed to *Ulva* spores that swim and probe a substrate for a suitable location. The attachment of diatoms depends on the expression of their adhesive/locomotory polymers and their compatibility with the surface.

In general, the number of attached cells was slightly higher on the hydrophilic surfaces. This was unexpected because the rinsing process typically removes more cells from hydrophilic than from hydrophobic surfaces because the strength of adhesion is typically greater on the latter. In this study, the initial

attachment period was quite short and it may be that diatoms require more time to adhere strongly to the hydrophobic surfaces.

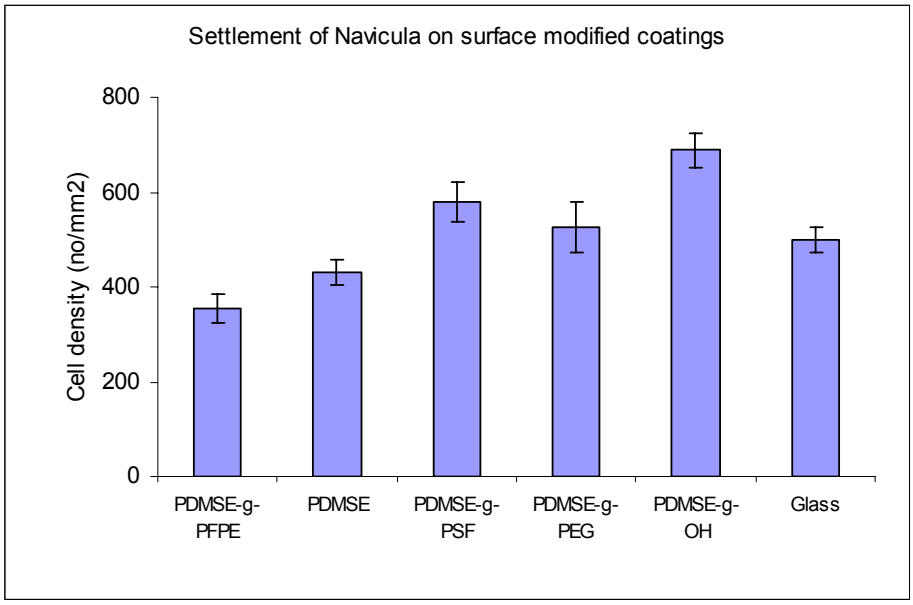

Figure 6-18: Density of *Navicula* cells on surface-modified coatings after settlement and gentle washing. Each bar is the mean of 90 counts, 30 from each of 3 replicates. Bars show 95% confidence limits.

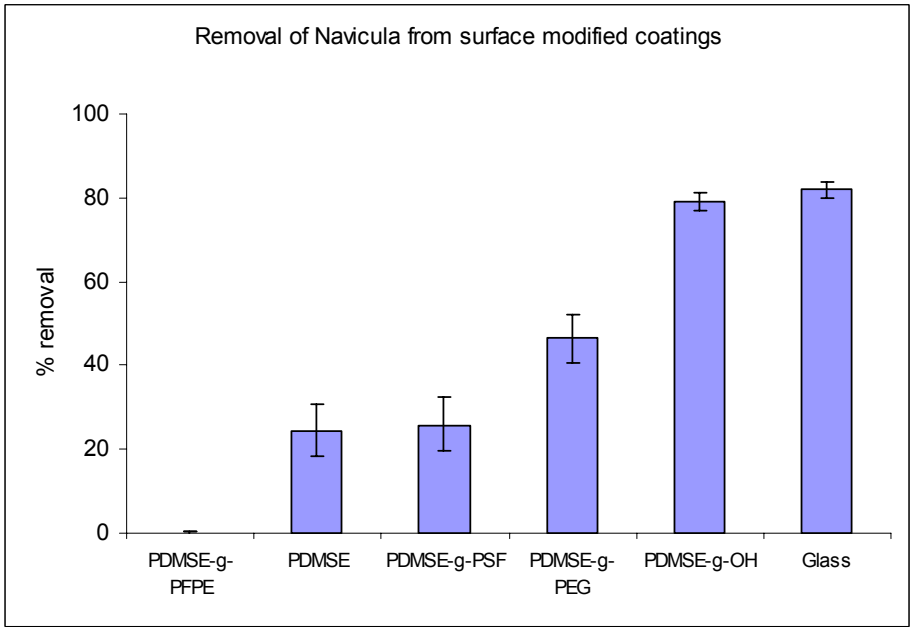

Figure 6-19: Detachment plotted as % removal following a 1 h settlement period + 2 h incubation. Each point represents the mean percentage removal of *Navicula* cells from 90 observations of controls and 90 observations of treatments from 3 replicate slides. Bars represent 95 % confidence limits derived from arcsine transformed data.

Diatoms exhibited greater release from surfaces with increasing wettability (Figure 6-19). This is in agreement with data from other experiments in which attachment strengths to surfaces with different wettabilities have been studied e.g. Finlay et al., (2002) [199]; Holland et al. (2004) [90]. The strong correlation of the diatom release data with substrate wettability show the efficacy of these surface grafts in evaluating the bioresonse.

***Ulva* zoospore settlement and release data**

A second full study of the chemically modified and patterned slides was launched during the 2005 spring season when spores were next available. This study evaluated a set of uniformly smooth slides two sets of patterned slides, the 2 μm sharklets and 5 μm deep, 5 μm wide channels separated by 5 μm ridges. The smooth slides and patterned slides were assayed with two separate spore batches. Thus the flat areas on the patterned slides were also evaluated.

Data were analyzed for statistical trends using the Fusion Pro software package. This program allows for the data analysis of designed experiments to determine and model the significant factors within the design. A factorial multi-level experimental design was analyzed at a 95% confidence level to determine statistically significant variables and at lower confidence levels to ascertain trends with respect to topography type (3 levels), and substrate wettability (5 levels) on various spore density measurements. All comparisons described in the text as statistically significant are significant at a 95% confidence level. The data for the smooth study was evaluated separately from the patterned slides, as these two groups were run with separate spore batches. The sharklet and

channel data sets were evaluated separately and together to more fully explain the trends.

Table 6-6: Slides shipped for zoospore assay: full experiment to analyze bioresponse with respect to surface chemistry modifications and topography

Number of Slides	Formulation	Topography	Date Shipped
6	Unmodified PDMSe	Smooth	3/05
6	PDMSe-OH	Smooth	3/05
6	PDMSe + mPEG-silane	Smooth	3/05
6	PDMSe + GPS + s-PSf	Smooth	3/05
6	PDMSe + GPS + s-PSf	Smooth	3/05
6	Unmodified PDMSe	Sharklet	3/05
6	PDMSe-OH	Sharklet	3/05
6	PDMSe + mPEG-silane	Sharklet	3/05
6	PDMSe + GPS + s-PSf	Sharklet	3/05
6	PDMSe + GPS + s-PSf	Sharklet	3/05
6	Unmodified PDMSe	Channel	3/05
6	PDMSe-OH	Channel	3/05
6	PDMSe + mPEG-silane	Channel	3/05
6	PDMSe + PSf-silane	Channel	3/05
6	PDMSe + mPFPE-silane	Channel	3/05

Smooth. On uniformly smooth surfaces, substrate wettability is a statistically significant variable for spore density before and after exposure to flow (Figure 6-20). Values for spore density before and after flow increase with decreasing wettability. This was unexpected as the previous spore density after exposure to flow had exhibited a minimum at PDMSe. For this batch of slides, the PDMSe-g-PEG and PDMSe-OH both exhibited lower spore density after flow than the PDMSe. The PDMSe-g-PFE had the highest spore counts before and after flow.

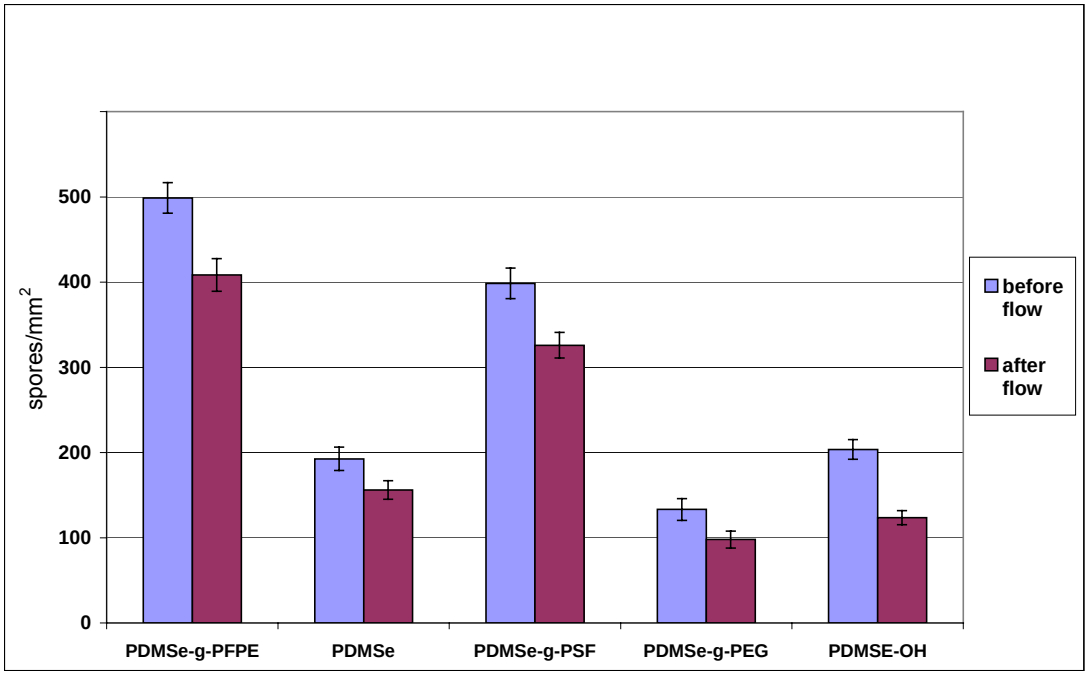

Figure 6-20: Number of spores attached to the surface of modified PDMSe before and after exposure to a shear stress of 53 Pa. Each bar is the mean of 90 counts, 30 from each of 3 replicates. Bars show 95% confidence limits.

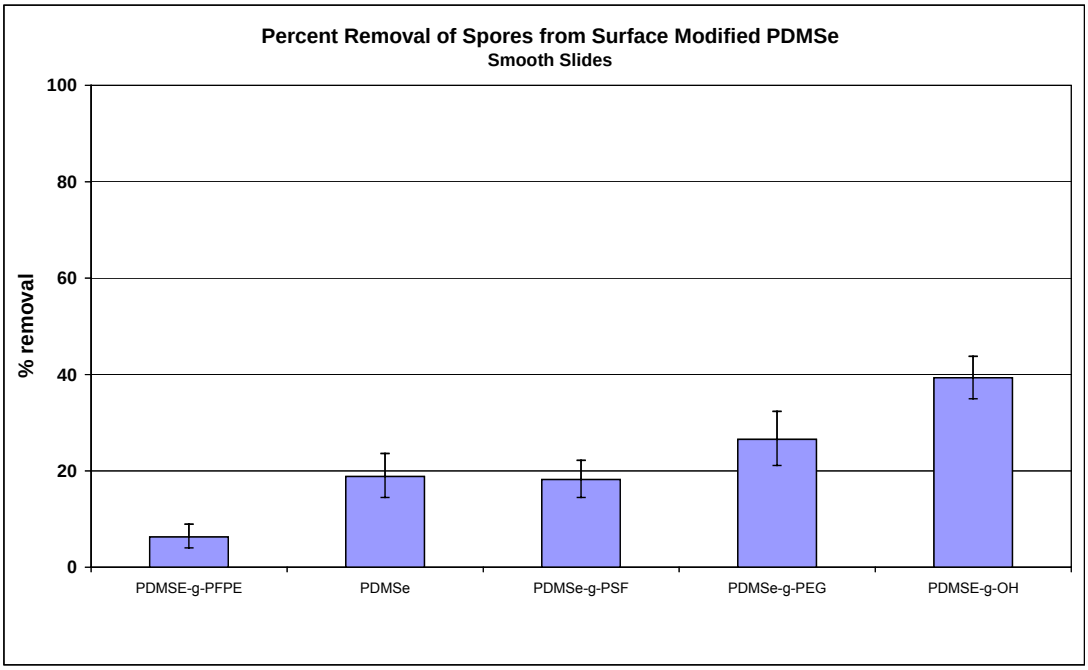

Figure 6-21: Percent removal after exposure to flow. Each point represents the mean percentage removal of *Ulva* zoospores from 90 observations of controls and 90 observations of treatments from 3 replicate slides. Bars represent 95 % confidence limits derived from arcsine transformed data.

Percent removal, alternately, was correlated with increasing surface wettability, although overall, percentage removal was relatively low (maximum 40%) (Figure 6-21). Settlement is higher on the PFPE and PSf-modified surfaces then on the other three surfaces.

Sharklet. The patterned area was approximately 1 inch square and was located in the middle of the slide. The number of spores settled on the flat and patterned areas before flow (Figure 6-22) and after flow (Figure 6-23) are shown. The spore density after flow for the flat area of the patterned slide exhibited the Baier trend with the minimum at PDMSe as predicted and as seen in the previous sharklet study. Also, as in the previous sharklet study, the patterned area of the slide did not follow the same trend as the flat area. It cannot be determined at this time whether this was due to pattern fidelity or some other unknown factor.

The sharklet pattern reduced settlement on all chemically modified PDMSe surfaces compared to the adjacent flat areas. In the previous study, there was only a slight decrease in settlement for the patterned areas. For this study, the fidelity was greatly improved. Topography was seen to have a more profound effect on spore settlement than surface chemistry as determined by the statistical analysis, which ranked the importance of the variables as such. The majority of spores that did settle on the sharklet patterned areas were settled in defects. The greatest reduction in settlement for the sharklet relative to the flat was seen on the unmodified PDMSe. It is unclear if this is an effect of pattern fidelity or surface chemistry (Figure 6-25).

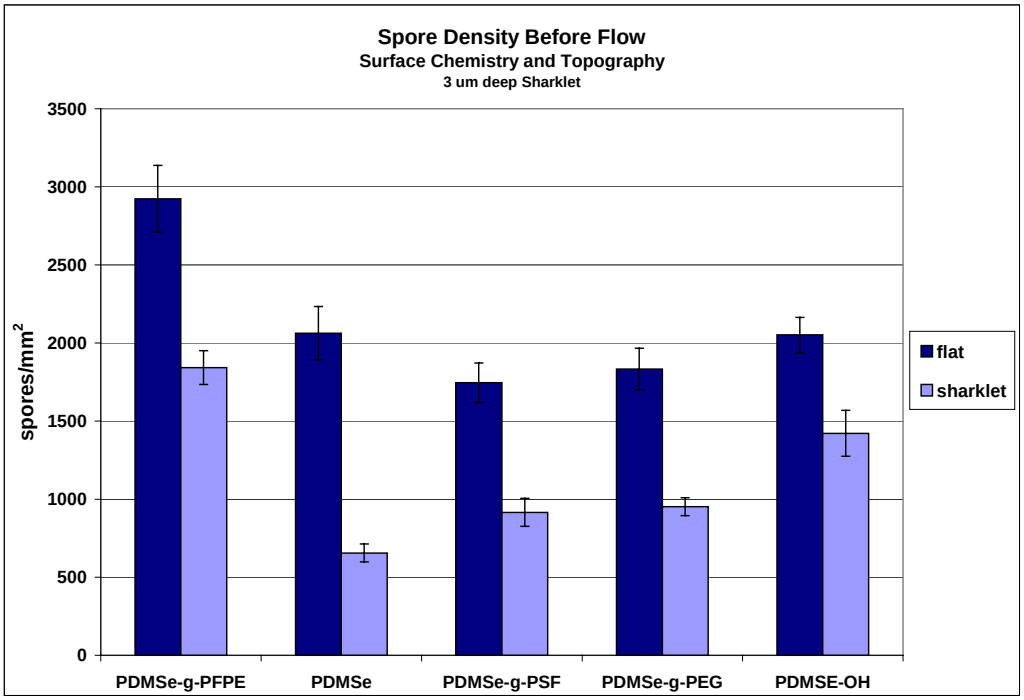

Figure 6-22: Number of spores attached to the surface of flat and sharklet patterned areas of modified PDMSe. Each bar is the mean of 90 counts, 30 from each of 3 replicates. Bars show 95% confidence limits.

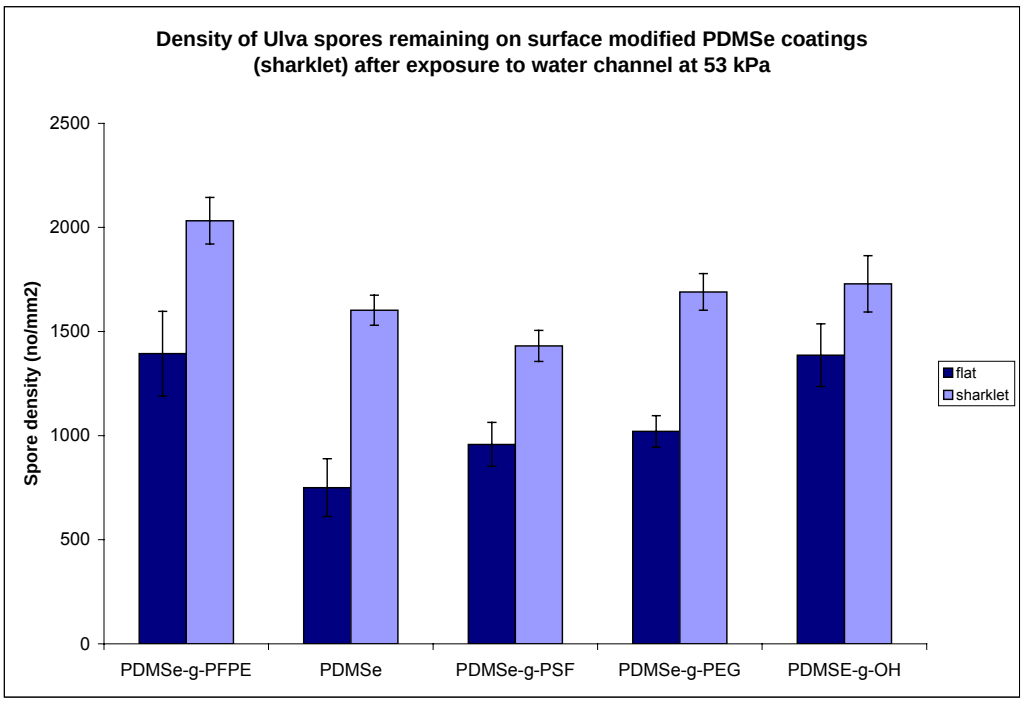

Figure 6-23: Number of spores attached after exposure to flow to the surface of flat and areas patterned with sharklets of modified PDMSe. Each bar is the mean of 90 counts, 30 from each of 3 replicates. Bars show 95% confidence limits

After exposure to water flow, few spores were removed from the sharklet patterned areas. This is as expected from all previous studies except the last one in which the spores were abnormally large. The spore density after flow was greater on the sharklet patterns of a given chemistry than on its flat area. It is also an interesting note that the Baier trend was once again detected for the spore density after flow on the flat portions of the slides.

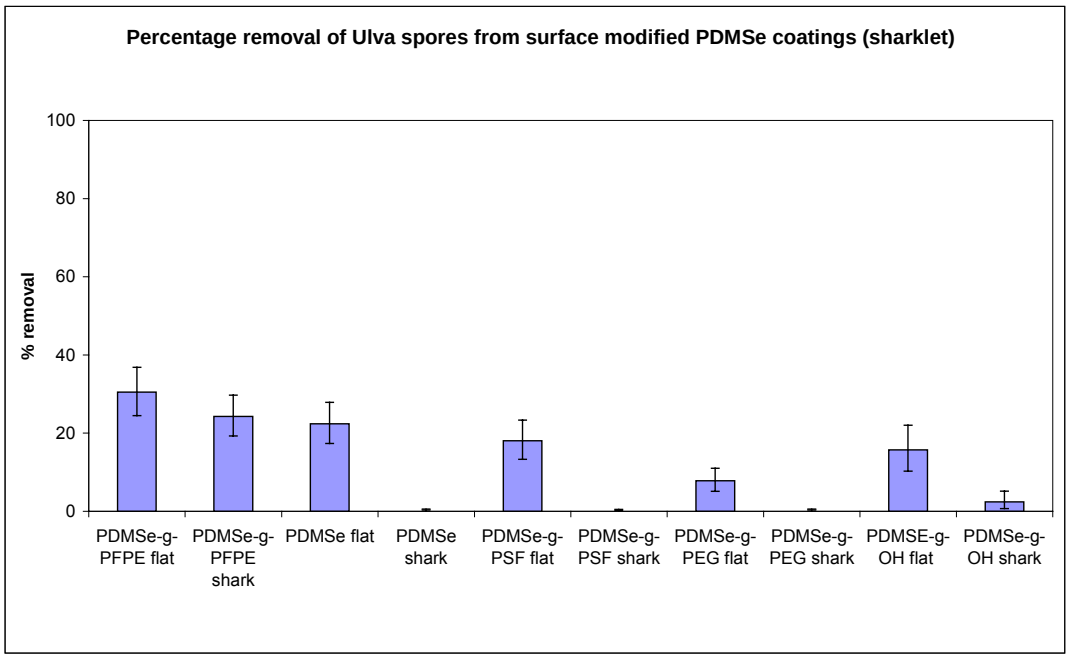

Figure 6-24: Percent removal after exposure to flow. Each point represents the mean percentage removal of *Ulva* zoospores from 90 observations of controls and 90 observations of treatments from 3 replicate slides. Bars represent 95 % confidence limits derived from arcsine transformed data.

Percentage removal from the flat areas of all samples was relatively low (Figure 6-23). Highest removal (30%) was from the PFPE grafted surface. Spores settled on both the flat and sharklet portions of the PDMSe-g-PFPE were settled in aggregates that protruded from the surface of the slide. Typically spores aggregates have greater attachment strength because all spores in these gregarious settlement groups are attached to the surface and enhance each

other's adhesive properties. This is not the case with the spore groups of the fluorinated surface. As these slides were removed from the spore solution, the slide immediately dewetted, gathering the spores together to form these aggregates such that the spores were not attached to the surface at all points.

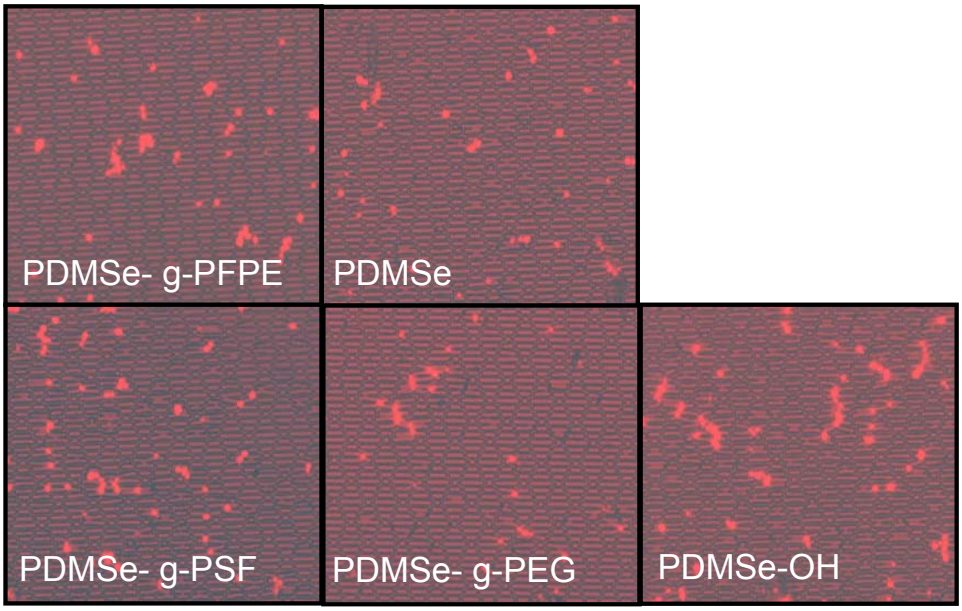

Figure 6-25: Images of *Ulva* spores on surface treated sharklet micropatterns

Channel. The 1 cm square patterned area was divided into three areas in which channels were either 5, 10 and 20 μm wide. All channels were 5μm deep and separated by 5 μm ridges. Spores were counted in the 5μm wide channels, but not for the 10 or 20 μm channels.

The spore settlement density was quite high. Figure 6-26 shows the number of spores settled on the flat area and the area with 5μm wide channels. Figure 6-27 shows the number of spores attached before and after flow.

The Baier trend was not seen for either the flat or patterned area of these slides. It should be noted that these slides were assayed at the same time as the sharklet samples that did exhibit the Baier trend. For the channel slides,

topography had a great influence on the settlement density. In all cases, higher numbers of spores settled on the area with 5μm wide channels compared to the flat surface.

Spores packed in the channels frequently deformed the channels/ridges (Figure 6-29). This had not bee seen in previous studies of the channels in the 2002-topography/oil addition studies. As was seen in these previous experiments, spore settlement in 5 μm wide channels is highly variable.

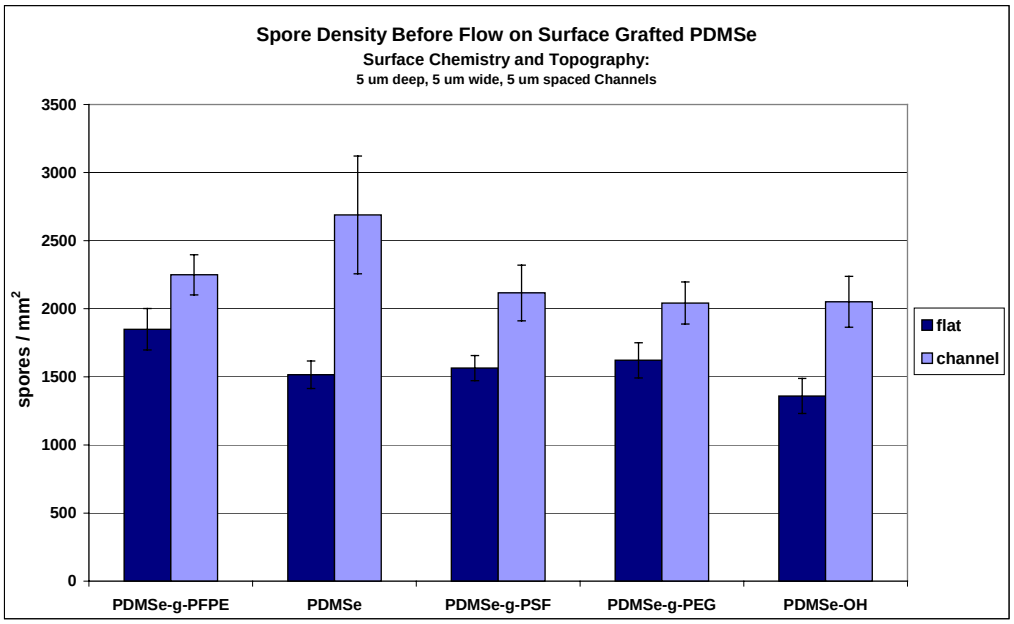

Figure 6-26: Number of spores attached to the surface of modified PDMSe. Each bar is the mean of 90 counts, 30 from each of 3 replicates. Bars show 95% confidence limits.

For all samples, there was higher percentage removal from areas with channels than the equivalent flat area. Removal from the channel area of the PSf-grafted surface was lower (~10% removal) than from all of the other surfaces (~40%). A similar trend was noted for the flat portions of the PSf-grafted.

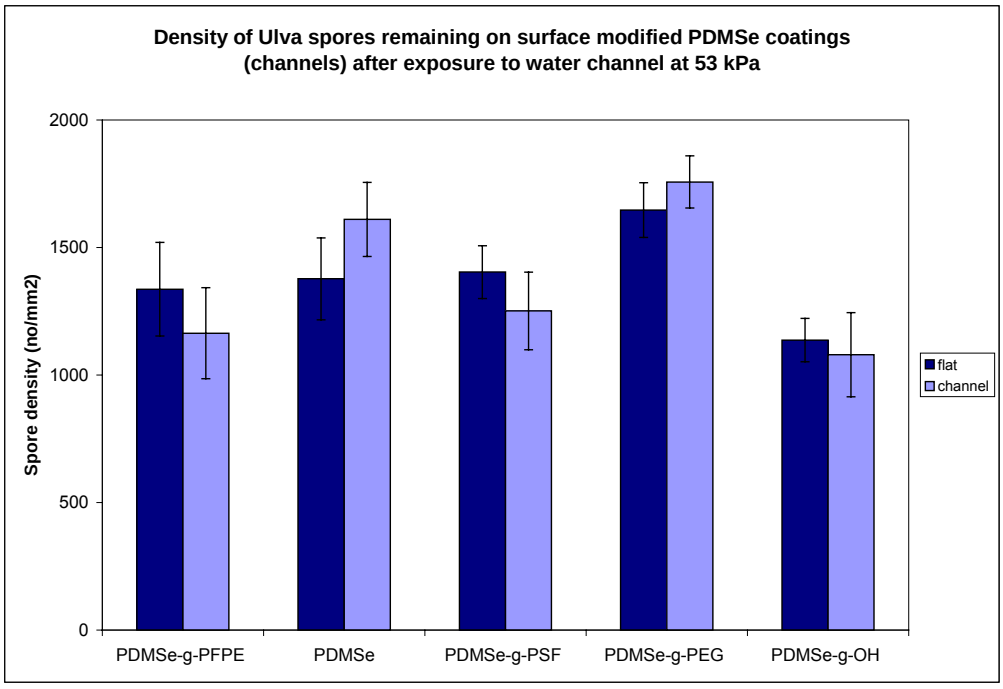

Figure 6-27: Number of spores attached to the surface of modified PDMSe before and after exposure to a shear stress of 53 Pa. Each bar is the mean of 90 counts, 30 from each of 3 replicates. Bars show 95% confidence limits.

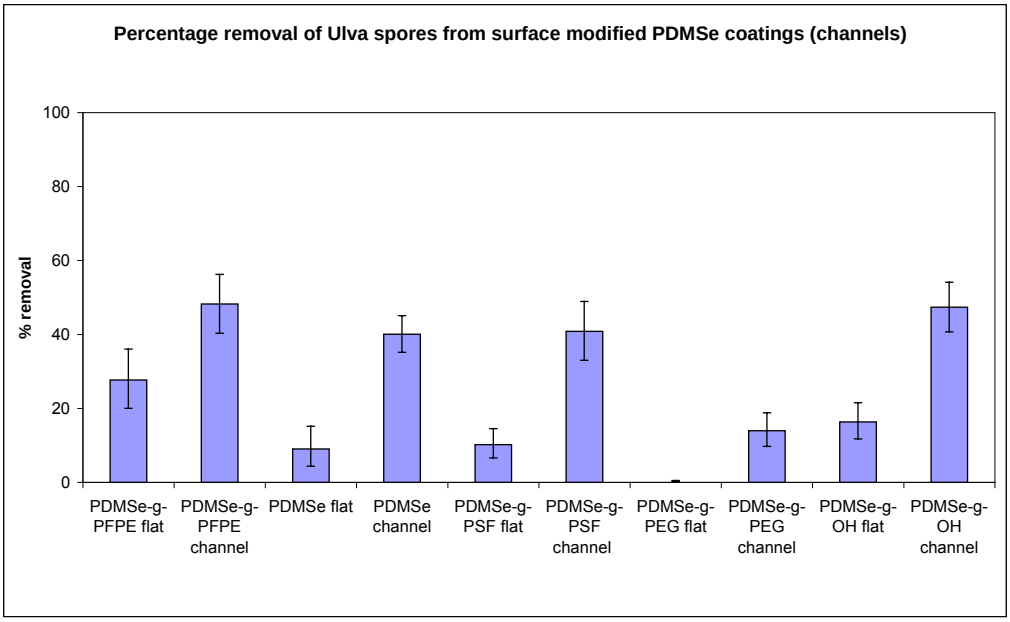

Figure 6-28: Percent removal after exposure to flow. Each point represents the mean percentage removal of *Ulva* zoospores from 90 observations of controls and 90 observations of treatments from 3 replicate slides. Bars represent 95 % confidence limits derived from arcsine transformed data.

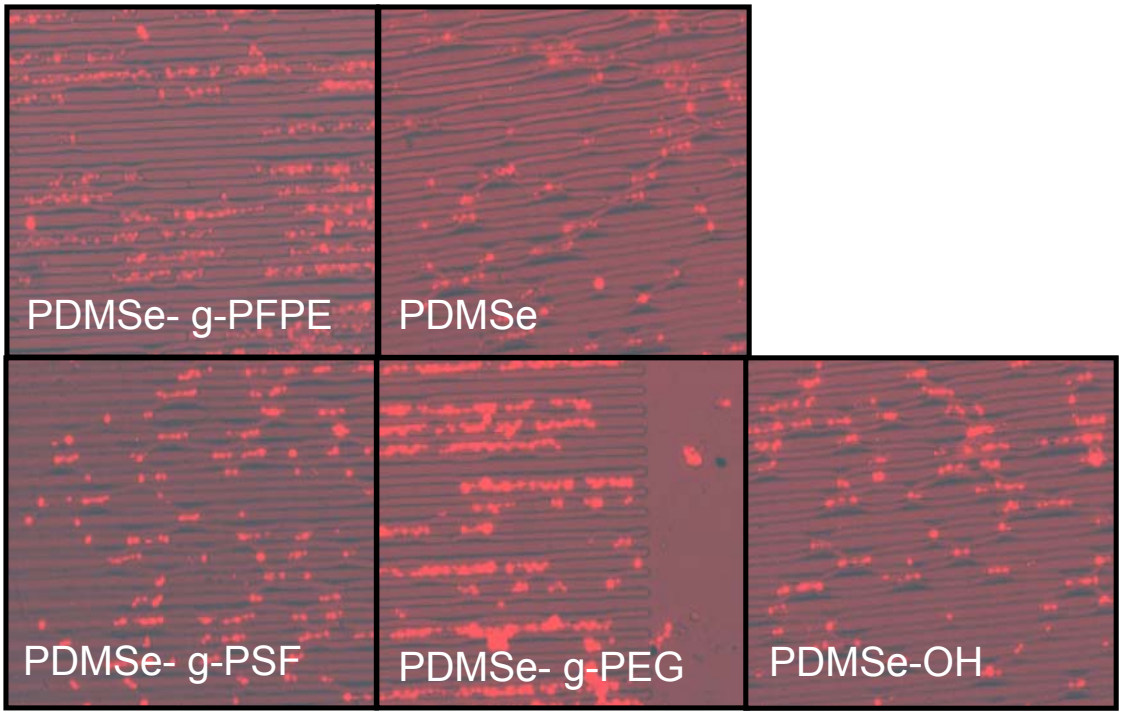

Figure 6-29: Images of *Ulva* zoospores settled in 5μm channels. Note how the spores have stressed the ridges inwards to conform to the spore body

Conclusions

These results show that the surface grafting of polymers allow for the evaluation of surface chemistry independently of bulk modulus. These substrates further allowed for the investigation of whether the existence of the Baier minimum reported in literature was related to the surface chemistry as indicated by Baier or the bulk modulus as indicated by Brady. The Baier curve was noted several times in the data set. However, the Baier minimum was not seen in all zoospore experiments. These results clearly show that one cannot rule out the existence of a Baier minimum for silicone elastomers. Further experimentation is strongly recommended using surface grafting of polymers.

Additionally, this system allowed for the dual evaluation of chemistry and topography. For the surface chemistries studied in this research, the

topographical effect dominates the effect of surface chemistry. For all chemistries evaluated, the sharklet dramatically reduces spore settlement relative to flat areas. For all chemistries evaluated, the 5μm channels increase spore settlement relative to flat. Therefore, the positive or negative thigmotactic response of these geometries transcends surface chemistry.

CHAPTER 7
CONCLUSIONS AND FUTURE WORK

Conclusions

NMR, FTIR, GPC, and iodometric titrations were used to analyze the Silastic T2® components. The combination of these techniques gave considerable information about the molecular structure and stoichiometric ratio of hydrides to vinyl groups that participate in the crosslinking of this elastomer. The elastomers were evaluated during and after curing to determine the effects of time, temperature and additives on the network structure. Contact angles were also used to assess that the surface energy of this elastomer remained constant at ~23 dynes/cm with the addition of these PDMS based additives.

The effect on *Ulva* settlement and adhesion to the PDMSe with respect to the addition of trimethylsilyl terminated polydimethyl siloxane oils was evaluated. This particular oil type did not enhance the foul release properties. The combination of oils and topography yielded a great deal of information as to the response of these zoospores. For instance, the presence of channels promoted spore attachment, but the addition of oils reduced this effect. Furthermore, there was generally lower settlement on the 1.5 μm deep features as compared to 5 μm features, but the differences became less pronounced on the surfaces with oil especially on the surface with pillars. The oils tended to decrease the thigmotactic effect of the topographies. The infilling of these topographies with

oil allowed for the indirect measurement of spore response to a smaller topographical dimension.

This led to the evaluation of smaller topographic scales and allowed for the discovery of the critical topographical dimension required to control spore response. This dimension, 2μm is just less than half the spore body width. Subsequent studies with novel geometries showed that the geometry of the feature is just as important as the size. A biomimetic pattern base on shark scales showed antifouling behaviour, whereas pillars of the same dimensions increased fouling. In order to more fully evaluate the response of spores to topography, these two different experiments 5μm channels and 2μm sharks were measured in the same assay and with the presence of surface grafts.

PDMSe coated glass microscope slides were surface grafted with various silane terminated polymers; mPEG-silane, mPFPE-silane, and PSf-silane. Samples were also evaluated that had been treated with either an isocyanatopropyltriethoxysilane or a glycidoxypropyltriethoxysilane and then subsequently coupled to hydroxyl terminated PFPE or sulfonated polysulfone. These surface grafts were evaluated with respect to change in water contact angle, chemical composition, and bulk modulus. The surface grafting was verified and grafting procedures were continually improved. The data for the finalized grafting procedure produced surface modified PDMSe with a range of captive air bubble water contact angles ranging from 95°- 30° and bulk moduli values ranging from 1.2 – 1.6 MPa. These surface modified elastomers were

subsequently assayed to determine bioresponse with respect to the alga *Ulva* and the diatom *Navicula*.

PFPE-g-PDMSe

In the majority of the spore assays, the PFPE modified PDMSe performs slightly worse than the unmodified PDMSe. This effect was not statistically significant in all cases. The general trends do seem to point to the possibility that the Baier minimum is real. So much research had been devoted to proving that bulk modulus and surface roughness were the reasons for the upturn at low surface energies in the Baier plot. However, since the original research of Baier and Fletcher, almost no one has discussed the possibility that the reason for the minimum is related to the fact that the surface free energy of bulk water is 22 dynes/cm.

This research points to the need for more research at the Baier minimum region and lower surface energy materials. One possible improvement on the studies performed here would be to provide more similar chemical structures, for instance, using fluorosilicones for the surface treatment. Another question is how the graft tails are affecting bioresponse. This research has not evaluated the nano-topography associated with a surface graft copolymer. Therefore we cannot know whether the performance of the PFPE-g-PDMSe related entirely to surface chemistry or is there another component such as nano-roughness. This problem can be addressed by producing silioxane graft species on the PDMSe.

PDMSe

The PDMS elastomer used in this research performs extremely well with respect to *Ulva* zoospores. This material is now used as the standard against

which all other experiment coatings are measured in the Callow lab and will be soon in the labs of other ONR approved bioassayists. The material is now well characterized and can be readily modified. In chapter 3 and 4, data were presented for the bulk modification of this material with oil additives to enhance the surface lubricity or change the bulk modulus. In chapter 4 and 6, topographical modifications of this material have been shown to be highly effective in modulating the bioresponse to this material. Finally, the surface can be modified readily with respect to chemistry as discussed in chapter 5.

PSf-g-PDMSe

Polysulfone surface treatments have been problematic throughout this research. The thickness problems associated with the coating were eliminated by obtaining hydroxyl-terminated polysulfone that could be derivatized with a silane. This process is facile and the DABCO catalyst is easily removed, as it is soluble in the methanol used to precipitate the derivatized polysulfone from solution. No problems with toxicity of these surfaces were observed. This process also allows for extension of this research to any polymer available with hydroxyl termination.

One of the main problems with the inclusion of this polymer as a surface graft in this research is the rigid polymer backbone. Regardless of how thin and regular we are able to produce the surface treatment; there will always be an increased surface modulus. The effect of surface versus bulk modulus has never been fully evaluated for marine biofouling. It has been suggested that bulk modulus is more important for higher organisms such as barnacles and tubeworms. Likewise it was suggested that surface modulus might be a more

important property for microfoulers such as diatoms and algae. This is an important facet of biofouling research that requires further evaluation.

It is possible that the inclusion of this polymer in the surface graft series may provide some indication of how higher modulus materials may perform in this assay with these topographies. Further analysis is suggested.

PEG-g-PDMSe

Poly(ethylene glycol) is now starting to come into the forefront of minimally fouling research. The use of PEG grafts on PDMSe are difficult to characterize, so many unanswered questions plague this research. At a recent Office of Naval Research review, researchers presented evidence that the density of PEG grafts on glass can affect bioresponse. If the density is too high, the surface is rigid and allows for the formation of fouling. Likewise if the density is too low, the foulants can avoid the PEG grafts entirely and foul the underlying substrate. Additionally, antidotal research has suggested that the molecular weight of the PEG grafts can change the bioresponse to these grafted surfaces. This surface requires extensively more characterization with spectroscopy techniques such as sum frequency generation spectroscopy, which could describe the orientation of the PEG grafts both in air and in water.

Future Work

This research clearly shows the efficacy of these surface graft copolymers to evaluate the dual response of chemistry and topography. In order to gain a better understanding of the factors affecting bioadhesion, it is necessary to replicate these chemical modifications on a higher bulk modulus material. One of the main problems associated with silicone based foul release coatings is poor

coating durability. This research has shown that topography can be used to generate either a positive or negative thigmotactic response regardless of surface chemistry. If these topographies also show a similar trend regardless of bulk modulus, then tougher coatings can be produced.

It was originally intended that similar surface modifications would be produced on both silicone and polysulfone to probe the combined effects of surface energy, topography, and bulk modulus on bioresponse. Solvent casting techniques used for the modified polysulfones did not allow for the production of substrates suitable for *Ulva* bioassays. The films produced were wavy and lacked transparency due to solvent casting techniques. Transparent samples that are strongly adhered to glass microscope slides are requisite for *Ulva* bioassays, and wavy substrates can more than triple the time required to assay a substrate.

This research on the modification of polysulfones should be revisited such that surface rather than bulk modified polysulfones are produced. The Udel polysulfone and even polystyrene can be surface modified using chlorosulfonic acid and a suitable non-solvent. It is possible to use solvent or melt processing techniques to impart the microtopographies onto the polysulfone. Surface modifications of the polymers will eliminate many of the problems associated with the bulk modification of the material. I would propose surface sulfonation of the Udel polysulfone, or alternately polystyrene, followed by grafting with commercially available glycidoxy terminated polymers. Available polymers include PEG and PDMS. Glycidoxypropyltriethoxy silane could also be used as

a coupling agent. The epoxy group would bind with the s-PSf surface leaving the triethoxysilane groups exposed. These groups could react with any hydroxyl or silane terminated polymers such as the polysulfone, PEG, and PFPE used in this dissertation.

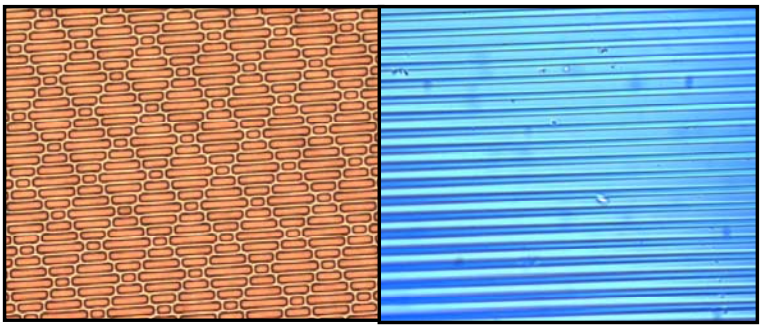

Figure 7-1: Sharklet microtopography replicated in polystyrene and channel microtopography replicated in polysulfone

Casting these materials against wafers is problematic in that the higher modulus materials tend to stick in the silicon wafer. Both of the images above were obtained by casting the polymers against a PDMSe mold. There are problems associated with the swelling of the PDMSe and concerns over residual solvent trapped in the polymer. The ideal material to perform these high modulus experiments would not utilize solvent casting. Ideally, the material would be a curable system that could be molded against the PDMSe replicates. The thermoset would have to be readily surface modified by the chemical techniques described above. The processes described in this dissertation are readily adaptable for a wide range of polymer systems, which will allow for the continuation of this research to narrow down and model these factors that affect bioresponse to polymers.

APPENDIX A
MATERIALS

Solvents

Ethanol [CAS 64-17-5]

$H_3C—CH_2—OH$

Source: Fisher Scientific

Molecular Weight: 46.07 g/mol

Purification and use: Ethanol was used in the silane deposition solutions and for rinsing the glass and silicone coated microscope slides. It was purchased either as 200 proof or 190 proof. 190 proof was used as received. 200 proof ethanol was diluted to produce a 95% aqueous ethanol solution with nanopure water.

Methanol [CAS 67-56-1]

$H_3C—OH$

Source: Fisher Scientific

Molecular Weight: 32.04 g/mol

Purification and use: Methanol was used for precipitating the sulfonated polysulfone post-sulfonation reaction and in the silane derivatization of the hydroxyl terminated polysulfone. It was used as received. The methanol used in the precipitation of sulfonated polysulfone was recovered via rotovap and reused.

n-Propanol [CAS 71-23-8]

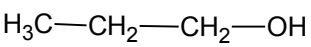

Source: Fisher Scientific

Molecular Weight: 76.14 g/mol

Purification and use: n-Propanol used in surface energy measurements was of the highest grade available and was used as received.

Water (nanopure)

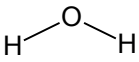

Source: Produced in-house

Molecular Weight: 18.02 g/mol

Purification and use: Nanopure water was obtained by filtration and dionization through a Barnstead NANOpure II unit (>15 MΩ-cm).

Chloroform

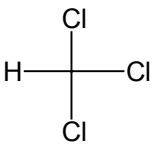

Source: Fisher Scientific

Molecular Weight: 119.38 g/mol

Purification and use: Chloroform was used to extract unreacted oils from the cured silicone elastomers prior to evaluation by XPS and was used as received.

Deuterated Chloroform

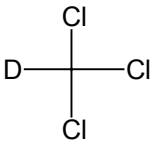

Source: Fisher Scientific

Molecular Weight: 119.38 g/mol

Purification and use: Deuterated chloroform was used for NMR of the siloxanes and was used as received.

Toluene [CAS 108-88-3]

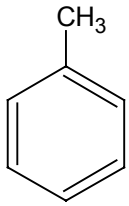

Source: Fisher Scientific

Molecular Weight: 92.14 g/mol

Purification and use: Toluene was used to separate the filler from the Silastic T2 components and was as received.

Methyl Iodide (Iodomethane) [CAS 74-88-4]

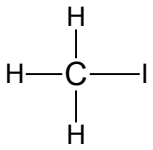

Source: Fisher Scientific: Cat no. M212I-100

Molecular Weight: 141.94 g/mol

Purification and use: Methyl iodide was used for contact angles in surface energy determination and was used as received.

Methylene Iodide (Diiodomethane) [CAS 75-11-6]

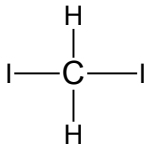

Source: Fisher Scientific

Molecular Weight: 267.83 g/mol

Purification and use: Methylene iodide was used for contact angles in surface energy determination and was used as received.

Acetonitrile [CAS 75-0-8]

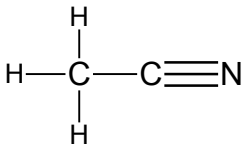

Source: Fisher Scientific

Molecular Weight: 41.05 g/mol

Purification and use: Acetonitrile was used for contact angles in surface energy determination and was used as received.

N-N-Dimethylformamide [CAS 68-12-2]

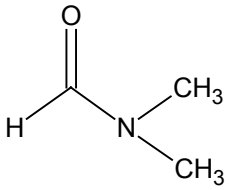

Source: Fisher Scientific

Molecular Weight: 73.09 g/mol

Purification and use: DMF was used as a solvent for sulfonated polysulfone and was used for contact angles in surface energy determination. DMF was purchased in its anhydrous form with a septum cap and used as received.

Formamide [CAS 75-12-7]

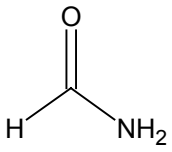

Source: Fisher Scientific

Molecular Weight: 45.04 g/mol

Purification and use: Formamide was used for contact angles in surface energy determination and was used as received.

1,1,2-Trichloroethane (Technical Grade) [CAS 79-00-5]

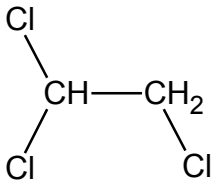

Source: Fisher Scientific

Molecular Weight: 133.41 g/mol

Purification and use: Trichloroethane was used as a solvent for polysulfone during the sulfonation procedure, silane derivatization procedure, and in the preparation of silane solutions for the surface modification of PDMSe. Technical grade trichloroethane was purchased at least two years prior to the beginning of this research. The opened bottle was used as found and contained molecular sieves. There were no modifications to the solvent bottle labeled.

1,1,2-Trichloroethane (98%) [CAS 79-00-5]

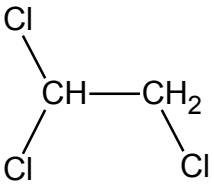

Source: Fisher Scientific

Molecular Weight: 113.41 g/mol

Purification and use: Technical grade 1,1,2-trichloroethane was (previous entry) was discontinued. 98% pure trichloroethane was purchased and an unknown impurity was found to react with chlorosulfonic acid, dramatically decreasing the yield for the polysulfone sulfonation. The new solvent was triple distilled over sodium hydride drying agent and stored with molecular sieves.

1,1,2-trichloro-1,2,2-trifluoroethane

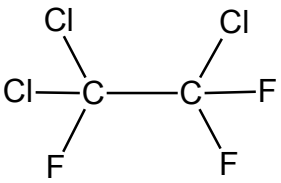

Source: University of Florida ChemSwap Program

Molecular Weight: 187.38 g/mol

Purification and use: Trichlorotrifluoroethane was used as a solvent for the fluorinated polymers, in the silane derivatization of hydroxyl-terminated perfluoropolyether, and in the production of the silane solution for the surface modification of the PDMSe substrates. Trichlorotrifluoroethane was used as received.

Polymers

Silastic T2® Base Resin

Source: Essex Brownell, a distributor for Dow-Corning, Corp.

Purification and use: Purchased in 45-gallon drum and transferred to 1-liter containers prior to use.

Silastic T2® Curing Agent

Source: Essex Brownell, a distributor for Dow-Corning, Corp.

Purification and use: Purchased in 4.5-gallon drum and transferred to 1-liter containers prior to use.

Trimethylsiloxane terminated polydimethylsiloxane oils

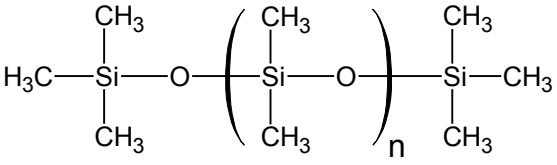

Source: Gelest, Inc.

Purification and use: Oils were used as received and incorporated in the polydimethylsiloxane elastomers.

Product Code	Viscosity (cSt)	Molecular Weight (g/mol)
DMS-T15	50	3,780
DMS-T25	500	17,250
DMS-T35	5,000	49,350

Vinyl terminated polydimethylsiloxane oils

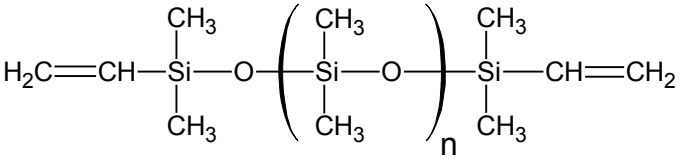

Source: Gelest, Inc.

Purification and use: Oils were used as received and incorporated in the polydimethylsiloxane elastomers.

Product Code	Viscosity (cSt)	Molecular Weight (g/mol)
DMS-V00	0.7	3,780
DMS-T03	2-3	17,250
DMS-T31	1,000	49,350

m-PEG-silane

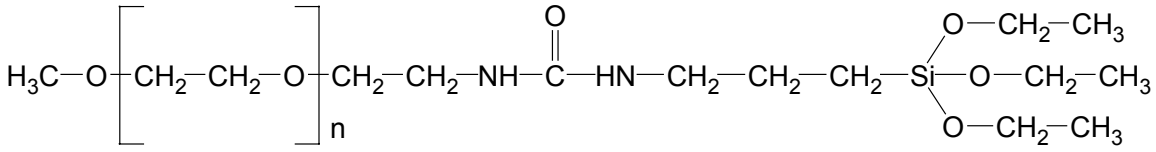

Source: BioLink Life Sciences or Nektar Therapeutics

Molecular Weight: 5,099 g/mol

Purification and use: m-PEG-silane was obtained as a white powder that was stored in the freezer and used without further purification. It was used for the surface modification of the polydimethylsiloxane elastomers.

m-PFPE-OH

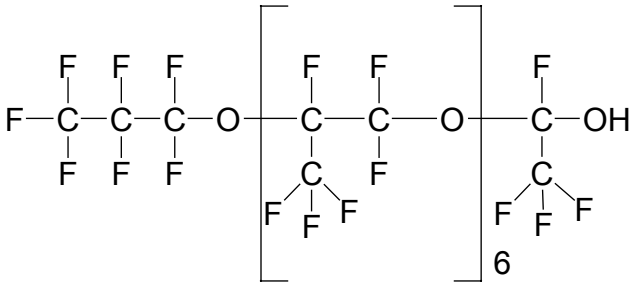

Source: Sample from the DeSimone group at the University of North Carolina

Molecular Weight: reported by the UNC group as ~ 1,200 g/mol

Purification and use: The polymer was a clear liquid and was derivatized with silane functionality without further purification.

m-PFPE-silane

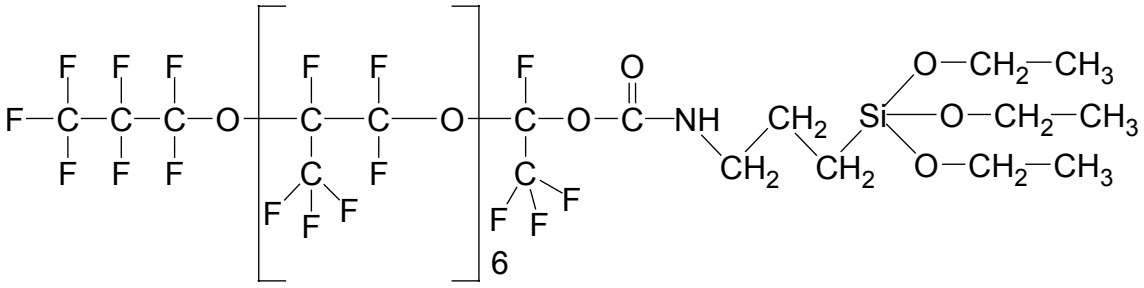

Source: Sample from Dupont

Molecular Weight: ~1,200 g/mol

Purification and use: The polymer was a yellowish liquid and was used as received for the surface modification of PDMSe substrates.

Polysulfone (Udel P-1700)

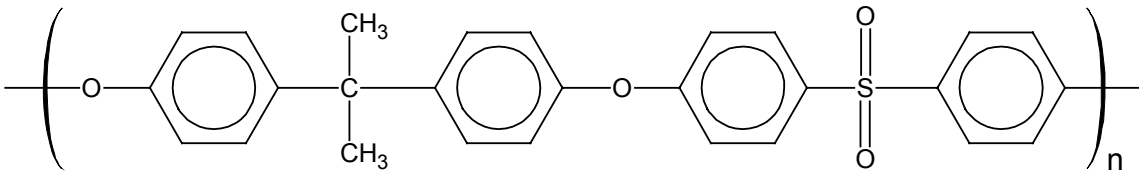

Source: Sample from Solvay Advanced Polymers

Molecular Weight: ~35 kg/mol

Purification and use: This polymer was received in pellet form. It was dried in a 140°C oven for 4 hours or overnight per manufacturers instructions prior to dissolution in trichloroethane for the sulfonation reaction.

Hydroxyl terminated Polysulfone

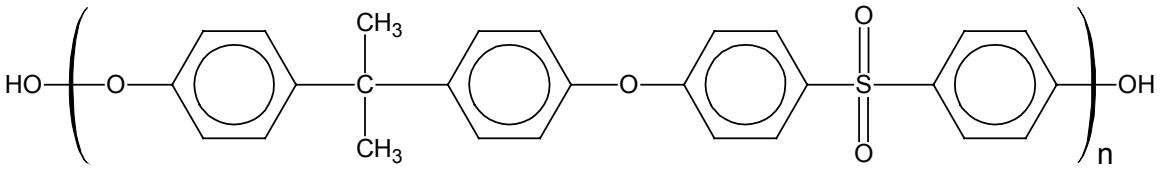

Source: Polysciences, Inc.

Molecular Weight: ~35 kg/mol

Purification and use: This polymer was received as a fine white powder and was used as received.

Coupling Agents

Hexamethyldisilazane [999-99-37]

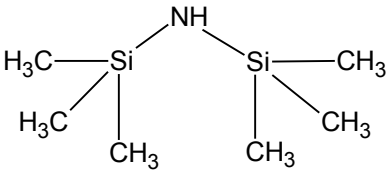

Source: Sigma Aldrich

Molecular Weight: 161.4 g/mol

Purification and use: Hexamethyldisilazane was store under nitrogen. Hexamethyldisilazane was used to treat glass plates to make them minimally adhesive with respect to the silicone elastomers.

Allyltrimethoxysilane [2550-04-1]

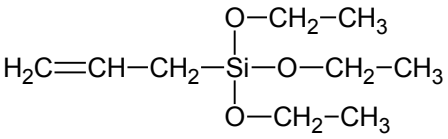

Source: Gelest, Inc

Molecular Weight: 204.34 g/mol

Purification and use: Allyltriethoxysilane was used as received and stored under nitrogen in a desiccator after opening. Allyltriethoxysilane was used to treat glass slides to promote adhesion with respect to the silicone elastomers.

Glycidoxypropyltriethoxysilane [2530-83-8]

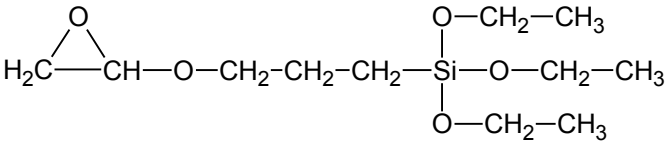

Source: Gelest, Inc.

Molecular Weight: 236.34 g/mol

Purification and use: Glycidoxypropyltriethoxysilane was used as received and stored under nitrogen in a desiccator after opening.

Glycidoxypropyltriethoxysilane was used as a coupling agent to tether sulfonated polysulfone to polydimethylsiloxane elastomers.

Isocyanatoproyltriethoxysilane [24801-88-5]

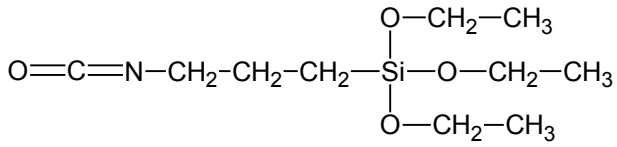

Source: United Chemical Technologies, Inc.

Molecular Weight: 247.4 g/mol

Purification and use: Isocyanatopropyltriethoxysilane was used as received and stored under nitrogen in a desiccator after opening.

Isocyanatopropyltriethoxysilane was used to derivatize hydroxyl-terminated polymers.

Miscellaneous

Ammonia (Household grade)

NH_3 (Ammonium hydroxide in water, <3N NH_4OH (<5% as ammonia, NH_3))

Source: Kash n' Karry

CAS: 1336-21-6

Molecular Weight: 17.03 g/mol

Purification and use: Aqueous ammonia solution was used as received.

Wij's Solution, 0.2N ICl in Glacial Acetic Acid

CAS: [7553-56-3], [7782-50-5], and [64-19-7]

Source: Fisher Scientific

Purification and use: Wij's solution was used for iodometric titrations as received and stored in the dark.

Sodium Thiosulfate

Source: Fisher Scientific

Molecular Weight: g/mol

Purification and use: was used as received.

Starch Indicator

Source: Fisher Scientific

Molecular Weight: g/mol

Purification and use:

Glacial Acetic Acid

Source: Acros Organics

Molecular Weight: g/mol

Purification and use: Acetic acid was used as received.

Hydrochloric Acid, 37% (aq)

Source: Acros Organics

Molecular Weight: 108.64 g/mol

Purification and use: HCl was used as received and diluted to 3M concentration with nanopure water.

Potassium Hydroxide

Source: Fisher Scientific

Molecular Weight: g/mol

Purification and use: was used as received.

Chlorotrimethylsilane, 98% [75-77-4]

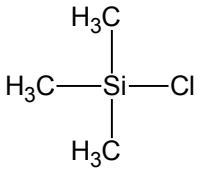

Source: Acros Organics

Molecular Weight: 108.64 g/mol

Purification and use: Chlorotrimethylsilane was used as received in the sulfonation reaction.

Chlorosulfonic Acid

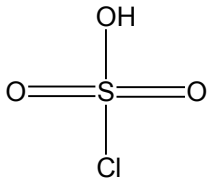

Source: Fisher Scientific

Molecular Weight: 92.14 g/mol

Purification and use: Toluene was used as received.

1,4-Diazabicyclo[2.2.2]-octane (DABCO) [280-57-9]

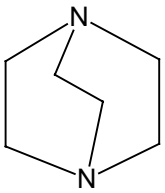

Source: Sigma Aldrich

Molecular Weight: 112.18 g/mol

Purification and use: DABCO was received as a white crystalline substance and was used as received as a catalyst for the derivatization of the polymer endgroups.

Glass Microscope Slides

Source: Fisher Scientific

Purification and use: Glass microscope slides were cleaned by passing through a very clean Bunsen burner flame. The slides were subsequently treated with a coupling agent to promote adhesion of the Silastic T2® elastomer.

PET release films

Source: McMaster-Carr

Purification and use: PET film was cleaned with acetone and ethanol and was used to prevent adhesion of the Silastic T2® elastomer to the glass plates.

Glass Plates

Source: Shay's Glass

Purification and use: Glass plates were cleaned with acetone and ethanol and then treated with hexamethyldisilazane to minimize adhesion to the Silastic T2® elastomer.

APPENDIX B
ABBREVIATIONS

ACN: Acetonitrile

AF: Antifouling

ATR: Attenuated total reflectance spectroscopy

ATS: Allyltriethoxysilane

CSA: Chlorosulfonic acid

CTMS: Chlorotrimethylsilane

DABCO:1,4-Diazabicyclo[2.2.2]-octane

DMF: Dimethyl formamide

etOH: Ethanol

FR: Foul release

FTIR: Fourier transform infrared spectroscopy

GPC: Gel permeation chromatography

GPS: Glycidoxypropyltriethoxysilane

HCl: Hydrochloric acid

HMDS: Hexamethyldisilazane

ICPES: Isocyanatopropyltriethoxysilane

KOH : Potassium hydroxide

MeI: Methyl iodide

MeI_2: Methylene iodide

meOH: Methanol

mPEG-silane: Mono-methoxy polyethylene glycol, silane terminated

mPFPE-OH: Mono-methoxy perfluoropolyether, hydroxyl terminated

mPFPE-silane: Mono-methoxy perfluoropolyether, silane terminated

NMR: Nuclear magnetic resonance spectroscopy

ONR: Office of Naval Research

PDMS: Polydimethylsiloxane

PDMSe: Polydimethylsiloxane elastomer

PDMSe-OH: Hydrolyzed polydimethyl siloxane elastomer

PDMSe-g-PEG: Polydimethylsiloxane elastomer surface grafted with polyethylene glycol

PDMSe-g-PFPE: Polydimethylsiloxane elastomer surface grafted with perfluoropolyether

PDMSe-g-PSf: Polydimethylsiloxane elastomer surface grafted with polysulfone

PEG: Polyethylene glycol

PEO: Polyethylene oxide

PFPE: Perfluoropolyether

PMHS: Poly(methyl hydride) siloxane

PMMA: Poly(methyl methacrylate)

PSf: Polysulfone

PSf-OH: Polysulfone, dihydroxyl terminated

PSf-silane: Polysulfone, disilane terminated

PT-PDMSe: Plasma treated polydimethylsiloxane elastomer

PU: Polyurethane

RTV: Room temperature vulcanized

SAMs: Self-assembled monolayers

SEM: Scanning electron microscopy

TBT: Tributyltin tin

TCE: Trichloroethane

TGA: Thermal gravimetric analysis

TMS: Trimethylsiloxy

XPS: X-ray photoelectron spectroscopy

LIST OF REFERENCES

1. Pasmore, M., Todd, P., Pfiefer, B., and Bowman, C.N. Effect of Polymer Surface Properties on the Reversibility of Attachment of *Pseudomonas Aeruginosa* in the Early Stages of Biofilm Development*. Biofouling* **2002**, *18*(1), p. 65-71.

2. Costerton, J.W. and Stewart, P.S. Biofilms and Device-Related Infections. in *Persistent Bacterial Infections*, Nataro, J.P., Blaster, M.J., and Cunningham-Rundles, S., Editors; ASM Press: Washington DC. 2000, p. 423–439.

3. Brady, J., Robert F. A Fracture Mechanical Analysis of Fouling Release from Nontoxic Antifouling Coatings*. Progress in Organic Coatings* **2001**, *43*(1-3), p. 188-192.

4. Christiaen, A.-C. Evaluation of the Durability of Elastomeric Easy Release Coatings. Virginia Tech, Blacksburg, VA, 1998.

5. Brady, R.F. and Singer, I.L. Mechanical Factors Favoring Release from Foul Release Coatings*. Biofouling* **2000**, *15*(1-3), p. 73-81.

6. Keough, M.J. and Raimondi, P.T. Responses of Settling Invertebrate Larvae to Bioorganic Films: Effects of Two Different Types of Films*. Journal of Experimental Marine Biology and Ecology* **1995**, *185*, p. 235-253.

7. Singer, I.L., Kohl, J.G., and Patterson, M. Mechanical Aspects of Silicone Coatings for Hard Foulant Control*. Biofouling* **2000**, *16*(2-4), p. 301-309.

8. Callow, M.E. Ship-Fouling: The Problems and Methods of Control*. Biodeterioration Abstracts* **1996**, *10*, p. 411-421.

9. Hills, J.M. and Thomason, J.C. The Effect of Scales of Surface Roughness on the Settlement of Barnacle (*Semibalanus Balanoides*) Cyprids*. Biofouling* **1998**, *12*, p. 57-69.

10. Hills, J.M. and Thomason, J.C. A Multi-Scale Analysis of Settlement Density and Pattern Dynamics of the Barnacle *Semibalanus Balanoides. Marine Ecology-Progress Series* **1996**, *138*(1-3), p. 103-115.

11. Hills, J.M. and Thomason, J.C. Settlement of Barnacle Larvae Is Governed by Euclidean and Not Fractal Surface Characteristics. *Functional Ecology* **1999**, *13*(6), p. 868-875.

12. Baier, R.E. and Meyer, A.E. Surface Analysis of Fouling-Resistant Marine Coatings*. Biofouling* **1992**, *6*, p. 165-180.

13. Meyer, A.E. and Baier, R.E. Nontoxic Control of Zebra Mussels: Surface Chemistry/Physics of Biological Adhesion. in *Proc Electric Utility Zebra Mussel Control Tech Conf Electric Power Research Institute*. 1992, p. 45-58.

14. Taylor, G.T., Zheng, D., Lee, M., Troy, J.P., Gyananath, G., and Sharma, S.K. Influence of Surface Properties on Accumulation of Conditioning Films and Marine Bacteria on Substrata Exposed to Oligotrophic Waters*. Biofouling* **1997**, *11*(1), p. 31-57.

15. Ista, L.K., Callow, M.E., Finlay, J.A., Coleman, S.E., Nolasco, A.C., Simons, R.H., Callow, J.A., and Lopez, G.P. Effect of Substratum Surface Chemistry and Surface Energy on Attachment of Marine Bacteria and Algal Spores*. Applied and Environmental Microbiology* **2004**, *70*(7), p. 4151-4157.

16. Joint, I., Callow, M.E., Callow, J.A., and Clarke, K.R. The Attachment of *Enteromorpha* Zoospores to a Bacterial Biofilm Assemblage*. Biofouling* **2000**, *16*, p. 151-158.

17. O'Connor, N.J. and Richardson, D.L. Effects of Bacterial Films on Attachment of Barnacle *Balanus Improvisus Darwin* Larvae Laboratory and Field Studies*. Journal of Experimental Marine Biology and Ecology* **1996**, *206*, p. 69-81.

18. O'Connor, N.J. and Richardson, D.L. Attachment of Barnacle (*Balanus Amphitrite Darwin*) Larvae: Responses to Bacterial Films and Extracellular Materials*. Journal of Experimental Marine Biology and Ecology* **1998**, *226*, p. 115-129.

19. Lau, S.C.K. and Qian, P.-Y. Inhibitory Effect of Phenolic Compounds and Marine Bacteria on Larval Settlement of the Barnacle *Balanus Amphitrite Amphitrite Darwin. Biofouling* **2000**, *16*(1), p. 47-58.

20. Bohn, C. Dynamic Antifouling Structures and Actuators Using EAPComposites. Doctoral, University of Florida, Gainesville, Fl, 2004.

21. Abbott, A., Abel, P.D., Arnold, D.W., and Milne, A. Cost Benefit Analysis of the Use of Tributyltin: The Case for a Treatment Approach*. The Science of the Total Environment* **2000**, *258*, p. 5-19.

22. Strandenes, S.P. The Second Order Effects on Commercial Shipping of Restrictions on the Use of Tributyltin*. The Science of the Total Environment* **2000**, *258*, p. 111-117.

23. Champ, M.A. A Review of Organotin Regulatory Strategies, Pending Actions, Related Costs and Benefits*. The Science of the Total Environment* **2000**, *258*, p. 21-71.

24. Evans, S.M., Birchenough, A.C., and Brancato, M.S. The Tributyltin Ban: Out of the Frying Pan into the Fire? *Marine Pollution Bulletin* **2000**, *40*(3), p. 204-211.

25. *Commodities Analysis*, in Wallstreet Journal. 2003.

26. U.S. Navy, www. navy.mil, 2003.

27. Ingle, M. *Navy Pespectives and Requirements for New Hull Coatings*. in *ONR Coatings and Biofouling Program Review*. 2005. Baltimore, MD.

28. Lugo, F., Hoipkemeier, S., and Moke, M. Personal Communication, February 07, 2002.

29. Mickelberry, K., Moke, M., and Hoipkemeier, S. Personal Communication, February 09, 2002.

30. Abel, P.D. Tributyltin: Towards a Better Way to Regulate Pollutants*. The Science of the Total Environment* **2000**, *258*, p. 1-4.

31. Alzieu, C. Environmental Impact of Tributyltin: The French Experience*. The Science of the Total Environment* **2000**, *258*, p. 99-102.

32. Gadd, G.M. Microbial Interactions with Tributyltin Compounds: Detoxification, Accumulation, and Environmental Fate*. The Science of the Total Environment* **2000**, *258*, p. 119-127.

33. Jacobson, A.H. and Willingham, G.L. Sea-Nine Antifoulant: An Environmentally Acceptable Alternative to Organotin Antifoulants*. The Science of the Total Environment* **2000**, *258*, p. 103-110.

34. Voulvoulis, N., Scrimshaw, M.D., and Lester, J.N. Comparative Environmental Assessment of Biocides Used in Antifouling Paints*. Chemosphere* **2002**, *47*, p. 789-795.

35. Miller, S.M. Techniques for Evaluation of Chemicals as Marine Antifoulants*. Industrial and Engineering Chemistry Research* **1964**, *3*(3), p. 226-230.

36. Santillo, D., Johnston, P., and Langston, W.J. Tributyltin Antifoulants: A Tale of Ships, Snails and Imposex. in *Late Lessons from Early Warnings: The Precautionary Principle 1896–2000*. 2001, p. 135-148.

37. Alzieu, C. Tributyltin Case Study of a Chronic Contaminant in the Coastal Environment*. Ocean and Coastal Management* **1998**, *40*, p. 23-36.

38. Boxall, A.B.A., Comber, S.D., Conrad, A.U., Howcroft, J., and Zaman, N. Inputs, Monitoring and Fate Modeling of Antifouling Biocides in UK Estuaries*. Marine Pollution Bulletin* **2000**, *40*(11), p. 898-905.

39. Kiil, S., Weinell, C.E., Pedersen, M.S., and Dam-Johansen, K. Analysis of Self-Polishing Antifouling Paints Using Rotary Experiments and Mathematical Modeling*. Industrial and Engineering Chemistry Research* **2001**, *40*, p. 3906-3920.

40. Hall, L.W. and Anderson, R.D. A Deterministic Ecological Risk Assessment for Copper in European Saltwater Environments*. Marine Pollution Bulletin* **1999**, *38*(3), p. 207-218.

41. Matthiessen, P., Reed, J., and Johnson, M. Sources and Potential Effects of Copper and Zinc Concentrations in the Estuarine Waters of Essex and Suffolk, United Kingdom*. Marine Pollution Bulletin* **1999**, *38*(10), p. 908-920.

42. Muller, W. and Nowacki, L. Ship's Hull Coated with Antifouling Silicone Rubber*.* US:**3,702,778,** 1972.

43. Milne, A. Anti-Fouling Marine Compositions*.* US:**4,025,693,** 1977.

44. Griffith, J.R. Non-Toxic Antifouling Systems*.* US:**5,449,553,** 1995.

45. Schumacher, J.F., Estes, T.G., Carman, M.L., Wilson, L.H., Wendt, D.E., Callow, M.E., and Brennan, A.B. *Shark Inspired Non-Toxic Coatings for Non-Fouling Marine Applications*. in *American Chemical Society Meeting & Exposition*. 2005. Washington, DC USA.

46. Callister, W.D.J. Materials Science and Engineering. 5th ed; John Wiley & Sons, Inc: 1999.

47. Johnson, K.L., Kendall, K., and Roberts, R.D. Surface Energy and the Contact of Elastic Solids. *Proceedings of the Royal Society of London* **1971**, *324*(1558), p. 301-313.

48. Kohl, J.G. and Singer, I.L. Pull-Off Behavior of Epoxy Bonded to Silicone Duplex Coatings. *Progress in Organic Coatings* **1999**, *36*(1-2), p. 15-20.

49. Johnson, R.E., Jr. and Dettre, R.H. Wettability and Contact Angles. *Surface and Colloid Science* **1969**, *2*, p. 85-153.

50. Singhvi, R., Stephanopoulos, G., and Wang, D.I.C. Effects of Substratum Morphology on Cell Physiology - Review. *Biotechnology and Bioengineering* **1994**, *43*(8), p. 764-771.

51. Eginton, P.J., Gibson, H., Holah, J., Handley, P.S., and Gilbert, P. The Influence of Substratum Properties on the Attachment of Bacterial-Cells. *Colloids and Surfaces B-Biointerfaces* **1995**, *5*(3-4), p. 153-159.

52. van Kooten, T.G. and von Recum, A.F. Cell Adhesion to Textured Silicone Surfaces: The Influence of Time of Adhesion and Texture on Focal Contact and Fibronectin Fibril Formation. *Tissue Engineering* **1999**, *5*(3), p. 223-240.

53. Curtis, A.S.G., Casey, B., Gallagher, J.O., Pasqui, D., Wood, M.A., and Wilkinson, C.D.W. Substratum Nanotopography and the Adhesion of Biological Cells. Are Symmetry or Regularity of Nanotopography Important? *Biophysical Chemistry* **2001**, *94*(3), p. 275-283.

54. Wong, J.Y., Leach, J.B., and Brown, X.Q. Balance of Chemistry, Topography, and Mechanics at the Cell-Biomaterial Interface: Issues and Challenges for Assessing the Role of Substrate Mechanics on Cell Response. *Surface Science* **2004**, *570*(1-2), p. 119-133.

55. Nath, N., Hyun, J., Ma, H., and Chilkoti, A. Surface Engineering Strategies for Control of Protein and Cell Interactions. *Surface Science* **2004**, *570*(1-2), p. 98-110.

56. Karuri, N.W., Liliensiek, S., Teixeira, A.I., Abrams, G., Campbell, S., Nealey, P.F., and Murphy, C.J. Biological Length Scale Topography Enhances Cell-Substratum Adhesion of Human Corneal Epithelial Cells. *Journal of Cell Science* **2004**, *117*(15), p. 3153-3164.

57. Andersson, M., Berntsson, K., Nosson, P., Gatenholm, P. Microtextured Surfaces: Towards Macrofouling Resistant Coatings. *Biofouling* **1999**, *14*(2), p. 167-178.

58. Kerr, A. and Cowling, M.J. The Effects of Surface Topography on the Accumulation of Biofouling. *Philosophical Magazine* **2003**, *83*(24), p. 2779-2795.

59. Li, X.Q., Liu, T.Q., and Chen, Y.T. The Effects of the Nanotopography of Biomaterial Surfaces on *Pseudomonas Fluorescens* Cell Adhesion. *Biochemical Engineering Journal* **2004**, *22*(1), p. 11-17.

60. Holm, E.R., Cannon, G., Roberts, D., Schmidt, A.R., Sutherland, J.P., and Rittschof, D. The Influence of Initial Surface Chemistry on Development of the Fouling Community at Beaufort, North Carolina. *Journal of Experimental Marine Biology and Ecology* **1997**, *215*, p. 189-203.

61. Berntsson, K.M., Jonsson, P.R., Lejhall, M., and Gatenholm, P. Analysis of Behavioural Rejection of Micro-Textured Surfaces and Implications for Recruitment by the Barnacle *Balanus Improvisus. Journal of Experimental Marine Biology and Ecology* **2000**, *251*, p. 59–83.

62. Petronis, S., Berntsson, K., Gold, J., and Gatenholm, P. Design and Microstructuring of Polydimethylsiloxane Surfaces for Improved Marine Biofouling Resistance. *Journal of Biomaterials Science-Polymer Edition* **2000**, *11*(10), p. 1051-1072.

63. Hoipkemeier-Wilson, L., Schumacher, J., Carman, M., Gibson, A., Feinberg, A., Callow, M., Finlay, J., Callow, J., and Brennan, A. Antifouling Potential of Lubricious, Micro-Engineered, PDMS Elastomers against Zoospores of the Green Fouling Alga Ulva (Enteromorpha). *Biofouling* **2004**, *20*(1), p. 53-63.

64. Granhag, L.M., Finlay, J.A., Jonsson, P.R., Callow, J.A., and Callow, M.E. Roughness-Dependent Removal of Settled Spores of the Green Alga *Ulva* (Syn. *Enteromorpha*) Exposed to Hydrodynamic Forces from a Water Jet. *Biofouling* **2004**, *20*(2), p. 117-122.

65. Wenzel, R.N. Surface Roughness and Contact Angle. *Journal of Physical and Colloid Chemistry* **1949**, *53*, p. 1466-1467.

66. Cassie, A.B.D. and Baxter, S. Wettability of Porous Surfaces. *Faraday Society Transactions* **1944**, *40*, p. 546-551.

67. Bico, J., Marzolin, C., and Quere, D. Pearl Drops. *Europhysics Letters* **1999**, *47*(2), p. 220-226.

68. Bico, J., Tordeux, C., and Quere, D. Rough Wetting. *Europhysics Letters* **2001**, *55*(2), p. 214-220.

69. Bico, J., Thiele, U., and Quere, D. Wetting of Textured Surfaces. *Colloids and Surfaces A: Physicochemical and Engineering Aspects* **2002**, *206*(1-3), p. 41-46.

70. Callow, M.E. and Callow, J.A. Substratum Location and Zoospore Behaviour in the Fouling Alga *Enteromorpha. Biofouling* **2000**, *15*(1-3), p. 49-56.

71. Weiss, P. Experiments on Cell and Axon Orientation in Vitro: The Role of Colloidal Exudates in Tissue Organization. *Journal of Experimental Zoology* **1946**, *100*, p. 353-386.

72. Dunn, G.A. and Heath, J.P. New Hypothesis of Contact Guidance in Tissue-Cells. *Experimental Cell Research* **1976**, *101*(1), p. 1-14.

73. den Braber, E.T., de Ruijter, J.E., Smits, H.T., Ginsel, L.A., von Recum, A.F., and Jansen, J.A. Effect of Parallel Surface Microgrooves and Surface Energy on Cell Growth. *Journal of Biomedical Materials Research* **1995**, *29*(4), p. 511-8.

74. Curtis, A. and Wilkinson, C. Topographical Control of Cells. *Biomaterials* **1997**, *18*, p. 1573-1583.

75. Schmidt, J.A. and von recum, A.F. Texturing of Polymer Surfaces at the Cellular-Level. *Biomaterials* **1991**, *12*(4), p. 385-389.

76. Schmidt, J.A. and von Recum, A.F. Macrophage Response to Microtextured Silicone. *Biomaterials* **1992**, *13*(15), p. 1059-1069.

77. Von Recum, A.F. and Van Kooten, T.G. The Influence of Micro-Topography on Cellular Response and the Implications for Silicone Implants. *Journal of Biomaterial Science* **1995**, *7*(2), p. 181-198.

78. Bhatia, S.N., Yarmush, M.L., and Toner, M. Controlling Cell Interactions by Micropatterning in Co-Cultures: Hepatocytes and 3t3 Fibroblasts. *Journal of Biomedical Materials Research* **1997**, *34*, p. 189-199.

79. Harrison, R.G. On the Stereotropism of Embryonic Cells. *Science* **1911**, *34*, p. 279.

80. Bechert, D.W., Hoppe, G., and Reif, W.E. On the Drag Reduction of the Shark Skin. *AIAA Shear Flow Control Conference Proceedings* **1985**, *0546*.

81. Bechert, D.W. and Bartenwerfer, M. The Viscous Flow on Surfaces with Longitudinal Ribs. *Journal of Fluid Mechanics* **1989**, *206*, p. 105-129.

82. Barthlott, W. and Neinhuis, C. Purity of the Sacred Lotus, or Escape from Contamination in Biological Surfaces. *Planta* **1997**, *202*(1), p. 1-8.

83. Afsar, A., De Nys, R., and Steinberg, P. The Effects of Foul-Release Coatings on the Settlement and Behaviour of Cyprid Larvae of the Barnacle *Balanus Amphitrite Amphitrite Darwin. Biofouling* **2003**, *19*(Supplement), p. 105-110.

84. Berglin, M. and Gatenholm, P. The Nature of Bioadhesive Bonding between Barnacles and Fouling-Release Silicone Coatings. *Journal of Adhesion Science and Technology* **1999**, *13*(6), p. 713-727.

85. Berglin, M. and Gratenholm, P. The Barnacle Adhesive Plaque: Morphological and Chemical Differences as a Response to Substrate Properties. *Colloids and Surfaces B-Biointerfaces* **2003**, *28*(2-3), p. 107-117.

86. Callow, M.E. and Callow, J.A. Enhanced Adhesion and Chemoattraction of Zoospores of the Fouling Alga *Enteromorph*a to Some Foul Release Silicone Elastomers. *Biofouling* **1998**, *13*(2), p. 157-172.

87. Callow, M.E. and Fletcher, R.L. The Influence of Low Surface-Energy Materials on Bioadhesion - a Review. *International Biodeterioration & Biodegradation* **1994**, *34*(3-4), p. 333-348.

88. Clarkson, N. and Evans, L.V. Raft Trial Experiments to Investigate the Antifouling Potential of Silicone Elastomer Polymers with Added Biocide. *Biofouling* **1995**, *9*(2), p. 129-143.

89. Estarlich, F.F., Lewey, S.A., Nevell, T.G., Thorpe, A.A., Tsibouklis, J., and Upton, A.C. The Surface Properties of Some Silicone and Fluorosilicone Coating Materials Immersed in Seawater. *Biofouling* **2000**, *16*(2-4), p. 263-275.

90. Holland, R., Dugdale, T.M., Wetherbee, R., Brennan, A.B., Finlay, J.A., Callow, J.A., and Callow, M.E. Adhesion and Motility of Fouling Diatoms on Silicone Elastomers. *Biofouling* **2004**, *20*(6), p. 323-329.

91. Nevell, T.G., Edwards, D.P., Davis, A.J., and Pullin, R.A. The Surface Properties of Silicone Elastomers Exposed to Seawater. *Biofouling* **1996**, *10*(1-3), p. 199-212.

92. Thomas, J., Choi, B.-C., Fjeldheim, R., and Boudjouk, P. Silicones Containing Pendant Biocides for Antifouling Coatings. *Biofouling* **2004**, *20*(4-5), p. 227-236.

93. Truby, K., Wood, C.D., Stein, J., Cella, J., Carpenter, J., Kavanagh, C., Swain, G., Wiebe, D., Lapota, D., Meyer, A., Holm, E., Wendt, D., Smith, C., and Montemarano, J. Evaluation of the Performance Enhancement of Silicone Biofouling-Release Coatings by Oil Incorporation. *Biofouling* **2000**, *15*(1-3), p. 141-150.

94. Wood, C.D., Truby, K., Stein, J., Wiebe, D., Holm, E.R., Wendt, D., Smith, C., Kavanagh, C.J., Montemarano, J., Swain, G.W., and Meyer, R. Temporal and Spatial Variations in Macrofouling of Silicone Fouling-Release Coatings. *Biofouling* **2000**, *16*(2-4), p. 311-322.

95. Wynne, K.J., Swain, G.W., Fox, R.B., Bullock, S., and Uilk, J. Two Silicone Nontoxic Fouling Release Coatings: Hydrosilylation Cured Polydimethylsiloxane and Calcium Carbonate Filled, Ethoxysiloxane Cured Rtv11. *Biofouling* **2000**, *16*(2-4), p. 277-+.

96. Bullock, S., Johnston, E.E., Willson, T., Gatenholm, P., and Wynne, K.J. Surface Science of a Filled Polydimethylsiloxane-Based Alkoxysilane-Cured Elastomer: Rtv11. *Journal of Colloid and Interface Science* **1999**, *210*, p. 18-36.

97. Callow, M.E., Jennings, A.R., Brennan, A.B., Seegert, C., Gibson, A., Wilson, L., Feinberg, A., Baney, R., and Callow, J.A. Microtopographic Cues for Settlement of Zoospores of the Green Fouling Alga *Enteromorpha*. *Biofouling* **2002**, *18*(3), p. 237-245.

98. Feinberg, A.W., Gibson, A.L., Wilkerson, W.R., Seegert, C.A., Wilson, L.H., Zhao, L.C., Baney, R.H., Callow, J.A., Callow, M.E., and Brennan, A.B. Investigating the Energetics of Bioadhesion on Microengineered Siloxane Elastomers: Characterizing the Topography, Mechanical Properties, and Surface Energy and Their Effect on Cell Contact Guidance. in *Synthesis and Properties of Silicones and Silicone-Modified Materials*, Clarson, Fitzgerald, Owen, Smith, and Dyke, V., Editors; ACS. 2003.

99. Feinberg, A.W., Seegert, C., Wilkerson, W.R., Gibson, A., Wilson, L., Baney, R., and Brennan, A.B. Characterization of Chemically and Topographically Modified Siloxane Elastomer. *Abstracts of Papers of the American Chemical Society* **2001**, *221*, p. 255-POLY.

100. Gray, N.L., Banta, W.C., and Loeb, G.I. Aquatic Biofouling Larvae Respond to Differences in the Mechanical Properties of the Surface on Which They Settle: Short Communication. *Biofouling* **2002**, *18*(4), p. 269-273.

101. Gustavsson, T.G., Gubanski, S.M., Hillborg, H., and Gedde, U.W. Aging of Silicone Rubber Materials in Marine Environment*. IEEE* **2000**.

102. Hills, J.M., Thomason, J.C., Milligan, J.L., and Richardson, T. Do Barnacle Larvae Respond to Multiple Settlement Cues over a Range of Spatial Scales? *Hydrobiologia* **1998**, *376*, p. 101-111.

103. Kohl, J.G., Singer, I.L., and Griffith, J.R. Evaluating the Durability of Silicone Duplex Coating Using a Scratch Tester*. Rubber Chemistry and Technology* **2000**, *73*, p. 607-618.

104. Burnell, T.B., Carpenter, J.C., Carroll, K.M., Cella, J.A., Resue, J.A., Rubinsztajn, G., Serth-Guzzo, J., Stein, J., Truby, K.E., Webb, K.K., Schultz, M., Swain, G.W., and Zimmerman, R. Advances in Nontoxic Silicone Biofouling Release Coatings*. GE Global Research Report Technical Information Series* **1997**.

105. Burnell, T., Cella, J., Espinoza, R., Rubinsztajn, S., and Stein, J. New Silicone, Nontoxic Foul-Release Coating System*. GE Global Research Report Technical Information Series* **1997**.

106. Wood, C.D., Truby, K., Stein, J., Wiebe, D., Holm, E., Wendt, D., Smith, C., Kavanagh, C., Montemarano, J., Swain, G., and Meyer, A. Temporal and Spatial Variations in Macro-Fouling of Silicone Fouling-Release Coatings*. GE Global Research Report Technical Information Series* **1999**.

107. Stein, J., Truby, K., Wood, C.D., Stein, J., Gardner, M., Swain, G., Kavanagh, C., Kovach, B., Schultz, M., Wiebe, D., Holm, E., Montemarano, J., Wendt, D., Smith, C., and Meyer, A. Silicone Foul Release Coatings: Effect of the Interaction of Oil and Coating Functionalities on the Magnitude of Macrofouling Attachment Strengths*. GE Global Research Report Technical Information Series* **2002**.

108. Stein, J., Truby, K., Wood, C.D., Takemori, M., Vallance, M., Swain, G., Kavanagh, C., Kovach, B., Schultz, M., Wiebe, D., Holm, E., Montemarano, J., Wendt, D., Smith, C., and Meyer, A. Structure-Property Relationships of Silicone Biofouling-Release Coatings: Effect of Silicone Network Architecture on Pseudobarnacle Attachment Strengths*. GE Global Research Report Technical Information Series* **2002**.

109. Kovach, B.S., Kavanagh, C.J., Swain, G.W., Darkangelo-Wood, C., Stein, J., Truby, K., Holm, E., Montemarano, J., Meyer, A., and Wiebe, D. A through-Hull Drag Meter to Evaluate the Performance of Fouling-Release Coatings*. GE Global Research Report Technical Information Series* **2003**.

110. Holm, E., Kavanagh, C., Meyer, A., Wiebe, D., Nedved, B., Wendt, D., Smith, C.M., Swain, G., Darkangelo-Wood, C., Truby, K., Stein, J., and Montemarano, J. Adhesion of Marine Fouling to Silicone Surfaces: Relationships between Organisms and Material Properties*. GE Global Research Report Technical Information Series* **2003**.

111. Meyer, A., Baier, R., Wood, C.D., Stein, J., Truby, K., Holm, E., Montemarano, J., Kavanagh, C., Nedved, B., Smith, C., Swain, G., and Wiebe, D. Contact Angle Study of the Mechanism of Easy-Release from Oil-Amended Silicone Paints before and after Long-Term Biofouling Exposure*. GE Global Research Report Technical Information Series* **2003**.

112. Kavanagh, C.J., Swain, G.W., Kovach, B.S., Stein, J., Darkangelo-Wood, C., Truby, K., Holm, E., Montemarano, J., Meyer, A., and Wiebe, D. Screening of Fouling-Release Coatings by Barnacle Adhesion Strength*. GE Global Research Report Technical Information Series* **2003**.

113. Swain, G.W., Kavanagh, C.J., Kovach, B.S., Darkangelo-Wood, C., Stein, J., Truby, K., Holm, E., Montemarano, J., Meyer, A., and Wiebe, D. The Antifouling Performance of Non-Toxic Silicone Fouling Release Coatings for a Small Planing Craft*. GE Global Research Report Technical Information Series* **2003**.

114. Wiebe, D., Holm, E.R., Swain, G., Kavanagh, C.J., Meyer, A.E., Stein, J., Wood, C.D., Truby, K., Wendt, D., Smith, C.M., and Montemarano, J. Variations in Surface Coverage and Performance of Oil-Enhanced Foul-Release Coatings*. GE Global Research Report Technical Information Series* **2003**.

115. Warrick, E.L., Pierce, O.R., Polmanteer, K.E., and Saam, J.C. Silicone Elastomer Developments 1967-1977*. Rubber Chemistry and Technology* **1978**, *52*, p. 437-525.

116. Chaudhury, M.K. and Whitesides, G.M. Direct Measurement of Interfacial Interactions between Semispherical Lenses and Flat Sheets of Poly(Dimethylsiloxane) and Their Chemical Derivatives*. Langmuir* **1991**, *7*, p. 1013-1025.

117. Chaudhury, M.K. Interfacial Interaction between Low-Energy Survaces*. Materials Science and Engineering Review* **1996**, *R16*, p. 97-159.

118. Newby, B.-m.Z. and Chaudhury, M.K. Effect of Interfacial Slippage on Viscoelastic Adhesion*. Langmuir* **1997**, *13*, p. 1805-1809.

119. She, H., Malotky, D., and Chaudhury, M.K. Estimation of Adhesion Hysteresis at Polymer/Oxide Interfaces Using Rolling Contact Mechanics. *Langmuir* **1998**, *14*, p. 3090-3100.

120. Newby, B.-m.Z. and Chaudhury, M.K. Friction in Adhesion. *Langmuir* **1998**, *14*, p. 4865-4872.

121. Chaudhury, M.K. Rate-Dependent Fracture at Adhesive Interface. *Journal of Physical Chemistry: B* **1999**, *103*, p. 6562-6566.

122. She, H. and Chaudhury, M.K. Estimation of Adhesion Hysteresis Using Rolling Contact Mechanics. *Langmuir* **2000**, *16*, p. 622-625.

123. Schmidt, D.L., Brady, R.F., Lam, K., Schmidt, D.C., and Chaudhury, M.K. Contact Angle Hysteresis, Adhesion, and Marine Biofouling. *Langmuir* **2004**, *20*(7), p. 2830-2836.

124. Jelvestam, M., Edrud, S., Petronis, S., and Gatenholm, P. Biomimetic Materials with Tailored Surface Micro-Architecture for Prevention of Marine Biofouling. *Surface and Interface Analysis* **2003**, *35*(2), p. 168-173.

125. Baier, R.E. Surface Properties Influencing Biological Adhesion. in *Adhesion in Biological Systems*, Manly, R.S., Editor; Academic Press: New York. 1970, p. 15-50.

126. Baier, R.E. *Influence of the Initial Surface Conditions of Materials on Bioadhesion*. in *Proceedings of the 3rd International Congress on Marine Corrosion and Fouling*. 1973. Gaithersburg, MD: National Bureau of Standards.

127. Dexter, S.C., Sullivan, J.D., Williams III, J., and Watson, S.W. Influence of Substrate Wettability on the Attachment of Marine Bacteria to Various Surfaces. *Applied Microbiology* **1975**, *30*(1), p. 298-308.

128. Dexter, S.C. Influence of Substratum Critical Surface Tension on Bacterial Adhesion-in Situ Studies. *Journal of Colloid and Interface Science* **1979**, *70*(2), p. 346-354.

129. Fletcher, M. and Loeb, G.I. Influence of Substratum Chemistry on the Attachment of a Marine Pseudomonad to Solid Surfaces. *Applied and Environmental Microbiology* **1979**, *37*, p. 67-72.

130. Rolland, J.P., Hagberg, E.C., Denison, G.M., Carter, K.R., and Simone, J.M.D. High-Resolution Soft Lithography: Enabling Materials for Nanotechnologies. *Angewandte Chemie-International Edition* **2004**, *43*, p. 5796-5799.

131. Ayambem, A., Mecham, S.J., Sun, Y., Glass, T.E., and McGrath, J.E. Endgroup Substituent Effects on the Rate/Extent of Network Formation and Adhesion for Phenylethynyl-Terminated Poly(Arylene Ether Sulfone) Oligomers. *Polymer* **2000**, *41*(13), p. 5109-5124.

132. Mecham, J.B. Direct Polymerization of Sulfonated Poly(Arylene Ether) Random Copolmers and Poly(Imide) Sulfonated Poly(Arylene Ether) Segmented Copolymers: New Candidate Materials for Proton Exchange Membrane Fuel Cell Material Systems. Virginia Tech, Blacksburg, VA, 2001.

133. Mecham, S. Synthesis and Characterization of Phenylethynyl Terminated Poly(Arylene Ether Sulfone) as Thermosetting Structural Adhesives and Composite Matrices. Virginia Tech, Blacksburg, VA, 1997.

134. Rao, V.L. Polyether Sulfones. *Journal of Macromolecular Science-Reviews in Macromolecular Chemistry and Physics* **1999**, *C39*(4), p. 655-711.

135. Rao, V.L. and Rao, M.R. Synthesis and Characterization of Poly(Ether Sulfone) Copolymers. *Journal of Applied Polymer Science* **1998**, *69*(4), p. 743-750.

136. Rao, V.L., Sabeena, P.U., and Ninan, K.N. Synthesis and Properties of Polyether Ketone and Polyether Ketone Sulfone Copolymers. *European Polymer Journal* **1998**, *34*(3-4), p. 567-570.

137. Rao, V.L., Sabeena, P.U., Rao, M.R., and Ninan, K.N. Synthesis and Characterization of Poly(Ether Sulfone) and Poly(Ether Sulfone Ketone) Copolymers. *Journal of Applied Polymer Science* **1999**, *73*(11), p. 2113-2121.

138. Noshay, A. and Roberson, L.M. Sulfonated Polysulfone. *Journal of Applied Polymer Science* **1976**, *20*, p. 1885-1903.

139. Noshay, A. and McGrath, J.E. Block Copolymers. in; Academic Press: 1977, 516.

140. Flemming, H.-C. and Schaule, G. Biofouling on Membranes - a Microbiological Approach. *Desalination* **1988**, *70*(1-3), p. 95-119.

141. Todd, J.S., Zimmerman, R., Crews, P., and Alberte, R.S. The Antifouling Activity of Natural and Synthetic Phenolic Acid Sulphate Esters. *Phytochemistry* **1993**, *34*(2), p. 401-404.

142. Alexandratos, S.D. Synthesis and Purification of Zosteric Acid. US:**5,990,336,** 1999.

143. Stanley, M.S., Callow, M.E., Perry, R., Alberte, R.S., Smith, R., and Callow, J.A. Inhibition of Fungal Spore Adhesion by Zosteric Acid as the Basis for a Novel, Nontoxic Crop Protection Technology. *Phytopathology* **2002**, *92*(4), p. 378-383.

144. Nojiri, C., Okano, T., Jacobs, H.A., Park, K.D., Mohammad, S.F., Olsen, D.B., and Kim, S.W. Blood Compatibility of Polyethylene Oxide Grafted Polyurethane and Hema/Styrene Block Copolymer Surfaces. *Journal of Biomedical Materials Research* **1990**, *24*, p. 1151-1171.

145. Desai, N.P. and Hubbell, J.A. Biological Responses to Polyethylene Oxide Modified Polyethylene Terephthalate Surfaces. *Journal of Biomedical Materials Research* **1991**, *25*, p. 829-843.

146. Han, D.K., Jeong, S.Y., Kim, Y.H., Min, B.G., and Cho, H.I. Negative Cilia Concept for Thromboresistance: Synergistic Effect of Polyethylene Oxide and Sulfonate Groups Grafted onto Polyurethanes. *Journal of Biomedical Materials Research* **1991**, *25*, p. 561-575.

147. Lee, J.H., Lee, H.B., and Andrade, J.D. Blood Compatibility of Polyethylene Oxide Surfaces. *Progress in Polymer Science* **1995**, *20*, p. 1043-1079.

148. Höcker, H. and Klee, D. Polymers for Biomedical Applications: Improvement of the Interface Compatibility. *Advances in Polymer Science* **2000**, *149*, p. 1-57.

149. Inglis, W., Sanders, G.H.W., Williams, P.M., Davies, M.C., Roberts, C.J., and Tendler, S.J.B. A Simple Method for Biocompatible Polymer Based Spatially Controlled Adsorption of Blood Plasma Proteins to a Surface. *Langmuir* **2001**, *17*(23), p. 7402-7405.

150. Cuvelier, D., Rossier, O., Bassereau, P., and Nassoy, P. Micropatterned "Adherent/Repellent" Glass Surfaces for Studying the Spreading Kinetics of Individual Red Blood Cells onto Protein-Decorated Substrates. *European Biophysics Journal with Biophysics Letters* **2003**, *32*(4), p. 342-354.

151. Gupta, B. and Anjum, N. Plasma and Radiation-Induced Graft Modification of Polymers for Biomedical Applications. *Advances in Polymer Science* **2003**, *162*, p. 35-61.

152. Rixman, M.A., Dean, D., and Ortiz, C. Nanoscale Intermolecular Interactions between Human Serum Albumin and Low Grafting Density Surfaces of Poly(Ethylene Oxide). *Langmuir* **2003**, *19*(22), p. 9357-9372.

153. Qiu, Y.X., Klee, D., Pluster, W., Severich, B., and Hocker, H. Surface Modification of Polyurethane by Plasma-Induced Graft Polymerization of Poly(Ethylene Glycol) Methacrylate. *Journal of Applied Polymer Science* **1996**, *61*(13), p. 2373-2382.

154. Jo, S. and Park, K. Surface Modification Using Silanated Poly(Ethylene Glycol). *Biomaterials* **2000**, *21*, p. 605-616.

155. Delamarche, E., Geissler, M., Bernard, A., Wolf, H., Michel, B., Hilborn, J., and Donzel, C. Hydrophilic Poly(Dimethylsloxane) Stamps for Microcontact Printing. *Advanced Materials* **2001**, *13*(15), p. 1164-+.

156. Papra, A., Bernard, A., Juncker, D., Larsen, N.B., Michel, B., and Delamarche, E. Microfluidic Networks Made of Poly(Dimethylsiloxane), Si, and Au Coated with Polyethylene Glycol for Patterning Proteins onto Surfaces. *Langmuir* **2001**, *17*(13), p. 4090-4095.

157. Csucs, G., Michel, R., Lussi, J.W., Textor, M., and Danuser, G. Microcontact Printing of Novel Co-Polymers in Combination with Proteins for Cell-Biological Applications. *Biomaterials* **2003**, *24*(10), p. 1713-1720.

158. Revzin, A., Tompkins, R.G., and Toner, M. Surface Engineering with Poly(Ethylene Glycol) Photolithography to Create High-Density Cell Arrays on Glass. *Langmuir* **2003**, *19*(23), p. 9855-9862.

159. Kofinas, P., Athanassiou, V., and Merrill, E.W. Hydrogels Prepared by Electron Irradiation of Poly(Ethylene Oxide) in Water Solution: Unexpected Dependence of Cross-Link Density and Protein Diffusion Coefficients on Initial Peo Molecular Weight. *Biomaterials* **1996**, *17*(15), p. 1547-1550.

160. McPherson, T., Kidane, A., Szleifer, I., and Park, K. Prevention of Protein Adsorption by Tethered Poly(Ethylene Oxide) Layers: Experiments and Single-Chain Mean-Field Analysis. *Langmuir* **1998**, *14*(1), p. 176-186.

161. Delamarche, E., Donzel, C., Kamounah, F.S., Wolf, H., Geissler, M., Stutz, R., Schmidt-Winkel, P., Michel, B., Mathieu, H.J., and Schaumburg, K. Microcontact Printing Using Poly(Dimethylsiloxane) Stamps Hydrophilized by Poly(Ethylene Oxide) Silanes. *Langmuir* **2003**, *19*(21), p. 8749-8758.

162. Chen, H., Brook, M.A., and Sheardown, H. Silicone Elastomers for Reduced Protein Adsorption. *Biomaterials* **2004**, *25*(12), p. 2273-2282.

163. Gan, D.J., Mueller, A., and Wooley, K.L. Amphiphilic and Hydronhobic Surface Patterns Generated from Hyperbranched Fluoropolymer/Linear Polymer Networks: Minimally Adhesive Coatings Via the Crosslinking of Hyperbranched Fluoropolymers. *Journal of Polymer Science Part a-Polymer Chemistry* **2003**, *41*(22), p. 3531-3540.

164. Gudipati, C.S., Greenlief, C.M., Johnson, J.A., Prayongpan, P., and Wooley, K.L. Hyperbranched Fluoropolymer and Linear Poly(Ethylene Glycol) Based Amphiphilic Crosslinked Networks as Efficient Antifouling Coatings: An Insight into the Surface Composition, Topographies, and Morphologies. *Journal of polymer Science A: Polymer Chemistry* **2004**, *42*, p. 6193-6208.

165. Akizawa, T., Kino, K., Koshikawa, S., Ikada, Y., Kishida, A., Yamashita, M., and Imamura, K. Efficiency and Biocompatibility of a Polyethylene Glycol Grafted Cellulosic Membrane During Hemodialysis. *Transactions of the American Society of Artificial Internal Organs* **1989**, *35*, p. 333-335.

166. Park, J.H., Park, K.D., and Bae, Y.H. Polydimethylsiloxane-Based Polyurethanes with Polyethylene Glycol Grafts: Synthesis, Characterization and Platelet Adhesion Study. *Biomaterials* **1999**, *20*, p. 943-953.

167. Han, D.K., Park, K.D., Ahn, K.-D., Jeong, S.Y., and Kim, Y.H. Preparation and Surface Characterization of Polyethylene Oxide-Grafted and Heparin-Immobilized Polyurethanes. *Journal of Biomedical Materials Research* **1989**, *23*(A1), p. 87-104.

168. Han, D.K., Park, K.D., Jeong, S.Y., Kim, Y.H., Kim, U.Y., and Min, B.G. In Vivo Biostability and Calcification-Resistance of Surface-Modified PU-PEO-SO_3. *Journal of Biomedical Materials Research* **1993**, *27*, p. 1063-1073.

169. Nojiri, C., Okano, T., Park, K.D., and Kim, S.W. Suppression Mechanisms for Thrombus Furmation on Heparin-Immobilized Segmented Polyurethane Ureas. *Transactions of the American Society of Artificial Internal Organs* **1988**, *34*, p. 386-398.

170. Makamba, H., Kim, J.H., Lim, K., Park, N., and Hahn, J.H. Surface Modification of Poly(Dimethylsiloxane) Microchannels. *Electrophoresis* **2003**, *24*(21), p. 3607-3619.

171. Wilkerson, W.R. Contribution of Modulus to the Contact Guidance of Endothelial Cells on Microtextured Siloxane Elastomers. Masters, University of Florida, Gainesville, Fl, 2001.

172. Abbasi, F. and Mirzadeh, H. Adhesion between Modified and Unmodified Poly(Dimethylsiloxane) Layers for a Biomedical Application. *International Journal of Adhesion and Adhesives* **2004**, *24*(3), p. 247-257.

173. Chu, P.K., Chen, J.Y., Wang, L.P., and Huang, N. Plasma-Surface Modification of Biomaterials. *Materials Science & Engineering R-Reports* **2002**, *36*(5-6), p. 143-206.

174. Fritz, J.L. and Owen, M.J. Hydrophobic Recovery of Plasma-Treated Polydimethylsiloxane. *Journal of Adhesion* **1995**, *54*, p. 33-45.

175. Olander, B., Wirsen, A., and Albertsson, A.-C. Argon Microwave Plasma Treatment and Subsequent Hydrosilylation Grafting as a Way to Obtain Silicone Biomaterials with Well-Defined Surface Structures. *Biomacromolecules* **2002**, *3*, p. 505-510.

176. Olander, B., Wirsen, A., and Albertsson, A.-C. Silicone Elastomer Surface Funtionalized with Primary Amines and Subsequently Coupled with Heparin. *Biomacromolecules* **2003**, *4*, p. 145-148.

177. Everaert, E., van der Mei, H.C., and Busscher, H.J. Adhesion of Yeasts and Bacteria to Fluoro-Alkylsiloxane Layers Chemisorbed on Silicone Rubber. *Colloids and Surfaces B-Biointerfaces* **1998**, *10*(4), p. 179-190.

178. Silver, J.H., Lin, J.C., Lim, F., Tegoulia, V.A., Chaudhury, M.K., and Cooper, S.L. Surface Properties and Hemocompatibility of Alkyl-Siloxane Monolayers Supported on Silicone Rubber: Effect of Alkyl Chain Length and Ionic Functionality. *Biomaterials* **1999**, *20*(17), p. 1533-1543.

179. Price, C., Waters, M.G.J., Williams, D.W., Lewis, M.A.O., and Stickler, D. Surface Modification of an Experimental Silicone Rubber Aimed at Reducing Initial Candidal Adhesion. *Journal of Biomedical Materials Research* **2002**, *63*(2), p. 122-128.

180. Aziz, T., Waters, M., and Jagger, R. Surface Modification of an Experimental Silicone Rubber Maxillofacial Material to Improve Wettability. *Journal of Dentistry* **2003**, *31*(3), p. 213-216.

181. Perutz, S., Kramer, E.J., Baney, J., and Hui, C.-Y. Adhesion between Hydrolyzed Surfaces of Poly(Dimethylsiloxane) Networks. *Macromolecules* **1997**, *30*, p. 7964-7969.

182. Bhattacharya, S., Datta, A., Berg, J.M., and Gangopadhyay, S. Studies on Surface Wettability of Poly(Dimethyl) Siloxane (PDMS) and Glass under

Oxygen-Plasma Treatment and Correlation with Bond Strength. *Journal Of Microelectromechanical Systems* **2005**, *14*(3), p. 590-598.

183. Miyaji, F., Iwai, M., Kokubo, T., and Nakamura, T. Chemical Surface Treatment of Silicone for Inducing Its Bioactivity. *Journal of Materials Science-Materials in Medicine* **1998**, *9*(2), p. 61-65.

184. DePalma, D. Surface Hydrolysis of Polydimethylsiloxane Elastomers. Masters, University of Florida, Gainesville, Fl, 1992.

185. Thanawala, S.K. and Chaudhury, M.K. Surface Modification of Silicone Elastomer Using Perfluorinated Ether. *Langmuir* **2000**, *16*(3), p. 1256-1260.

186. Chen, H., Zhang, Z., Chen, Y., Brook, M.A., and Sheardown, H. Protein Repellant Silicone Surfaces by Covalent Immobilization of Poly(Ethylene Oxide). *Biomaterials* **2005**, *26*(15), p. 2391-2399.

187. Fateh-Alavi, K., Gallstedt, M., and Gedde, U.W. The Effect of Antioxidants on the Surface Oxidation and Surface Cracking of Crosslinked Polydimethylsiloxane. *Polymer Degradation and Stability* **2001**, *74*, p. 49-57.

188. Baier, R.E., Meyer, A.E., and Forsberg, R.L. Certification of Properties of Nontoxic Fouling-Release Coatings Exposed to Abrasion and Long-Term Immersion. *Naval Research Reviews* **1997**, *99*, p. 60-65.

189. Smith, A.L. Analysis of Silicones. 1978.

190. Launer, P.J. Infrared Assessment of Organosilicon Compounds: Spectra Structure Correlations. in *Silicon Coumpounds: Silanes and Silicones - a Survey of Properties and Chemistry by Gelest, Inc*, Arkles, B. and Larson, G., Editors. 2004.

191. Leblanc, J.L. Rubber-Filler Interactions and Rheological Propertiesin Filled Compounds. *Progress in Polymer Science* **2002**, *27*, p. 627-687.

192. Hecht, A.-M., Horkay, F., and Geissler, E. Structure of Polymer Solutions Containing Fumed Silica. *Physical Review Letters* **2001**, *64*, p. 1-6.

193. Karlsson, A. New Analytical Methods for Silicone Elastomers Used in Drug Delivery Systems. Royal Institute of Technology, Stockholm, 2003.

194. Wilkerson, W.R., Seegert, C.A., Feinberg, A.W., Zhao, L.C., Callow, M.E., Baney, R., and Brennan, A.B. Bioadhesion Studies on Microtextured

Siloxane Elastomers*. Abstracts of Papers of the American Chemical Society* **2001**, *221*, p. 253-POLY.

195. Gibson, A. Chemical Modification of Silicone Elastomer for Controlled Biological Interactions on Microtextured Surfaces. Masters, University of Florida, Gainesville, Fl, 2001.

196. Good, R.J. Contact Angle, Wetting, and Adhesion: A Critical Review*. Journal of Adhesion Science and Technology* **1992**, *6*(12), p. 1269-1302.

197. Callow, J.A., Stanley, M.S., Wetherbee, R., and Callow, M.E. Cellular and Molecular Approaches to Understanding Primary Adhesion in *Enteromorpha*: An Overview*. Biofouling* **2000**, *16*(2-4), p. 141-150.

198. Schultz, M., Finlay, J.A., Callow, M.E., and Callow, J.A. A Turbulent Channel Flow Apparatus for the Determination of the Adhesion Strength of Microfouling Organisms*. Biofouling* **2000**, *15*(4), p. 243-251.

199. Finlay, J.A., Callow, M.E., Ista, L.K., Lopez, G.P., and Callow, J.A. The Influence of Surface Wettability on the Adhesion Strength of Settled Spores of the Green Alga *Enteromorpha* and the Diatom *Amphora. Integrative and Comparative Biology* **2002**, *42*(6), p. 1116-1122.

200. Callow, M.E., Callow, J.A., Pickett-Heaps, J., and Weatherbee, R. Primary Adhesion of *Enteromorpha (Chlorophyta, Ulvales)* Propogules: Quantitative Settlement Studies and Video Microscopy*. Journal of Phycology* **1997**, *33*, p. 938-947.

201. Guillard, R.R. and Ryther, J.H. Studies of Marine Planktonic Diatoms: 1. *Cyclotella Nana Hustedt* and *Detonula Confervacea (Cleve) Gran. Canadian Journal of Microbiology* **1962**, *8*(2), p. 229-&.

202. Swain, G., Anil, A.C., Baier, R.E., Chia, F.S., Conte, E., Cook, A., Hadfield, M., Haslbeck, E., Holm, E., Kavanagh, C., Kohrs, D., Kovach, B., Lee, C., Mazzella, L., Meyer, A.E., Qian, P.Y., Sawant, S.S., Schultz, M., Sigurdsson, J., Smith, C., Soo, L., Terlizzi, A., Wagh, A., Zimmerman, R., and Zupo, V. Biofouling and Barnacle Adhesion Data for Fouling-Release Coatings Subjected to Static Immersion at Seven Marine Sites*. Biofouling* **2000**, *16*(2-4), p. 331-344.

203. Abbasi, F., Mirzadeh, H., and Katbab, K. Modification of Polysiloxane Polymers for Biomedical Applications: A Review*. Polymer International* **2001**, *50*, p. 1279-1287.

BIOGRAPHICAL SKETCH

Leslie Hoipkemeier Wilson, daughter of Steven and Lori Hoipkemeier, was born on September 8, 1978 in Monterey, California where here father was attending Naval Postgraduate School. Leslie has one sister, Casey Hoipkemeier Bergen. The family moved to Virginia Beach, Virginia when Leslie was just two-years old. Leslie attended Kempsville High School in Virginia Beach, Virginia, where she met a most influential teacher, Mrs. Duvall. Whilst serving as Mrs. Duvall's teaching assistant, Leslie aided her in developing a curriculum to teach polymer chemistry to elementary school students. It was then that Leslie's desire to work in the field of polymer chemistry developed.

The following fall, Leslie began her matriculation at The College of William and Mary in Williamsburg, Virginia. In September of 1996, Leslie began her undergraduate research under the advisement of Dr. David Kranbuehl. Leslie graduated with high honors with her bachelors in chemistry with a minor in physics in May of 2000. Her honors thesis was entitled, "Use of Frequency Dependent Electromagnetic Sensing Techniques to Monitor Gelation Properties of Methacrylate-based Systems and the Degradation of Nylon PA-11." At William and Mary, Leslie met Clifford Adams Wilson II, who became her husband in July 2000.

For her graduate work, Leslie attended the University of Florida and specialized in Materials Science and Engineering. She was inducted into Tau

Beta Pi, the National Engineering Honor Society and Alpha Sigma Mu, thu Materials Engineering Honor Society. During her five years at the university she worked on the development of minimally adhesive coating systems under the advisement of Dr. Anthony Brennan and with financial assistance from The Office of Naval Research. She was proud to be carrying on the proud tradition of Hoipkemeier engineers and felt honored to work on a project for the US Navy.